Technical Report ECOM-01870-189 November 1967

IMPEDANCE CHARACTERISTICS OF PUMPED VARACTORS

C. E. L. Technical Report No. 7695-189

Contract No. DA28-043-AMC-01870(E)

DA Project No. 1 PO 21101 AO42. 01.02

Prepared by

David E. Oliver

COOLEY ELECTRONICS LABORATORY
Department of Electrical Engineering
The University of Michigan
Ann Arbor, Michigan

for

U. S. Army Electronics Command, Fort Monmouth, N. J.

ABSTRACT

Since the publication in 1956 by Manley and Rowe of their now famous study of power flow in nonlinear reactive media, a considerable amount of work has been reported on the analysis of pumped varactor diode circuits. However all these studies have been limited in generality by two simplifying assumptions: the limitation of the pump voltage to low amplitudes, and the restriction of signal power flow to only a few sidebands. The first of these assumptions excludes the possibility of harmonic generation by the nonlinear diode, while the second presupposes the existence of ideal filters in the linear circuitry.

This study is concerned with an analysis of pumped varactor diode circuits without these two restrictions. Because the governing nonlinear equations are extremely complex and are insoluble using algebraic techniques, recourse was made to numerical techniques utilizing the digital computer. The input impedances of several basic pumped varactor diode circuits were analyzed theoretically by determining a suitable model for each circuit and then predicting its

impedance characteristics. The results showed good correlation with experimental measurements, indicating the adequacy of the circuit model, and the validity of the analysis methods.

In developing an accurate circuit model, a number of interesting and useful results were discovered. It was shown that several circuit parameters, which had never before been considered important, significantly affect circuit behavior. These parameters include: the exact nature of the diode depletion layer capacity-voltage characteristic; the circuit termination at the pump harmonic frequencies and their sidebands; the minority carrier lifetime of the semiconductor material; and the character of the electric fields in the diode junction.

The relationships between the exact expressions derived here and those obtained using the assumptions of previous workers were explored and clarified. A practical technique was developed for experimentally measuring the pump voltage amplitude across the diode junction. This method is useful for all save the smallest pump voltage magnitudes and does not depend upon the presence of rectified current flow through the diode.

The most significant outcome of this study is the development of a circuit model which can accurately characterize a varactor diode circuit. This model together with mathematical techniques developed here makes possible the accurate analysis of this type of circuit.

TABLE OF CONTENTS

TABLE OF CONTENTS (Cont.)

LIST OF TABLES

LIST OF SYMBOLS

Symbol	Meaning	Defined by or first used in
ω	angular frequency	Section 1.1
ω_p	angular frequency of the pump	Section 1.1
ω_1	angular frequency of the applied input signal	Section 1.1
ℓ, n, m	dummy subscript integers	Section 1.1
ω_{mn}	$m\omega_p + n\omega_1$	Eq. 1.1
q_t	total charge stored in varactor junction	Eq. 2.1
v_t	total voltage across varactor junction	Eq. 2.1
C	varactor junction capacity	Eq. 2.1
C_a	varactor junction capacity at zero bias	Eq. 2.1
ϕ	semiconductor contact potential	Eq. 2.1
M	non-integer exponent	Eq. 2.1
f	function of one variable	Eq. 2.2
Q_c	constant of integration	Eq. 2.3
V_{Bias}	bias voltage across diode	Eq. 2.4
V_N	normalized time varying voltage component across abrupt junction diode	Eq. 2.4
Q_{Bias}	DC charge stored in diode junction	Eq. 2.5
Q_N	normalized time varying charge component in abrupt junction diode	Eq. 2.5
K_1, K_2	normalization in constants	Eq. 2.5
S	elastance of diode	Eq. 2.9

LIST OF SYMBOLS (Cont.)

Symbol	Meaning	Defined by or first used in
S_s	normalized small signal elastance at the bias point	Eq. 2.9
C_N	normalized capacity of abrupt junction diode	Eq. 2.13
S_N	normalized elastance of abrupt junction diode	Eq. 2.14
V_L	normalized time varying voltage across linear junction diode	Eq. 2.16
Q_L	normalized time varying charge in linear junction diode	Eq. 2.16
C_L	normalized capacity of linear diode	Eq. 2.17
S_L	normalized elastance of linear diode	Eq. 2.18
x	distance from junction	Section 2.3
t	time (real)	Section 2.3
q	magnitude of charge on an electron	Section 2.3
p_n	thermal-equilibrium hole density in n-region	Section 2.3
τ	lifetime of holes in the base	Section 2.3
j_p	current density due to holes	Section 2.3
P(x, t)	excess hole density in n-region	Section 2.3
D	diffusion constant for holes	Eq. 2.22
E	magnitude of retarding electric field	Eq. 2.22
μ	mobility of holes	Eq. 2.22
K	Boltzmann constant	Eq. 2.23
T	junction temperature	Eq. 2.23

LIST OF SYMBOLS (Cont.)

Symbol	Meaning	Defined by or first used in
I_{Total}	total current through diode which is attributable to diffusion	Eq. 2.25
I_p	current transported by motion of holes	Eq. 2.25
I_e	current transported by motion of electrons	Eq. 2.25
e	2.718281827	Eq. 2.27
σ_ω	component of hole density of frequency ω and $x=0$	Eq. 2.28
σ_0	DC component of hole density at $x=0$	Eq. 2.28
j	$\sqrt{-1}$	Eq. 2.29
I_ω	diffusion current through diode at frequency ω	Eq. 2.30
β	electric field term	Eq. 2.30
V_ω	voltage component at frequency ω	Eq. 2.32
Y_ω	junction admittance due to diffusion	Eq. 2.33
P_n	normalized hole density	Eq. 2.33
I_{DC}	direct current through junction	Eq. 2.34
L_s	diode series inductance	Section 2.4
C_p	diode package capacitance	Section 2.4
R_s	diode series resistance	Section 2.4
B_j	imaginary part of junction admittance	Section 2.4
G_j	real part of junction admittance	Section 2.4
P_{mn}	power entering the reactance at ω_{mn}	Eq. 2.35

LIST OF SYMBOLS (Cont.)

Symbol	Meaning	Defined by or first used in
P'_p	power entering the reactance at the pump	Eq. 2.36
ω_u	$\omega_p + \omega_1$, upper sideband frequency	Eq. 2.36
P_u	power entering the reactance of the upper sideband	Eq. 2.36
ω_ℓ	$\omega_p - \omega_1$, lower sideband frequency	Eq. 2.38
P_ℓ	power entering the reactance of the lower sideband	Eq. 2.38
P_{nu}	power entering the reactance at $n\omega_p + \omega_1$	Eq. 2.40
$P_{n\ell}$	power entering the reactance at $n\omega_p - \omega_1$	Eq. 2.40
Q_p	pump component of charge	Eq. 3.2
q_s	signal component of charge	Eq. 3.2
v_s	signal voltage across junction	Eq. 3.3
S_n	complex Fourier coefficient of elastance at frequency $n\omega_p$	Eq. 3.6
i_s	signal current through varactor	Eq. 3.8
$I_{n\omega_p \pm \omega_1}$	component of signal current at frequency $n\omega_p \pm \omega_1$	Eq. 3.8
$V_{n\omega_p \pm \omega_1}$	component of signal voltage at frequency $n\omega_p \pm \omega_1$	Eq. 3.12
ω_n	special notation for signal frequency components	Table 3.1
I_n	signal current component at frequency ω_n	Eq. 3.14
V_n	signal voltage component at frequency ω_n	Eq. 3.14

LIST OF SYMBOLS (Cont.)

Symbol	Meaning	Defined by or first used in
$[S]$	depletion layer impedance matrix	Eq. 3.15
$[i_s]$	signal current through depletion layer capacity	Eq. 3.15
$[v_s]$	signal voltage across junction	Eq. 3.15
Z_{mm}	m, n element in [S]	Eq. 3.16
V_p	pump component of varactor voltage	Eq. 3.21
C_n	complex Fourier coefficient of depletion layer capacity at frequency $n\omega_p$	Eq. 3.21
$[C]$	pumped diode depletion layer admittance matrix	Eq. 3.22
Y_{mn}	m, n element in [C]	Eq. 3.23
$[Y'(n)]$	n-frequency admittance matrix	Eq. 3.29
α_{mn}	submatrix of $[Y'(n)]$	Eq. 3.30
θ_n	submatrix of $[Y'(n)]^{-1}$	Eq. 3.31
β_{mn}	m, n element of the α_{22}^{-1} matrix	Eq. 3.32
γ	pumping "hardness" coefficient	Eq. 3.34
Q_M	normalized charge	Section 4.2
V_M	normalized time varying component of voltage	Section 4.2
ω_o	small signal resonant frequency	Section 4.2
a	amplitude of sinusoidal waveform	Section 4.2
Υ	phase angle	Eq. 4.8
V	normalized voltage across tuned circuit	Eq. 4.8

LIST OF SYMBOLS (Cont.)

Symbol	Meaning	Defined by or first used in
I_{IN}	current source	Eq. 4.7
Q	quality factor of circuit	Eq. 4.7
L	inductance	Eq. 4.7
α	small parameter	Eq. 4.7
∂C	change in capacity	Eq. 4.11
δ_ω	frequency deviation from resonance	Eq. 4.16
E_{in}	amplitude of voltage source	Eq. 4.17
ϵ_t	perturbation of q_t	Eq. 4.19
q_0	amplitude of sinusoidal charge	Eq. 4.20
ν, ζ, ψ	normalization constants	Eq. 4.22
$Q_A(n)$	coefficient of $\cos n\omega_p t$	Eq. 5.1
$Q_B(n)$	coefficient of $\sin n\omega_p t$	Eq. 5.1
s	complex Laplace parameter	Eq. 5.3
Z	Thevenin equivalent impedance	Section 5.2
L_1	primary inductance	Section 5.2
L_2	secondary inductance	Section 5.2
M_1	mutual inductance between L_1 and L_2	Section 5.2
C_s	parasitic coil capacity	Section 5.2
G	inductor loss	Section 5.2
Z_L	impedance of ideal inductor	Section 5.2
X_L	reactance of shorted transmission line	Section 5.2

LIST OF SYMBOLS (Cont.)

Symbol	Meaning	Defined by or first used in
R_L	resistance of shorted transmission line	Section 5.2
ω_L	resonant frequency of transmission line	Section 5.2
Z_0	characteristic impedance of line	Section 5.2
a' and b'	inner and outer diameters of coaxial line	Section 5.2
σ	conductivity	Section 5.2
V_{LIN}	voltage across linear circuit	Eq. 5.8
E_A	cosine component of E_{in}	Eq. 5.9
E_B	sine component of E_{in}	Eq. 5.9
R(n)	resistance at nth harmonic	Eq. 5.11
X(n)	reactance at nth harmonic	Eq. 5.11
I_{in}	current source	Eq. 5.15
Q_m	estimate for Q_p after m iterations	Eq. 5.19
ϵ_m	error after m iterations	Eq. 5.20
Q_{Am}	estimate for Q_A after m iterations	Eq. 5.30
Q_{Bm}	estimate for Q_B after m iterations	Eq. 5.30
$\epsilon_A(n)_m$	coefficient of $\cos n\omega_p t$ in series for ϵ_m	Eq. 5.31
$\epsilon_B(n)_m$	coefficient of $\sin n\omega_p t$ in series for ϵ_m	Eq. 5.31
Z_{LR}	impedance of lossy inductor	Eq. 5.37
Z_{coil}	impedance of inductor with parasitic capacity	Eq. 5.39

LIST OF SYMBOLS (Cont.)

Symbol	Meaning	Defined by or first used in
ω_c	coil self resonant frequency	Eq. 5.41
δ_m	equation error after m iterations	Section 5.4
ϵ'_m	correction term in mth iteration	Eq. 5.12
$[Z_s]$	linear signal impedance matrix	Section 5.5
Z_n	nth element in $[Z_s]$	Section 5.5
$[V_s]$	input signal matrix	Section 5.5
V'_1	component of input signal at ω_1	Eq. 5.55
I_N	Norton current source	Eq. 6.1
I_{LIN}	current through linear network	Eq. 6.1
I_d	diffusion current through diode	Eq. 6.1
I_p	current through barrier layer capacity	Eq. 6.1
I_A	cosine component of I_N	Eq. 6.2
I_B	sine component of I_N	Eq. 6.2
Y	admittance of linear circuit	Eq. 6.3
G(n)	conductance at nth harmonic	Eq. 6.4
B(n)	susceptance at nth harmonic	Eq. 6.4
V_A	cosine component of V_p	Eq. 6.11
V_B	sine component of V_p	Eq. 6.11
E_N	voltage source	Section 6.3
ϵ_{max}	error in initial approximation to solution	Section 6.3
V'_m	estimate for V_p after m iterations	Eq. 6.12

LIST OF SYMBOLS (Cont.)

Symbol	Meaning	Defined by or first used in
V_{Am}	cosine component of V'_m	Eq. 6.12
V_{Bm}	sine component of V'_m	Eq. 6.12
F_m, G_m	constants in mth iteration	Eq. 6.15
$[I_s]$	input signal current matrix	Eq. 6.19
$[I_{1s}]$	signal current through linear circuit	Eq. 6.19
$[I_{ds}]$	signal current through diffusion capacity	Eq. 6.19
$[Y_s]$	linear admittance matrix	Eq. 6.22
Y_n	nth element in Y_s	Eq. 6.23
P_p	carrier density due to pump	Eq. 6.28
ρ_n	excess hole density component at $x=0$, at frequency $n\omega_p$	Eq. 6.28
P_s	carrier density due to signal	Eq. 6.29
$[Y_d]$	diffusion admittance matrix	Eq. 6.34
$[Y_t]$	total admittance	Eq. 6.35
M_2	mutual inductance	Section 7.2
L_3	inductance	Section 7.2
C_{B1}, C_{B2}, C_{B3}, C_{B4}	blocking capacitor	Section 7.2
C_{f1}, C_{f2}, C_{f3}	feed through capacitor	Section 7.2
C_{R1}, C_{R2}	varactor diode	Section 7.2
F	frequency term in matrix	Eq. A.3

LIST OF SYMBOLS (Cont.)

Symbol	Meaning	Defined by or first used in
$B_{m,n}$	cofactor of β_{mn}	Eq. A. 4
F'	frequency term in matrix	Eq. A. 5
G_{in}	input admittance to ladder network	Eq. A. 7
S_M	elastance of M law diode	Eq. B. 4
Q_M	normalized time varying charge in M law diode	Eq. B. 5
K_3	normalization constant	Eq. B. 5
N	general non-integer exponent	Eq. B. 7
K'_N	normalized elastance or capacitance	Eq. B. 7
Kn	normalized coefficient	Eq. B. 10
G'_n	real part of $-1/jn\omega_p Z(n\omega_p)$	Fig. C. 1
Y'_n	imaginary part of $-1/jn\omega_p Z(n\omega_p)$	Fig. C. 1
$\delta_A(n)_m$	coefficient of $\cos n\omega_p t$	Eq. D. 2
$\delta_B(n)_m$	coefficient of $\sin n\omega_p t$	Eq. D. 2
$\epsilon'_A(n)_m$	coefficient of $\cos \omega_p t$	Eq. D. 3
$\epsilon'_B(n)_m$	coefficient of $\sin \omega_p t$	Eq. D. 3
$R'_{(n)}$	real part of $-[1 + Z(n\omega p)]$	Eq. D. 4
$X'_{(n)}$	imaginary part of $-[1 + Z(n\omega p)]$	Eq. D. 4
r, s	integer dummy indices	Eq. D. 7
I_F	forward current	Eq. E. 2
R_p	resistor in pulse circuit	Eq. E. 2
E_F	pulse generator output before switching	Eq. E. 2

LIST OF SYMBOLS (Cont.)

Symbol	Meaning	Defined by or first used in
E_R	pulse generator output after switching	Eq. E. 2
V_F	diode voltage before switching	Eq. E. 2
V_R	diode voltage after switching	Eq. E. 3
T_s	length of reverse current pulse	Eq. E. 3
I_R	reverse current	Eq. E. 4

LIST OF ILLUSTRATIONS

LIST OF ILLUSTRATIONS (Cont.)

LIST OF ILLUSTRATIONS (Cont.)

LIST OF APPENDICES

CHAPTER I

INTRODUCTION

1.1 Statement of the Problem

This thesis is concerned with analysis of the input impedance characteristics of a pumped varactor diode circuit. This analysis, which includes both theoretical and experimental studies, avoids simplifying assumptions which would restrict the accuracy and generality of the results.

Although the response of pumped varactor diode circuits to small input signals has been studied extensively , most of this effort has been concentrated upon low-noise amplifying devices. Reflection type parametric amplifiers have received particularly wide-spread attention, although both parametric up-converters and phase-shift amplifiers have also been discussed frequently. Despite the multitude of studies reported on parametric circuit development, no general study of the behavior of these circuits has been reported. Certain assumptions are inherent in all the published analyses and cause appreciable error in many cases. This study examines the response of some simple pumped varactor circuits using a method free from these assumptions. Consequently, the analysis presented here is more accurate than any previously reported study. It is capable of accurately predicting pumped diode circuit behavior, even under conditions of hard pumping where the applied pump power is of such magnitude that the diode conducts over part of the pump cycle.

The operation and terminology of pumped varactor circuits are conveniently reviewed by considering Fig. 1.1 which shows all the basic elements present in a pumped varactor circuit in block diagram form. These elements are

1) A varactor diode. This is a semiconductor PN junction designed for operation under reverse-biased conditions such that the principal impedance component comes from the nonlinear voltage-dependent depletion layer capacitance.

2) A linear network. This network may include lumped or distributed circuit components. It contains a load resistor which absorbs the output signal, as well as the impedances associated with the external sources. It may also contain filters designed to separate the various frequency components generated in the parametric action.

3) A current or voltage source at frequency ω_p. The function of the source is similar to that of the local-oscillator in a mixer circuit. In parametric circuits it is usually designated as the pump.

4) A current or voltage source at frequency ω_1. This source provides the signal to be processed through amplification or frequency conversion.

The pump at frequency ω_p and the input signal at frequency ω_1 are coupled parametrically by the nonlinearity of the varactor

capacitance. In general, the resulting signal contains all positive frequencies in the set

$$\omega_{mn} = m\,\omega_p + n\,\omega_1;\ n,\ m = 0,\ \pm1,\ \pm2,\ \ldots \qquad (1.1)$$

In practice, the amplitude of the input signal is small compared with the pump amplitude to minimize the nonlinearity of the signal processing. The frequency of the input signal, ω_1, is usually smaller than the pump frequency ω_p. The frequencies are then restricted to the set

$$\omega_m = m\omega_p + \ell\omega_1 \qquad (1.2)$$

where as before

$$m = 0,\ 1,\ 2,\ \ldots$$

but for linear processing to occur, ℓ can have only three values

$$\ell = 0,\ -1,\ +1$$

The components at frequencies where $\ell = 0$ are the pump and its harmonics. The largest and most important of these is the pump fundamental ($m = 1$, $\ell = 0$). First order approximations, which are valid at small pump amplitudes, ignore all other components and treat both pump voltage (or current) and the resulting variations in diode capacity (or elastance) as sinusoidal. For "hard" or large amplitude

pumping, the sinusoidal approximations are often not valid, and more accurate analytical methods are required.

Components at frequencies where $\ell = -1$, or $+1$ have the same information content as the input signal. Frequencies in this set are denoted as signal frequencies. The output signal may be taken at any of these signal frequencies. However, it is usually taken at ω_1, $\omega_p + \omega_1$, or $\omega_p - \omega_1$.

1.2 Review of Literature

The literature on pumped circuits principles dates back more than a century to Faraday and Rayleigh, who showed that oscillation can be produced in a mechanical resonant system by supplying energy or "pumping" at a frequency twice that of the fundamental resonant frequency of the system (Ref. 1). Prior to World War I, the principle was expanded to include frequency ratios other than two-to-one and was applied to electrical networks. In 1916, Alexanderson built a "Magnetic Amplifier" (Ref. 2). Although he was primarily interested in modulation, or up-conversion, he did present data showing that negative resistance and parametric gain could exist.

The next really significant advance occurred during World War II when it was discovered by Torrey and Whitmer (Ref. 3) that certain microwave diodes had a nonlinear contact capacitance and could be used for amplification. Shortly thereafter, van der Ziel recognized the potential for building a low-noise amplifier (Ref. 4). However, it was

not possible to realize this potential until 1954 when Uhlir and his co-workers at Bell Telephone Laboratories developed low-loss silicon nonlinear capacitors (varactors) (Refs. 5 and 6).

Since that time, developments have been rapid, (Ref. 7) The Manley-Rowe relations which describe the power flow at various frequencies in an arbitrary nonlinear reactance were published in 1956, (Refs. 8 and 9). In April 1957, Suhl (Ref. 10) proposed construction of a parametric amplifier using a nonlinear ferrite material, and in July of that year experimental realization was reported (Ref. 11).

Bloom and Chang (Ref. 12) in their paper of Dec. 1957 considered theoretically the performance of parametric amplifiers using nonlinear inductors, and the following year both Heffner and Wade (Ref.13) and Rowe (Ref. 14) published analyses of parametric amplifiers utilizing nonlinear capacitors. All these analyses assumed that the nonlinear element was varying sinusoidally at the pump frequency (ω_p). They also assumed that only two voltages were present: one at the original frequency (ω_1); and the other at the difference frequency or lower sideband ($\omega_p - \omega_1$).

Leenov (Ref. 15)in a study of varactor up-converters published in 1958 used a somewhat different set of assumptions. He assumed sinusoidal elastance (elastance is the reciprocal of capacitance) and the presence of only two currents at frequencies ω_1 and $\omega_p + \omega_1$. Three years later, Robinson (Ref.16) and Penfield and Rafuse (Ref. 17)

again assumed sinusoidal elastance and the existence of only a limited number of currents. They advocated analyses which limited the number of currents and treated the elastance variation as sinusoidal rather than the methods used in previous analyses which restricted the number of voltage components and treated capacitance variation as sinusoidal.

In a paper on parametric amplifier noise, Kurokawa and Uenohara (Ref. 18) discussed both the case in which two currents (at ω_1 and $\omega_p + \omega_1$) are allowed to flow as well as the case in which two voltages (also at ω_1 and $\omega_p + \omega_1$) are permitted to exist. Adams (Ref. 19) in a 1962 paper allowed both sideband currents to flow along with the input signal current: ω_1, $\omega_p + \omega_1$, and $\omega_p - \omega_1$. He also relaxed the capacitance waveform assumption somewhat by considering a second harmonic component in addition to the fundamental.

Korpel and Ramasaway's (Refs. 20, 21) 1965 study of pumped varactor input conductance was premised on essentially the same assumptions as that of Adams (Ref. 19), except that they recognized that the average capacity of a varactor is dependent upon pump amplitude.

1.3 Topics of Investigation

The objective of this study is the accurate analysis of pumped varactor diode circuit behavior. Detailed study of a general circuit, such as that shown in Fig. 1. 1, does not yield results which are directly applicable to circuit design. To make the problem tractable, while

retaining some generality, it was decided to study the circuits in Figs. 1.2 and 1.3. These two circuits are simple, but they contain most features found in more complex, practical circuits. The results of the study of these basic circuits are directly applicable to the analysis of more complex networks.

The device shown in Fig. 1.2 is a very simple pumped varactor circuit. The circuit is assumed to be resonant near the pump frequency, so that a large voltage is produced across the diode with a small expenditure of power. Most varactor diode pump circuits utilize resonant tuning to minimize the pump power requirement.

The pump circuit resonance may also be adjusted for tuning at, or near, a sideband frequency. If the lower sideband ($\omega_p - \omega_1$) is near resonance, and the upper sideband is outside the passband, the device is a simple, negative-resistance parametric amplifier. The device can also be made to behave as a simple positive-resistance varactor up-converter by placing the upper sideband near resonance, and the lower sideband below the passband. If the sidebands are tuned symmetrically, the device behaves as an elementary double-sideband or phase-modulation circuit. The simple circuit in Fig. 1.2, thus can represent a large class of useful circuits.

The distributed circuit shown in Fig. 1.3 is somewhat more complex. Most pumped varactor circuits are actually built using distributed rather than lumped elements, and this simple transmission line circuit was chosen to represent this class of devices. The lumped

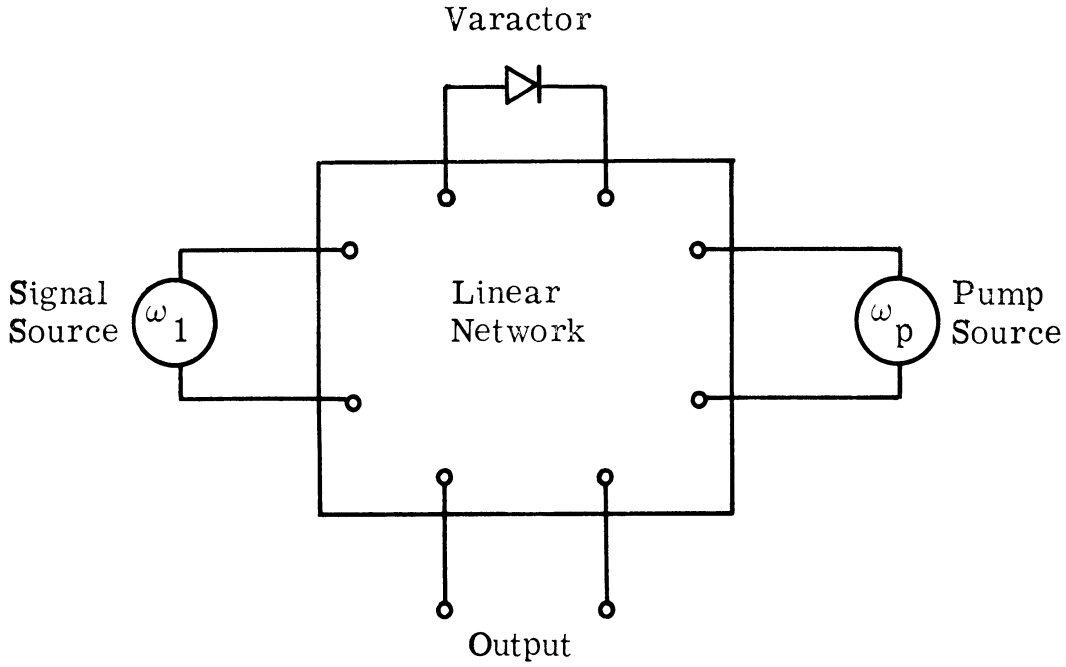

Fig. 1.1. The basic representation of a pumped varactor circuit

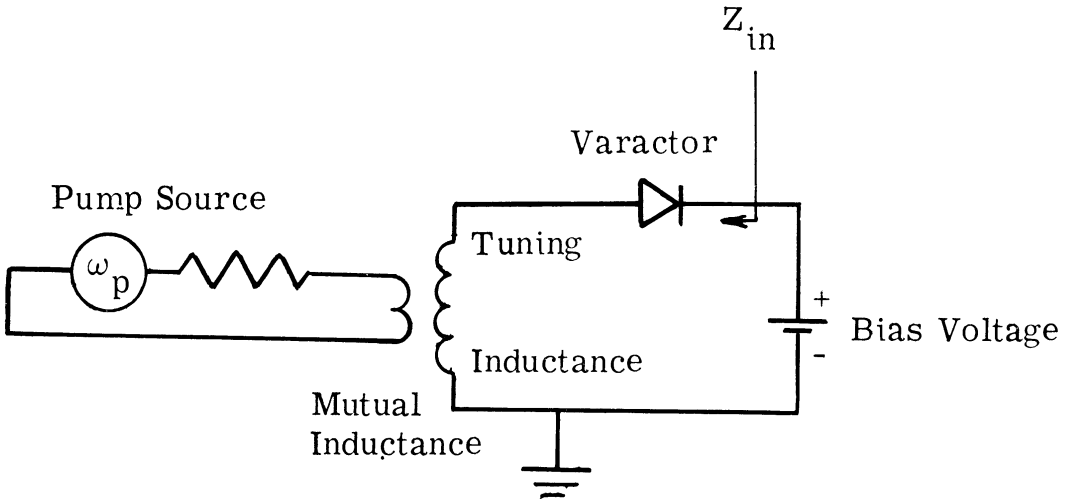

Fig. 1.2. Pumped varactor circuit consisting of lumped elements

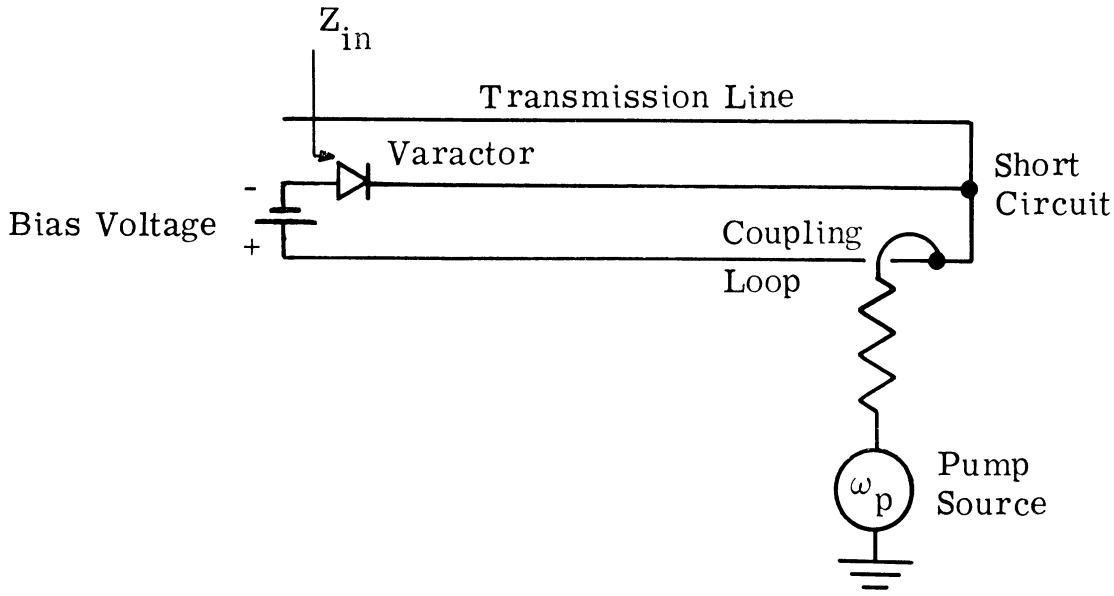

Fig. 1.3. Pumped varactor circuit consisting of a transmission line circuit

The input impedance for both circuits 1.2 and 1.3 is defined as the ratio of signal voltage (at frequency ω_1) to signal current. Currents and voltages are present at other frequencies (ω_1, $\omega_p+\omega_1$, $Z\omega_p+\omega_1$, ... etc.), and they affect the impedance significantly.

circuit (Fig. 1.2) has only one resonance (or passband), while the distributed circuit (Fig. 1.3) has an infinity of resonances. This results in marked differences in the circuit behavior.

The theoretical method used to determine the behavior of both circuits will include four steps:

(1) The pump voltage waveform will be found by solution of a nonlinear differential equation. Once the voltage across the diode is known, its small signal capacity can be computed easily at every instant of time during the pump cycle. Under these circumstances it is unnecessary to assume that the diode capacitance (or elastance) is sinusoidal, since this quantity can be computed as accurately as desired.

(2) The capacitance (or elastance) found in (1) will be expressed as a Fourier series, with the fundamental at the pump frequency, (ω_p) and additional terms at harmonics of the pump.

(3) The Fourier coefficients found in (1) and (2) will be inserted into the harmonic balance equations. These describe the mixing of the pump and its harmonics with the input signal (at frequency ω_1).

(4) The set of harmonic balance equations will be solved, and the impedance at the input signal frequency will be found.

The whole process will be systematized so that all four steps of the computation can be carried out on the digital computer.

1.4 Thesis Organization

Chapter II is a discussion of background material that is necessary for the remainder of this study. Two important but unrelated topics are discussed: (a) the properties of varactor diodes, and (b) the Manley-Rowe general energy relations.

Chapter III discusses the harmonic balance equations. These are a general formulation of mixing in a lossless, nonlinear reactance. A discussion of the assumptions made by others and the relationships between these assumptions and the exact expressions is included.

Chapter IV is a short discussion of pump stability in varactor circuits. The conditions under which the circuit is unstable are determined, and compared with experimental results. The comparison indicates that the simplified method of analysis which is developed in this chapter is adequate for at least a quantitive understanding.

Chapter V is a theoretical study of pumped diode circuits (Figs. 1.2 and 1.3) under conditions of small signal pumping. The nonlinear differential equation describing pump circuit behavior is set up and a method for solving it is presented. However, the solution is not in closed form, necessitating use of numerical methods for a specified set of input conditions.

Chapter VI is a theoretical study of diffusion or conduction effects in the circuit of Fig. 1.2. The results are applicable even under conditions of very hard pumping, where the diode is reverse-biased with a DC voltage, but is driven into forward conduction during a portion of the pump cycle by the large AC pump voltage.

Chapter VII contains all the numerical results from the studies of Chapters V and VI, as well as the results of a rather extensive experimental investigation. The experimental and numerical results are then compared and discussed. This chapter closes with the conclusions of the study.

CHAPTER II

FUNDAMENTAL PROPERTIES OF PUMPED VARACTORS

2. 1 Introduction

The performance of a pumped varactor circuit is intimately dependent upon the characteristics of the diode. The diode capacity-voltage relationship, the diode resistance, the carrier lifetime, etc., all significantly influence circuit behavior. Thus, it is appropriate to review some fundamental properties of varactor diodes prior to setting up and solving the nonlinear equations describing the circuit behavior.

In the next two sections, 2. 2 and 2. 3, the basic equations describing varactor diodes are first set down and then put in special forms which will be utilized in later chapters. A circuit model which accurately characterizes the varactor is presented in Section 2. 3, and is used throughout the remainder of this paper.

Some additional background material of a different nature is discussed in Section 2. 4, where the Manley-Rowe equations are presented. These are the general energy relations which describe the lossless varactor mixing process. Unfortunately, they can provide only a limited description of circuit performance, and hence are not used quantitatively in this paper. They can provide some important insights into circuit behavior, however; some of this insight will be particularly useful in Chapter VII , where the numerical results of the computer

programs and the experimental results are set down and interpreted.

2.2 Barrier-Layer Capacity

Modern varactor diodes are made from p-n semiconductor junctions, which exhibit a nonlinear capacitance when biased in the voltage range between forward conduction and reverse breakdown. A varactor diode is built to utilize this nonlinear reactive effect while minimizing the bulk series resistance of the semiconductor material.

Figure 2.1 shows the DC voltage current characteristics of a typical microwave varactor. The current in the forward direction increases exponentially, doubling in magnitude every 18 mv. In the reverse direction, breakdown typically occurs between -5 and -150 volts, depending upon the method of manufacture. In between, the conduction current is negligible and the device shows a voltage dependent capacitance called the barrier, or depletion layer capacity. The physical origins of this capacity are thoroughly discussed by several authors (Refs. 22, 23, 24, 25, 26), whose results are only summarized here.

Under reverse bias, the barrier layer capacity is the principal factor in determining the capacity of the varactor diode. At forward bias, however, the diffusion capacity associated with current flow may become important (Ref. 27).

The barrier layer capacity of a p-n junction is independent of frequency up to at least 20 GHz (Ref. 28). It can be expressed approximately as:

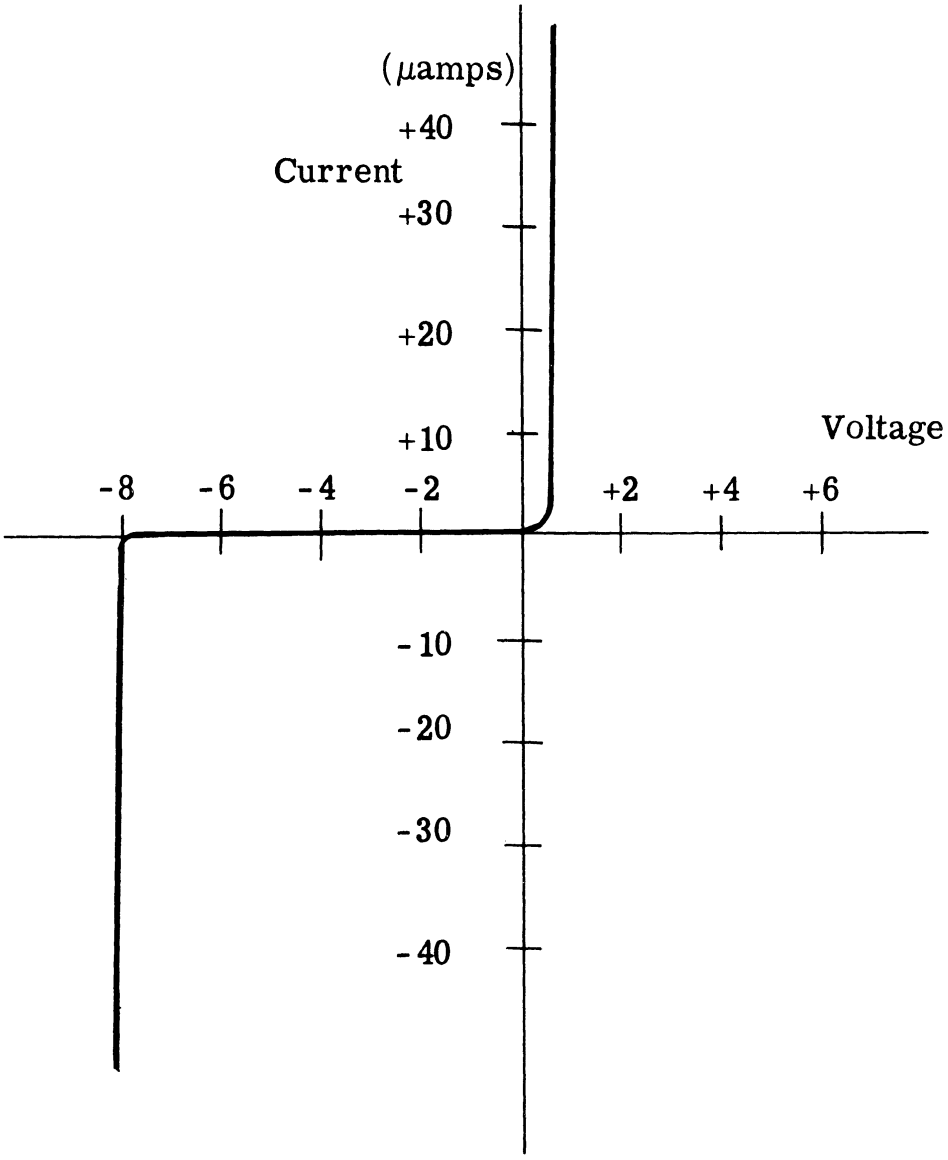

Fig. 2. 1. Typical varactor DC characteristics

$$\frac{dq_t}{dv_t} \triangleq C = \frac{C_a}{\left(1 - \frac{v_t}{\phi}\right)^{\frac{1}{M}}} \qquad (2.1)$$

where

v_t = applied voltage

C_a = junction capacity at zero bias

ϕ = contact potential

q_t = charge stored in junction

and $M = 2$ for an abrupt junction device

$M = 3$ for a graded junction device

The value of ϕ varies from 0.5 to 1.2 volts depending upon the semiconductor material and the manufacturing process. The exponent $\frac{1}{M}$ is a function only of the junction configuration. Actual devices can often be closely approximated by using a value between 0.25 and 0.50 for the exponent, and then adjusting the value of ϕ for the best curve fit.

Figure 2.2 shows the measured capacitance-voltage curve of a typical alloy junction varactor along with a very close approximation of the form (2.1).

In Chapters V and VI, where the circuit equations are set up and then solved, it is necessary to have an expression of the following from which relates voltage to charge:

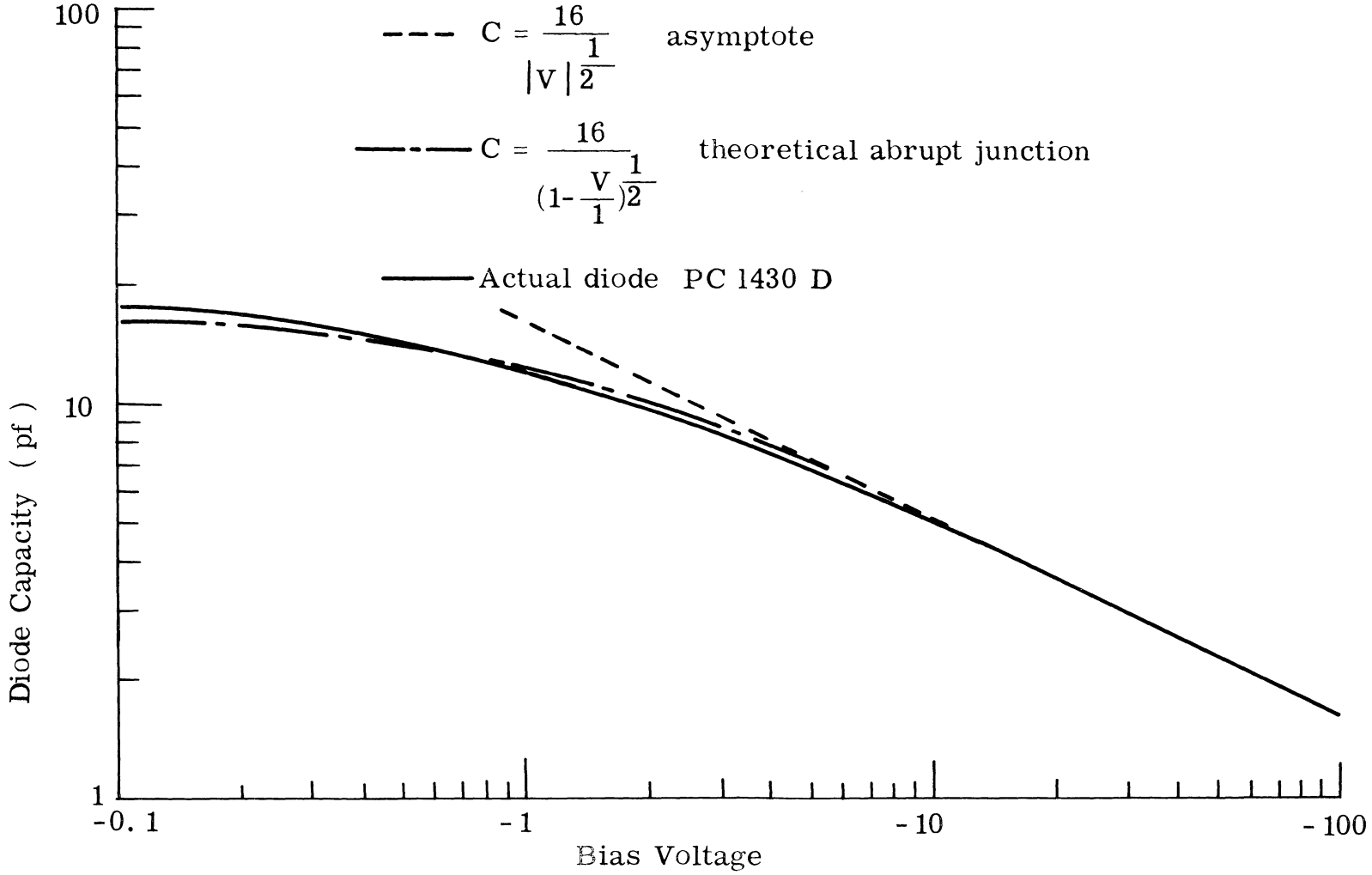

Fig. 2.2. Typical varactor capacitance characteristics

$$v_t = f(q_t) \tag{2.2}$$

In the abrupt junction case, a relation of this form can be obtained from Eq. 2.1. The first step is to find the charge stored in the junction. This is done simply by integrating Eq. 2.1.

$$q_t = -2\, C_a\, \phi \left(1 - \frac{v_t}{\phi}\right)^{\frac{1}{2}} + Q_c \tag{2.3}$$

where Q_c is a constant of integration.

It is convenient here to introduce new variables. Let both the total voltage and charge be the sum of two terms. The first term is dependent only upon DC bias; the second is a function of the time varying signals. K_1 and K_2 are constants which will be used to scale both V_N and Q_N, and thus obtain the simplest possible form for expression (2.2).

$$v_t = V_{Bias} + K_1 V_N(t) \tag{2.4}$$

$$q_t = Q_{Bias} + K_2 Q_N(t) \tag{2.5}$$

Combining Eqs. 2.3, 2.4 and 2.5

$$Q_{Bias} + K_1 Q_N(t) = -2\, C_a\, \phi \left(1 - \frac{V_{Bias}}{\phi} - \frac{K_1 V_N(t)}{\phi}\right)^{\frac{1}{2}} + Q_c \tag{2.6}$$

Q_c can now be chosen so that $Q_N(t)$ is zero when $V_N(t)$ is zero.

$$Q_c = Q_{Bias} - 2 C_a \phi \left(1 - \frac{V_{Bias}}{\phi}\right)^{\frac{1}{2}} \qquad (2.7)$$

Equation 2.6 can be combined with Eq. 2.7, solved for $V_N(t)$ and rewritten

$$V_N(t) = \frac{-(\phi - V_{Bias})}{K_1} \left[\frac{K_2^2 Q_N^{\,2}(t)}{(Q_{Bias} - Q_c)^2} - \frac{K_2 2 Q_N(t)}{(Q_{Bias} - Q_c)}\right] \qquad (2.8)$$

The small signal elastance at the bias point is found from Eq. 2.8.

$$S_s \triangleq \left.\frac{d\, V_N(t)}{d\, Q_N(t)}\right|_{\substack{\text{limit} \\ Q_N \to 0}} = \frac{2(\phi - V_{Bias})}{(Q_{Bias} - Q_c)} \frac{K_2}{K_1} \qquad (2.9)$$

Expressions 2.1, 2.8, and 2.9 can now be scaled by normalizing both signal and impedance to convenient values:

(1) Normalize the impedance level by setting the small signal elastance at the bias point equal to one daraf.

$$S_s = 1 \qquad (2.10)$$

(2) Normalize the signal level by setting the "total DC bias" equal to

$$V_{Bias} - \phi = K_{-1} \qquad (2.11)$$

Then from Eq. 2.9, Eq. 2.10, and Eq. 2.11, K_2 can be written as:

$$K_2 = \frac{-(Q_{Bias} - Q_c)}{2}$$

The normalized equation for voltage (Eq. 2.8) now becomes

$$V_N(t) = Q_N(t) + \frac{Q_N(t)^2}{4} \tag{2.12}$$

This is the desired expression having the form of Eq. 2.2.

In normalized form, the equation for capacitance (Eq. 2.1) becomes

$$C_N(t) = \frac{1}{[1 + V_N(t)]^{\frac{1}{2}}} \tag{2.13}$$

The small signal elastance can be computed from Eq. 2.12

$$S_N(t) = \frac{d\, V_N(t)}{d\, Q_N(t)} = 1 + \frac{Q_N(t)}{2} \tag{2.14}$$

In Eqs. 2.12 through 2.14, the variables are constrained by the following limits:

$$\begin{aligned} Q_N(t) &\geq -2 \\ V_N(t) &\geq -1 \\ S_N(t) &\geq 0 \end{aligned} \tag{2.15}$$

The same procedure can, of course, also be carried through for the diode having a linear variation of the majority carrier concentration in the junction area.

$$V_L(t) = -1 + \left[1 + \frac{2}{3} Q_L(t)\right]^{\frac{3}{2}} \tag{2.16}$$

$$C_L(t) = \frac{1}{\left[1 + V_L(t)\right]^{\frac{1}{3}}} \tag{2.17}$$

$$S_L(t) = \left[1 + \frac{2}{3} Q_L(t)\right]^{\frac{1}{2}} \tag{2.18}$$

The normalization here is carried out exactly as in the abrupt junction case (Eqs. 2.10 and 2.11). The limits, however, are different.

$$\begin{aligned} Q_L(t) &\geq -\frac{3}{2} \\ V_L(t) &\geq -1 \\ S_L(t) &\geq 0 \end{aligned} \tag{2.19}$$

2.3 Diffusion Capacity

Diffusion capacity arises from conduction processes in a p-n junction, which occur through charge carriers (electrons and holes) being injected across the junction, and diffusing into the region on the opposite side. Once across the junction they continue to exist as minority carriers having a finite lifetime, and traveling with a finite velocity.

The circuit effect of this process is a frequency-dependent capacity with a large associated loss. For mixing processes, this compares unfavorably with the low loss, frequency independent capacity formed by the p-n junction depletion layer. This section includes a short discussion of some p-n junction physics, for, unlike the depletion layer capacity which is treated in several references, there appears to be no adequate discussion of the mixing processes occurring in diffusion capacity.

To compute the diffusion capacitance, it is necessary to make several idealizing assumptions concerning the nature of the p-n junction.

The assumptions made in this paper can be summarized as follows (Refs. 25, 27, 29, 30, 31).

1) The problem can be reduced to one dimensional variations along the x-axis. This assumption introduces little error, for in all practical configurations, the radii of the junction and the area of the junction are both much greater than the junction thickness.

2) The device can be represented by a step junction, in which the doping changes discontinuously at the junction. A depletion region which is swept free of charge carriers is formed around this junction. The potential across the depletion region is the sum of the applied voltage plus the contact potential. Although this assumption is an obvious over-simplification, exact computations for some special cases show it to be surprisingly good (Refs. 32, 26).

3) The energy of the charge carriers can be described by Boltzmann statistics. This condition is applicable for varactor diodes constructed of silicon and germanium and for most GaAs diodes . However, it may break down for GaP.

4) The p-region is so heavily doped that the electron current can be neglected. Forward current then is carried entirely by holes, which leave the p-region to become minority carriers in the n-region. Reverse current is due to holes originating in the n-region, which are swept across the junction into the p-region. This assumption is consistent with current device fabrication techniques for silicon devices.

5) A retarding electric field which is assumed to be constant with distance exists in the n-region. This assumption is clearly at odds with the step junction approximation. It represents only a first order approximation to the actual fields in the junction.

6) The n-region is long compared with the diffusion length of holes in the material. This is a valid assumption for most devices, but is only approximately satisfied for some low loss epitaxial devices which have very thin n-type layers.

7) The hole current is constant throughout the depletion layer. Both transit time across the depletion layer and hole recombination in this layer are neglected. This assumption is almost always valid for germanium PN junction, but is less accurate for silicon.

8) The minority-carrier densities are small compared with majority carrier densities. This is the "low level injection" assumption (Ref. 29). It allows both the carrier lifetime and mobility to be treated as constants. This assumption is always valid for low current levels, but breaks down under conditions of high currents and high resistivitity n-type materials.

Under these assumptions, the continuity equation is valid for holes in the n-region.

$$\frac{-\partial j_p(x,t)}{\partial x} = q\frac{\partial P(x,t)}{\partial t} + q\frac{P(x,t)}{\tau} \qquad (2.20)$$

where

$j_p(x,t)$ is the current density due to holes (p-type carriers)

q is the magnitude of the charge on an electron

$P(x,t)$ is the excess hole density above p_n

p_n is the normal thermal-equilibrium density of holes in the n-region

τ is the lifetime of holes in the n-type material.

Since the carrier density cannot be less than zero, $P(x,t)$ has a lower limit given by

$$P(x,t) \geq -p_n \qquad (2.21)$$

The transport equation for holes in the presence of an electric field also is valid in this situation.

$$-j_p(x,t) = qD\frac{\partial P(x,t)}{\partial x} + qE\mu P(x,t) \qquad (2.22)$$

where

D is the diffusion constant for holes in the n-region

E is the magnitude of the retarding field

μ is the mobility of holes in the n-region

The diffusion constant and the mobility are related by the so-called Einstein relationship

$$\frac{\mu}{D} = \frac{q}{KT} \qquad (2.23)$$

Differentiating Eq. 2.22 with respect to x and combining it with the continuity equation (2.20) yields an equation which describes hole flow in the n-region.

$$D\frac{\partial^2 P(x,t)}{\partial x^2} = \frac{\partial P(x,t)}{\partial t} + \frac{P(x,t)}{\tau} - \mu E\frac{\partial P(x,t)}{\partial x} \qquad (2.24)$$

Since this is a linear differential equation, superposition and a variety of transform techniques are applicable.

In general, the current through any cross section of the diode is carried by both holes and electrons, that is,

$$I_{\text{Total}} = I_p + I_e \qquad (2.25)$$

However, one of the assumptions made here (assumption number 4) is that the current across the junction itself is carried entirely by holes. Then, taking the coordinate system origin at the junction, the total current is given by

$$I(t)_{\text{Total}} = I_p\Big|_{x=0} = -q\,DA\,\frac{\partial P(x,t)}{\partial x}\Big|_{x=0} - q\,AE\mu\,P(o,t) \qquad (2.26)$$

where

A is the area of the junction.

The final important relationship to be introduced in this section comes from Boltzmann statistics. It gives the instantaneous density of excess carriers at the junction in terms of the instantaneous voltage across the junction (Ref. 33).

$$P(o,t) = p_n\left(e^{\frac{q}{KT}\,v_t(t)} - 1\right) \qquad (2.27)$$

This equation, in contrast to the equations describing hole flow in the n-region, is nonlinear.

To compute the diffusion capacity of a PN junction at a general frequency ω, assume that the excess hole density at the junction has a component σ_ω at that frequency plus a constant term, σ_o.

$$P(o,t) = \mathrm{Re}\left\{\sigma_\omega \epsilon^{j\omega t} + \sigma_o\right\} \tag{2.28}$$

The only restrictions on σ_o is that

$$-|\sigma_\omega| + \sigma_o \geq -p_n$$

The behavior of holes in the base region can now be expressed as a boundary value problem. The coordinate system is set up so that the base region extends indefinitely in the positive direction starting at $x=0$.

$$D\frac{\partial^2 P(x,t)}{\partial x^2} = \frac{\partial P(x,t)}{\partial t} + \frac{P(x,t)}{\tau} - \mu E\frac{\partial P(x,t)}{\partial x} \tag{2.29}$$

$$P(o,t) = \mathrm{Re}\left\{\sigma_\omega \epsilon^{j\omega t} + \sigma_o\right\}$$

$$P(\infty,t) = 0$$

$$I(t)_{\text{Total}} = -q\,DA\frac{\partial P(x,t)}{\partial x}\bigg|_{x=0} - q\,AE\mu\,P(o,t)$$

The solution to this boundary value problem can be found using conventional techniques. Since the differential equation for the excess hole density is linear, the component of current at frequency ω is dependent only upon σ_ω and is independent of any other signal component which may be present.

Using the set of equations (2.29), the component of current at frequency ω is found to be

$$I_\omega = \frac{q\,A(1+j\omega\tau)\,\sigma_\omega}{\frac{\tau}{2}\left(\frac{qF}{KT}\right)\left[1+\sqrt{1+\beta(1+j\omega\tau)}\right]} \qquad (2.30)$$

where

$$\beta = \frac{4\,K^2\,T^2}{D\tau\,q^2\,F^2}$$

The voltage across the diode can be obtained from the Boltzmann relation, (Eq. 2.27).

$$v_t(t) = \mathrm{Re}\left\{\frac{KT}{q}\,\ell n\left(1+\frac{\sigma_o+\sigma_\omega\,e^{j\omega t}}{p_n}\right)\right\} \qquad (2.31)$$

If σ_ω is assumed to be small, this can be simplified and the voltage component at ω identified.

$$V_\omega = \frac{KT}{q}\left(\frac{\sigma_\omega}{\sigma_o+p_n}\right) \qquad (2.32)$$

If σ_o contains any time varying components, the situation is somewhat more complex due to frequency mixing. This case is discussed in Chapter VI.

The admittance of the junction is found from Eqs. 2.30 and 2.32. Diffusion capacity is defined as the imaginary part of this admittance divided by ω.

$$Y_\omega = \frac{I_\omega}{V_\omega} = \frac{(\frac{q}{KT})\, q\, A(1+j\omega\tau)(\sigma_o + p_n)}{\frac{\tau}{2}\frac{qE}{KT}\left[1+\sqrt{1+\beta(1+j\omega\tau)}\right]} \tag{2.33}$$

or

$$Y_\omega = \frac{\frac{q}{KT}\, P_n(1+j\omega\tau)\, e^{\frac{q}{KT}\, V_{Bias}}}{\left[1+\sqrt{1+\beta(1+j\omega\tau)}\right]}$$

where

$$P_n = \frac{q\, A\, p_n}{\frac{\tau}{2}\frac{qE}{KT}}$$

Under these conditions, the DC current through the junction is

$$I_{DC} = \frac{P_n\left(e^{\frac{q}{KT}\, V_{Bias}} - 1\right)}{(1+\sqrt{1+\beta})} \tag{2.34}$$

where V_{Bias} is the DC voltage, and σ_o is the excess carrier density associated with this voltage.

It is interesting to compare Eq. 2.33 with that for depletion layer capacity (2.1). Both depletion layer and diffusion capacity are functions only of the instantaneous diode voltage. Depletion layer capacity, however, is frequency independent and lossless, while diffusion capacity is not frequency independent and has a large loss associated with it at all frequencies.

Some further comparison of diffusion and depletion layer capacity can be made with a numerical example. The data presented here was obtained experimentally on a high quality diode having a measured capacity-voltage relationship of the form in Eq. 2.1. The measurement techniques, together with a more complete set of data are presented in Appendix E. The results are merely summarized here.

Carrier lifetime	$\tau = 0.5\ \mu\text{sec}$
"Normalized carrier density"	$P_n = 10^{-12}$ amps
Electric field term	$\beta = 0.1$
Junction field	$E = 600$ volts/cm
Capacity at zero voltage	$C_a = 33.1$ pf
Contact potential	$\phi = 1$ volt

The following table (Table 2.1) was computed by using this data in Eqs. 2.1 and 2.33. It illustrates clearly why the diffusion capacity can be neglected at reverse-bias voltages, and why it is important under forward-bias conditions.

Bias Voltage	DC Current	Depletion-layer Capacity	Diffusion Capacity @ 1 Mc	Diffusion Capacity @ 1000 Mc
+ 0.5	0.24 ma	47.0 pf	4500 pf	390 pf
+ 0.4	4.45 μ amps	42.9 pf	89 pf	7.1 pf
+ 0.2	0.0015 μ amps	37.1 pf	0.028 pf	2.4×10^{-3} pf
0	0	33.1 pf	9.6×10^{-6} pf	0.79×10^{-6} pf
- 4.0	--	14.8 pf	--	--
-10.0	--	10.0 pf	--	--

Table 2.1. Comparison of Capacities

The actual reverse current of the diode is several orders of magnitude larger than the values calculated above using P_n. This additional current is carried by holes and electrons which are generated thermally within the depletion region, and are then immediately swept out by the electric field.

Diffusion capacity changes by a factor of about 10 for every 60 mv change in junction potential.

2.4 Varactor Equivalent Circuit

Varactor operation can be described by the equivalent circuit in Fig. 2.3 (Refs. 5, 17, 34, 35, 36). The diode package is characterized by the package capacity C_p, and a series inductance L_s. The impedances of this equivalent circuit cannot be attributed to individual effects, but must be considered as a lumped equivalent circuit. The values in the equivalent circuit hold only at one frequency, and at other frequencies the parameters have to be re-evaluated.

The junction itself is usually formed on a base of n-type material. To achieve a reasonable reverse breakdown voltage, this material must have a high resistivity (Ref. 37). The resulting "bulk" resistivity is the major source of loss in varactor diodes. Usually, it is independent of both voltage and frequency. However, some high quality epitaxial varactors are formed on very thin base layers (Ref. 38). Changes in voltage, which change the width of the depletion layer, cause an appreciable percent change in base width for these diodes.

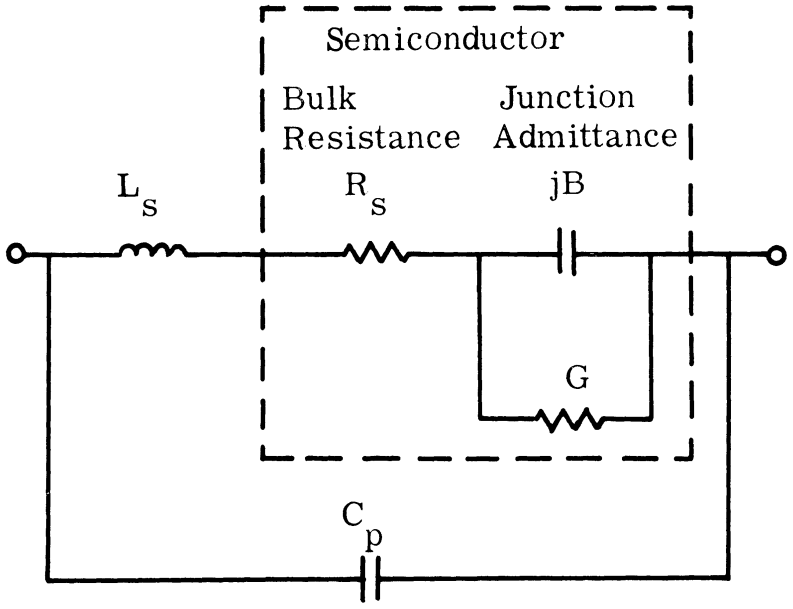

Fig. 2.3. Varactor Equivalent Circuit

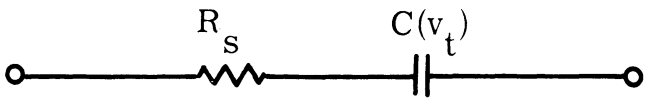

Fig. 2.4. Uhlir varactor model

The total admittance of the junction consists of the admittance of the barrier layer capacity in parallel with the admittance due to diffusion effects. The nature of these admittances are discussed in Sections 2.2 and 2.3. Measurements by Eng (Refs. 24, 39) indicate that for some devices skin effects on the semiconductor surface are important. To account for this he proposes that a linear network consisting of two resistors and one capacitor be placed across the junction.

The reactances of the package and of the skin effect are small and can often be neglected, but in any case, they are linear and can be lumped into the external circuit. If, in addition, R_s can be considered independent of voltage, the diode model reduces to the so-called Uhlir Model, Fig. 2.4 (Ref. 5). This model usually includes only the effects of barrier layer capacity, but may be easily extended to include diffusion effects as well. It will be used throughout the remainder of this paper.

2.5 Manley-Rowe Relations

The relationships which describe the real power flow through a nonlinear capacitor were first derived by Manley and Rowe (Refs. 8, 9):

$$\sum_{m=0}^{\infty} \sum_{n=-\infty}^{\infty} \frac{m P_{mn}}{m\omega_p + n\omega_1} = 0$$

$$\sum_{m=-\infty}^{\infty} \sum_{n=0}^{\infty} \frac{n P_{mn}}{m\omega_p + n\omega_1} = 0 \qquad (2.35)$$

where P_{mn} is the power entering the reactance at frequency $m\omega_p + n\omega_1$.

Usually power entering is taken as positive, while power leaving is taken as negative. These relationships are applicable to a lossless capacitance and give the inherent limitations governing power flow at a set of frequencies.

2.5.1 Single Sideband Up-converters. The circuit which allows power to flow at only three frequencies ω_1, ω_p, and $\omega_p + \omega_1$ is termed an upper sideband up-converter. Power is applied to the circuit at the signal and the pump, while the output is taken at their sum (upper sideband). The Manley-Rowe relationships (Eq. 2.35) in this case reduce to

$$\frac{P'_p}{\omega_p} + \frac{P_u}{\omega_u} = 0$$

$$\frac{P_1}{\omega_1} + \frac{P_u}{\omega_u} = 0 \qquad (2.36)$$

where $\omega_u = \omega_p + \omega_1$, i e., the upper sideband. P'_p is the power supplied by the pump, and P_1 is the power supplied by signal source. A little algebra reduces these to

$$P_u = -P_1 - P'_p$$

$$\frac{P_1}{\omega_1} = \frac{P'_p}{\omega_p} \qquad (2.37)$$

$$\frac{-P_u}{P_1} = \frac{\omega_u}{\omega_1}$$

The first of these equations (2.37) is simply conservation of energy; the power out at upper sideband is the sum of power in at signal and pump. The second shows that the two sources contribute to the converted power in the ratio of their frequencies. The third equation predicts that the conversion gain from ω_1 to ω_u is proportional to the frequency ratio.

The circuit which utilizes the lower sideband, i. e., $\omega_\ell = \omega_p - \omega_1$ in addition to the signal and pump is called a parametric amplifier. For these frequencies, Eq. 2.35 reduces to

$$\frac{P'_p}{\omega_1} + \frac{P_\ell}{\omega_\ell} = 0$$

$$\frac{P_1}{\omega_1} - \frac{P_\ell}{\omega_\ell} = 0 \qquad (2.38)$$

These equations reduce immediately to

$$P_1 = \frac{P_\ell}{\omega_\ell}\,\omega_1 \qquad (2.39)$$

Power is not supplied at P_ℓ (i.e., $P_\ell < 0$); and therefore, $P_1 < 0$. This means more power is leaving the circuit at ω_1 than is supplied. The resultant circuit effect is a negative resistance at ω_1 and at ω_ℓ. This is in contrast to the upper sideband up-converter in which the signal source supplies a net positive power to the circuit, which results in a positive resistance.

2.5.2 Multiple Sideband Up-converter. In the most general linear case, power is allowed to flow at the set of frequencies (1.2). The second of the Manley-Rowe relations (2.35) then reduces to

$$\frac{P_1}{\omega_1} - \frac{P_\ell}{\omega_\ell} + \frac{P_u}{\omega_u} - \frac{P_{2\ell}}{2\omega_p - \omega_1} + \frac{P_{2u}}{2\omega_1 + \omega_1} - \frac{P_{3\ell}}{3\omega_1 - \omega_1} + \frac{P_{3u}}{3\omega_p + \omega_1} + \ldots = 0 \qquad (2.40)$$

Here $P_{n\ell}$ and P_{nu} denote the power flow at the lower and upper sidebands of the nth pump harmonic (i.e., at $n\omega_p - \omega_1$ and $n\omega_p + \omega_1$). The power flow at the signal frequency is

$$P_1 = \omega_1 \left\{ \frac{P_\ell}{\omega_\ell} + \frac{P_{2\ell}}{2\omega_p - \omega_1} + \frac{P_{3\ell}}{3\omega_p - \omega_1} + \ldots - \frac{P_u}{\omega_u} - \frac{P_{2u}}{2\omega_p + \omega_1} - \frac{P_{3u}}{3\omega_p + \omega_1} - \ldots \right\} \qquad (2.41)$$

Now P_ℓ, $P_{2\ell}$, $P_{3\ell}$, ... P_u, P_{2u}, P_{3u}, ... < 0 because power is supplied to the circuit only at ω_1 and ω_p. Thus, power output at any of the upper sidebands (P_u, P_{2u}, P_{3u}, ...) causes power to flow into the circuit at ω_1; but power output at any of the lower sidebands (P_ℓ, $P_{2\ell}$, $P_{3\ell}$, ...) causes power to flow out of the circuit at ω_1. The resultant circuit effect is that the lower sidebands tend to cause negative resistance at ω_1, while the upper sidebands tend to cause positive resistance at ω_1. By virtue of the frequency ratios, the power at the upper and lower sidebands of the pump fundamental usually determine the sign of this resistance, but the sidebands of the pump harmonics can sometimes be significant.

CHAPTER III

HARMONIC BALANCE RELATIONS

3.1 Introduction

The objective of this chapter is to present the Harmonic Balance Relations (Ref. 40). These are a general formulation for parametric circuit analysis.

In Section 3.2, a set of linear equations relating diode voltage to currents is developed by expanding the diode depletion layer elastance in a Fourier series. In this set of equations, diode currents are the independent variables. The dual set of equations involving diode depletion layer capacitance, and an independent set of voltages is presented in Section 3.3. The relationships developed in these two sections form an essential step in the computation of the input impedance; and they will be used in both Chapters V and VI.

The two sets of equations are compared in Section 3.4. It is shown that the two sets of equations are intimately related to the two types of assumptions which have been made previously by workers in this field, and the relationship between these two types of assumptions are explored and clarified. This provides a convenient framework in which to examine the exact analysis presented in succeeding chapters.

3.2 Elastance Expansion

The small signal (differential) elastance of a varactor diode can be written as a function of the total charge stored in the junction, such that

$$S(q_t) = \frac{1}{C(q_t)} = \frac{dv_t}{dq_t} \tag{3.1}$$

where $S(q_t)$ represents the small-signal elastance and $C(q_t)$ the small-signal capacitance; v_t is the total potential across the junction and q_t is the charge.

This definition of elastance is consistent with the definition of varactor incremental elastance as used by Penfield and Rafuse (Ref. 17).

The potential across the junction can also be expressed as a function of charge. If the charge consists of a large component Q_p due to the "pump" source plus a "small signal" charge q_s, v_t can be written in the form of a Taylor series expansion

$$v_t(q_t) = v_t(Q_p + q_s) = V(Q_p) + \left.\frac{dv_t}{dq_t}\right|_{q_t = Q_p} q_s + \left.\frac{d^2 v_t}{dq_t^2}\right|_{q_t = Q_p} \frac{q_s^2}{2} + \cdots \tag{3.2}$$

where

$$q_t = Q_p + q_s$$

Now let

$$v_t = V(Q_p) + v_s$$

The first term is simply the voltage due to the pump in the absence of any signal. The remainder of the expansion is an expression for the signal voltage v_s.

$$v_s = \left.\frac{dv_t}{dq_t}\right|_{q_t=Q_p} q_s + \left.\frac{d^2v_t}{dq_t^2}\right|_{q_t=Q_p} \frac{q_s^2}{2} + \ldots \qquad (3.3)$$

When q_s is small [and $v(q_t)$ is sufficiently smooth], the first term of the expression is dominant, and the relationship between the signal voltage and signal charge may be approximated by the linear equation.

$$v_s \approx \left.\frac{dv_t}{dq_t}\right|_{q_t=Q_p} q_s \qquad (3.4)$$

whenever

$$q_s << Q_p.$$

This expression can be rewritten by using the definition of elastance in Eq. 3.1

$$v_s \approx S(Q_p)\, q_s \qquad (3.5)$$

If the charge due to the pump is periodic with frequency ω_p, a Fourier expansion may be written for the depletion layer elastance

$S(Q_p)$.

$$S(Q_p) = \sum_{n=-\infty}^{\infty} S_n \, e^{jn\omega_p t} \tag{3.6}$$

where

$S_n = S^*_{-n}$ because $S(Q_p)$ is a real quantity.

Now diode small-signal voltages and currents must be found. These must satisfy Eqs. 3.5 and 3.6 and be consistent with the constraints imposed by whatever linear network which is connected to the terminals of the diode. It is easy to show that if the external signal source is sinusoidal at frequency ω_1, these conditions are satisfied when the signal current consists of components at the positive frequencies in the set.

$$n\omega_p \pm \omega_1 \qquad\qquad n = 0, \; 1, \; \ldots \tag{3.7}$$

That is

$$i_s = \sum_{n=-\infty}^{\infty} I_{(n\omega_p+\omega_1)} \, e^{j(n\omega_p+\omega_1)t} + \sum_{n=-\infty}^{\infty} I_{(n\omega_p-\omega_1)} \, e^{j(n\omega_p-\omega_1)t} \tag{3.8}$$

The charge must be of the form

$$q_s = \int i_s \, dt = \sum_{n=-\infty}^{+\infty} \frac{I_{(n\omega_p+\omega_1)} \, e^{j(n\omega_p+\omega_1)t}}{j(n\omega_p+\omega_1)}$$

$$+ \sum_{n=-\infty}^{+\infty} \frac{I_{(n\omega_p-\omega_1)} \, e^{j(n\omega_p-\omega_1)t}}{j(n\omega_p-\omega_1)} \qquad (3.9)$$

Equations 3.5, 3.6 and 3.9 can be combined to obtain the signal voltage, v_s, across the diode.

$$v_s = \sum_{m,\, n=-\infty}^{+\infty}{}' \frac{S_m \, I_{(n\omega_p+\omega_p)} \, e^{j[(n+m)\omega_p+\omega_1]t}}{j(n\omega_p+\omega_1)}$$

$$+ \sum_{m,\, n=-\infty}^{+\infty}{}' \frac{S_m \, I_{(n\omega_p-\omega_1)} \, e^{j[(n+m)\omega_p-\omega_1]t}}{j(n\omega_p-\omega_1)} \qquad (3.10)$$

It is clear from Eq. 3.10 that v_s contains the same set of frequencies as i_s, that is, all the frequencies in the set (3.7). In particular there are no voltages (and thus no currents) at any frequencies in the set

$$\begin{matrix} n\omega_p \pm 2\omega_1 \\ \\ n\omega_p \pm 3\omega_1 \end{matrix} \qquad n = 0,\ 1,\ 2 \ldots \qquad (3.11)$$

The presence of these components would not be consistent

with the linear equation (3.4). However, if the signal amplitude becomes large, the higher order terms in Eq. 3.3 cannot be neglected and the additional components appear. From a practical point of view, their existence means that the signal is being processed nonlinearly. They can always be rendered insignificant simply by reducing the signal amplitude. No signal frequencies other than those in (3.7) can exist if linearity is to hold.

Equation 3.10 can be rearranged and written in the form

$$v_s = \sum_{m,\,n=-\infty}^{+\infty} \frac{S_{n-m}\, I_{(m\omega_p+\omega_1)}\, e^{j(n\omega_p+\omega_1)t}}{j(m\omega_p+\omega_1)}$$

$$+ \sum_{m,\,n=-\infty}^{+\infty} \frac{S_{n-m}\, I_{(m\omega_p-\omega_1)}\, e^{j(n\omega_p-\omega_1)t}}{j(m\omega_p-\omega_1)}$$

The individual terms in this equation can now be identified, and the signal voltage can be written as

$$v_s = \sum_{n=-\infty}^{+\infty} V_{(n\omega_p+\omega_1)}\, e^{j(n\omega_p+\omega_1)t} + \sum_{n=-\infty}^{+\infty} V_{(n\omega_p-\omega_1)}\, e^{j(n\omega_p-\omega_1)t} \qquad (3.12)$$

where the voltage coefficients can be identified as (Ref. 40)

$$V_{(n\omega_p+\omega_1)} = \sum_{m=-\infty}^{+\infty} \frac{S_{n-m}\, I_{(m\omega_p+\omega_1)}}{j(m\omega_p+\omega_1)}$$

$$V_{(n\omega_p-\omega_1)} = \sum_{m=-\infty}^{+\infty} \frac{S_{n-m}\, I_{(m\omega_p-\omega_1)}}{j(m\omega_p-\omega_1)} \qquad (3.13)$$

Because both v_s and i_s are real quantities

$$V_{(n\omega_p+\omega_1)} = V^*_{(-n\omega_p-\omega_1)}$$

and

$$I_{(n\omega_p+\omega_1)} = I^*_{(-n\omega_p-\omega_1)}$$

It is convenient here to introduce some special notation. Each signal frequency in the set (3.7) can be assigned a subscript according to the scheme of Table 3.1.

	Special Notation for Signal Frequency Components				
Frequency	ω_1	$\omega_p-\omega_1$	$\omega_p+\omega_1$	$2\omega_p-\omega_1$	$2\omega_p+\omega_1$ . . .
Special notation	ω_1	ω_2	ω_3	ω_4	ω_5 . . .

Table 3.1. Frequency Notation

Lower sidebands are assigned even subscripts, while upper sidebands are denoted by odd subscripts. The relationship between positive frequency components and those at negative frequency can now be written as

$$I_n = I^*_{-n}$$

$$V_n = V^*_{-n}$$

The coefficients of Eq. 3.13 can be expressed conveniently in terms of this special notation. The results for the first few coefficients are written out here:

$$V_1 = \frac{S_0 I_1}{j\omega_1} + \frac{S_1 I_{-2}}{-j\omega_2} + \frac{S_{-1} I_3}{j\omega_3} + \frac{S_2 I_{-4}}{-j\omega_4} + \frac{S_{-2} I_5}{j\omega_5} + \cdots$$

$$V_2 = \frac{S_1 I_{-1}}{-j\omega_1} + \frac{S_0 I_2}{j\omega_2} + \frac{S_2 I_{-3}}{-j\omega_3} + \frac{S_{-1} I_4}{j\omega_4} + \cdots$$

$$V_3 = \frac{S_1 I_1}{j\omega_1} + \frac{S_2 I_{-2}}{-j\omega_2} + \frac{S_0 I_3}{j\omega_3} + \frac{S_3 I_{-4}}{-j\omega_4} + \cdots$$

$$V_4 = \frac{S_2 I_{-1}}{-j\omega_1} + \cdots \qquad (3.14)$$

$$\vdots$$

The complete set of signal voltage components may be found in this manner. They may easily be expressed in matrix form. The signal voltage, v_s, can now be written as a column matrix, which is the product of a square impedance matrix [S] which represents pumped depletion layer impedance and a column matrix $[i_s$, which represents the signal currents.

To obtain a consistant set of signal currents, take the complex conjugate of all the even rows in Eq. 3.14. The resulting matrix is written in terms of V_n and I_n for n odd and V_{-n} and I_{-n} for n even. The first few terms of the matrix are written out in Eq. 3.15.

$$\begin{bmatrix} V_1 \\ V_{-2} \\ V_3 \\ V_{-4} \\ V_5 \\ V_{-6} \\ \\ \\ \\ \end{bmatrix} = \begin{bmatrix} -j\frac{S_0}{\omega_1} & j\frac{S_1}{\omega_2} & -j\frac{S_{-1}}{\omega_3} & j\frac{S_2}{\omega_4} & \cdots \\ -j\frac{S_{-1}}{\omega_1} & j\frac{S_0}{\omega_2} & -j\frac{S_{-2}}{\omega_3} & j\frac{S_1}{\omega_4} & \cdots \\ -j\frac{S_1}{\omega_1} & j\frac{S_2}{\omega_2} & -j\frac{S_0}{\omega_3} & j\frac{S_3}{\omega_4} & \cdots \\ -j\frac{S_{-2}}{\omega_1} & j\frac{S_{-1}}{\omega_2} & -j\frac{S_{-3}}{\omega_3} & j\frac{S_0}{\omega_4} & \cdots \\ -j\frac{S_2}{\omega_1} & j\frac{S_3}{\omega_2} & -j\frac{S_1}{\omega_3} & j\frac{S_4}{\omega_4} & \cdots \\ -j\frac{S_{-3}}{\omega_1} & \cdots & \cdots & \cdots & \cdots \\ \vdots & & & & \end{bmatrix} \times \begin{bmatrix} I_1 \\ I_{-2} \\ I_3 \\ I_{-4} \\ I_5 \\ \vdots \end{bmatrix} \qquad (3.15)$$

$$[v_s] = [S] \times [i_s$$

The elements of the impedance matrix are of the form

$$Z_{mn} = \frac{j\, S_{\ell(m,n)}}{(-1)^n\, \omega_n} \qquad (3.16)$$

where $\ell(m, n)$ is an integer and is given by

$$\ell(m,n) = (-1)^n \left(\frac{2n - 1 + (-1)^n}{4}\right) - (-1)^m \left(\frac{2m - 1 + (-1)^m}{4}\right)$$

3.3 Capacitance Expansion

The harmonic balance equations in Section 3.2 were derived by defining elastance as

$$S(q_t) = \frac{dv_t}{dq_t} \tag{3.17}$$

and by expressing the voltage across the diode junction as a function of the charge stored in the junction

$$v_t = v_t(q_t) \ . \tag{3.18}$$

The computations were carried up to a point where a signal voltage matrix was equated to the product of an impedance matrix and a current matrix (Eq. 3.15).

In this section, an alternate approach is presented. The charge stored in the junction is expressed as a function of the voltage across the junction.

$$q_t = q_t(v_t) \tag{3.19}$$

Capacity can be defined as

$$C(v_t) = \frac{dq_t(v_t)}{dv_t} \tag{3.20}$$

This definition of capacitance is consistent with the definition used by Rowe (Ref. 14), and Heffner's definition of "incremental capacity" (Ref. 41). Heffner (Ref. 41) contains a complete discussion on the definition of capacity.

For a periodic pump voltage, the depletion layer capacitance can be expressed in a Fourier series

$$C(V_p) = \sum_{n=-\infty}^{\infty} C_n \, e^{jn\omega pt} \tag{3.21}$$

The arguments from this point on are the dual of the arguments in Section 3.2, and the computations are carried on in exactly the same manner. The results can be expressed in matrix form. The signal currents are written as column matrix $i_s]$. This is the product of an admittance matrix, $[C]$, which represents depletion layer admittance, and a column matrix, $[v_s$, which represents the signal voltages.

The first few terms of the resulting expression are written out in Eq. 3.22 .

$$
\begin{bmatrix} I_1 \\ I_{-2} \\ I_3 \\ I_{-4} \\ I_5 \\ I_{-6} \\ \vdots \end{bmatrix} = \begin{bmatrix} j\omega_1 C_0 & j\omega_1 C_1 & j\omega_1 C_{-1} & j\omega_1 C_2 & \cdots \\ -j\omega_2 C_{-1} & -j\omega_2 C_0 & -j\omega_2 C_{-2} & -j\omega_2 C_1 & \cdots \\ j\omega_3 C_1 & j\omega_3 C_2 & j\omega_3 C_0 & j\omega_3 C_3 & \cdots \\ -j\omega_4 C_{-2} & -j\omega_4 C_{-1} & -j\omega_4 C_{-3} & -j\omega_4 C_0 & \cdots \\ j\omega_5 C_2 & j\omega_5 C_3 & j\omega_5 C_1 & j\omega_5 C_4 & \cdots \\ \vdots & \vdots & \vdots & \vdots & \ddots \end{bmatrix} \times \begin{bmatrix} V_1 \\ V_{-2} \\ V_3 \\ V_{-4} \\ V_5 \\ V_{-6} \\ \vdots \end{bmatrix}
$$

$$
[i_s] = [C] \times [v_s] \tag{3.22}
$$

The Y_{mn} term of the matrix has the value

$$
Y_{mn} = j(-1)^{m+1} C_{\ell(m,n)} \tag{3.23}
$$

where

$\ell(m, n)$ is an integer

and, as before, can be expressed as

$$
\ell(m,n) = (-1)^n \left[\frac{2n-1+(-1)^n}{4}\right] - (-1)^m \left[\frac{2m-1+(-1)^m}{4}\right]
$$

3.4 Short Circuit and Open Circuit Assumptions

Equations 3.15 and 3.22 are two representations of the most general case of small signal varactor mixing. They are, however, exceedingly large and unwieldy. Thus far, most workers have chosen not to deal directly with them, but rather to make simplifying

assumptions. All the assumptions have one common goal: reduction of the infinite matrices to finite matrices.

Many of the authors referred to in the literature review (Section 1.2) (Refs. 13, 42, 18, 19, 20, 21, 43, 4, 14) choose to deal with the set of admittance equations (Eq. 3.22). They reduce this matrix to a manageable size by making the so-called "short circuit" assumptions. The voltages are the independent quantities. The unwanted voltages are assumed to be shorted out by ideal filters. In addition, the diode is represented by a capacitance varying periodically.

This is usually a sinusoid, although a few authors (Refs. 19, 20) have accounted for a second harmonic component in addition to the fundamental.

On the other hand, some authors (Refs. 15, 16, 18, 17) deal with the impedance matrix (Eq. 3.15). To reduce the size of this matrix, they make a different set of assumptions, called the "open circuit" assumptions. Only a finite number of currents are permitted to flow through the diode junction. The currents are treated as the independent quantities and the voltages are the dependent quantities. Ideal filters prevent currents from flowing at the unwanted frequencies, i.e., open circuit them. In this case, the diode is represented as an elastance varying sinusoidally at the pump frequency.

It has been argued that the open-circuit assumptions correspond more closely to the physical situation than do the short-circuit assumptions, due to the presence of the diode lead inductance,

which has a reactance increasing with frequency. However it is possible for the circuit external to the diode to present a reactance which resonates in series with the diode lead inductance and thus provides a short-circuit termination.

In practice, the presence of the diode series resistance usually results in some power dissipation at all sideband frequencies, and neither assumption is strictly valid.

3.4.1 Two-Frequency Case. Most of the early parametric amplifier work was done by considering only two frequencies and using the "short circuit assumptions." In this case, signal voltages are present only at the input frequency, ω_1, and the lower sideband ω_2. The voltages at other frequencies are shorted out, and while currents may flow at the shorted frequencies, they are unimportant because there is no power flow. In this case (3.22) reduces to the two frequency short circuit equation.

$$\begin{bmatrix} I_1 \\ I_{-2} \end{bmatrix} = \begin{bmatrix} j\omega_1 C_0 & j\omega_1 C_1 \\ -j\omega_2 C_{-1} & -j\omega_2 C_0 \end{bmatrix} \times \begin{bmatrix} V_1 \\ V_{-2} \end{bmatrix} \qquad (3.24)$$

On the other hand, the "open circuit assumptions" can also be used. In the two-frequency case, signal currents exist only at frequencies ω_1 and ω_2; and voltages at other frequencies are of no interest. These assumptions reduce Eq. 3.15 to the two-frequency open circuit equation.

$$\begin{bmatrix} V_1 \\ V_{-2} \end{bmatrix} = \begin{bmatrix} -j\frac{S_0}{\omega_1} & j\frac{S_1}{\omega_2} \\ -j\frac{S_{-1}}{\omega_1} & j\frac{S_0}{\omega_2} \end{bmatrix} \times \begin{bmatrix} I_1 \\ I_{-2} \end{bmatrix} \qquad (3.25)$$

The relationship between the open and short circuit assumptions may easily be seen by inverting Eq. 3.24 to obtain voltage in terms of current (Ref. 18).

$$\begin{bmatrix} V_1 \\ V_{-2} \end{bmatrix} = \begin{bmatrix} \frac{-j\,C_0}{\omega_1(C_0^2 - C_1C_{-1})} & \frac{-j\,C_1}{\omega_2(C_0^2 - C_1C_{-1})} \\ \frac{j\,C_{-1}}{\omega_1(C_0^2 - C_1C_{-1})} & \frac{j\,C_0}{\omega_2(C_0^2 - C_1C_{-1})} \end{bmatrix} \times \begin{bmatrix} I_1 \\ I_{-2} \end{bmatrix} \qquad (3.26)$$

Equation 3.26 is identical with (3.24) if one defines

$$S_0 \triangleq \frac{C_0}{C_0^2 - |C_1|^2} \quad \text{and} \quad S_1 \triangleq \frac{C_1}{C_0^2 - |C_1|^2} .$$

The open circuit and short circuit assumptions also give identical results for the other two frequency cases in which power is permitted to flow only at the input signal frequency, ω_1, and at the upper sideband frequency, ω_3.

3.4.2 Three-Frequency Case. The relationship between the open circuit and short circuit assumptions for three or more

frequencies is somewhat more complex. For the short circuit assumption assuming only three non-zero voltages, three non-trivial currents, and sinusoidal capacitance, Eq. 3.22 reduces to

$$\begin{bmatrix} I_1 \\ I_{-2} \\ I_3 \end{bmatrix} = \begin{bmatrix} j\omega_1 C_0 & j\omega_1 C_1 & j\omega_1 C_{-1} \\ -j\omega_2 C_{-1} & -j\omega_2 C_0 & 0 \\ j\omega_3 C_1 & 0 & j\omega_3 C_0 \end{bmatrix} \times \begin{bmatrix} V_1 \\ V_{-2} \\ V_3 \end{bmatrix} \qquad (3.27)$$

From Eq. 3.15 the open circuit assumption for the three frequency case reduces to

$$\begin{bmatrix} V_1 \\ V_{-2} \\ V_3 \end{bmatrix} = \begin{bmatrix} -j\frac{S_0}{\omega_1} & j\frac{S_1}{\omega_2} & -j\frac{S_{-1}}{\omega_3} \\ -j\frac{S_{-1}}{\omega_1} & j\frac{S_0}{\omega_2} & 0 \\ -j\frac{S_1}{\omega_1} & 0 & -j\frac{S_0}{\omega_3} \end{bmatrix} \times \begin{bmatrix} I_1 \\ I_{-2} \\ I_3 \end{bmatrix} \qquad (3.28)$$

Equation 3.27 can be inverted to give voltages in terms of currents, but if this is done, the resulting equation is not the same as Eq. 3.28. In particular, the terms on the diagonal have different forms. In Eq. 3.28, these are just the impedances of ordinary frequency independent elastances. The elastances in the diagonal terms of the inverted Eq. 3.27 lack the property of frequency independence.

For the three-frequency case, the open and short circuit

assumptions yield different results.

3.4.3 n-Frequency Case. The open circuit and the short circuit assumptions also yield different results for the n frequency case ($n > 2$). It will be shown here that only in the limit as $n \to \infty$ can the two assumptions become compatible.

This will be demonstrated by inverting the n-frequency admittance matrix which is a square (n by n) matrix. It will be proved that only as this matrix becomes infinitely large does the inversion procedure result in an impedance matrix.

The mathematical techniques used in this section follow those of Desoer (Ref. 44). Desoer, however, was concerned with the errors produced by truncating an admittance matrix of the form (3.22). In this section the relationship between the admittance formulation of reactive mixing and the impedance formulation will be explored.

If the capacitance variation is sinusoidal, the general admittance matrix equation (3.22) reduces to the simpler $[Y'(n)]$ matrix (Eq. 3.29) in the n-frequency case.

$$
[\,Y'(n)\,] = \left[\begin{array}{ccc:ccccccc}
j\omega_1 C_0 & j\omega_1 C_1 & j\omega_1 C_{-1} & 0 & 0 & 0 & 0 & 0 & 0 & \cdots \\
-j\omega_2 C_{-1} & -j\omega_2 C_0 & 0 & -j\omega_2 C_1 & 0 & 0 & 0 & 0 & 0 & \cdots \\
j\omega_3 C_1 & 0 & j\omega_3 C_0 & 0 & j\omega_3 C_{-1} & 0 & 0 & 0 & 0 & \cdots \\
\hdashline
0 & -j\omega_4 C_{-1} & 0 & -j\omega_4 C_0 & 0 & -j\omega_4 C_1 & 0 & 0 & 0 & \cdots \\
0 & 0 & j\omega_5 C_1 & 0 & j\omega_5 C_0 & 0 & j\omega_5 C_{-1} & 0 & 0 & \cdots \\
0 & 0 & 0 & -j\omega_6 C_{-1} & 0 & -j\omega_6 C_0 & 0 & -j\omega_6 C_1 & 0 & \cdots \\
0 & 0 & 0 & 0 & j\omega_7 C_1 & 0 & j\omega_7 C_0 & 0 & j\omega_7 C_{-1} & \cdots \\
0 & 0 & 0 & 0 & 0 & -j\omega_8 C_{-1} & 0 & -j\omega_8 C_0 & 0 & \cdots \\
0 & 0 & 0 & 0 & 0 & 0 & j\omega_9 C_1 & 0 & j\omega_9 C_0 & \cdots \\
\cdot & \cdot & \cdot & \cdot & \cdot & \cdot & \cdot & \cdot & \cdot & \cdot \\
\cdot & \cdot & \cdot & \cdot & \cdot & \cdot & \cdot & \cdot & \cdot & \cdot \\
\cdot & \cdot & \cdot & \cdot & \cdot & \cdot & \cdot & \cdot & \cdot & \cdot
\end{array}\right] \qquad (3.29)
$$

The $[Y'(n)]$ matrix of Eq. 3.29 is shown partitioned into submatrices as follows:

α_{11} - 3 x 3 matrix

$\alpha_{12}(n)$ - (n-3) x 3 matrix

$\alpha_{21}(n)$ - 3 x (n-3) matrix

$\alpha_{22}(n)$ - (n-3) x (n-3) matrix

$$[Y'(n)] = \left[\begin{array}{c|c} \alpha_{11} & \alpha_{12}(n) \\ \hline \alpha_{21}(n) & \alpha_{22}(n) \end{array}\right] \tag{3.30}$$

Because $\alpha_{12}(n)$ and $\alpha_{21}(n)$ each have only two non-zero terms, the computation of the nine elements in the upper right hand corner of the $[Y'(n)]$ matrix is relatively simple. After some manipulation the resulting inverse matrix can be written as

$$[Y'(n)]^{-1} = \left[\begin{array}{c|c} \theta_1(n)^{-1} & \begin{matrix} . & . \\ . & . \end{matrix} \\ \hline \begin{matrix} . & . \\ . & . \end{matrix} & \begin{matrix} . & . \\ . & . \end{matrix} \end{array}\right] \tag{3.31}$$

where:

$$\theta_1(n) = \begin{bmatrix} j\omega_1 C_1 & j\omega_1 C_1 & j\omega_1 C_{-1} \\ -j\omega_2 C_{-1} & -j\omega_2 C_0 + \beta_{11}(n)\,\omega_2\omega_4 C_1 C_{-1} & -\beta_{12}(n)\,\omega_2\omega_5 C_1 C_1 \\ j\omega_3 C_1 & -\beta_{21}(n)\,\omega_3\omega_4 C_{-1} C_{-1} & j\omega_3 C_0 + \beta_{22}(n)\,\omega_3\omega_5 C_1 C_{-1} \end{bmatrix} \tag{3.32}$$

$\beta_{11}(n)$, $\beta_{12}(n)$, $\beta_{21}(n)$, and $\beta_{22}(n)$ are the upper four elements in the α_{22}-1 matrix. They are evaluated in Appendix A, and only the results are set down here:

$$\beta_{11}(n) = \frac{1}{-j\omega_4 C_0 \left\{ 1 - \dfrac{\gamma^2}{1-\gamma^2 \;\; \dfrac{}{1-\gamma^2} \;\; \ddots} \right\}} \tag{3.33}$$

$$\beta_{22}(n) = \frac{1}{j\omega_5 C_0 \left\{ 1 - \dfrac{\gamma^2}{1-\gamma^2 \;\; \dfrac{}{1-\gamma^2} \;\; \ddots} \right\}} \tag{3.34}$$

$$\beta_{12}(n) = \beta_{21}(n) = 0$$

where the pumping "hardness" coefficient is defined by

$$\gamma^2 = \frac{C_1 C_{-1}}{C_0^{\,2}}$$

and

$$\beta_{11}(4) = \beta_{11}(5) = \frac{1}{-j\,\omega_4\,C_0}$$

$$\beta_{22}(4) = \beta_{22}(5) = \frac{1}{j\,\omega_5\,C_0}$$

in expressions (3.33) and (3.34), the quantity γ^2 appears $\left(\frac{n}{2} - 2\right)$ times for n even and $\left(\frac{n}{2} - \frac{5}{2}\right)$ times for n odd.

It is also shown in Appendix A that in the infinite frequency case, the expansion can be written in the simple form:

$$\beta_{11}(\infty) = \frac{1}{-j\,\omega_4\,C_0\left(\frac{1}{2} + \sqrt{\frac{1}{4} - \gamma^2}\right)} \tag{3.35}$$

$$\beta_{22}(\infty) = \frac{1}{j\,\omega_5\,C_0\left(\frac{1}{2} + \sqrt{\frac{1}{4} - \gamma^2}\right)} \tag{3.36}$$

$$\beta_{12}(\infty) = \beta_{21}(\infty) = 0 \tag{3.37}$$

Now Eq. 3.32 can be inverted, and the resulting matrix examined to see which values of $\beta_{11}(n)$ and $\beta_{22}(n)$ yield the proper impedance elements. From Eqs. 3.15 and 3.16 all the impedance matrix elements must be of the form $Z_{mn} = \frac{j\,S_{\ell(m,n)}}{(-1)^n\,\omega^n}$ where $S_{\ell(m,n)}$ is independent of frequency.

The $Z_{11}(n)$ term of $\theta^{-1}(n)$ can be computed by inspection.

$$Z_{11}(n) = \frac{\omega_2 \omega_3}{|\theta_{(n)}|} \left[C_0^2 + j\beta_{11}(n)\omega_4 C_0 C_1 C_{-1} - j\beta_{22}(n)\omega_5 C_0 C_1 C_{-1} + \beta_{11}(n)\beta_{22}(n)\omega_4\omega_5 C_1^2 C_{-1}^2 \right] \quad (3.38)$$

where $|\theta_{(n)}|$ denotes the value of the determinate of the $\theta(n)$ matrix.

But from the impedance matrix (Eq. 3.15)

$$Z_{11}(n) = \frac{S_0(n)}{j\omega_1} \quad (3.39)$$

Combining Eqs. 3.38 and 3.39

$$S_0(n) = \frac{j\omega_1\omega_2\omega_3}{|\theta_{(n)}|} \left[C_0^2 + j\beta_{11}(n)\omega_4 C_0 C_1 C_{-1} - j\beta_{22}(n)\omega_5 C_0 C_1 C_{-1} + \beta_{11}(n)\beta_{22}(n)\omega_4\omega_5 C_1^2 C_{-1}^2 \right] \quad (3.40)$$

The same procedure can be done for $Z_{22}(n)$ and $Z_{33}(n)$. The results are

from $Z_{22}(n)$

$$S_0(n) = \frac{j\omega_1\omega_2\omega_3}{|\theta_n|} \left[C_0^2 - j\beta_{22}(n)\omega_5 C_0 C_{-1} C_1 - C_1 C_{-1} \right] \quad (3.41)$$

from Z_{33}

$$S_0(n) = \frac{j\omega_1\omega_2\omega_3}{|\theta_n|} \left[C_0^2 + j\beta_{11}(n)\omega_4 C_0 C_1 C_{-1} - C_1 C_{-1} \right] \quad (3.42)$$

Now the elastances in Eqs. 3.40, 3.41 and 3.42 are all equal. Combining (3.40), (3.41), (3.42)

$$\beta_{11}(n)\,\omega_4 = -\beta_{22}(n)\,\omega_5 \tag{3.43}$$

$$\beta_{22}(n) = \frac{1}{j\,\omega_5\,C_0\left(\frac{1}{2}+\sqrt{\frac{1}{4}-\gamma^2}\right)} \tag{3.44}$$

Equations 3.43 and 3.44 are identical to Eqs. 3.35 and 3.36. This means that the infinite short circuit matrix is the only matrix which can yield the correct form of the open circuit matrix.

Now that the infinite matrix case is known to be the correct one, all the terms may be found. The first few are written out in Eq. 3.45. Equation 3.45 is the inverse of Eq. 3.29 only for the infinite frequency case.

$$\begin{bmatrix} -j\frac{S_0}{\omega_1} & +j\frac{S_1}{\omega_2} & -j\frac{S_{-1}}{\omega_3} & \cdots \\ -j\frac{S_{-1}}{\omega_1} & +j\frac{S_0}{\omega_2} & -j\frac{S_{-2}}{\omega_3} & \cdots \\ -j\frac{S_1}{\omega_1} & +j\frac{S_2}{\omega_2} & -j\frac{S_0}{\omega_3} & \cdots \\ \vdots & \vdots & \vdots & \ddots \\ \vdots & \vdots & \vdots & \ddots \end{bmatrix} \tag{3.45}$$

where

$$S_0 = \frac{1}{C_0 \sqrt{1 - 4\gamma^2}}$$

$$S_0 = \frac{1}{C_0} (1 + 2\gamma^2 + 6\gamma^4 + 20\gamma^6 + 70\gamma^8 + 252\gamma^{10} + \ldots)$$

$$S_1 = - \frac{C_1 (1 - \sqrt{1 - 4\gamma^2})}{2C_0^2 \gamma^2 \sqrt{1 - 4\gamma^2}} \qquad (3.46)$$

$$S_1 = - \frac{C_1}{C_0^2} (1 + 3\gamma^2 + 10\gamma^4 + 35\gamma^6 + 126\gamma^8 + \ldots)$$

$$S_2 = \frac{4C_1^2}{C_0^3 \sqrt{1 - 4\gamma^2} (1 + \sqrt{1 - 4\gamma^2})^2}$$

$$S_2 = \frac{C_1^2}{C_0^3} (1 + 4\gamma^2 + 15\gamma^4 + 56\gamma^6 + 210\gamma^8 + \ldots)$$

$$\gamma^2 = \frac{C_1 C_{-1}}{C_0^2}$$

The following procedure provides further insight into the relationship between the open circuit and the short circuit equations:

The capacitance considered in the short circuit matrix (Eq. 3.29) has the form

$$C = C_0 + C_1 e^{j\omega t} + C_{-1} e^{-j\omega t} \tag{3.47}$$

The corresponding elastance is

$$S \triangleq \frac{1}{C} = \frac{1}{C_0}\left(1 + \frac{C_1}{C_0} e^{j\omega t} + \frac{C_{-1}}{C_0} e^{-j\omega t}\right)^{-1} \tag{3.48}$$

This may be expanded and the coefficients of like exponentials collected. After some labor, the results can be expressed as an infinite Fourier series.

$$S = S_0 + S_1 e^{j\omega t} + S_2 e^{j2\omega t} + \ldots\ldots + S_{-1} e^{-j\omega t} + S_{-2} e^{-j2\omega t} + \ldots\ldots \tag{3.49}$$

where

$$S_0 = \frac{1}{C_0}(1 + 2\gamma^2 + 6\gamma^4 + 20\gamma^6 + 70\gamma^8 + \ldots) \tag{3.50}$$

$$S_1 = -\frac{C_1}{C_0^2}(1 + 3\gamma^2 + 10\gamma^4 + 35\gamma^6 + \ldots)$$

$$S_2 = \frac{C_1^2}{C_0^3}(1 + 4\gamma^2 + 15\gamma^4 + 56\gamma^6 + \ldots)$$

The elastance coefficients in Eqs. 3.50 are identical with the elastance coefficients in the infinite short circuit matrix (Eqs. 3.45 and 3.46).

A comparison of Eq. 3.48 with Eq. 3.49 shows that an infinite Fourier series in elastance is required to correctly represent a sinusoidal capacitance variation. It is now easily seen why only the

infinite elastance (open circuit) matrix is equivalent to a capacitance (short circuit) matrix.

3.5 Summary

In this chapter, the harmonic balance equations were developed. The results can be expressed either as an infinite set of impedance equations (3.15), or as an infinite set of admittance equations (3.22). These two sets of equations are the key to the entire paper, and the majority of the material in subsequent chapters is devoted to solving them. In the next two chapters, the elastance coefficients which are the individual elements of the matrix are computed. These elastance coefficients are then substituted in the matrix which is then inverted to obtain the input impedance.

The open and short circuit approximations were discussed at some length. They clearly illustrate the assumptions made by other workers, and thus provide a background for this more exact study.

CHAPTER IV

STABILITY

4.1 Introduction

The harmonic balance equations in the preceding chapter form the basis for the analysis of pumped diode input impedance. In deriving these equations, it is assumed that the pump voltage and charge are periodic and can be expressed in a Fourier series with the fundamental at frequency ω_p. The purpose of this chapter is to examine the validity of this assumption. Particular emphasis is placed upon those effects which result from nonlinear causes, and which affect the stability of the circuit.

Although the linear voltage-current relations of the signal are the primary concern in this paper, it is important to study nonlinear instability effects for two reasons:

(1) They affect the pump voltage-current relations. This in turn affects both the magnitude and phase of the Fourier coefficients of elastance, and thus the signal.

(2) Under certain conditions, they cause the pump to become unstable. Thus, some pump voltage-frequency combinations are inaccessible.

The next section is devoted to a discussion of the "Ferroresonant effect." It is a particularly serious form of instability, since

it occurs frequently in a high Q tuned circuit driven near resonance. Almost all pumped varactor circuits use a tuning technique of this type to obtain a large pump voltage across the varactor with minimum pump power expenditure. In Section 4.3, instabilities of a high Q tuned circuit are examined with the aid of Mathier's equation.

4.2 The Ferroresonant Effect

In this section, the "Ferroresonant" effect (Refs. 20, 21, 45, 46, 47) is examined using an approximate method which yields quantitive agreement with theory. The diode capacity is treated as a linear capacitor whose magnitude is dependent upon pump voltage magnitude. This allows the use of familiar impedance concepts to explain an inherently nonlinear phenomenon.

In Appendix B, it is shown that the pump voltage across a reverse-biased junction diode may be expressed as:

$$V_M = \left[1 + Q_M\right]^{\frac{M}{M-1}} - 1 \qquad \text{(B.6)}$$

where Q_M is the normalized charge due to the pump, and the small signal capacity at the bias point is normalized to one farad. The exponent, M, not necessarily an integer, usually takes values ranging from 5 down to 2, depending upon the impurity distribution in the diode. $M = 2$ for an ideal abrupt (alloy) junction, and $M = 3$ for an ideal linear (diffused) junction device.

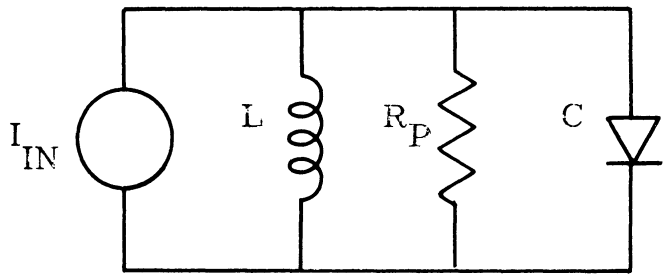

Fig. 4.1. Parallel RLC network excited by a current source

Consider now a circuit of the type shown in Fig. 4.1. The diode capacity is tuned by the inductor, and the circuit is sinusoidally excited at a frequency near ω_0, the small signal resonant frequency of the circuit. In this case, $\omega_0 = (L)^{-\frac{1}{2}}$ because the small signal capacity has been normalized to one.

If losses are small, the voltage is approximately sinusoidal.

$$V_M \approx a \cos \omega t \tag{4.1}$$

$$0 \leq |a| < 1$$

From Eq. B.6 the charge can now be written as

$$Q_M = (1 + a \cos \omega t)^{1 - \frac{1}{M}} - 1 \tag{4.2}$$

Equation 4.3 has the same form (except for a constant) as Eq. B.9 where

$$N = \frac{M}{1 - M} \tag{4.3}$$

Thus, it may be expanded using the techniques developed in Appendix B, and the charge flowing at the fundamental frequency can be written in the form of Eq. B.13.

$$Q_{(\omega)} = (a + .095\, a^3 + .034\, a^5 + .025\, a^7 + \cdots) \cos \omega t \tag{4.4}$$

By Eq. 4.1 this can be written as

$$Q_{(\omega)} = (1 + .095\, a^2 + .034\, a^4 + .025\, a^6 + \cdots)\, V_M \qquad (4.5)$$

which can be put in the common form

$$Q_{(\omega)} = C(a)\, V_M \qquad (4.6)$$

where

$$C(a) = (1 + .095\, a^2 + .034\, a^4 + .025\, a^6 + \cdots)$$

Kirchhoff's current law applied to the current at frequency ω which flows in the circuit of Fig. 4.1 yields the following equation,

$$\frac{d\, Q_{(\omega)}(t)}{dt} + \frac{\int V_M\, dt}{L} + \frac{V_M(t)}{R_p} - I_{IN}(t) = 0 \qquad (4.7)$$

where $I_{IN} = I \cos(\omega t + \Upsilon)$.

All terms in this expression are sinusoidal at frequency ω. Combine Eqs. 4.1, 4.6, and 4.7 and perform the indicated operations. The resulting relation may be expressed in exponential form:

$$e^{+j\omega t}\left[\frac{ja\omega\, C(a)}{2} - \frac{ja}{2\omega L} + \frac{a}{2R_p} - \frac{I\, e^{j\Upsilon}}{2}\right] +$$

$$e^{-j\omega t}\left[\frac{-ja\omega\, C(a)}{2} + \frac{ja}{2\omega L} + \frac{a}{2R_p} - \frac{I\, e^{-j\Upsilon}}{2}\right] = 0$$

The coefficients of $e^{+j\omega t}$ and $e^{-j\omega t}$ must both equal zero. Setting the coefficient of $e^{+j\omega t}$ to zero results in the familiar expression:

$$V = \frac{j\omega LI}{\frac{j}{Q} + [1 - \omega^2 LC(a)]} \tag{4.8}$$

where

$$Q \approx \frac{R_p}{\omega_0 L} \quad \text{and} \quad V = a\, e^{-j\Upsilon}$$

For convenience, the analysis is conducted with

$$|V|^2 = \frac{\omega^2 L^2 I^2}{\frac{1}{Q^2} + [1 - \omega^2 LC(a)]^2} \tag{4.9}$$

From Eq. 4.5, the capacitance C(a) may be represented by the approximate form

$$C(a) \approx (1 + \alpha |V|^2) \triangleq C(V) \tag{4.10}$$

where α is small, and

$$|V|^2 < 1$$

Substituting this value in Eq. 4.9 and differentiating with respect to frequency, there follows

$$\frac{d|V|^2}{d\omega} = \frac{2\omega L^2 I_{IN}^2 + 4V^2 \omega\, LC(V)[1 - \omega^2 LC(V)] - \frac{2V^2}{\omega Q^2}}{\frac{1}{Q^2} + [1 - \omega^2 LC(V)]^2 - 2\omega^2 L\, \delta C[1 - \omega^2 LC(V)]} \tag{4.11}$$

where the change in capacity is

$$\delta C = \alpha |V|^2$$

From inspection of the denominator of this expression, it is apparent that under certain circumstances, the slope of the response curve of V^2 as a function of ω will become infinite. A jump in output will occur as the frequency of the exciting current passes through the appropriate value.

The circumstances under which this effect occurs are found by setting the denominator equal to zero and solving for the frequency. After some algebra, it is found that the required expression is

$$\omega = \omega_0 \left\{ \frac{1 + 2\delta C \pm \delta C \left\{ 1 - \frac{\left[1 + \frac{1}{\delta C}\right]\left[3 + \frac{1}{\delta C}\right]}{Q^2} \right\}^{\frac{1}{2}}}{1 + 3\delta C} \right\}^{\frac{1}{2}} \qquad (4.12)$$

It follows that the jump frequencies are always less than the resonant frequency, and that these frequencies are real only if

$$1 \geq \frac{\left[1 + \left(\frac{1}{\delta C}\right)\right]\left[3 + \left(\frac{1}{\delta C}\right)\right]}{Q^2} \qquad (4.13)$$

It is also apparent that the jump frequencies are a function of the magnitude of the applied signal voltage.

Condition (4.13) may be rewritten as

$$\delta C \geq \frac{(Q^2 + 1)^{\frac{1}{2}} + 2}{Q^2 - 3} \tag{4.14}$$

Output jumps occur at two frequencies when this inequality is satisfied, and at one frequency when equality occurs. Figure 4.2 is a graphical plot of the relation:

$$\delta C = \frac{(Q^2 + 1)^{\frac{1}{2}} + 2}{Q^2 - 3} \tag{4.15}$$

This curve divides the area into two regions, with no output jumps in the region below the curve and jumps at two frequencies in the region above it. It indicates that the ferroresonant effect may be avoided in a varactor diode circuit by reducing either the circuit Q or the applied signal level.

Experimental measurements qualitatively confirmed the theoretical results. Figure 4.3 shows three voltage-frequency curves for a diode-loaded tuned circuit. When the level is small, δC is below the threshold value for jumps, and a conventional response occurs, as shown in Fig. 4.3(a). As the level is increased by 10 db, the passband of the response becomes asymmetrical, as shown in Fig. 4.3(b). Increase in the level by a further 10 db gives an output jump at one frequency, demonstrated in Fig. 4.3(c).

The voltage amplitude at which the jump in output occurs may also be found by setting the denominator of expression 4.11 equal

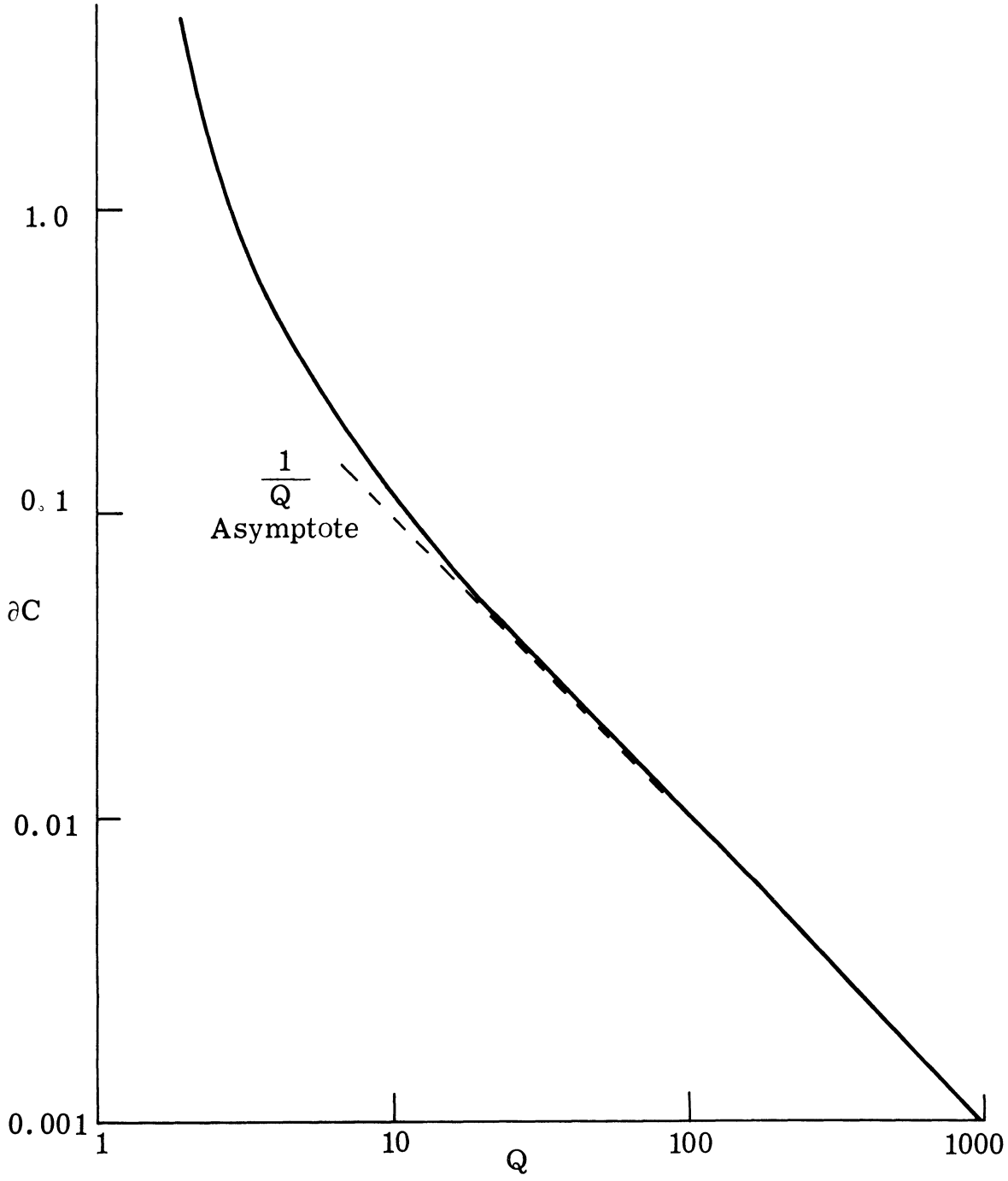

Fig. 4.2. Fractional increase in average capacity necessary to produce the ferroresonant effect

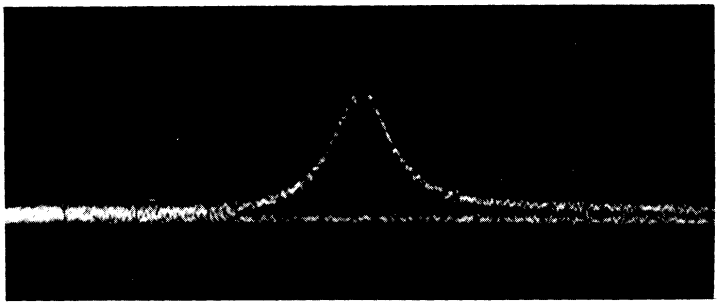

(a)

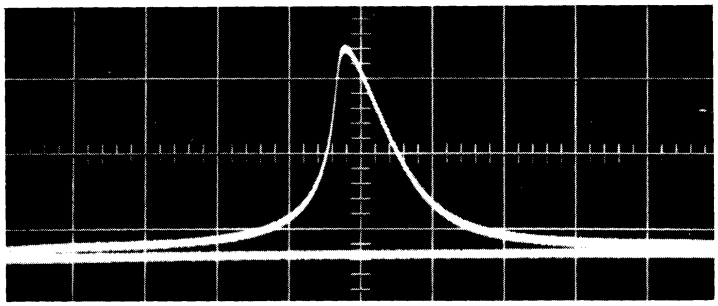

(b)

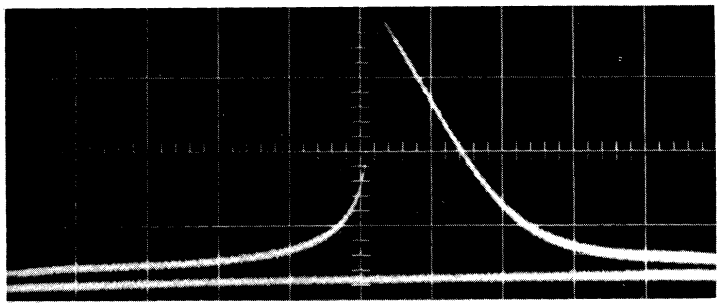

(c)

Fig. 4.3. Frequency response curves for parallel resonant circuit containing a varactor diode

to zero. Using the substitution

$$\omega = \omega_0 + \delta_\omega \quad \text{where } \delta_\omega << \omega_0 \text{ to simplify the algebra,}$$

the expression reduces to

$$\alpha V^2 = \frac{-4\frac{\delta_\omega}{\omega_0} \pm \sqrt{4\frac{\delta_\omega^2}{\omega_0^2} - \frac{3}{Q^2}}}{3\left(1 + \frac{2\delta_\omega}{\omega_0}\right)} \tag{4.16}$$

This expression is plotted for various values of Q in Fig. 4.4. Each value of Q defines a parabolic area, on the voltage-frequency plane, within which the circuit is unstable. The circuit is stable in the region between the parabola corresponding to a given Q and the coordinate axes.

The experimental result of Fig. 4.5 illustrates this effect clearly. The photograph in this figure shows the frequency response of a diode tuned circuit. The vertical axis is response voltage, and the horizontal axis is frequency, with the small signal resonant frequency ω_0 occurring at the right-hand edge of the photograph. The input frequency was swept continuously as the amplitude was slowly reduced. The light areas indicate conditions under which the circuit is stable, while the dark areas indicate circuit instability since the oscilloscope trace did not remain in the unstable regions long enough to record an image.

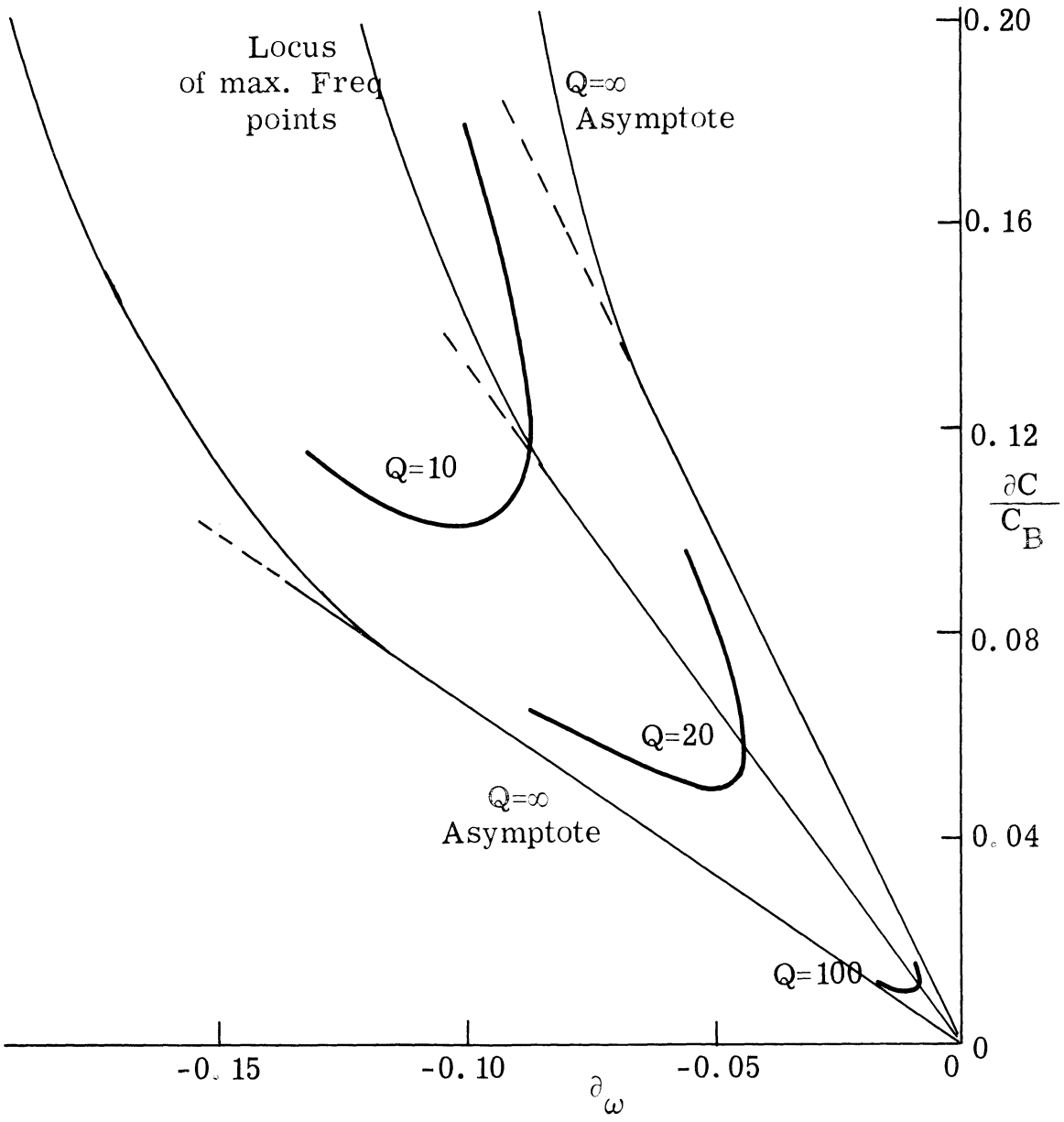

Fig. 4.4. Theoretical results showing region of ferroresonant instability

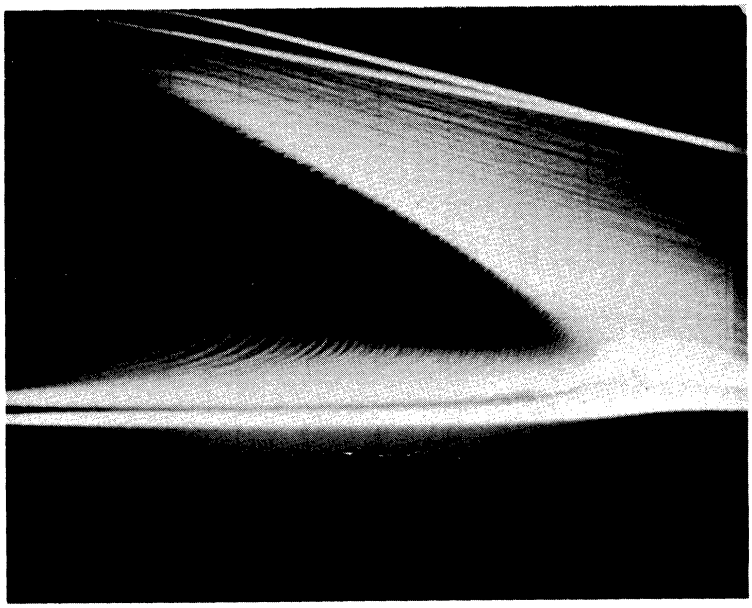

Fig. 4.5. Experimental results showing region of ferroresonant instability

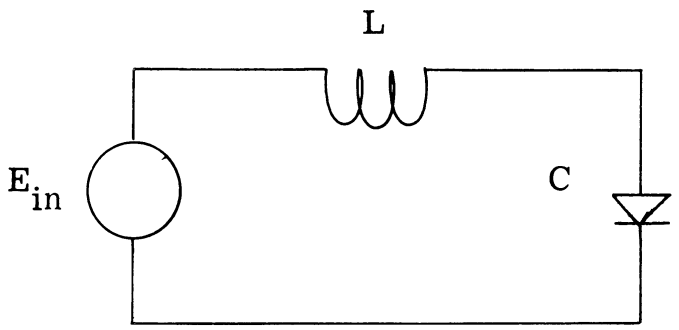

Fig. 4.6. Series resonant circuit containing a varactor diode

4.3 Other Instabilities

Consider a series LC circuit excited by a constant sinusoidal voltage source $E_{in} \cos \omega t$ (Fig. 4.6). The normalized differential equation of the circuit is

$$E_{in} \cos \omega t = L \frac{d^2 Q_N}{dt^2} + V_N + R_s \dot{Q}_N \tag{4.17}$$

where Q_N is the charge stored in the capacitor, i.e., the integral of the current, and V_N is the voltage across the capacitor. For an abrupt (alloy) junction varactor diode, the relationship between AC voltage and charge was found in Section 2.2 and can be written as

$$V_N = Q_N(t) + \frac{Q_N(t)^2}{4} \tag{2.12}$$

Substituting this relationship, the differential equation for Q becomes

$$\frac{d^2 Q_N}{dt^2} = \frac{1}{L} \left[E_{in} \cos \omega t - Q_N - \frac{Q_N^2}{4} \right] \tag{4.18}$$

This equation can be checked for stability by perturbing q_t slightly, i.e., letting Q_N change to $Q_N + \epsilon_t$, where $\epsilon_t << Q_N$. Substituting this into Eq. 4.16 the following differential equation for ϵ is obtained.

$$\frac{d^2 \epsilon_t}{dt^2} + R_s \frac{d\epsilon_t}{dt} + \epsilon_t \left(\frac{1}{L} + \frac{Q_N}{2L} \right) = 0 \tag{4.19}$$

If the solution for ϵ_t is stable, the circuit is stable. However, if ϵ_t is unstable (i.e., ϵ_t becomes large without limit) the circuit is unstable, since it indicates that a very small perturbation in the circuit causes the charge and the current circulating in the circuit to increase without limit.

If E_{in} is small (i.e., $E_{in} << 1$) then Q_N can be approximated by a sinusoidal function

$$Q_N \approx q_0 \cos \omega t \qquad \text{where} \quad q_0 << 1 \tag{4.20}$$

The differential equation for ϵ_t then becomes

$$\frac{d^2 \epsilon_t}{dt^2} + R_s \frac{d\epsilon_t}{dt} + \frac{\epsilon_t}{L} \left(1 + \frac{q_0 \cos \omega t}{2}\right) = 0 \tag{4.21}$$

This differential equation is a form of Mathieu's equation. It can be put in canonical form by making the following substitution for the independent variable, and thereby removing the first derivative term (Refs. 48, 49)

$$\epsilon_t(t) = f(t)\, e^{-\frac{R_s}{2} t}$$

and then making the following substitutions:

$$\nu = \frac{\omega t}{2}$$

$$\zeta = \frac{4}{\omega^2 L} - \frac{R_s^2}{\omega^2}$$

$$\psi = \frac{-q_0}{\omega^2 L}$$

Then

$$\frac{d^2 f}{d\nu^2} + (\zeta - 2\psi \cos 2\nu) f = 0 \qquad (4.22)$$

This equation has been extensively studied and the results tabulated. For a study of stability it is sufficient to note from the tabulated information that for $\psi << 1$ (i.e., $q_0 << 1$) the solutions are unstable only for very small regions near: $\sqrt{\zeta} = 0, 1, 2, 3, \ldots n \ldots$

Since $\omega = \frac{2\omega_0}{\sqrt{\zeta}}$, the circuit can therefore be expected to be unstable when

$$\omega = \infty, 2\omega_0, \omega_0, \frac{2}{3}\omega_0, \frac{1}{2}\omega_0, \frac{2}{5}\omega_0, \ldots \qquad (4.23)$$

The instability at ω_0 has already been discussed; it is the ferroresonant effect. Physically, the instabilities at the other frequencies are related to harmonic and subharmonic oscillations. Many of these oscillations have been observed experimentally.

The insights resulting from the simple analysis presented here are sufficient to understand both the numerical results of the theory and the phenomenon observed during the experiments.

CHAPTER V

DEPLETION LAYER CAPACITY

5.1 Introduction

In Chapter III, a linear relationship (Eq. 3.15) which relates signal currents to signal voltage was developed. The parameters in this expression are the Fourier coefficients of varactor elastance which for signals of small amplitude are completely independent of signal. Two iterative techniques for computing the coefficients of elastance are developed in Sections 5.1 through 5.4 of this chapter. These procedures are applicable to situations where the diode is reversed biased in such a way that conduction and diffusion effects can be neglected, so that the diode can be characterized by its depletion layer capacity. Once these elastance coefficients are known, the input impedance at the signal frequency is computed using conventional matrix techniques which are outlined in Section 5.5.

The computation of the time varying elastance is the subject of the next three sections. Since the Fourier coefficients of this elastance are independent of both signal amplitude and frequency, they can be computed with any signal which is convenient. In this paper, the elastance is computed using a signal of zero amplitude; that is, all signal voltage sources are replaced with short circuits, and all signal current sources are replaced by open circuits. Of course, the pump

source remains in the circuit. The resultant simplified circuit is termed the pump circuit, and its use permits considerable simplification, for now only the effect of one source need be considered when computing the elastance.

In determining the behavior of the pump circuit, only the "steady state" solution is considered. The circuit is presumed to be stable and to generate neither free nor subharmonic oscillations. This, of course, is at odds with the results of Chapter IV, where it was shown that instabilities are to be expected in this type of nonlinear circuit. The "steady state" solutions then, must be carefully examined to determine whether they are solutions of the physical problem.

Under the "steady state" conditions, all currents and voltages in the circuit as well as the diode elastance can be expressed as a Fourier series with the fundamental at the pump frequency ω_p. However in much of the work which follows it is more convenient to deal with the charge stored in the diode junction. It is also periodic in ω_p and can be expressed as

$$Q_p(t) = \frac{Q_A(0)}{2} + \sum_{n=1}^{\infty} Q_A(n) \cos n\omega_p t + \sum_{n=1}^{\infty} Q_B(n) \sin n\omega_p t \qquad (5.1)$$

or the equivalent exponential form

$$Q_p(t) = \sum_{n=-\infty}^{\infty} \left[\frac{Q_A(n)}{2} - j \frac{n}{|n|} \frac{Q_B(n)}{2} \right] e^{jn\omega_p t} \qquad (5.2)$$

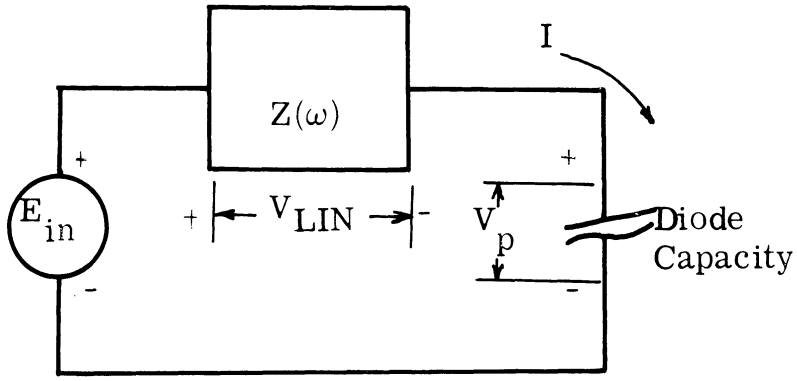

Fig. 5. 1. Thevenin equivalent pump circuit

In much of this work it is expedient to express voltages and charges in terms of frequency, rather than time by using the conventional Laplace Transform. Using this notation, Q_p can be written as

$$Q_p(s) = L\{Q_p(t)\} = \frac{1}{2} \sum_{n=-\infty}^{\infty} \left[\frac{Q_A(n) - j \frac{n}{|n|} Q_B(n)}{s - jn\omega_p} \right] \qquad (5.3)$$

Because all currents, voltages, charges, etc. can be expressed in Fourier series form, the Laplace transform and the inverse transform exist, and in fact,can always be determined with relative ease.

5.2 Pump Circuit Configuration

Figure 5.1 illustrates the pump circuit configuration used in this chapter. By referring back to the basic representation of a pumped varactor circuit shown in Fig. 1.1, it can be seen that the linear portion of the circuit as seen from the diode terminals has been replaced by an equivalent Thevenin circuit. The nonlinear varactor diode remains unaltered, and is not included in the equivalent circuit.

Because of the nonlinear element, the Thevenin equivalent impedance concept must be treated with some care. Usually, the entire circuit is linear, and voltages and currents are present at only one frequency, that of the voltage source. The introduction of the nonlinear diode complicates matters somewhat, for now voltage and currents may appear at frequencies other than that of the source. For each frequency component, the Thevenin equivalent circuit

must have the same (linear) voltage-current relation as the original circuit.

Figure 5.2 shows examples of two types of pumped diode circuits which are considered in this chapter. Figure 5.2a shows a simple circuit composed of lumped elements. The capacity of the varactor diode is series resonant with the inductor L_2 at a frequency near that of the pump source. Pump power is coupled into the circuit through the mutual inductance M_1. It can usually be assumed that the pump generator is sinusoidal at frequency ω_p, and that losses in the circuit are small. Under these conditions, the Thevenin voltage generator is sinusoidal, and the equivalent impedance can be closely approximated by the network in Fig. 5.4. Here R_s represents the diode loss, while G accounts for both inductor loss and generator resistance; C_s is the parasitic capacity of the inductor.

In the ideal case when all losses and the parasitic capacitance can be neglected, the Thevenin impedance reduces to

$$Z_L(\omega) = j\omega L \tag{5.4}$$

Figure 5.2b shows a simple distributed parametric circuit. A length of transmission line is shorted at one end and tuned to resonance near the pump frequency by a varactor diode placed across the opposite end. A loop near the shorted end couples pump power into the circuit. If the coupling is weak, and ohmic losses small, then the Thevenin impedance can be put in the form:

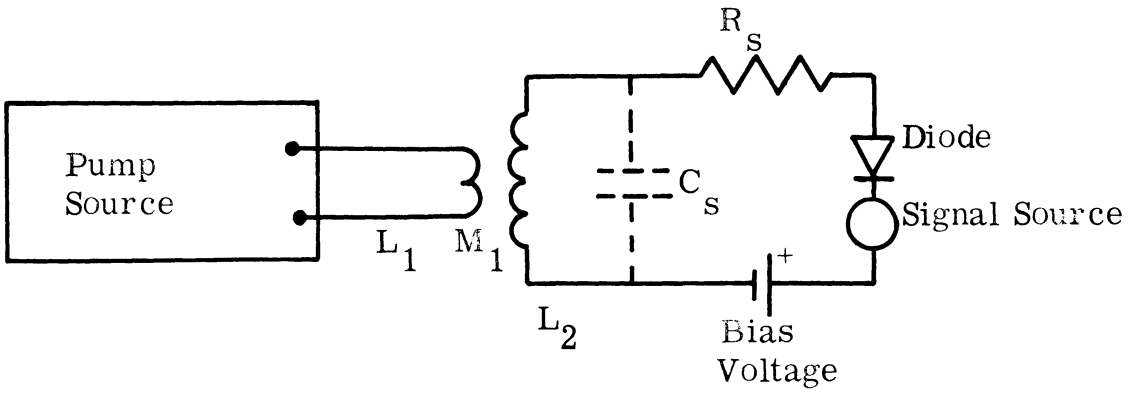

Fig. 5.2 a. Lumped circuit

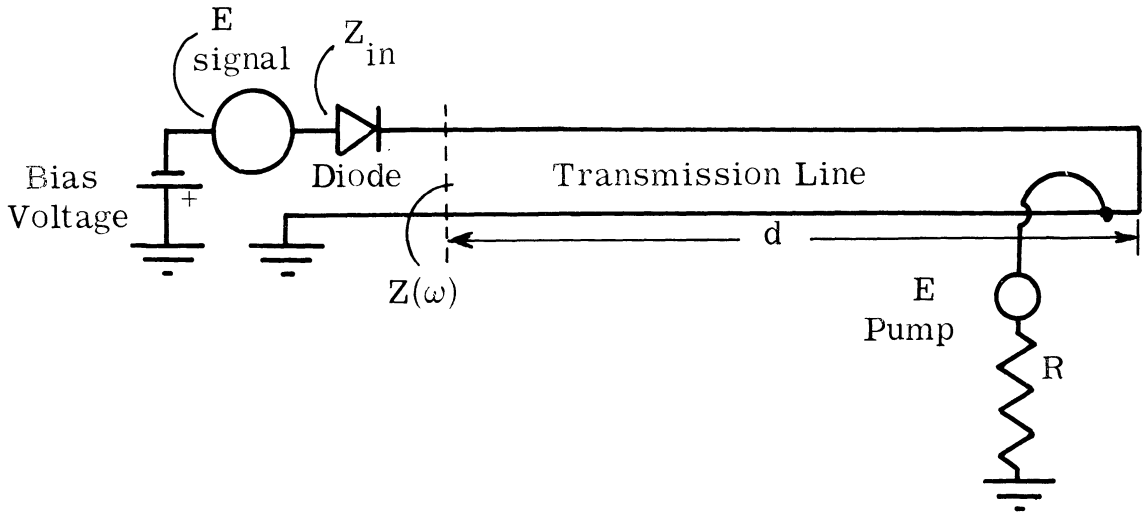

Fig. 5.2 b. Distributed Circuit

Fig. 5.2. Practical pumped varactor circuits

$$Z(\omega) = j X_L(\omega) + R_L(\omega) + R_s \qquad (5.5)$$

Except for frequencies very near the resonances of the line, the reactance takes the familiar tangent form:

$$X_L(\omega) = Z_0 \tan\left(\frac{\pi\omega}{2\omega_L}\right) \qquad (5.6)$$

and for the common case of an air dielectric coaxial line the distributed losses can be computed using conventional approximate techniques (Ref. 50)

$$R_L(\omega) = \frac{37.6 \times 10^3 \left(\frac{1}{a'} + \frac{1}{b'}\right)\left(\frac{\pi\omega}{4\omega_L} + \frac{1}{4}\sin\left(\frac{\pi\omega}{\omega_L}\right)\right)}{\sqrt{\sigma\omega}\,\cos^2\left(\frac{\pi\omega}{2\omega_L}\right)} \qquad (5.7)$$

where

Z_0 is the characteristic impedance of the line

ω_L is the radian frequency at which the line is one-quarter wavelength long

a' and b' are the inner and outer conductor diameters in meters

σ is the conductivity of the material in mhos/meter.

A comparison of Eqs. 5.4 and 5.6 indicates that although both impedances can be adjusted to resonate with the diode at the pump frequency, the impedances at harmonics of the pump can be considerably different. The inductor presents a higher impedance to each succeeding harmonic;

the line, because of the nature of the tangent function, need not follow such a regular pattern. Indeed, the line can be adjusted so that either a zero or pole of impedance falls at any harmonic. If the line length and the characteristic impedance are varied together in a manner such that the tuning of the pump fundamental remains constant, the tuning (and, therefore, the amplitudes) of the harmonics change. These simple circuits then provide a convenient means for studying the effects of higher harmonics upon a varactor circuit.

Now referring back to the circuit of Fig. 5. 1 it is clear that

$$E_{in}(t) = V_{LIN}(t) + V_p(t) \tag{5.8}$$

This equation is the basic pump circuit equation. The three voltages are discussed in the following three paragraphs.

a. The Pump Voltage. The pump source is assumed to be sinusoidal at frequency ω_p. Thus, the open circuit Thevenin voltage, $E_{in}(t)$, which would be present if the diode were removed, i. e., open circuited, is also sinusoidal at ω_p. The varactor DC voltage bias is taken into account by the relations developed in Chapter II and need not be included. In general, the time origin is arbitrary, and $E_{in}(t)$ takes the form:

$$E_{in}(t) = E_A \cos \omega_p t + E_B \sin \omega_p t \tag{5.9}$$

b. The Diode Voltage. In the abrupt junction reversed biased case, the voltage-charge relations for the diode were discussed in Section 2.2. Equation 2.12 is of particular value here:

$$V_p(t) = Q_p(t) + \frac{Q_p(t)^2}{4} \qquad (2.12)$$

The subscripts have been changed from N to p. This minor change in notation was made to emphasize the fact that all the voltages and charges (currents) considered in this section are due to the pump only. Here, V_p and Q_p are normalized according to the scheme in Section 2.2 and must satisfy the inequalities of Eq. 2.15.

$$V_p \geq -1$$

$$Q_p(t) \geq -2$$

In the remainder of this chapter, this abrupt junction equation will be used. The choice of the abrupt junction was arbitrary; the linear diode (Eq. 2.16), or measured data could have been used.

c. The Network Voltage. Using the complex frequency notation introduced earlier, the voltage across the linear circuit can be easily expressed in terms of the charge.

$$V_{LIN}(s) = s\,Z(s)\,Q_p(s) \qquad (5.10)$$

Here, the linear circuit components have been transformed in the

usual manner into complex impedances. The impedances of the network at the pump and its harmonics are important enough to justify a special notation. The impedance of the linear network at the nth harmonic of the pump is denoted as

$$Z(n\omega_p) = R(n) + j\,X(n) \tag{5.11}$$

where

$$n = 1, 2, \ldots$$

The voltage across the linear network in the time domain can now be found by combining Eqs. 5.1, 5.10 and 5.11

$$V_{LIN}(t) = \sum_{n=1}^{\infty} n\omega_p \left[Q_B(n)\,R(n) - Q_A(n)\,X(n)\right] \cos n\omega_p t$$

$$- \sum_{n=1}^{\infty} n\omega_p \left[Q_A(n)\,R(n) + Q_B(n)\,X(n)\right] \sin n\omega_p t \tag{5.12}$$

The advantages of using the complex frequency notation are easily seen by comparing Eq. 5.10 with Eq. 5.12.

A convenient form for the differential equation describing pump circuit behavior can be obtained by combining Eqs. 2.12, 5.8 and 5.10.

$$0 = E_{in}(s) - s\,Z(s)\,Q_p(s) - L\left\{Q_p(t) + \frac{Q_p^{\,2}(t)}{4}\right\} \tag{5.13}$$

This can be solved for $Q_p(t)$ and rewritten.

$$Q_p(t) = L^{-1}\left\{\frac{1}{+ sZ(s)}\left[E_{in}(s) - L\left\{\frac{Q_p^{\,2}(t)}{4} + Q_p(t)\right\}\right]\right\} \qquad (5.14)$$

where the $L^{-1}\{\ \}$ notation denotes the inverse Laplace transform.

This equation is closely related to Lalesco's Nonlinear Integral Equation (Ref. 51). However, the sequence method ordinarily used to solve this type of equation fails to converge in some instances. One circuit of particular interest for which the usual method does not converge is shown in Fig. 5.2b. In the next section, a scheme which is useful in this case will be presented.

The quantity that will be treated as the forcing function in Eq. 5.14 has not yet been determined. It can be selected in a variety of ways, of which letting E_{in} be the forcing function, and allowing $Q_p(t)$ be the unknown is perhaps the most natural. In this chapter, however, a different choice is made. The forcing function is $Q_A(1)$, the fundamental cosine component of charge at the pump frequency. $Q_B(1)$ is set equal to zero; this is simply equivalent to choosing a time origin. E_{in} and all the remaining components of $Q_p(t)$ are now the unknowns. Physically, this is equivalent to replacing the voltage source in the circuit of Fig. 5.1 by a current source in parallel with an ideal filter (Fig. 5.3). The filter short circuits all frequencies except ω_p; at this frequency it is an open circuit. The current source is

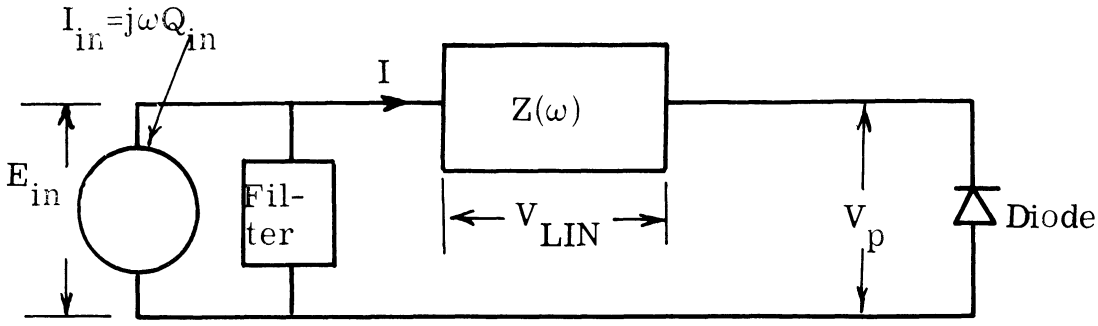

Ideal filter is an open circuit at the pump frequency; a short circuit for all other frequencies.

Fig. 5.3. Pump circuit configuration used in Chapter V

$$I_{in}(t) = -\omega_p Q_A(1) \sin \omega_p t \qquad (5.15)$$

It is clear that under stable conditions nothing has been altered by making this change in driving functions, for by the "substitution theorem" (Ref. 52) a voltage source which is delivering a current of I amperes to a load may be replaced by a current source of magnitude I with no change in the external circuit. However this choice of a driving function along with the constraint of only a "steady state" solution does force the solution to the differential equation to be stable and periodic in ω_p. Unfortunately the physical circuit is not so constrained and as discussed in Chapter IV, can become unstable under certain conditions. Thus, an important step in characterizing the pump circuit behavior involves examination of the steady state solutions to determine whether, in fact, it is a stable solution of the physical problem. This can be carried out in a straightforward manner by noting the behavior of $\frac{\partial |E_{in}|}{\partial |I_{in}|}$ at a constant frequency. Whenever this term is positive; that is, whenever the magnitude of voltage increases with current, the circuit is stable. However, if $\frac{\partial |E_{in}|}{\partial |I_{in}|}$ is negative or zero, that is, if the voltage magnitude decreases with current magnitude, the circuit is unstable, and the "steady state" solution is meaningless.

This can be proven quite simply by recalling the results of Chapter IV, where the stability of a network driven by a current source of constant magnitude is determined by examining the expression for

$\frac{\partial |V|}{\partial \omega}$ and searching for the conditions under which the expression becomes infinite; that is, where the denominator becomes zero. The dual is also true; the stability of a network such as Fig. 5.1 which is driven by a voltage source can be determined by examining the expression for $\frac{\partial |I|}{\partial \omega}$ and searching for the conditions under which the denominator becomes zero (Ref. 45).

Following the same technique as used in Chapter IV, the current at the fundamental frequency in the circuit of Fig. 5.1 can be put in the following form:

$$|I_{in}| = \frac{A\left(|E_{in}|, |I_{in}|, \omega\right)}{B\left(|E_{in}|, |I_{in}|, \omega\right)} \tag{5.16}$$

where A and B are functions of the indicated variables.

Now this circuit is unstable when the denominator of $\frac{\partial |I_{in}|}{\partial \omega}$ equals zero, the voltage E_{in} being held constant. That is, when

$$0 = \left(B + I_{in} \frac{\partial B}{\partial |I_{in}|} - \frac{\partial A}{\partial |I_{in}|}\right) \tag{5.17}$$

Replacing the voltage source by a current source as is done in Fig. 5.3 does not change the voltage-current relationship of the network. If now the function $\frac{\partial |E_{in}|}{\partial |I_{in}|}$ with frequency being held constant is examined, this function has zeros at

$$0 = \left(B + I_{in} \frac{\partial B}{\partial |I_{in}|} - \frac{\partial A}{\partial |I_{in}|} \right) \tag{5.18}$$

This is, of course, the same condition under which the circuit by the voltage source becomes unstable. For the circuits considered here, the $\frac{\partial |E_{in}|}{\partial |I_{in}|}$ function has either one zero, or two zeros which bound a negative region. These points correspond to the instability regions discussed in the previous chapter.

5.3 An Iterative Technique Applicable to Single Tuned Circuits

The preceding sections presented the basic pump circuit equation and explained the selection of the driving function and the dependent variable. In this section, an iterative technique is introduced for solving the equation.

The basic scheme used to solve the equation is to

(1) Substitute an estimate for $Q_p(t)$ into the right side of the equation and perform the indicated operations. The result is a "better" estimate for $Q_p(t)$.

(2) This new estimate for $Q_p(t)$ can be substituted back into the right side of the equation.

(3) The process is repeated until the resulting estimate is as close to the correct answer as desired.

Formally, the process can be set down as follows:

The solution to Eq. 5.14 is the limit of the infinite sequence of functions: $Q_0(t)$, $Q_1(t)$, $Q_2(t)$, ... $Q_m(t)$ ...

and

$$Q_p(t) = \lim_{m \to \infty} Q_m(t) \tag{5.19}$$

It is clear that in order to be a useful process, $Q_m(t)$ must converge uniformly to $Q_p(t)$. A sufficient condition for convergence is that the error become smaller after each iteration. Thus

$$|\epsilon_{m+1}(t)| < |\epsilon_m(t)| \tag{5.20}$$

for all m and all t. $\epsilon_m(t)$ is the error after m iterations, and $\epsilon_{m+1}(t)$ is the error after m+1 iterations.

$$\epsilon_m(t) = Q_m(t) - Q_p(t) \tag{5.21}$$

$$\epsilon_{m+1}(t) = Q_{m+1}(t) - Q_p(t) \tag{5.22}$$

After m iterations, the estimate for $Q_{m+1}(t)$ is computed from Eq. 5.14, 5.21, and 5.22 using the procedure outlined above.

$$Q_{m+1}(t) = Q_p(t) + \epsilon_{m+1}(t) = L^{-1}\left\{\frac{1}{s\,Z(s)}\left[E_m(s) - L\left\{\frac{\left(Q_p(t) + \epsilon_m(t)\right)^2}{4} + Q_p(t) + \epsilon_m(t)\right\}\right]\right\} \tag{5.23}$$

Multiplying this out and substituting in the value of Q_p as determined by Eq. 5.13, Eq. 5.23 becomes

$$\epsilon_{m+1}(t) = -L^{-1}\left\{\frac{1}{s\,Z(s)}\;L\left\{\frac{Q_p(t)\,\epsilon_m(t)}{2} + \frac{\epsilon_m(t)^2}{4} + \epsilon_m(t)\right\}\right\} \qquad (5.24)$$

From this equation, an estimate can be made for the conditions under which the sequence will converge when

$$|\epsilon_{m+1}(t)| < |\epsilon_m(t)| \qquad (5.25)$$

In order to make this estimate, some bounds must first be placed on $Q_p(t)$ and $\epsilon_m(t)$. A lower limit for $Q_p(t)$ can be obtained from the fundamental equations derived for the abrupt junction diode.

$$Q_p(t) \geq -2 \qquad (5.26)$$

One crude approximation of $Q_p(t)$ is that it is sinusoidal. Certainly, this estimate should not be in error by more than a factor of 2.

Then

$$|Q_p(t)| \leq 2 \qquad (5.27)$$

In Eq. 5.1, $Q_p(t)$ is written in the form of a Fourier series. The fundamental term has been selected as the driving function, and thus is a known quantity. It can be reasonably expected that the fundamental will be the largest term in the solution, and that the sum of all the harmonics will not be larger than the fundamental. Then, by Eq. 5.27, and because the initial (and worst) estimate of $Q_p(t)$ is just this

fundamental term, an upper limit can be placed on the error

$$|\epsilon_m(t)| < 1 \tag{5.28}$$

for all m.

Now substitute Eq. 5.25 into Eq. 5.24. By Eq. 5.28, the $\epsilon_m(t)^2/4$ term is small compared with the other terms and may be neglected. After taking the transform

$$|\epsilon_{m+1}(s)| < \frac{2|\epsilon_m(s)|}{|s\ Z(s)|} \tag{5.29}$$

Thus, $|\epsilon_{m+1}(s) < |\epsilon_m(s)|$ whenever $|s\ Z(s)| > 2$. The equation is set up such that only the pump and its harmonics are present, and the iteration scheme is devised such that error term exists only at the harmonics. So

$$Q_m(t) = \frac{Q_A(0)_m}{2} + \sum_{n=1}^{\infty} Q_A(n)_m \cos n\omega_p t + \sum_{n=1}^{\infty} Q_B(n)_m \sin n\omega_p t \tag{5.30}$$

$$\epsilon_m(t) = \frac{\epsilon_A(0)_m}{2} + \sum_{n=1}^{\infty} \epsilon_A(n)_m \cos n\omega_p t + \sum_{n=1}^{\infty} \epsilon_B(n)_m \sin n\omega_p t \tag{5.31}$$

Then, the sequence will converge if

$$|n\omega_p\ Z(n\omega_p)| > 2 \tag{5.32}$$

for n = 2, 3, 4, ...

With the aid of Eq. 5.32, the convergence of the iteration process can now be examined for specific circuit configurations.

a. Ideal Inductor. If the coil is ideal and all losses in the circuit can be neglected, then the Thevenin equivalent impedance reduces to an inductance and

$$Z_L(\omega) = j\omega L \tag{5.33}$$

The impedance at the nth harmonic of pump frequency is

$$Z_L(n\omega_p) = jn\omega_p L \tag{5.34}$$

The coil is usually chosen to resonate with the small signal diode capacity (1 farad) at a frequency near the pump. Then

$$\omega_p^2 L \approx 1 \tag{5.35}$$

and

$$|n\omega_p Z_L(n\omega_p)| \approx n^2 \tag{5.36}$$

for n = 2, 3, 4, ...

The criterion of Eq. 5.32 is satisfied in this case, and the iteration procedure will converge for this circuit configuration.

b. Inductor with Series Resistance. In practice, the diode is not ideal and its losses must be accounted for; in this event, the Thevenin equivalent circuit may be approximated by an ideal inductor

in series with a resistance. The impedance at the nth harmonic is

$$Z_{LR}(n\omega_p) = jn\omega_p L + R_s \tag{5.37}$$

As in the previous example, the inductor is usually chosen to be resonant with the small signal diode capacity near the pump frequency. Then

$$|n\omega_p Z_{LR}(n\omega_p)|^2 \approx [n^2]^2 + [n\omega_p R_s]^2 > [n^2]^2 \tag{5.38}$$

for $n = 2, 3, 4, \ldots$

The criterion for convergence (Eq. 5.32) is satisfied in this case for all values of resistance.

c. Inductor with Parasitic Capacitance. The parasitic capacitance associated with all real inductors can be very important. The impedance of an ideal inductor increases linearly with frequency. It therefore presents a large impedance to the higher pump harmonics, and thus tends to prevent currents from flowing at these frequencies. The circuit approximates the so-called open circuit conditions, in which all currents except those at a few selected frequencies are prevented from flowing.

In contrast, the impedance of a real inductor with parasitic

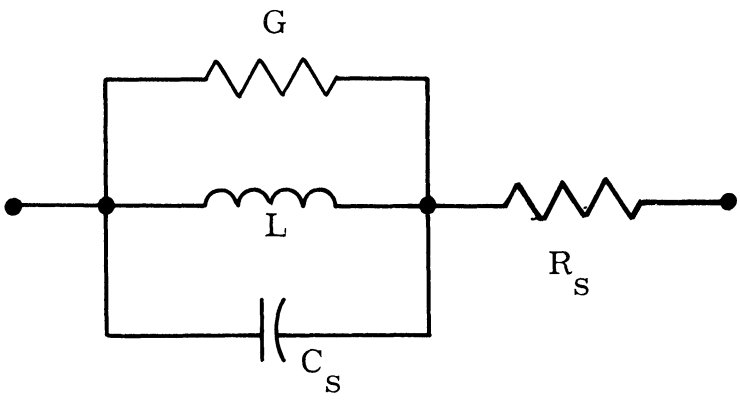

Fig. 5.4. Equivalent circuit for an inductor with parasitic capacity

capacity goes toward zero above the self resonant frequency. This tends to short circuit the higher harmonics of pump. The circuit then approximates the so-called short circuit conditions, in which no voltages exist except at a few selected frequencies.

If losses are ignored, the impedance of the circuit of Fig. 5.4 at the nth harmonic is

$$Z_{\text{Coil}}(n\omega_p) = \frac{jn\omega_p L}{1 - n^2 \omega_p{}^2 LC_s} \tag{5.39}$$

In this case, there are two resonant frequencies. The first is the frequency at which the coil is series resonant with the small signal capacity of the diode. This is near the pump fundamental.

$$\frac{\omega_p{}^2 L}{1 - \omega_p{}^2 LC_s} \approx 1 \tag{5.40}$$

The second is ω_c , the self-resonant frequency of the coil. It can be defined as

$$\omega^2_c = \frac{1}{LC_s} \tag{5.41}$$

Combining Eqs. 5.39, 5.40 and 5.41 with the approximate criterion for convergence, (Eq. 5.32), a condition for ω_c is obtained.

$$\omega_c > \sqrt{3}\ \omega_p \tag{5.42}$$

This is a reasonable value which most coils satisfy.

Other circuit configurations are easily checked for convergence in the same manner. In general, the larger the impedance, the faster the convergence. It should be clear that the sequence will not converge for all circuit configurations. For example, the criterion for convergence (Eq. 5.32) could not be satisfied if a zero of impedance happened to occur at some harmonic of the pump.

5.4 An Iterative Technique Applicable to Distributed Circuits

An iteration technique for solving the pump circuit differential equation was developed in the previous section. It was shown that the sequence does converge to the correct result for single tuned circuits; it was also made clear in the discussion that the sequence does not converge for all circuit configurations. In particular, the sequence does not converge for the distributed circuit of Fig. 5.2b. In this section an iterative technique is presented which was developed to solve this circuit. But, it is shown that the sequence will converge for any circuit. This new technique is more complex than the previously considered procedure, and generally, the computer running time is longer.

The basic scheme used to solve the equation is to

(1) Substitute an estimate for $Q_p(t)$ into the right side of Eq. 5.13 and perform the indicated operations. The result is $\delta(t)$, the equation error (Ref. 53).

(2) Using the equation error $\delta(t)$ and the estimate for $Q_p(t)$, compute an approximate value for the "solution error" $\epsilon(t)$ which is the difference between $Q_p(t)$ and the estimate.

(3) A new estimate for $Q_p(t)$ can easily be computed knowing both the old estimate and the "solution error" associated with it.

(4) This three-step process is repeated until the resulting estimate is as close to the correct answer as desired.

Formally, the process can be set down as follows:

The solution to Eq. 5.13 is the limit of the infinite sequence of functions: $Q_0(t)$, $Q_1(t)$, $Q_2(t)$, . . . , $Q_m(t)$ . . .

and

$$Q_p(t) = \underset{m \to \infty}{\text{Limit}} \; Q_m(t)$$

Step (1) of the iteration procedure is implemented by computing the equation error. After m iterations, $Q_m(t)$ is the estimate for $Q_p(t)$, and $\delta_m(t)$ the equation error is

$$\delta_m(t) \triangleq E_m(t) - L^{-1}\left\{s\,Z(s)\,Q_m(s)\right\} - \left[Q_m(t) + \frac{Q_m^{\,2}(t)}{4}\right] \qquad (5.43)$$

Of course, by Eq. 5.13 the equation error is zero when the solution is found. Thus

$$\delta_m(t) = 0 \qquad \text{when} \qquad Q_m(t) = Q_p(t) \tag{5.44}$$

As before, $Q_m(t)$ can be written as the sum of an error term plus the correct charge, where the error (hopefully) is small

$$Q_m(t) = Q_p(t) + \epsilon_m(t) \tag{5.45}$$

$$|\epsilon_m(t)| << 1$$

In Step (2) of the iteration procedure, an estimate for the solution error, $\epsilon_m(t)$ is computed. Substitute (5.45) into (5.43) and use (5.13) to obtain $\delta_m(t)$ in terms of $\epsilon_m(t)$.

$$\delta_m(t) = -\epsilon_m(t) - \frac{Q_p(t)\,\epsilon_m(t)}{2} - L^{-1}\left\{s\,Z(s)\,\epsilon_m(s)\right\}$$

This is an algebraic equation for $\epsilon_m(t)$. For convenience, the solution will be written as

$$\epsilon_m(t) = -\delta_m(t)\left[1 + L^{-1}\left\{s\,Z(s)\right\} + \frac{Q_p(t)}{2}\right]^{-1} \tag{5.46}$$

This is an expression for the "solution error." It is a function of the "equation error" and circuit parameters (both of which are known), and the solution ($Q_p(t)$ is unknown).

Although $Q_p(t)$ is unknown, an estimate can be made for it:

$$Q_p(t) \approx Q_m(t) \tag{5.47}$$

From (5.46) and (5.47) an estimate can be made for the "solution error"

$$\epsilon_m(t) \approx \epsilon'_m(t) = -\delta_m(t) \left[1 + L^{-1}\{s\, Z(s)\} + \frac{Q_m(t)}{2}\right]^{-1} \qquad (5.48)$$

In Step (3) of the iteration procedure, a new estimate for the solution, $Q_p(t)$, is computed.

From Eq. 5.45

$$Q_p(t) = Q_m(t) - \epsilon_m(t) \qquad (5.49)$$

Therefore, (hopefully) a better estimate than $Q_m(t)$ can be made for $Q_p(t)$:

$$Q_p(t) \approx Q_m(t) - \epsilon'_m(t) \triangleq Q_{m+1}(t) \qquad (5.50)$$

From (5.49) and (5.50)

$$Q_{m+1}(t) = Q_p(t) + \epsilon_m(t) - \epsilon'_m(t) \qquad (5.51)$$

Equations 5.43 through 5.50 complete one iteration (the mth) in the sequence. If the procedure is to be useful, the equation error after m+1 iterations should be smaller than the equation error after only m iterations. That is

$$|\delta_{m+1}(t)| < |\delta_m(t)| \qquad (5.52)$$

should hold for all t.

Substitute (5.51) into (5.43), and use (5.45) to obtain the equation error after m+1 iterations in terms of the previous equation error. After some manipulation

$$\delta_{m+1}(t) = \frac{\delta_m(t)}{2}\,\epsilon'_m(t)\left[1 + L^{-1}\{s\,Z(s)\} + \frac{Q_m(t)}{2}\right]^{-1} - \frac{1}{4}\left(\epsilon'^{\,2}_m(t)\left[1 + L^{-1}\{s\,Z(s)\} + \frac{Q_m(t)}{2}\right]^{-1}\right)^2 \qquad (5.53)$$

$$\delta_{m+1}(t) = 0[\delta_m(t)^2]$$

Therefore, providing the operator $\left[1 + L^{-1}\{s\,Z(s)\} + \frac{Q_m(t)}{2}\right]$ and its inverse exist, the equation error is reduced quadratically each iteration. The reason is that the expression for $Q_{m+1}(t)$ is stationary with respect to small variations in $Q_m(t)$. Once the sequence has converged to a value close to the correct solution, the variational property assures rapid convergence. Of course, when the error is large, the convergence is not as fast. In practice, the sequence converges to six-place accuracy in from 3 to 6 trials.

Essentially, the iteration procedure described in this chapter is an extension of the so-called Newton-Raphson method. The nonlinear differential equation is first transformed into a set of simultaneous nonlinear algebraic equations. Each harmonic of the pump is

represented by two of these equations: one equation represents the cosine; the other represents the sine term. All the equations are coupled through the $Q^2/4$ nonlinearity.

The resulting set of nonlinear algebraic equations is then solved with the aid of a linearization procedure. Each approximation to the solution is found by using the preceding approximation as a starting point. A linearized set of equations is generated from the nonlinear set by expanding the nonlinear functions in a Taylor series about the approximate solution and using only the first two terms. The linear set of equations is then solved, and a (hopefully) better approximation to the solution is obtained. The process is repeated until the solution is as accurate as desired (or until it diverges).

The usefulness of the method depends upon how closely the linearized set of equations represents the nonlinear set in a neighborhood centered about the approximate solution but extending outward to include the actual solution. If the approximate solution is close to the actual solution, and if the function is smooth enough in a neighborhood which includes both, then $\epsilon_m^2(t)$ and higher powers can really be ignored (as was done throughout this section). The sequence method will then converge fast enough to be a useful process.

For the situation considered in this chapter, there are two reasons why the sequence will probably converge:

(1) The varactor voltage-charge relationship $\left(Q + \frac{Q^2}{4}\right)$ is a "mild" nonlinearity. In the region of interest ($-2 \leq Q \leq +2$), the

first two terms of the Taylor expansion adequately represent the function in a large neighborhood. The function is "smooth" enough so that the sequence will converge even with a bad initial approximation to the correct solution.

(2) The initial approximation (the first estimate) is always close to the correct solution. This is a basic study, and, rather than just a single solution for one pump level, it is desirable to determine circuit behavior for a variety of pumping levels. A family of solutions can thus be constructed starting with the smallest pump magnitude and building up toward hard pumping. For each pump level, the initial approximation is the solution previously found for a slightly smaller pump amplitude. The choice of a current source for the driving function forces all the solutions to be stable, and the diode voltage increases continuously with pump level. This insures that the solution found for one pump level will be a reasonable initial approximation for a slightly higher pump level.

5.5 Small Signal Equations

The procedures developed in the preceding two sections determine the behavior of the pump circuit in the absence of signal. They implement the first step in the determination of small signal input impedance. The second step is straightforward, and is outlined only briefly here.

Once the pump circuit behavior has been determined, the

result can be expressed in terms of the charge circulating through the diode.

$$Q_p(t) = \frac{Q_A(0)}{2} + \sum_{n=1}^{\infty} Q_A(n) \cos n\omega_p t + \sum_{n=1}^{\infty} Q_B(n) \sin n\omega_p t \qquad (5.1)$$

By Eq. 2.14, the small signal elastance (for an abrupt junction device) can also be written as a function of charge:

$$S(t) = 1 + \frac{Q_p(t)}{2} \qquad (2.14)$$

Equations 2.14 and 4.6 can easily be combined and the resulting small signal elastance can be expressed as an exponential Fourier series:

$$S[Q_p(t)] = \sum_{n=-\infty}^{\infty} S_n e^{jn\omega_p t} \qquad (3.5)$$

This elastance is a function only of pump.

In Chapter III, an expression (3.15) is derived which relates signal voltages across the junction to signal currents through the junction. The elements in this matrix are the elastance coefficients of Eq. 3.5.

Now the circuit of Fig. 1.1 may be redrawn to emphasize the signal circuit. This is shown in Fig. 5.5. The diode is represented as a time varying elastance of the form (3.5), where the coefficients

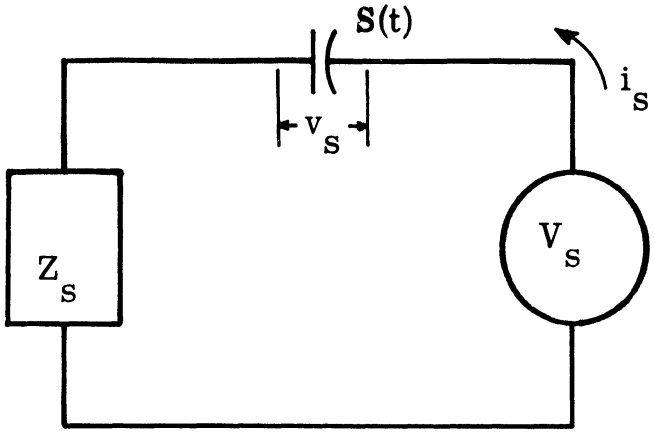

Fig. 5. 5. Signal circuit configuration used in Chapter V.

can now be computed. The relationship between the signal voltage appearing across the diode and the signal current is given by Eq. 3.15.

The linear portion of the circuit, including the impedance of the pump source can be replaced by a Thevenin equivalent impedance. This equivalent impedance, $[Z_s]$, must adequately model the circuit at the entire set of signal frequencies:

$$\omega_1, \omega_2, \omega_3, \cdots$$

The pump source may be removed since it is a linear current source and plays no direct role in the signal circuit. Its only purpose is to "pump" the diode, i.e., cause the diode elastance to vary periodically in time. The voltages around the circuit (Fig. 5.5) can be written in terms of the currents:

$$V_s] = [S] \times i_s] + [Z_s] \times i_s] \qquad (5.54)$$

$V_s]$ and $i_s]$ are column matrices

$[S]$ is a square matrix of the form (3.15)

$[Z_s]$ is a diagonal matrix representing the impedance of the linear network. The nth element of the matrix, denoted Z_n, is the impedance at the nth signal frequency, ω_n.

In the most common case, the signal source has only one frequency component (at ω_1).

The voltage matrix then reduces to

$$V_s] = \begin{bmatrix} V_1' \\ 0 \\ 0 \\ 0 \\ \cdot \\ \cdot \\ \cdot \end{bmatrix} \tag{5.55}$$

However, currents may still flow at all of the signal frequencies.

The $[Z_s]$ and the $[S]$ matrices can be combined as indicated in Eq. 5.54 and then simplified with the aid of Eq. 5.55. The result is Eq. 5.56. The input impedance of a small amplitude signal can be computed from this matrix by ordinary techniques. The method used in this paper was to reduce the matrix to its lower triangular form, by using the Gauss-Jordon technique. The input impedance is the (1, 1) element of the new matrix. Any method, however, will involve a large amount of labor if the matrix is large.

$$
\begin{bmatrix} V_1 \\ 0 \\ 0 \\ 0 \\ 0 \\ 0 \\ 0 \end{bmatrix} = \begin{bmatrix} -j\frac{S_0}{\omega_1} + Z_1 & j\frac{S_1}{\omega_2} & -j\frac{S_{-1}}{\omega_3} & j\frac{S_2}{\omega_4} & \cdots \\ -j\frac{S_{-1}}{\omega_1} & j\frac{S_0}{\omega_2} + Z_2^* & -j\frac{S_{-2}}{\omega_3} & j\frac{S_1}{\omega_4} & \cdots \\ -j\frac{S_1}{\omega_1} & j\frac{S_2}{\omega_2} & -j\frac{S_0}{\omega_3} + Z_3 & j\frac{S_3}{\omega_4} & \cdots \\ -j\frac{S_{-2}}{\omega_1} & j\frac{S_{-1}}{\omega_2} & -j\frac{S_{-3}}{\omega_3} & j\frac{S_0}{\omega_4} + Z_4^* & \cdots \\ -j\frac{S_{-2}}{\omega_1} & j\frac{S_3}{\omega_2} & -j\frac{S_1}{\omega_3} & & \\ -j\frac{S_{-3}}{\omega_1} & \vdots & \vdots & & \\ \vdots & & & & \end{bmatrix} \times \begin{bmatrix} I_1 \\ I_{-2} \\ I_3 \\ I_{-4} \\ I_5 \\ \vdots \end{bmatrix} \tag{5.56}
$$

5.6 Summary

In this chapter, a nonlinear differential equation which describes the behavior of the pump circuit was set up, and two iterative techniques for solving it were developed. These procedures involve the iteration of a sequence of solutions, and where properly used converge rapidly to the correct solution.

The first technique (Section 5.3) is useful for determining

the behavior of single tuned circuits in which the impedance at the harmonics is high compared with that of the diode. The second technique (Section 5.4) converges for any circuit configuration. The solution to the pump circuit is expressed in terms of the charge $Q_p(t)$, but it is clear that the result can also be expressed in terms of voltage or current. Once it is known, the Fourier coefficient of the elastance can be easily computed.

It was shown that these elastance coefficients can be substituted into the elastance matrix which describes the mixing process, and that the small signal input impedance can be obtained by manipulating the resulting impedance matrix.

The numerical results which are presented in Chapter 7 were obtained by algorithms of the procedures described in this chapter programmed for a digital computer. The flow diagrams are presented in Appendices C and D.

CHAPTER VI

DIFFUSION EFFECTS

6.1 Introduction

The circuit effects of depletion layer capacity have been treated in the previous chapter. The results of that chapter are valid if the voltage across the varactor is negative (reverse) at all times, so that the diode junction can be accurately characterized with frequency independent depletion layer capacity. However if positive (forward) voltages are applied to the diode, a second type of charge storage contributes to capacity. It is called diffusion capacity, and the purpose of this chapter is to determine its circuit effects. In Chapter II, the physical origin of diffusion capacity was thoroughly discussed, and this capacity was shown to be significant only for forward voltages, that is, when there is some direct current flow. For reverse voltages, it is negligible compared with depletion layer capacity.

Charge storage and diffusion effects are of interest primarily because in many cases, the pumping is hard enough to cause rectified direct current to flow through the diode. In most practical circuits, the varactor is operated with a reverse DC voltage bias on which the AC pump voltage is superimposed. This pump voltage is often so large that the diode is driven into forward conduction during each positive peak. In this situation, depletion layer capacity dominates the varactor characteristics most of the time, but for the

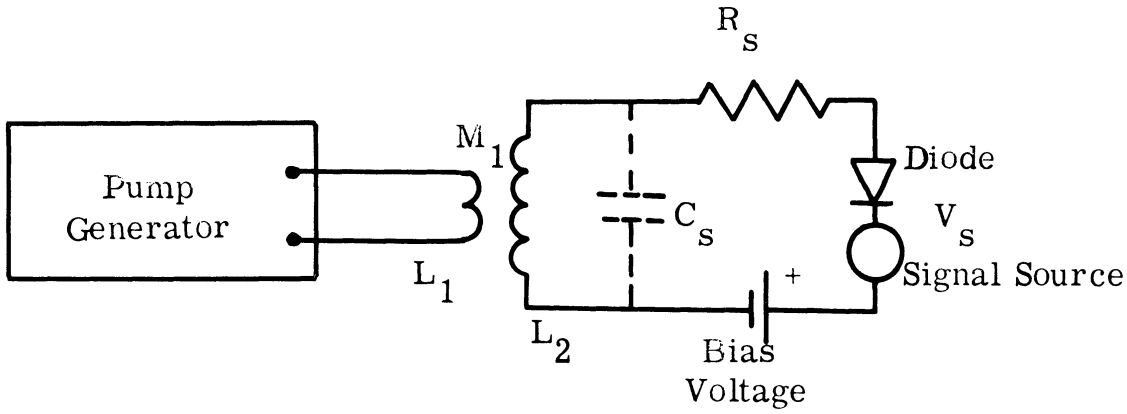

Fig. 6. 1. Varactor circuit used to investigate diffusion effects

positive part of every cycle, diffusion effects become important.

The organization of this chapter is similar to that of Chapter V. The behavior of the circuit in the absence of signal is treated first. Section 6.2 discusses a circuit representation which is useful when pump power is applied to the circuit. The nonlinear differential equation which results from this model is solved in Section 6.3.

The end result of this process is the determination of varactor voltage in the absence of signal. From this pump voltage, the input admittance of the diode can be computed for a signal of small amplitude. It is dependent upon the signal frequency, and is both time-varying at the frequency of the pump, and linear. In Section 6.4, an admittance matrix is generated which relates signal currents to signal voltages. The input admittance (or impedance) at the input signal frequency is then found by manipulating the matrix.

6.2 Pump Circuit Representation

The circuit of interest is shown in Fig. 6.1. It has exactly the same schematic configuration as the circuit of Fig. 5.2a. In Chapter V, however, only depletion layer (or barrier) capacity was of concern, and the voltage across the diode was always taken to be negative so that diffusion effects were negligible. In this chapter, there is no such restriction; both diffusion capacity and depletion layer capacity are of interest.

From the viewpoint of the circuit external to the diode,

diffusion effects and barrier layer effects appear in parallel. Physically, there is only one potential across the junction, the effects of which are experienced by all charge carriers. However, there are two components of charge (and therefore current). The first component consists of the mobile charge carriers which are drawn out of the depletion region by the electric field; their departure leaves some fixed charge centers unneutralized. This form of charge storage constitutes depletion layer capacity. The second component of charge results from the mobile charge carriers which have enough thermal energy to overcome the field in the depletion region. These carriers travel across the junction and are stored on the opposite side as minority carriers. These carriers constitute the charge stored by the diffusion capacity.

It is natural in this situation to treat voltage as the independent variable, and to reduce the pump circuit to its Norton equivalent (Fig. 6.2). Here, the linear portion of the circuit as viewed from the pump source, is replaced by a current source in parallel with an admittance. This equivalent circuit must have the same current-voltage relations at its terminals for all components of the pump. As in the previous chapter, it is assumed that the solution is periodic and stable, thus components exist only at the pump frequency and its harmonics. The diode is unchanged, although schematically, it can be split into two parts, a diffusion capacity and barrier capacity. The signal source is omitted entirely because this circuit is intended to

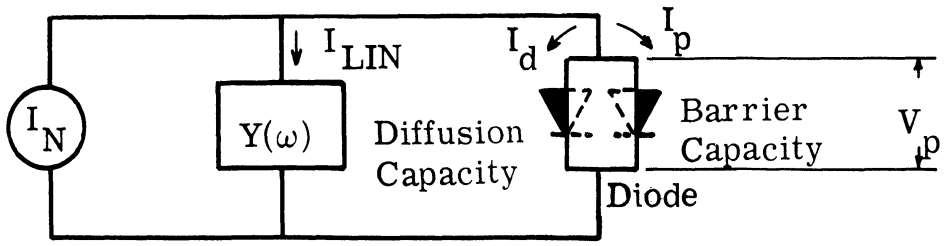

Fig. 6.2. Norton equivalent pump circuit

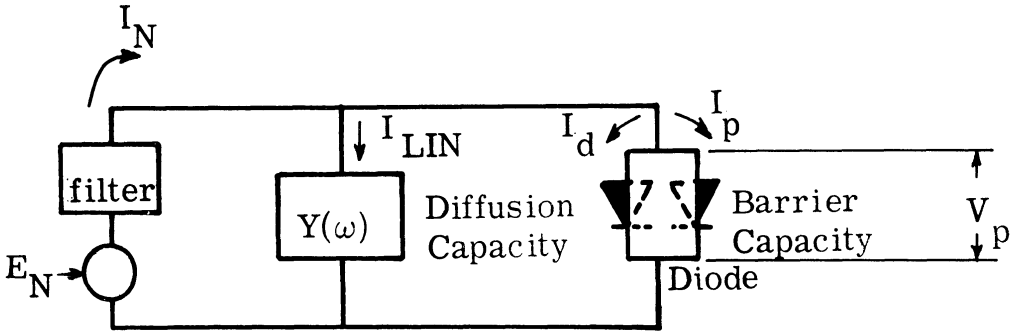

Ideal filter is a short circuit at the pump frequency;
an open circuit for all other frequencies

Fig. 6.3. Pump circuit configuration used in Chapter VI.

represent only the pump circuit.

The currents in the circuit of Fig. 6.2 must satisfy the elementary relationship

$$I_N = I_{LIN} + I_d + I_p \tag{6.1}$$

These four components of current can now be determined:

a. The Current Source. The pump source is assumed to be sinusoidal at frequency ω_p. Thus, the short circuit Norton current, $I_N(t)$, is also sinusoidal at ω_p. This is, of course, the current which would flow in the actual circuit if the diode was shorted. The varactor DC bias is also supplied by this source. In general, the time origin is arbitrary, and $I_N(t)$ takes the form

$$I_N(t) = I_{DC} + I_A \cos \omega_p t + I_B \sin \omega_p t \tag{6.2}$$

b. The Network Current. The current through the linear network can be determined in the usual manner

$$I_{LIN}(s) = Y(s)\ V_p(s) \tag{6.3}$$

It is assumed that currents and voltages exist only at the pump frequency, ω_p, and its harmonics. The admittance of the linear network at the nth harmonic of the pump fundamental is conveniently denoted as

$$Y(n) \triangleq Y(n\omega_p) = G(n) + j\ B(n) \tag{6.4}$$

c. The Barrier Capacity Current. As in previous chapters it will be assumed that the varactor can be modeled with an ideal abrupt junction diode. In this case, a convenient charge-voltage relationship, in which voltage is the independent variable, is given by Eq. 2.4.

$$q_t(t) = -2\, C_a\, \phi \left(1 - \frac{V_p(t)}{\phi}\right)^{\frac{1}{2}} + Q_c \qquad (2.4)$$

where Q_c is the constant of integration.

In the absence of signal,

$$q_t(t) = Q_{Bias} + Q_p(t) \ .$$

Q_c can be chosen so that $Q_p(t) = 0$, when $V_p(t) = 0$. This selection reduces Eq. 2.4 to the following form:

$$Q_p(t) = 2\, C_a\, \phi \left(1 - \sqrt{1 - \frac{V_p(t)}{\phi}}\right) \qquad (6.5)$$

The current through the barrier layer is the derivative (with respect to time) of the charge. This can be written in terms of complex frequency

$$I_p(s) = s\ Q_p(s) \qquad (6.6)$$

d. The Diffusion Current. As is the case for barrier layer capacity, the groundwork for the diffusion capacity model is set down in Section 2.3. A relationship between the junction voltage and the excess (over the thermal equilibrium density) density of charge carriers at the junction was set down there.

$$P(o,t) = p_n \left(e^{\frac{q}{KT} V_p(t)} - 1 \right) \tag{2.26}$$

Because the voltage under stable operating conditions is a periodic function of time, this expression can easily be transformed from the time domain into the frequency domain:

$$P(0,s) = p_n L \left\{ e^{\frac{q}{KT} L^{-1} \{V_p(s)\}} - 1 \right\} \tag{6.7}$$

The solution to the diffusion equation yields a linear relationship between the excess carrier density and current (Eq. 2.30). In the frequency domain, this relationship can be written as

$$I_d(s) = \frac{qA}{\frac{\tau}{2}\left(\frac{qE}{KT}\right)} \frac{(1+s\tau)\, P(0,s)}{\left(1 + \sqrt{1+\beta(1+s\tau)}\right)} \tag{6.8}$$

Equations 6.7, 6.8 and 2.33 can be combined to form a useful current-voltage relationship.

$$I_d(s) = \frac{P_n(1+s\tau)\, L\left\{e^{\frac{q}{KT} L^{-1}\{V_p(s)\}} - 1\right\}}{\left(1 + \sqrt{1+\beta(1+s\tau)}\right)} \qquad (6.9)$$

A nonlinear differential equation which describes the behavior of the pump circuit of Fig. 6.2 can be obtained by substituting into Eq. 6.1 the magnitudes of the various currents which are expressed in Eqs. 6.2, 6.3, 6.6 and 6.9. The result is

$$0 = -I_N(s) + V_p(s)\, Y(s) + 2sC_a\phi\, L\left\{1 - \sqrt{1 - \frac{1}{\phi} L^{-1}\{V_p(s)\}}\right\}$$
$$+ \frac{P_n(1+s\tau)}{\left(1 + \sqrt{1+\beta(1+s\tau)}\right)}\, L\left\{e^{\frac{q}{KT} L^{-1}\{V_p(s)\}} - 1\right\} \qquad (6.10)$$

6.3 Iterative Techniques

The technique for solving the nonlinear differential equation (Eq. 6.10) employed is basically an extension of the Newton-Raphson approach used in the last chapter. But before describing the procedure for solving the equation, it is first necessary to make a few remarks as to the nature of the solution and the choice of the forcing function.

Here, as in Chapter V, it is assumed that the circuit is stable and there are no oscillations of any kind. The solution to the differential equation can then be taken to be periodic, with the same period as the forcing function, and the pump voltage across the

varactor can be written as

$$V_p(t) = \frac{V_A(0)}{2} + \sum_{n=1}^{\infty} [V_A(n) \cos n\omega_p t + V_B(n) \sin n\omega_p t] \qquad (6.11)$$

The fundamental component of this voltage $[V_A(1) \cos \omega_p t + V_B(1) \sin \omega_p t]$ is selected as the forcing function. $V_A(1)$ can be arbitrarily set equal to zero; this is simply equivalent to selecting a time origin.

The physical significance of this rather unorthodox choice can be seen by comparing Figs. 6.2 and 6.3. The current source driving function $I_N(t)$, in Fig. 6.2 is replaced by a series combination of a voltage source, $E_N = \frac{V_A(0)}{2} + V_B(1) \sin \omega_p t$, and an ideal filter. This filter is a short circuit at DC and at ω_p; it acts as an open circuit at all other frequencies. The current flowing through this voltage source-filter combination, plus the voltage components at harmonics of the pump frequency, will be treated as the unknowns. The term E_N is selected to be the forcing function for three important reasons:

(1) The fundamental component of pump voltage has more physical significance than the Norton equivalent current source. Only when $Y(\omega)$ is much less than the impedance of the diode (the current pumping case) is the magnitude of the current source related to the degree of hardness with which the diode is being pumped. The pump voltage, on the other hand, is related to the diode capacity by Eq. 2.1

$$C(t) = \frac{C_a}{\left(1 - \frac{V_p(t)}{\phi}\right)^{\frac{1}{2}}} \qquad (2.1)$$

Although there is no simple relationship between $V_B(1)$ and the magnitude of the capacitance coefficient at the pump frequency, there is at least a one-to-one correspondence. The hardness of pumping increases smoothly with increasing pump voltage. Even this does not always hold with the Norton current source.

(2) It is assumed here that the diode is biased with a DC voltage source. It would be unreal to bias the diode with a DC current source.

(3) The magnitudes of all the voltage components at harmonics of the pump change smoothly as the fundamental voltage component increases. It will be seen later in this section that the initial approximation used to initiate the convergence procedure must differ from the correct solution by less than a predetermined error, ϵ_{max}.

The value of ϵ_{max} is "built into" the iterative procedure and if the initial error is greater than ϵ_{max}, the sequence will not converge. It is therefore necessary to control the relationship between the initial approximation and the correct solution. To implement this, a family of solutions is constructed starting with the smallest pump magnitude and building up toward hard pumping. For each pump level, the initial approximation is the solution previously

determined for a slightly smaller pump amplitude. The voltage source forcing function insures that the solutions change smoothly, and thus guarantee that the solution previously found will be a reasonable initial approximation.

Now that the forcing function has been established, an iteration procedure for solving Eq. 6.10 can be described. The solution to Eq. 6.10 is the limit of the infinite sequence of functions

$$V'_0(t),\ V'_1(t),\ V'_2(t),\ \cdots\ V'_m(t)\ \cdots$$

and

$$V_p(t) = \lim_{m \to \infty} V'_m(t) \tag{6.12}$$

The procedure for determining this sequence is identical with the Newton-Raphson technique described in Section 5.4, except for one detail which is involved with the nature of the exponential term.

It was explained in Chapter V that the usefulness of the Newton-Raphson method depends upon how accurately the nonlinear equations are represented by their linear approximations. Normally, the first two terms of Taylor's series are used as the approximation. This works well when the nonlinearity is not strong. This is the case in Chapter V, and also for the portion of Eq. 6.10 which deals with depletion layer capacity.

The function which describes diffusion capacity is more difficult to handle. The basic form of the function is

$$f(v) = e^{\frac{q}{KT} v} \tag{6.13}$$

and at room temperature,

$$\frac{q}{KT} \approx 40 . \tag{6.14}$$

It can be easily seen that the first two terms of Taylor's series fail to approximate this function accurately. In fact, if ϵ_{max}, the magnitude of the difference between the initial approximation and the correct solution, exceeds .020 volts, a Newton-Raphson sequence of the type used in Chapter V does not converge rapidly enough to be useful.

To increase the range of convergence, two sequences of constants, F_m and G_m, are used to improve the accuracy of the linear approximation. In the mth iteration, the exponential function is approximated by

$$f(V'_m + \epsilon) \approx F_m f(V'_m) + G_m f(V'_m) \epsilon \tag{6.15}$$

rather than the conventional two term Taylor's series approximation

$$f(V'_m + \epsilon) \approx f(V'_m) + \left.\frac{df(v)}{dv}\right|_{v=V'_m} \epsilon \tag{6.16}$$

The values of F_m and G_m are determined such that they minimize

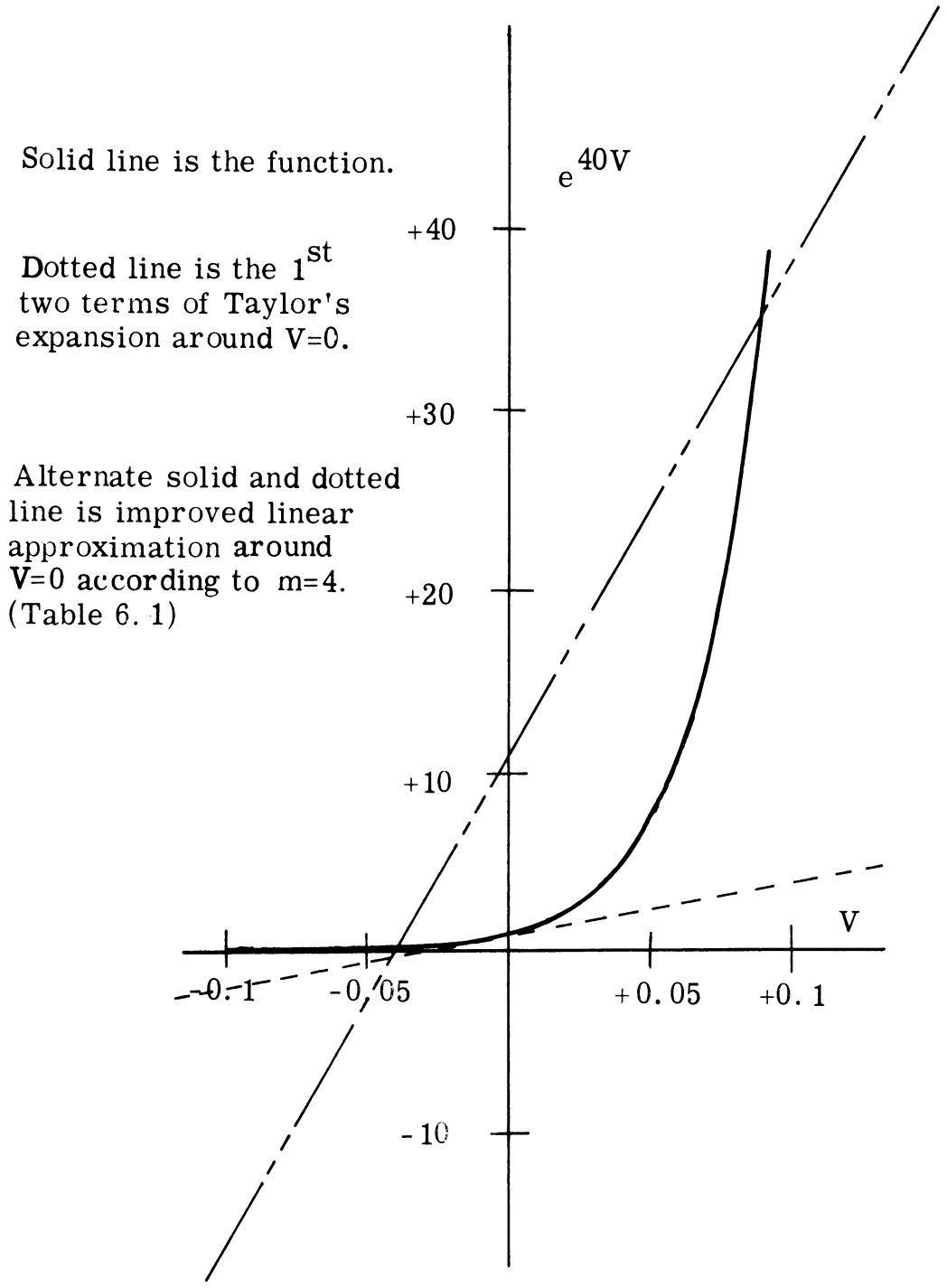

Fig. 6. 4 Exponential function and linear approximations

the maximum error between V as computed using the exact relationship (Eq. 6.13) and the approximate relationship (Eq. 6.15) over the range

$$V'_m - \epsilon_{max} \leq V \leq V'_m + \epsilon_{max} \qquad (6.17)$$

Figure 6.4 illustrates this graphically.

As the iterative sequence converges, i.e., as m increases, the error ϵ_{max} decreases, and the linear approximation can improve accordingly.

A useful sequence for F_m and G_m is shown in Table 6.1. It is assumed that the initial ϵ_{max} is less than 200 mv. This can always be achieved by constructing a family of solutions as explained earlier. If the initial ϵ_{max} is greater than 200 mv, the sequence may not converge, depending upon the relative magnitudes of the diffusion capacity and the depletion layer capacity terms.

Iteration Number, m	Max. Possible Error ϵ_{max}	F_m	G_m	Max. Possible Error Is Reduced To
1	200 mv	208.0	7450	163 mv
2	163 mv	73.5	2040	127 mv
3	127 mv	20.7	629	94 mv
4	94 mv	10.4	272	62 mv
5	62 mv	3.2	95	30 mv
6	30 mv	1.38	50	8.2 mv
7 and up	Use standard Newton-Raphson method	1.0	40	---

Table 6.1. Iteration Sequence

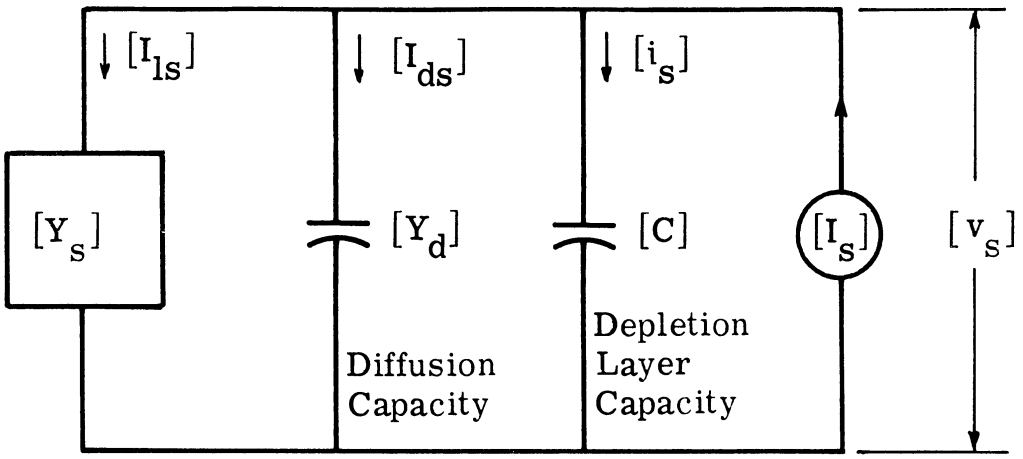

Fig. 6. 5. Signal circuit configuration used in Chapter VI.

6.4 Small Signal Equations

In the preceding two sections, a method was set down for determining the voltage, $V_p(t)$, across a varactor diode under conditions of hard pumping , but in the absence of signal. In this section, the signal is included, and the effect upon the signal of pumping the diode is determined. Figure 6.5 shows the circuit redrawn in a manner which emphasizes the signal circuit.

Admittance is used, because the depletion layer capacity appears in parallel with the diffusion capacity. The linear portion of the circuit, including the impedance of the pump source can be replaced by an equivalent (linear) admittance. This admittance must adequately model the linear circuit at the entire set of signal frequencies,

$$n\omega_p \pm \omega_1 \qquad n = 0,\ 1,\ \ldots \tag{3.7}$$

or from Table 3.1

$$\omega_1,\ \omega_2,\ \omega_3,\ \ldots \tag{6.18}$$

The pump source is not shown, since it is a linear voltage source at ω_p with zero impedance, and cannot interact with any component of signal. The signal source is represented by a current source.

The currents in the circuit of Fig. 6.5 must satisfy the elementary relationship.

$$[I_s] = [I_{ls}] + [I_{ds}] + [i_s] \tag{6.19}$$

a. The Driving Source. I_s is a current source, and is independent of the signal voltage, but the three other signal currents must be determined from the voltage-current relationships (the admittances) of the three elements.

b. The Depletion Layer Current. The admittance of the depletion layer capacity is represented by a matrix of the form of Eq. 3.22.

$$[i_s] = [C] \times [v_s \tag{6.20}$$

The individual elements of this matrix can be computed by first solving Eq. 6.10 for $V_p(t)$, the pump voltage across the diode as outlined in the previous section. In the abrupt junction case, the time varying capacity can then be computed by substituting $V_p(t)$ into Eq. 2.1.

$$C(t) = \frac{C_a}{\left(1 - \frac{V_p(t)}{\phi}\right)^{\frac{1}{2}}} \tag{2.1}$$

Since the pump voltage is periodic, the resulting capacity may be written as an exponential Fourier Series:

$$C[V_p(t)] = \sum_{n=-\infty}^{\infty} C_n e^{jn\omega_p t} \tag{6.21}$$

The capacitance coefficients in Eq. 6.21 when multiplied by the appropriate frequency form the individual elements in the matrix of Eq. 3.22.

c. The Network Current. The signal current through the linear network can be written as the product of a voltage matrix and an admittance matrix:

$$I_{ls}] = [Y_s] \times [v_s \tag{6.22}$$

The admittance of the linear network can be represented as a diagonal matrix of the form Eq. 6.23. The elements of this matrix are just the admittances (or the complex conjugate of the admittances) at the appropriate signal frequency. Recall that in deriving Eq. 3.22, it was necessary to take the complex conjugate of all the even rows in order to get a consistent set of signal voltages. It is desirable to have the admittance matrices compatible, and so the elements in all the even rows in Eq. 6.23 have also been conjugated.

$$[Y_s] = \begin{bmatrix} Y_1 & 0 & 0 & 0 & 0 & \\ 0 & Y^*_2 & 0 & 0 & 0 & \\ 0 & 0 & Y_3 & 0 & & \\ 0 & 0 & 0 & Y^*_4 & & \\ 0 & & & & \ddots & \\ \vdots & & & & & \vdots \end{bmatrix} \tag{6.23}$$

d. The Diffusion Current. The admittance of the diffusion capacity is also a matrix; the individual elements of which can be computed by using the pump voltage, $V_p(t)$. It was mentioned in Chapter II that parametric mixing occurs in diffusion capacity due to the nonlinear nature of the Boltzmann equation (Eq. 2.26). Mixing the nonlinear diffusion capacity is fundamental to the input admittance, and is described here in some detail.

The Boltzmann equation relates the excess density of mobile charge carriers at the junction to the instantaneous junction voltage.

$$P(0,t) = p_n\left(e^{\frac{q}{KT}\,v_t(t)} - 1\right) \tag{2.27}$$

When both pump and signal are present, the total voltage across the junction consists of both pump and signal components:

$$v_t(t) = V_p(t) + v_s(t) \tag{6.24}$$

$$v_t(t) = \sum_{n=-\infty}^{+\infty} \frac{\left(V_A(n) - j\frac{n}{|n|}\,V_B(n)\right)}{2}\, e^{jn\omega_p t} + \sum_{m=-\infty}^{+\infty} V_{(m\omega_p+\omega_1)}$$

$$e^{j(m\omega_p+\omega_1)t} + \sum_{m=-\infty}^{+\infty} V_{(m\omega_p-\omega_1)}\, e^{j(m\omega_p-\omega_1)t} \tag{6.25}$$

By exactly the same reasoning used in Chapter III, the pump voltage may be assumed to be much greater than the signal voltage. That is,

$$V_p(t) >> v_s(t) \tag{6.26}$$

Equations 6.24 and 6.25 may be substituted in Eq. 2.27 and the result simplified because of Eq. 6.26. The result is

$$P(0,t) = p_n e^{\frac{q}{KT}} \left[\sum_{n=-\infty}^{+\infty} \frac{\left(V_A(n) - j \frac{n}{|n|} V_B(n)\right)}{2} e^{jn\omega_p t} \right] - p_n$$

$$+ \frac{q}{KT} p_n \left(\sum_{m=-\infty}^{+\infty} V_{(m\omega_p+\omega_1)} e^{j(m\omega_p+\omega_1)t} + \sum_{m=-\infty}^{+\infty} V_{(m\omega_p-\omega_1)} \right.$$

$$\left. e^{j(m\omega_p-\omega_1)t} \right) \left(e^{\frac{q}{KT}} \left[\sum_{n=-\infty}^{+\infty} \frac{\left(V_A(n) - j \frac{n}{|n|} V_B(n)\right)}{2} e^{jn\omega_p t} \right] \right) \tag{6.27}$$

Now the individual terms in Eq. 6.27 may be identified. The first term on the right hand side is just the carrier density due to pump in the absence of signal. This component of carrier density is

$$P_p(t) \triangleq \sum_{n=-\infty}^{\infty} \rho_n e^{jn\omega_p t} = p_n e^{\frac{q}{KT}} \left[\sum_{n=-\infty}^{\infty} \frac{\left(V_A(n) + j \frac{n}{|n|} V_B(n)\right)}{2} e^{jn\omega_p t} \right] \tag{6.28}$$

The coefficients of this series, the ρ_n's, can be determined by first solving the pump circuit differential equation (Eq. 6.10) for the pump voltage, and then expanding Eq. 6.28.

The last term on the right hand side of Eq. 6.27 is the signal component of carrier density. By using the definition of Eq. 6.28, it may be written as

$$P_s(t) \triangleq \sum_{n=-\infty}^{+\infty} \sigma_{(n\omega_1+\omega_1)}\, e^{j(n\omega_p+\omega_1)t} + \sum_{n=-\infty}^{+\infty} \sigma_{(n\omega_p-\omega_1)}\, e^{j(n\omega_p-\omega_1)t}$$

$$= \frac{q}{KT}\, P_p(t) \left\{ \sum_{n=-\infty}^{+\infty} V_{(n\omega_p+\omega_1)}\, e^{j(n\omega_p+\omega_1)t} \right.$$

$$\left. + \sum_{n=-\infty}^{+\infty} V_{(n\omega_p-\omega_1)}\, e^{j(n\omega_p-\omega_1)t} \right\} \qquad (6.29)$$

and

$$\sum_{n=-\infty}^{+\infty} \sigma_{(n\omega_p+\omega_1)}\, e^{j(n\omega_p+\omega_1)t} + \sum_{n=-\infty}^{+\infty} \sigma_{(n\omega_p-\omega_1)}\, e^{j(n\omega_p-\omega_1)t}$$

$$= \frac{q}{KT} \left\{ \sum_{m,\, n=-\infty}^{+\infty} \rho_n\, V_{(m\omega_p+\omega_1)}\, e^{j[(m+n)\omega_p+\omega_1]t} + \right.$$

$$\left. \sum_{m,\, n=-\infty}^{+\infty} \rho_n\, V_{(m\omega_p-\omega_1)}\, e^{j[(m+n)\omega_p-\omega_1]t} \right\} \qquad (6.30)$$

The right hand side of Eq. 6.30 can now be rearranged, and the coefficients of the individual components identified.

$$\sigma_{(n\omega_p\pm\omega_1)} = \frac{q}{KT} \sum_{m=-\infty}^{\infty} \rho_m\, V_{[(n-m)\omega_p\pm\omega_1]} \qquad (6.31)$$

The relationship between the charge carrier density and the current was derived in Section 2.3. It is a linear relation which resembles an expression for admittance and it can be written as

$$I_{\omega} = \frac{P_n(1 + j\omega\tau)\ \sigma_{\omega}}{\left(1 + \sqrt{1 + \beta(1+j\omega\tau)}\right)} \tag{6.32}$$

The current due to diffusion at any signal frequency is found by combining Eq. 6.31 and Eq. 6.32.

$$I_{(n\omega_p \pm \omega_1)} = \frac{q\ P_n[1 + j(n\omega_p \pm \omega_1)\tau]}{KT\left(1 + \sqrt{1+\beta[1+j(n\omega_p \pm \omega_1)\tau]}\right)} \sum_{m=-\infty}^{\infty} \rho_m\ V_{[(n-m)\omega_p \pm \omega_1]} \tag{6.33}$$

This expression relates any one component of diffusion capacity signal current to all the components of signal voltage. It is convenient here to combine all the components of current into a single expression which has the same form as the matrix of Eq. 3.22.

$$I_{ds}] = [Y_d] \times [v_s \tag{6.34}$$

Where

$$[Y_d] = \begin{bmatrix} \frac{q}{KT} \frac{P_n(1+j\omega_1\tau)\,\rho_0}{1+\sqrt{1+\beta(1+j\omega_1\tau)}} & \frac{q}{KT} \frac{P_n(1+j\omega_1\tau)\,\rho_1}{1+\sqrt{1+\beta(1+j\omega_1\tau)}} & \frac{q}{KT} \frac{P_n(1+j\omega_1\tau)\,\rho_{-1}}{1+\sqrt{1+\beta(1+j\omega_1\tau)}} & \cdots \\ \frac{q}{KT} \frac{P_n(1-j\omega_2\tau)\,\rho_{-1}}{1+\sqrt{1+\beta(1-j\omega_2\tau)}} & \frac{q}{KT} \frac{P_n(1-j\omega_2\tau)\,\rho_0}{1+\sqrt{1+\beta(1-j\omega_2\tau)}} & \cdots & \\ \frac{q}{KT} \frac{P_n(1+j\omega_3\tau)\,\rho_1}{1+\sqrt{1+\beta(1+j\omega_3\tau)}} & \frac{q}{KT} \frac{P_n(1+j\omega_3\tau)\,\rho_2}{1+\sqrt{1+\beta(1-j\omega_2\tau)}} & \cdots & \\ \frac{q}{KT} \frac{P_n(1-j\omega_4\tau)\,\rho_{-2}}{1+\sqrt{1+\beta(1-j\omega_4\tau)}} & & & \\ \vdots & \vdots & \vdots & \vdots \end{bmatrix}$$

The final form of the admittance seen by the current source is obtained by combining Eqs. 6.19, 6.20, 3.22, 6.23, and 6.34. The result is written out in Eq. 6.35. I_s and v_s are column matrices, but to determine the input impedance, signal is applied only at one frequency, ω_1; and thus only one term of the I_s matrix is non-zero. However in computing the noise of a parametric amplifier, it is necessary to account for noise which is generated at frequencies other than ω_1, but is parametrically mixed with the pump and appears at the output. This can be done by assuming that the shot noise in the diode and the thermal noise in all the resistors are uncorrelated at all the signal frequencies. Noise due to each of these sources at any signal frequency can then be represented by an independent current source. In this case, I_s is a column matrix consisting of non-zero terms each of which represents the total noise generated at a particular signal frequency.

$$I_s] = [Y_s] \times [v_s + [Y_d] \times [v_s + [C] \times [v_s \qquad (6.35)$$

That is,

$$I_s] = [Y_t] \times [v_s$$

where

$$[Y_t] = [Y_s] + [Y_d] + [C]$$

The first few terms of the complete admittance matrix $[Y_t]$ are written out in Eq. 6.36.

$$
\left[Y_t\right] = \begin{bmatrix}
Y_1 + \frac{q}{KT}\,\frac{P_n(1+j\omega_1\tau)}{1+\sqrt{1+\beta+j\beta\omega_1\tau}}\,\rho_0 + j\omega_1 C_0 & \frac{q}{KT}\,\frac{P_n(1+j\omega_1\tau)}{1+\sqrt{1+\beta+j\beta\omega_1\tau}}\,\rho_1 + j\omega_1 C_1 \cdots \\
\frac{q}{KT}\,\frac{P_n(1-j\omega_2\tau)}{1+\sqrt{1+\beta-j\beta\omega_2\tau}}\,\rho_{-1} - j\omega_2 C_{-1} & Y_2^* + \frac{q}{KT}\,\frac{P_n(1-j\omega_2\tau)}{1+\sqrt{1+\beta-j\beta\omega_2\tau}}\,\rho_0 - j\omega_2 C_0 \cdots \\
\frac{q}{KT}\,\frac{P_n(1+j\omega_3\tau)}{1+\sqrt{1+\beta+j\beta\omega_3\tau}}\,\rho_1 + j\omega_3 C_1 & \frac{q}{KT}\,\frac{P_n(1+j\omega_3\tau)}{1+\sqrt{1+\beta+j\beta\omega_3\tau}}\,\rho_2 + j\omega_3 C_2 \cdots \\
\frac{q}{KT}\,\frac{P_n(1-j\omega_3\tau)}{1+\sqrt{1+\beta+j\beta\omega_4\tau}}\,\rho_{-2} - j\omega_4 C_{-2} & \\
\vdots & \vdots
\end{bmatrix}
\qquad (6.36)
$$

The C's and ρ's are determined by solving Eq. 6.10; β and P_n are constants of the diode

The input admittance at ω_1 can be obtained by manipulating this matrix. A number of schemes can be used, however, the method used here is to reduce the matrix to its lower triangular form. The desired admittance is then just the (1, 1) element of this new matrix.

6.5 Summary

In this chapter, the results of the previous chapter were extended to the hard pumping case. Both depletion layer and conduction effects have been accounted for. A nonlinear differential equation which describes the pump circuit was set up, and an iterative technique for solving it was presented. This iterative technique requires the use of a digital computer. Once the behavior of the pump has been determined, the signal is added to the circuit. The signal circuit behavior is expressed in a matrix formulation, the elements of which are determined by the pump circuit. The small signal input impedance is then obtained by manipulating this matrix.

The numerical results which are presented in Chapter VII were obtained by an algorithm of the procedures outlined in this chapter. The flow diagram of this program is similar to the one presented in Appendix D.

CHAPTER VII

EXPERIMENTAL WORK AND CONCLUSIONS

7.1 Introduction

Throughout the course of this research, a great deal of experimental work has been performed. This work was of considerable aid in the development of the theoretical portions of the thesis, particularly in the determination of accurate mathematical models for the varactor diode and its associated circuitry. The experiments were performed concurrently with the development of the theory, and as the work progressed, the theory and circuit model were constantly altered to conform with the observed facts. The result of this process is an accurate characterization for pumped varactor circuits, which can be utilized by an engineer to determine circuit behavior.

Three circuits were built and tested. The first two served mainly in the development of the depletion layer capacity theory of Chapter V. These two circuits are termed the "Lumped Circuit" and the "Distributed Circuit." The third circuit is termed the "Diffusion Circuit" and aided in the development of the theory presented in Chapter VI. A description of these circuits and the measurement methods is found in the next section.

In Section 7.3, the results of the experiments are presented along with the corresponding theoretical results. In general,

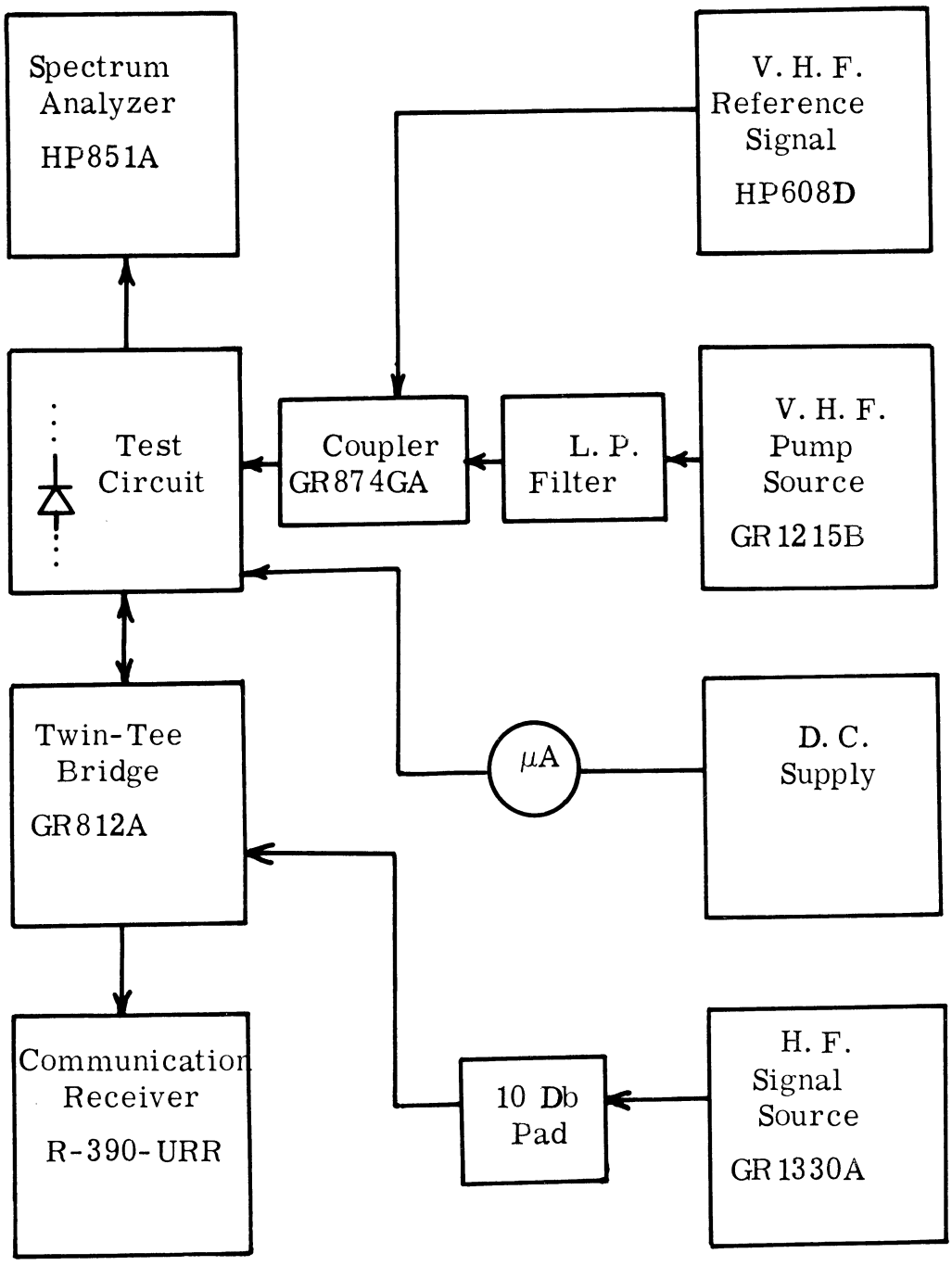

Fig. 7. 1. Block Diagram of measurement apparatus

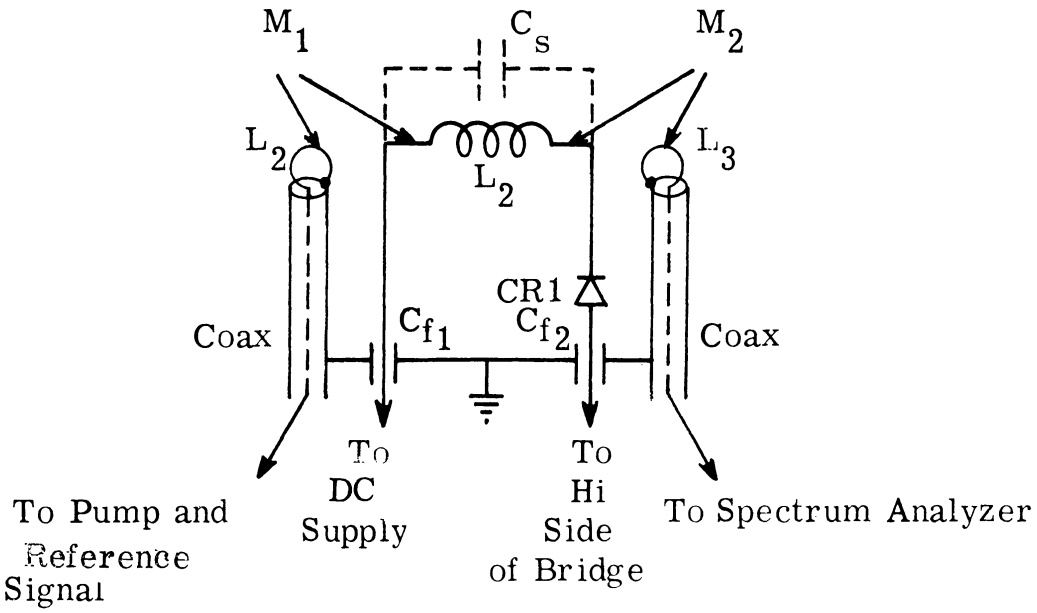

Fig. 7.2. Circuit used for measurement on lumped circuit and diffusion circuit

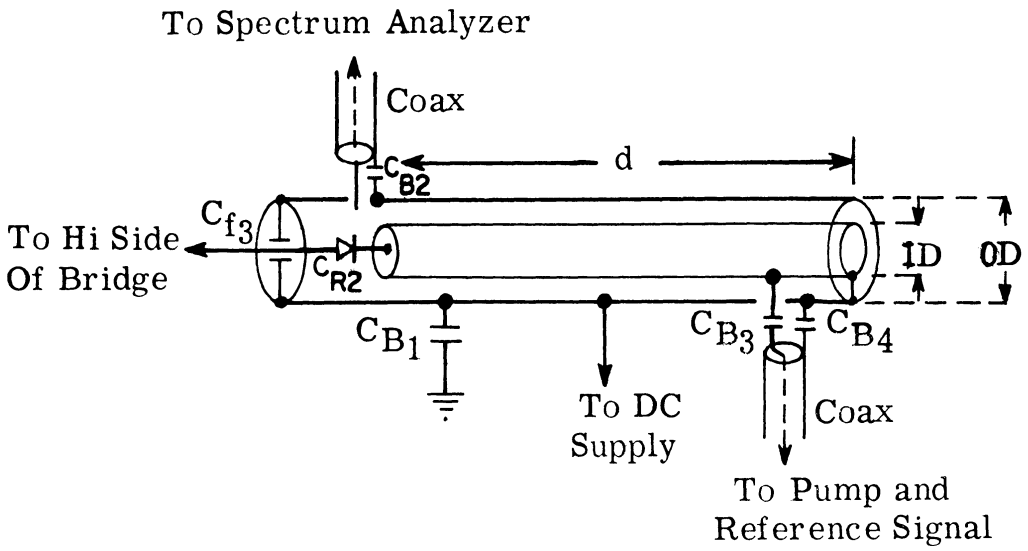

Fig. 7.3. Circuit used for measurements on distributed circuit

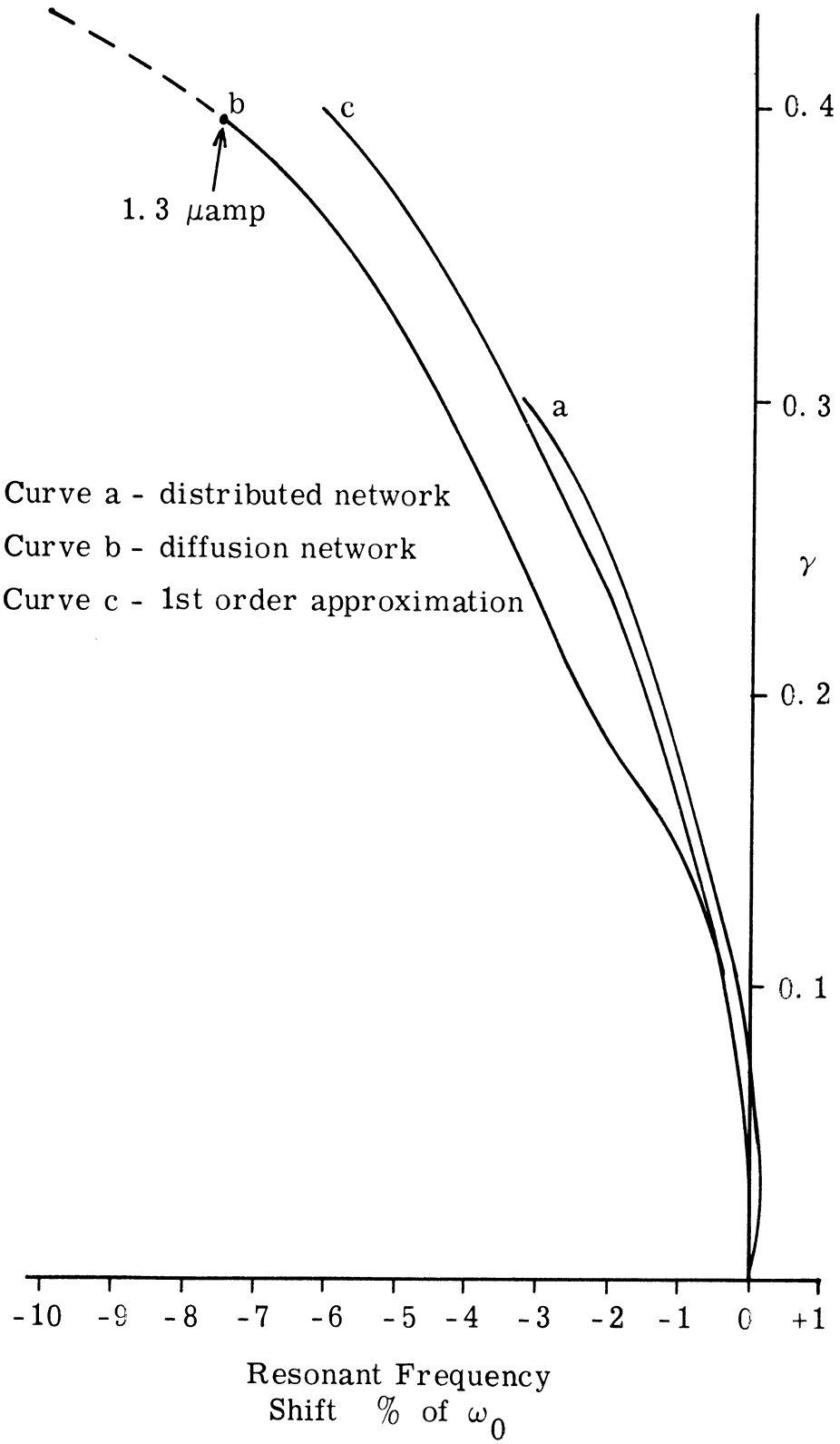

Fig. 7.4. Pumping hardness as a function of resonant frequency shift

excellent agreement is obtained between the experimental results and the theoretical results. The conclusions of this study are discussed in Section 7.4.

7.2 Experimental Methods

A block diagram of the measurement apparatus is shown in Fig. 7.1. The experimental setup is the same for each of the three circuits. The impedance of the varactor under test is measured at a High-Frequency signal (ω_1) on the parallel tee bridge, using the Communication's Receiver as a null-detector. The High-Frequency signal is of course supplied to the varactor circuit through the bridge. The frequency of this signal is in the 0.5 MHz to 10 MHz range.

DC bias is supplied to the varactor through a micro-amp meter which monitors the change in DC current with pump power.

It is necessary to make all the input impedance measurements under "small signal" conditions; that is, the signal components must be restricted to the set of frequencies (3.7). The presence of any components in the set (3.11) indicates that the small signal conditions are not satisfied. The spectrum analyzer is used to observe the amplitudes of these signal components, and if any undesired higher order sidebands are present, the signal source is attenuated until small signal conditions are obtained. In practice, the undesired signal components are always kept at least 20 Db down from the largest

component in the signal set.

The spectrum analyzer is also used in conjunction with the VHF reference signal to determine the pumping hardness. A definition of pumping hardness is

$$\gamma \triangleq \left| \frac{C_1}{C_0} \right| \tag{3.31}$$

or alternatively

$$\gamma \triangleq \left| \frac{S_1}{S_0} \right| \tag{7.1}$$

where the S's and C's are the Fourier coefficients of the exponential series. An adjustable inductive coupler permits a low amplitude VHF reference signal (ω_1) to be added to the pump power (ω_1). As explained below, this reference signal is useful in determining the pumping hardness. The frequency of both the reference signal and the pump are in the 60 MHz to 120 MHz range.

At these frequencies, there is no direct method to measure γ. However, an indirect method proved to be quite satisfactory. It is known that the average capacity of the varactor increases with pump voltage. Hence, the resonant frequency of the tuned circuit decreases with pump amplitude. To measure γ then, we simply insert the small amplitude VHF reference signal, and note the frequency of peak response. This will usually be slightly lower (0 - 10%)

than the unpumped resonant frequency of the circuit. In some cases, however it may actually be higher because the signal response depends not only upon the average capacity of the diode but also, and to a lesser extent, upon parametric mixing with the pump. The value of γ can be obtained by comparing the measured shift in resonant frequency with a plot of "γ versus shift" which can be computed using the theory.

This method of experimentally determining γ is simple and reasonably accurate. The only difficulty lies in finding the peak response points, for the response curve tends to flatten out (the circuit Q appears to become lower) as pumping increases.

Plots of "γ versus shift" are shown in Fig. 7.4. Curve "a" is for the distributed network which is described in (Fig. 7.3; Table 7.2) when it is pumped at resonance. Curve "b" is for the diffusion capacity circuit (Fig. 7.2; Table 7.1) when pumped at resonance. For a resonant frequency shift greater than about 7.5%, curve "b" has little meaning, for beyond this point the diode is drawing a measurable amount of DC current. It is much easier to read this current, and correlate it with γ than it is to measure the shift in resonant frequency. In fact, measurement of DC current is the accepted method of determining γ. However, it has not only the disadvantage of yielding no qualitative information when pumping is not hard enough to draw rectified current, but also may be inaccurate due to reverse avalanche current (Ref. 54).

Curve "c" is a first order approximation. It is derived in the following paragraph using the approximate relations developed in Appendix B.

For an abrupt junction diode (N= 2) and small current so that only the first terms of the expansions are important (B. 12) and (B. 13) can be combined with (B. 7) and (B. 9) to obtain

$$C_0 = (1 + .5a^2)\, C_B \tag{7.2}$$

$$C_1 = (-.5a)\, C_B \tag{7.3}$$

The shift in resonant frequency is given by

$$\delta_\omega \approx \frac{-\delta C \omega_0}{2 C_0} \tag{7.4}$$

Combining (7. 4) and (7. 2) and using (7. 3) in the definition of γ in Eq. 3. 31, an approximate relation between γ and δ_ω is obtained

$$\frac{\delta_\omega}{\omega_0} \approx -.38\gamma^2 \tag{7.5}$$

This is the approximate relationship plotted in Fig. 7. 4(c).

Figure 7. 2 shows the test circuits which were used for the lumped circuit and for the diffusion capacity measurements. The DC bias is returned to ground through the bridge. Element values

for both circuits are given in Table 7. 1.

	Lumped Circuit	Diffusion Capacity Circuit
Diode Type CR 1	PC 1430 D	PC 0622 C
Nominal Diode Capacity	7. 2 pf @ -4 volts	14. 6 pf @ -4 volts
Bias Voltage V_{Bias}	-18. 0 volts	-2. 0 volts
Diode Capacity at V_{Bias}	3. 7 pf	18. 4 pf
Inductor L_1	0. 93 μh	0. 179 μh
Inductor Stray Capacity C_s	0. 9 pf	0. 75 pf
Inductors L_2, L_3	Negligible	Negligible
Mutual Inductances M_1, M_2	Negligible	Negligible
C_{f1}	11000 pf	11000 pf
C_{f2}	1000 pf	1000 pf
Small Signal Resonance ω_0	76. 0 MHz	84 MHz
Small Signal Q	100	56

Table 7. 1. Lumped and Diffusion Capacity Circuit Parameters

Figure 7. 3 shows the test circuit built for measurements on a distributed circuit. Element values are given in Table 7. 2. The body of the cavity is machined of brass. DC bias is returned to ground through the bridge, while the cavity itself is at potential V_{Bias} from ground.

	Distributed Circuit
Diode Type CR2	PC 0642 C
Nominal Diode Capacity	13.4 pf @ -4 volts
Bias Voltage V_{Bias}	-25.0 volts
Diode Capacity at V_{Bias}	5.7 pf
I.D.	0.244 in.
O.D.	0.5625 in.
Length d	26.5 in.
C_{B1}	10 μf
C_{f2}, C_{f3}	1000 pf
C_{B3}, C_{B4}	4000 pf
Small Signal Resonance ω_0	100 MHz
Small Signal Q	140

Table 7.2. Distributed Circuit Parameters

7.3 Experimental and Comparative Theoretical Results

a. The Pump Circuit Solution. As described in the previous two chapters, the first step in determining the behavior of a pumped varactor circuit is to solve the pump circuit equation, that is, determine the circuit behavior with pump power applied, but with the signal amplitude at zero. The solution to this nonlinear equation takes the form of a nonsinusoidal periodic waveform, which if desired can be

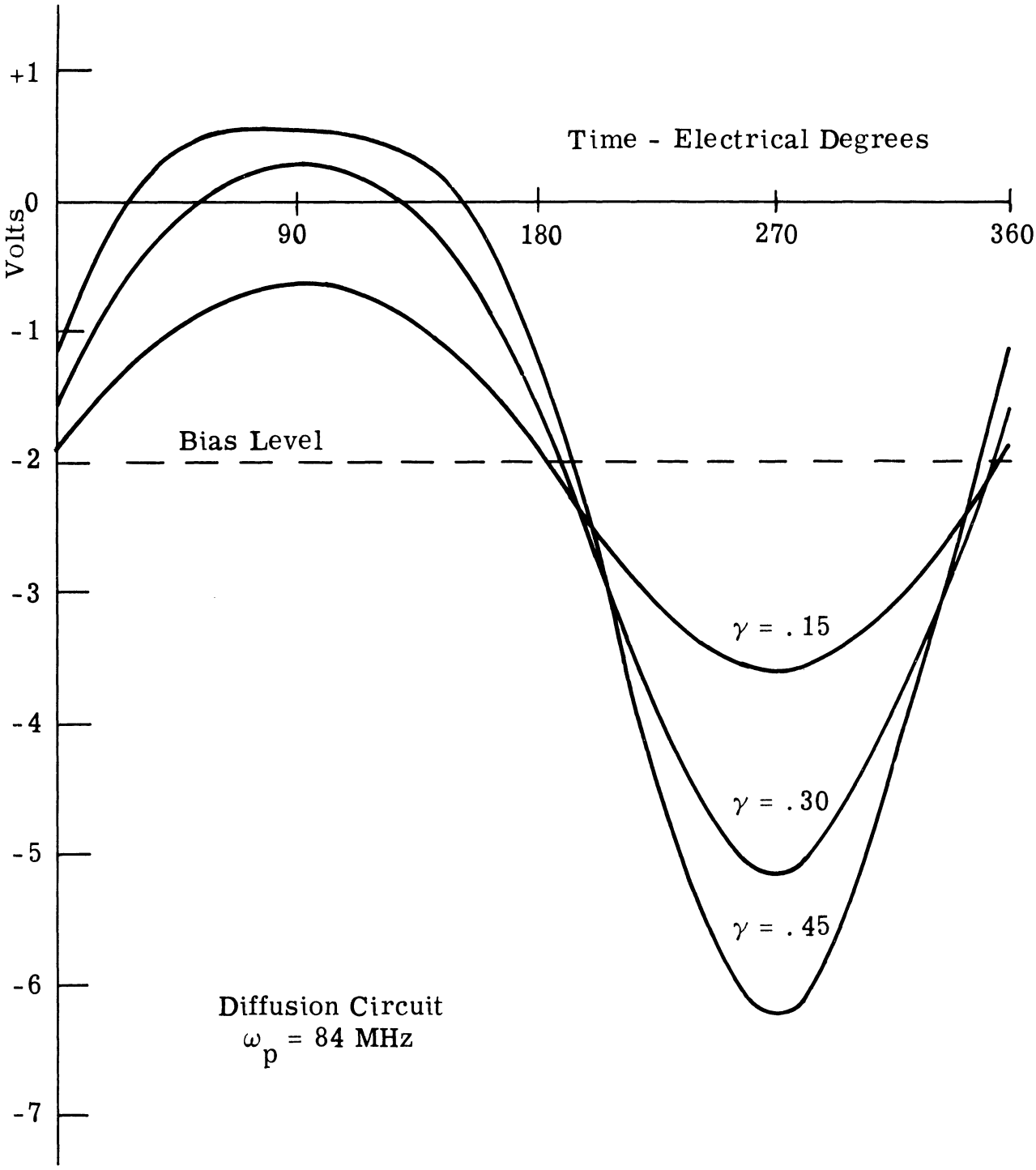

Fig. 7.5. Diode voltage waveforms

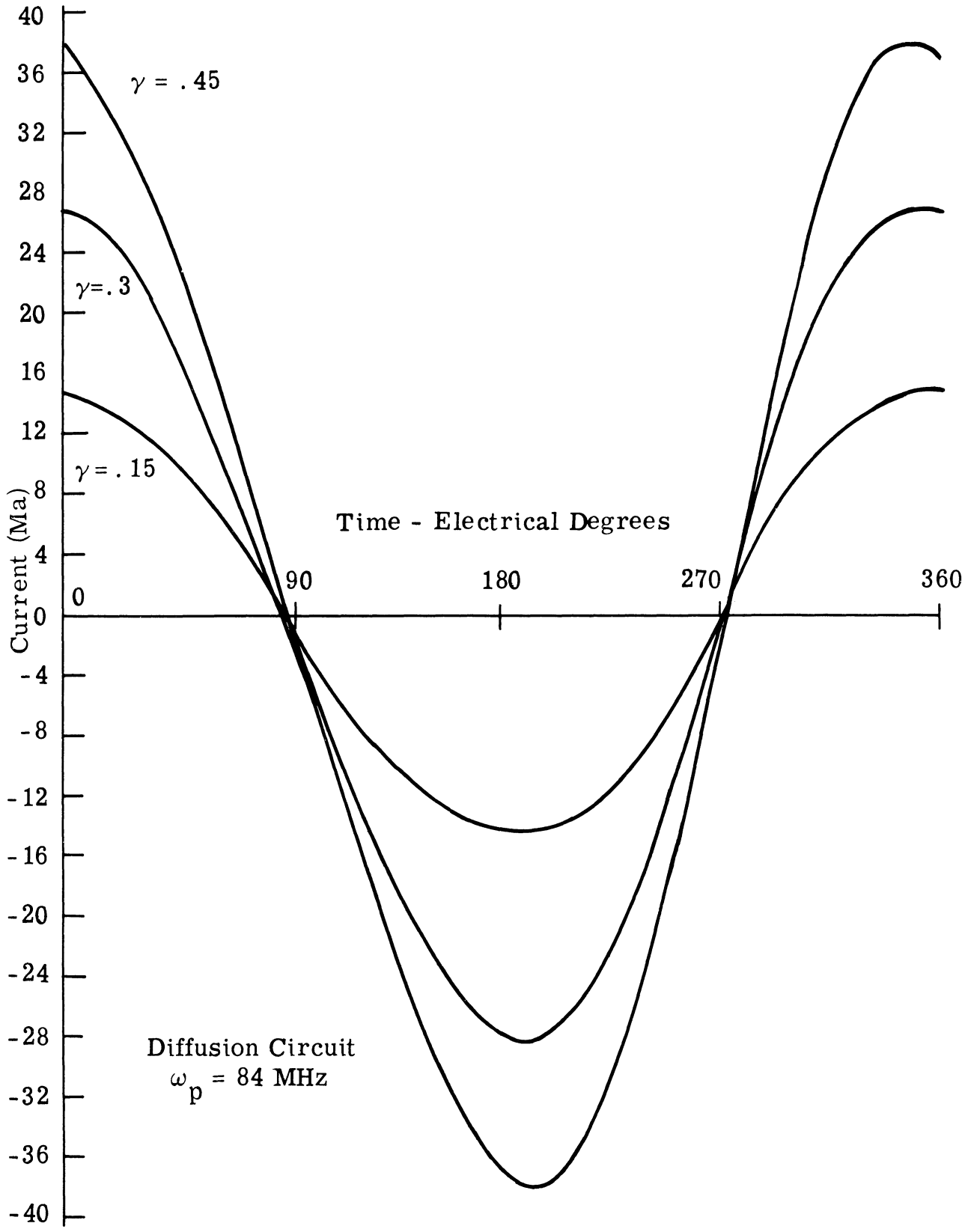

Fig. 7.6. Total current waveforms

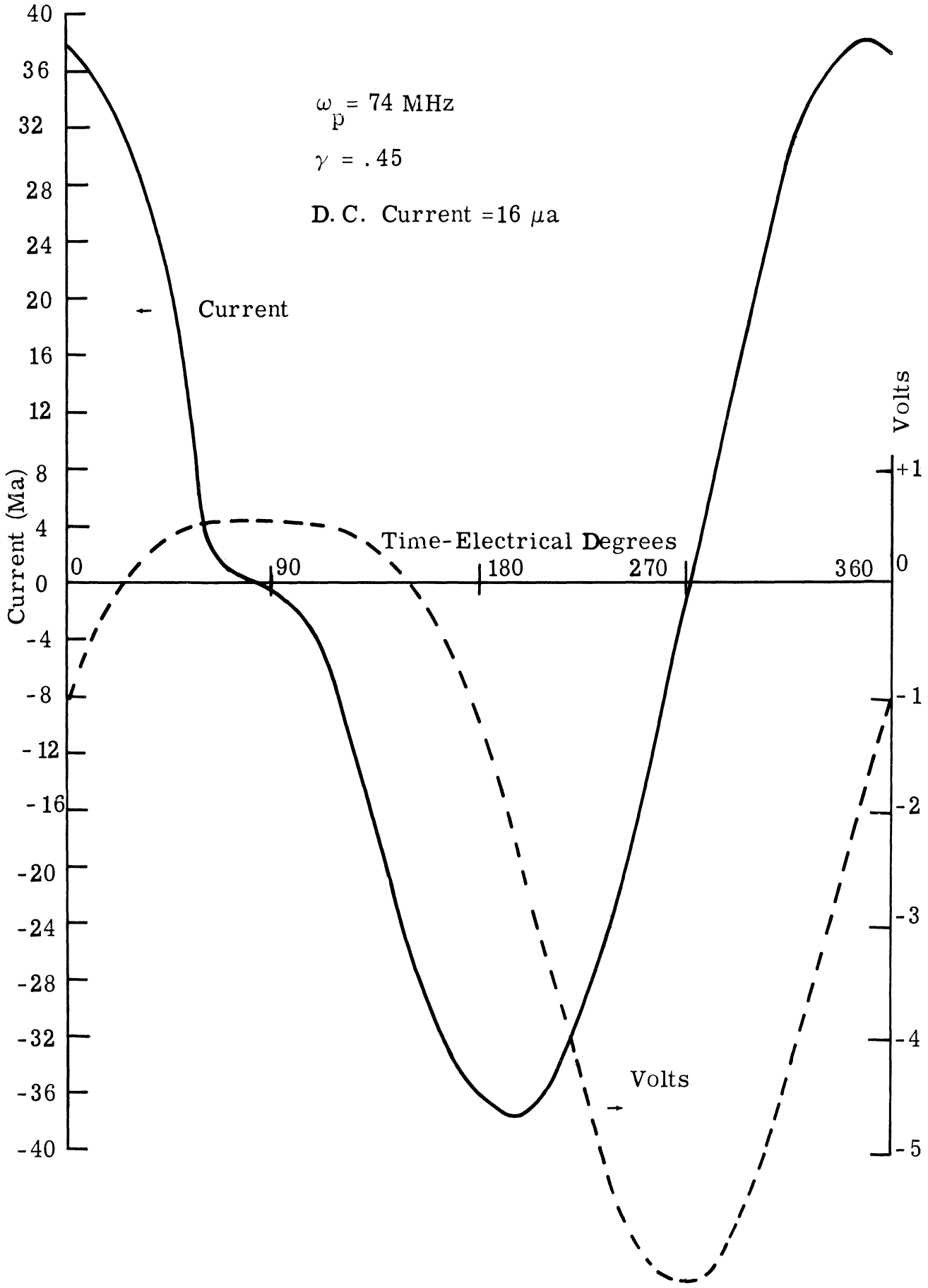

Fig. 7.7a. Barrier layer capacity current waveform

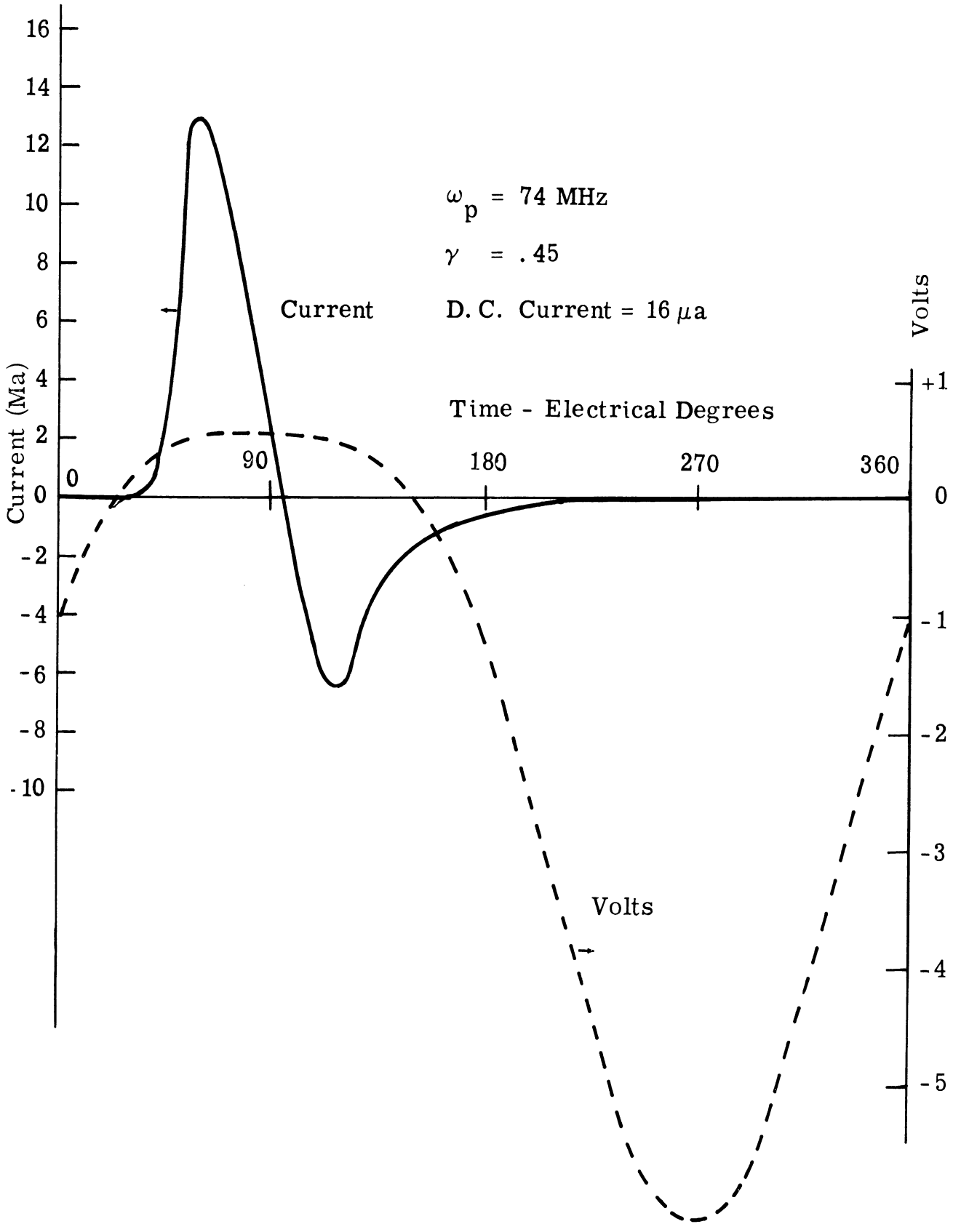

Fig. 7.7b. Diffusion current waveform

expressed as a Fourier series.

A few computed waveforms for the "Diffusion Circuit" are illustrated in Figs. 7.5 and 7.6. Figure 7.5 shows the voltage waveform across the diode for three values of pumping. The most notable feature is the clipping which occurs as the diode is driven into the region near zero voltage. Here, the capacity-voltage curve has the greatest curvature. As the pump level increases, the clipping becomes more pronounced as the diode is driven into forward conduction during the peak of the cycle. The characteristics for all the diodes used in the experiments are summarized in Appendix E.

The total current wave shape is shown in Fig. 7.6. By comparing 7.5 with 7.6, it can be seen that the current waveshape is more nearly sinusoidal than the voltage wave shape. This can be understood by noting that the inductor presents a high impedance to the harmonic components of current, and tends to open circuit them. For this particular circuit, the current source approximation, in which only the fundamental component of current is allowed to flow is a quite accurate approximation.

The currents shown in Fig. 7.6 are the total currents flowing through the diode. The two components of current are shown in Fig. 7.7. The portion of current due to barrier capacity is shown in Fig. 7.7a, while that current due to forward conduction and diffusion effects are shown in Fig. 7.7b. The diffusion currents for $\gamma = .15$ and $\gamma = 0.30$ are negligible.

The distinction between these components is important because the diffusion current produces shot noise, while the current flowing through the barrier capacity is noise free.

The double-spike waveform of the diffusion current occurs because the carrier lifetime is long compared with a period of the pump cycle. Hence, few of the carriers injected across the junction during the positive portion recombine, and when the voltage begins to decrease, they are swept back across the junction. In this regard, it is interesting to note that the current in the negative spike may actually be larger than the current in the positive spike. An avalanche effect may be initiated by the carriers coming back across the junction. The result may be a net reverse rather than a forward current (Ref. 54). This phenomenon was not observed during the course of these experiments.

b. The Elastance Coefficients. After the solution to the pump circuit has been computed, the next step in determining the behavior of a pumped varactor circuit is to calculate the elastance coefficients. Some theoretical results of these calculations is shown in Figs. 7.8 through 7.12. The magnitudes of the harmonic elastance coefficients for a variety of conditions are plotted as a function of S_1/S_0, that is as a function of γ. No direct experimental verification of this portion of the theory was obtained, for at these frequencies, it is impossible to measure the time varying capacity directly.

Figure 7.8 illustrates the harmonic elastance coefficients

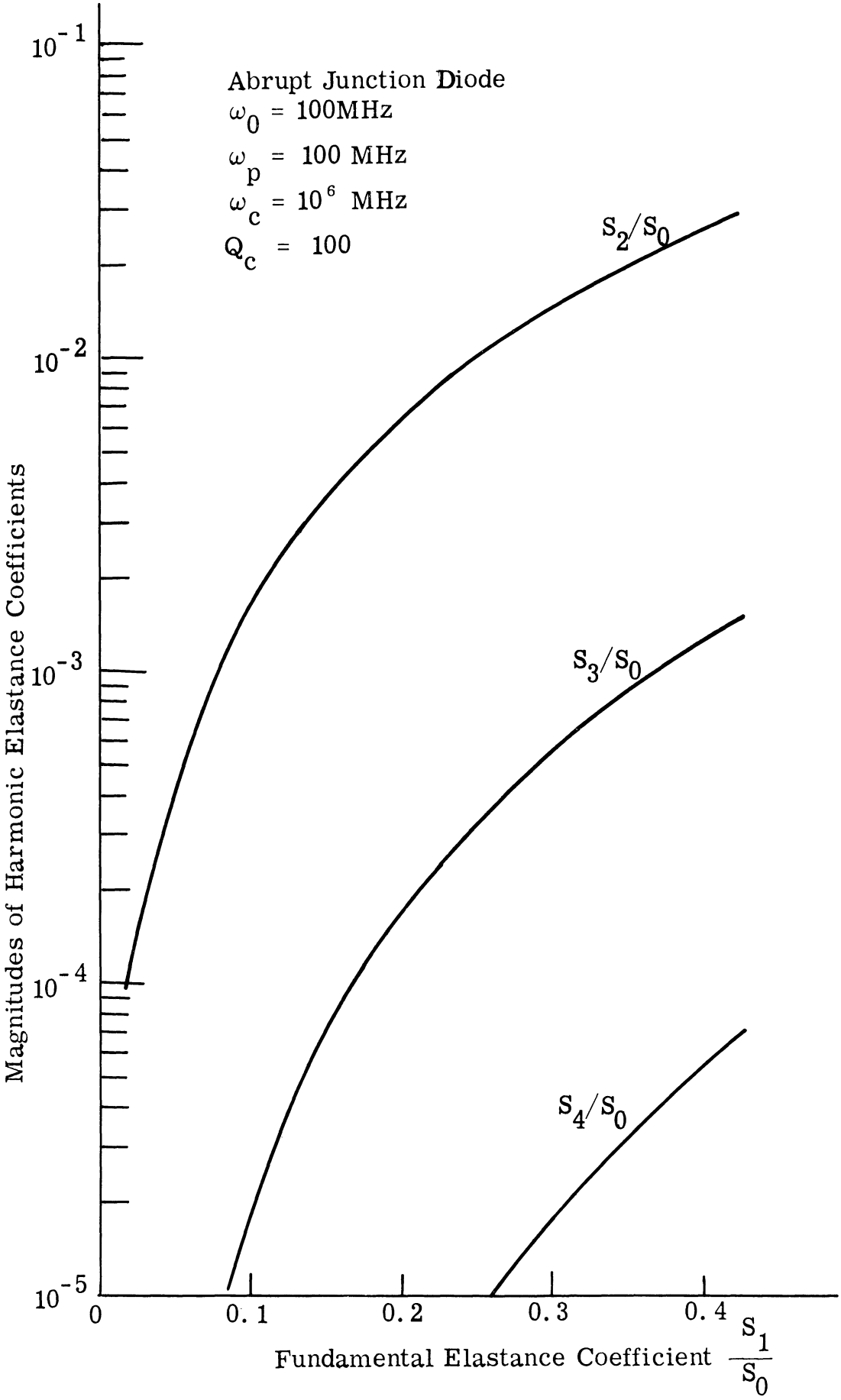

Fig. 7.8. Harmonic elastance coefficients for a lumped circuit

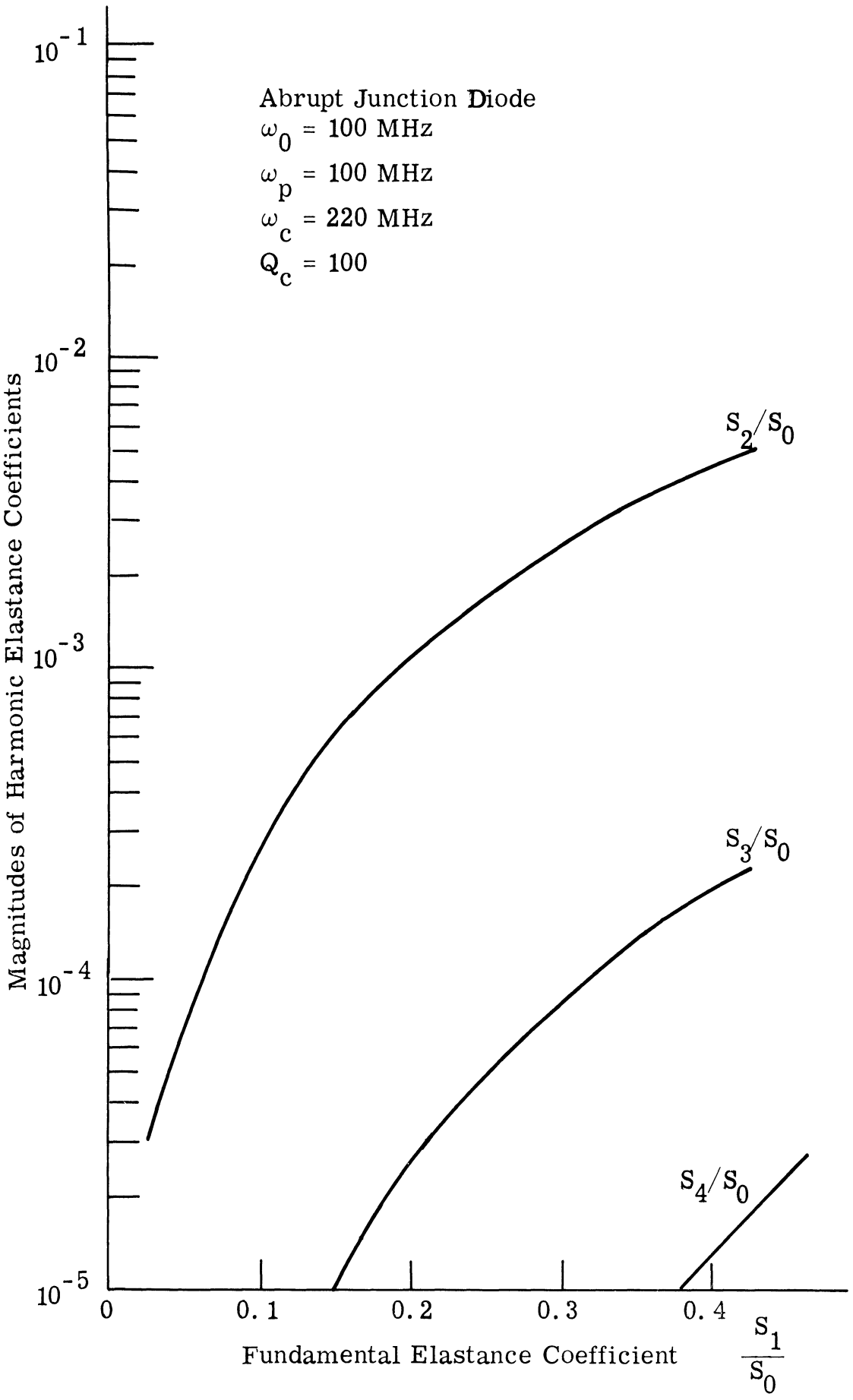

Fig. 7.9. Harmonic elastance coefficients for a lumped circuit with distributed capacity

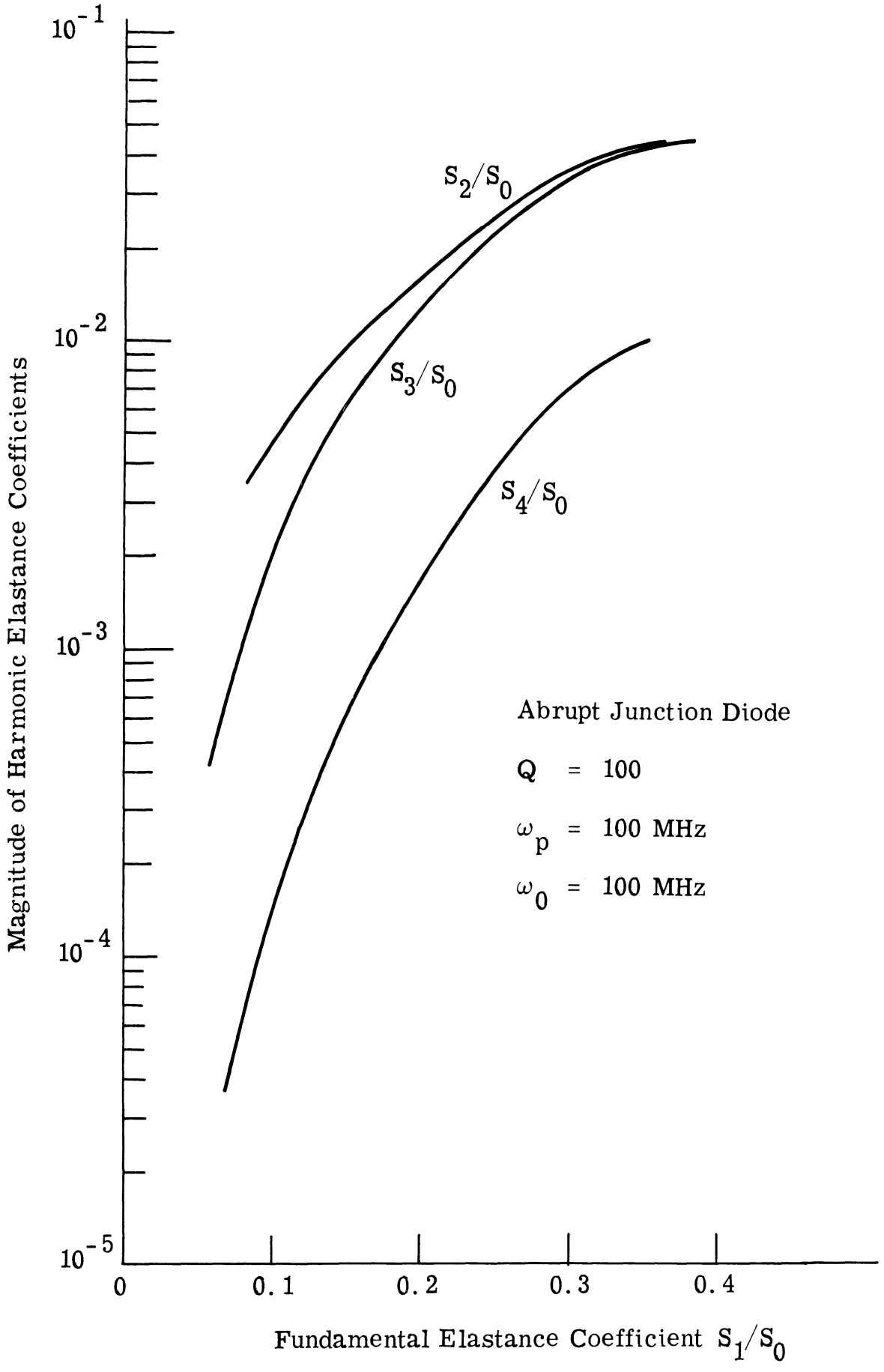

Fig. 7.10. Harmonic elastance coefficients for a distributed circuit

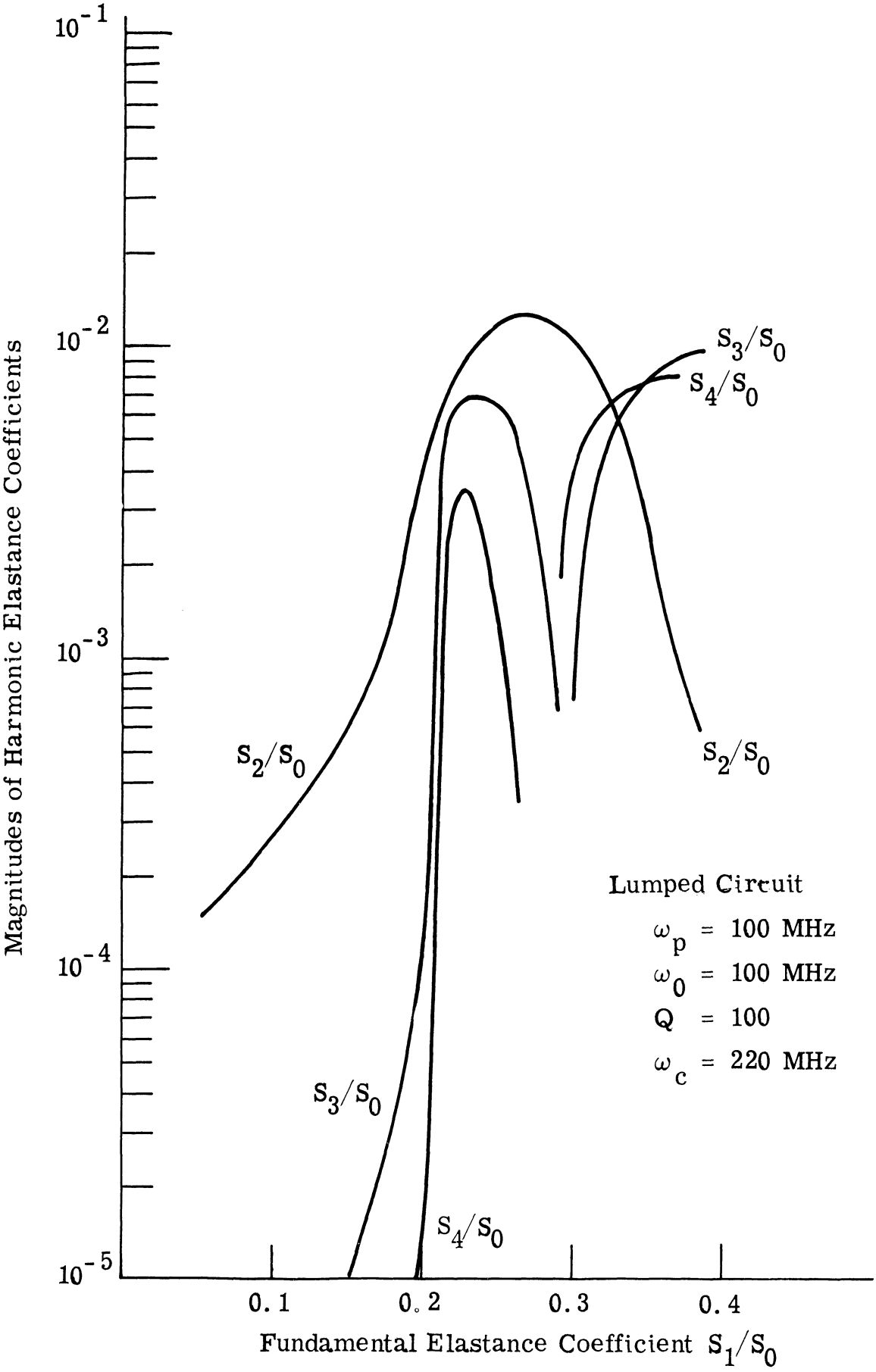

Fig. 7.11. Harmonic elastance coefficients for an actual diode

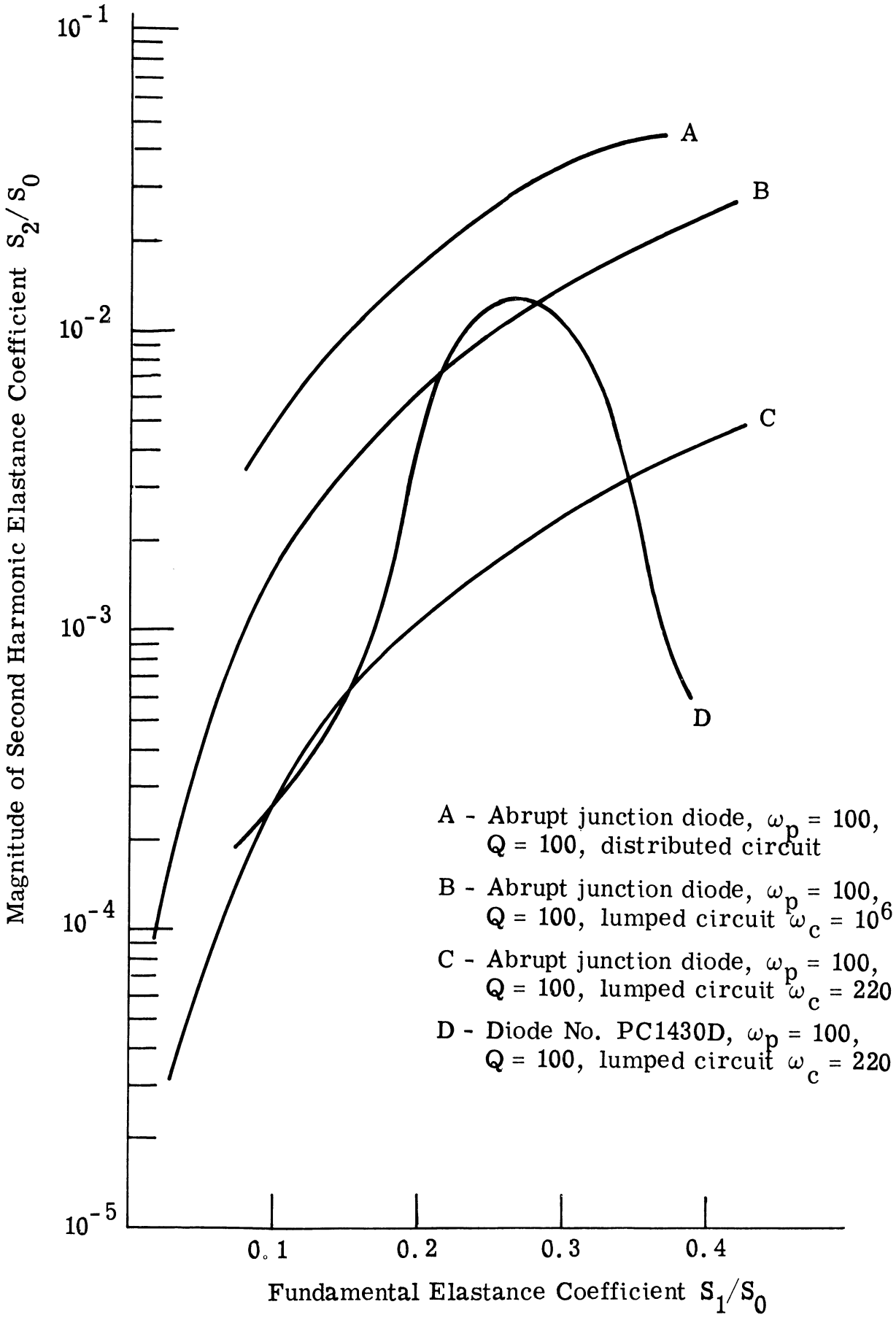

Fig. 7.12. Comparison of harmonic elastance coefficients for different circuit conditions

for a lumped circuit of the type shown in Fig. 7.2. The diode is assumed to be an ideal abrupt junction device having a characteristic of the form (Eq. 2.12). The self-capacity of the coil is assumed to be negligibly small. Figure 7.9 represents the same conditions, except that here the self-capacity of the coil has assumed a practical value, making the coil self-resonant at a frequency just above the second harmonic of the pump. The effect of the resulting pole of impedance can be clearly seen by comparing Fig. 7.8 with Fig. 7.9. It virtually open circuits the second harmonic, prevents current from flowing and lowers the harmonic content of the elastance.

Figure 7.10 illustrates the harmonic elastance coefficients for a distributed circuit of the type shown in Fig. 7.3. As in Figs. 7.8 and 7.9, the diode is assumed to be an abrupt junction device. However in contrast to the circuit conditions of Fig. 7.9, this circuit has an infinity of series type resonances or zeros. The most important of these resonances lies near the third harmonic of the pump. This zero of impedance virtually short circuits the third harmonic, which results in a large component of current flowing at this frequency and raises the harmonic content of the elastance.

These figures indicate that the magnitudes of the harmonic elastance coefficients are strongly dependent upon the circuit impedance at the harmonic frequencies. From Appendix B, note that if the commonly used open circuit approximations were used, all the harmonic elastance coefficients would be zero.

Figure 7.11 illustrates the harmonic elastance coefficients for the same conditions as those in Fig. 7.9 except that data on an actual diode rather than an idealized abrupt junction device was used for the computations. Each of the deep nulls in the curves is accompanied by a 180^{o} shift in phase.

Figure 7.12 is intended to summarize the results in Figs. 7.8 through 7.11. The second harmonic elastance coefficient is plotted for each of the conditions described above. The curves illustrate that elastance is dependent upon both the details of the capacity-voltage characteristic, and the circuit impedance at the harmonics of the pump.

c. The Determination of Input Impedance. The third step in the computation of input impedance is to insert the elastance coefficients into a small signal matrix, and manipulate this matrix to obtain the desired quantities. Some theoretical results along with the corresponding experimental values are illustrated in Figs. 7.13 through 7.19.

In contrast to the pump voltage, pump current, and elastance waveshape which are most difficult to measure experimentally, it is relatively easy to measure the input impedance by using the techniques described in the previous section. This in fact is one reason for emphasizing the input impedance. It is easy to measure, and, as will be shown, is also a sensitive function of the parameters which influence circuit behavior. These include the hardness of pumping, the diode capacity-voltage characteristics, the circuit impedances at the pump harmonics, the termination of the sidebands of both the pump

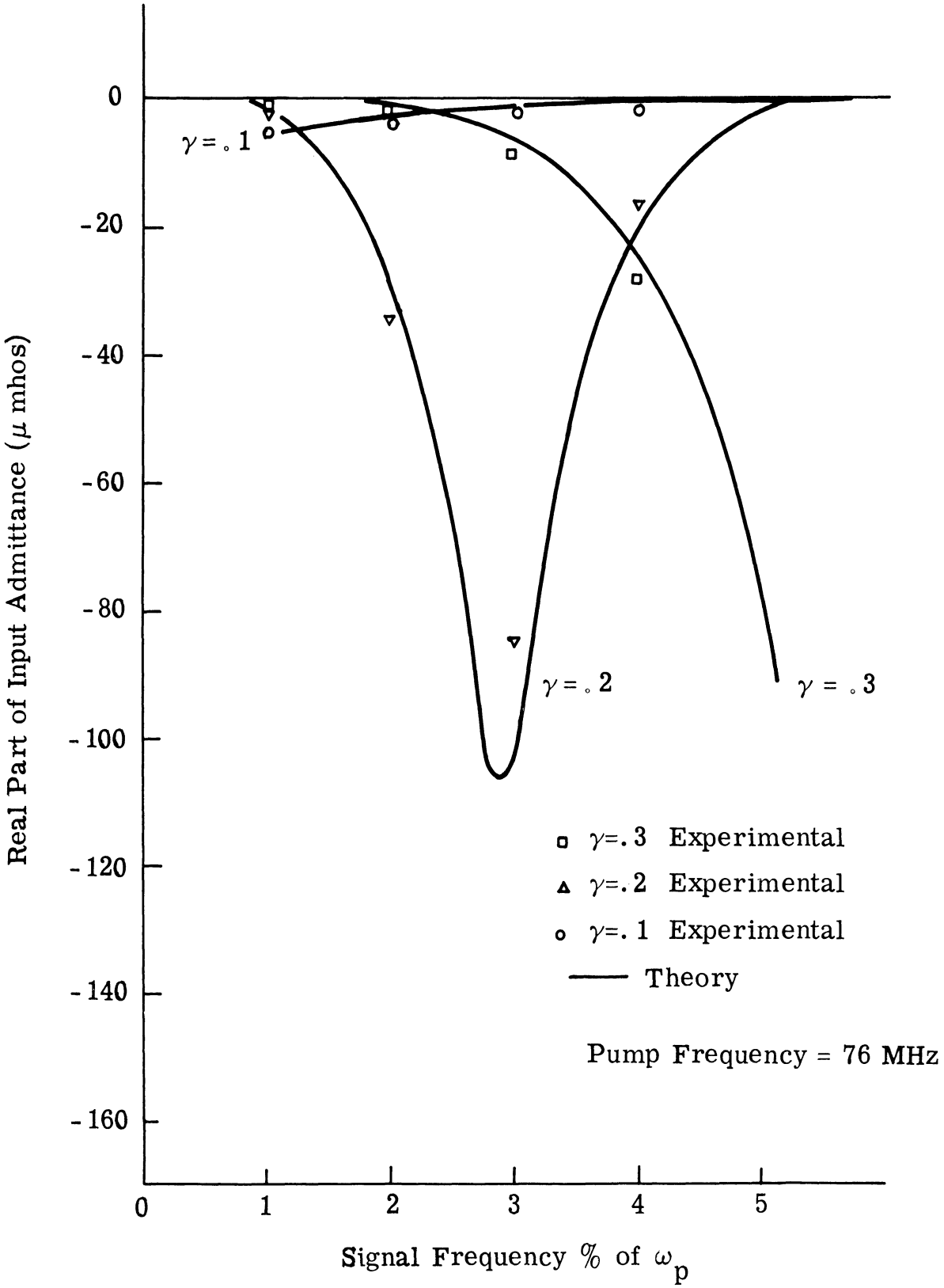

Fig. 7.13a. Real part of the input admittance of the lumped circuit

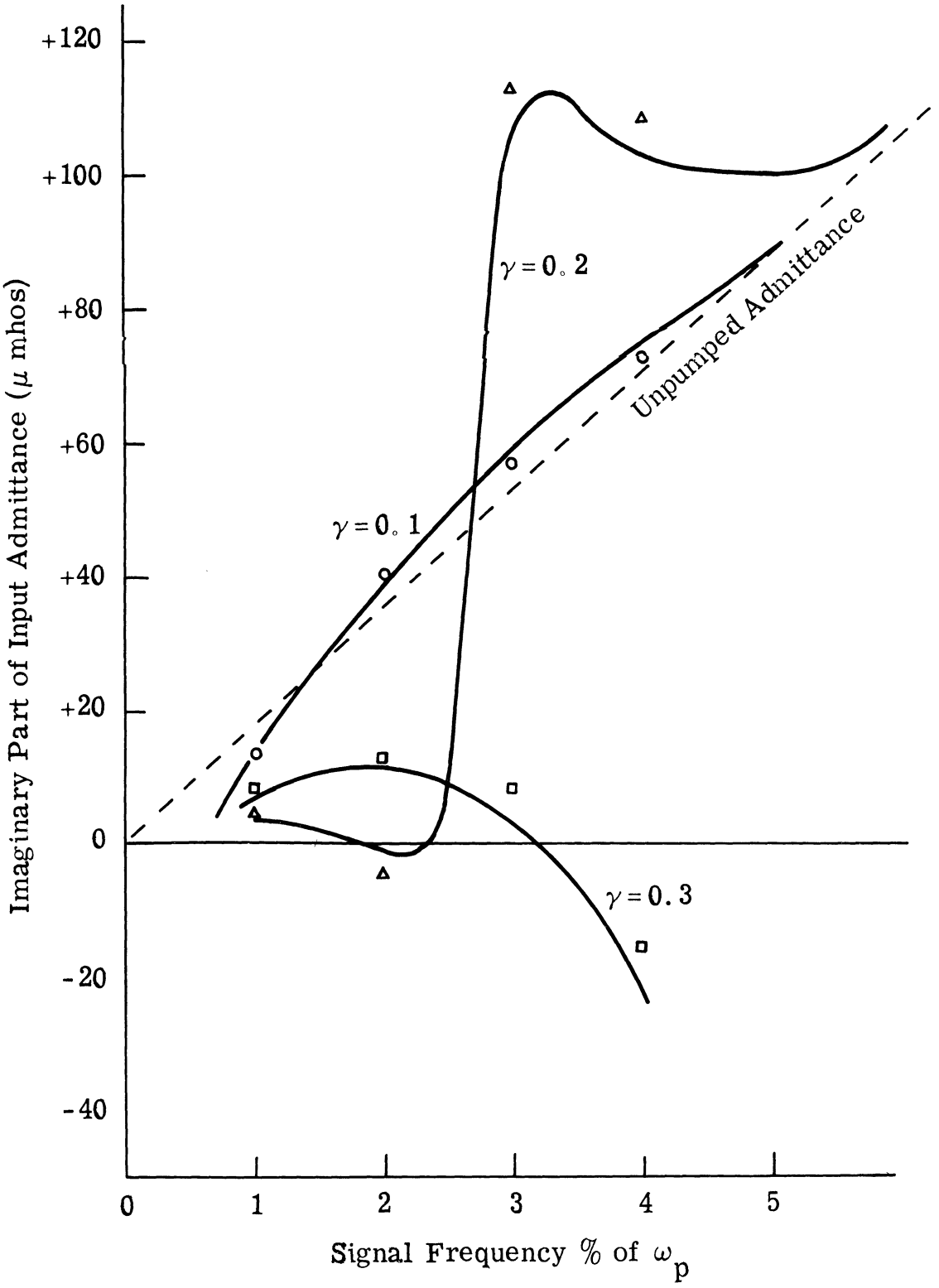

Fig. 7.13b. Imaginary part of the input admittance of the lumped circuit

fundamental and its harmonics, the electric fields in the diode junction the minority carrier density, the minority carrier lifetime, and the diode series resistance. For these reasons, the input impedance is an excellent media for exploring pumped varactor circuit behavior.

Figure 7.13 illustrates the input admittance of the "Lumped Circuit" for three values of γ. The pumping was not hard enough to draw rectified current or to cause diffusion effects to become important. All the results, then, are due to nonlinear depletion layer capacity. The experimental data is indicated by circles, while numerical results are shown as solid-lines. The abscissa quantities in all these figures is signal frequency (ω_1) normalized to the small signal resonant frequency of the circuit and expressed in percent, that is: $100 \times (\omega_1/\omega_0)$. The ordinate quantities are the input admittance of the varactor at the signal frequency. Both the real and imaginary parts of the admittance are expressed in μ-mhos. The real part of the unpumped diode admittance is zero μ-mhos, while the imaginary part is indicated by the straight dashed line. On each graph, data is shown for several values of γ.

The unpumped admittance of the circuit is 3.7 pf in parallel with 0 μ-mhos. Pumping is done at the small signal resonant frequency of the circuit (ω_0 = 76 MHz). The most striking feature exhibited by these curves is a series resonant type of effect--except that the signs of the real part as well as the imaginary part are opposite from those of a passive circuit.

This phenomenon can be understood (at least intuitively) by considering only the behavior of the pump lower sideband ($\omega_p - \omega_1$). By the Manley-Rowe relations, Section 2.4, the power dissipated at this sideband reflects as a negative resistance into the signal frequency.

The magnitude of power at the lower sideband is determined both by γ and the impedance; the maximum flow of power, of course, occurs for large γ and when the circuit is resonant at the frequency of the lower sideband. From Eq. 7.5, the resonant frequency of the circuit is seen to decrease with γ. Thus, as pump is increased, both the amplitude of the negative resistance curve, and the frequency at which it peaks, increase. The bandwidth of the curve is essentially determined by the Q of the unpumped circuit. For purposes of argument, the effect of other sidebands can be ignored, for they become further from resonance as pumping is increased. In the curve of Fig. 7.13, the amplitude of the ($\gamma = .3$) curve has a minimum at approximately 5.5% (4.2 MHz).

Figure 7.14 illustrates the results of three different methods for computing the input admittance. The Lumped Circuit with a value of $\gamma = 0.2$ is used as the example. The first method is the computer solution described in this paper. The results for this solution can be seen to yield results which correlate well with experiment.

The second method is the first order open circuit theory which assumes a sinusoidal elastance variation and the existence of

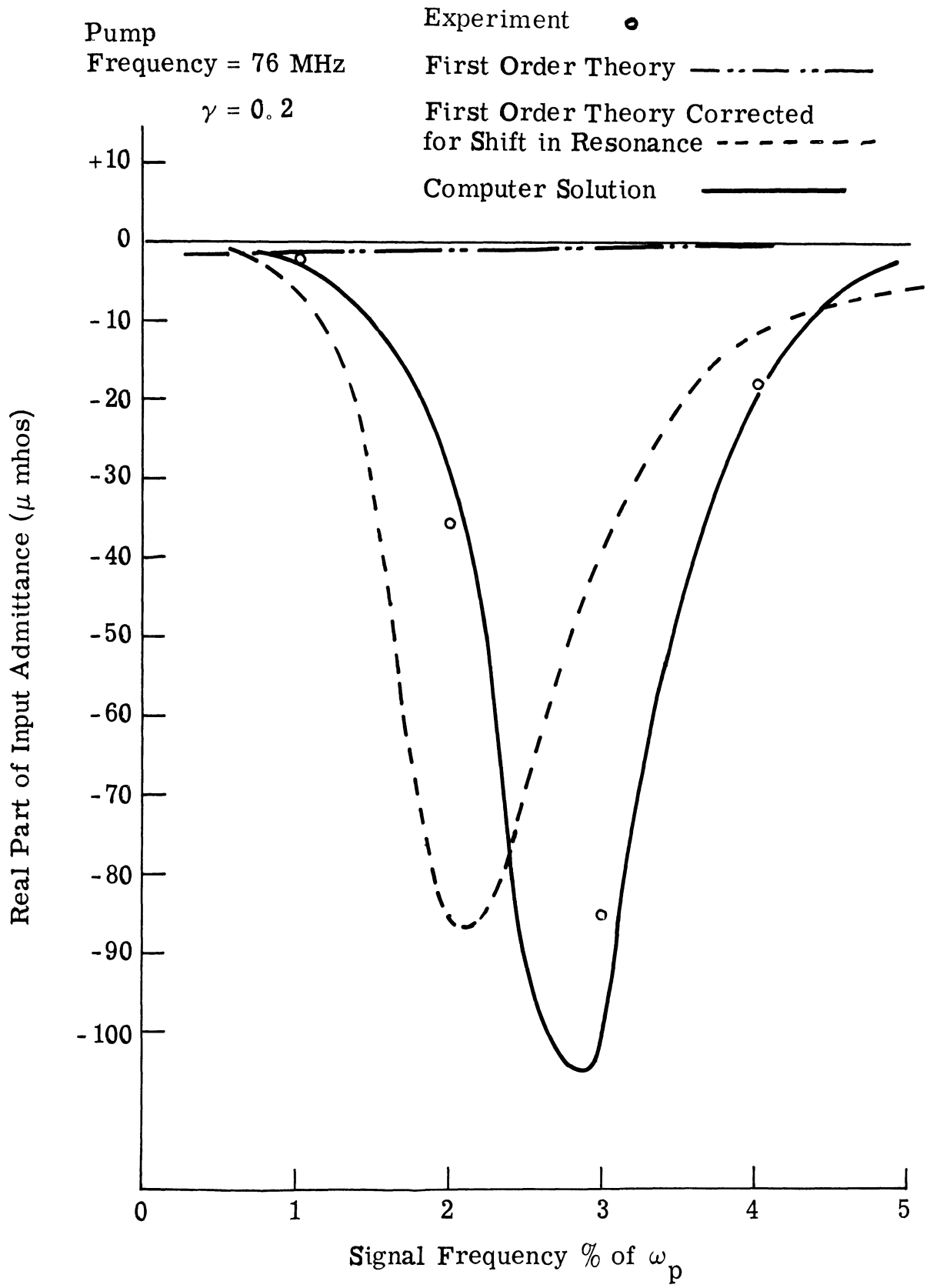

Fig. 7.14a. Comparison of methods for computing the real part of the input admittance of the lumped circuit

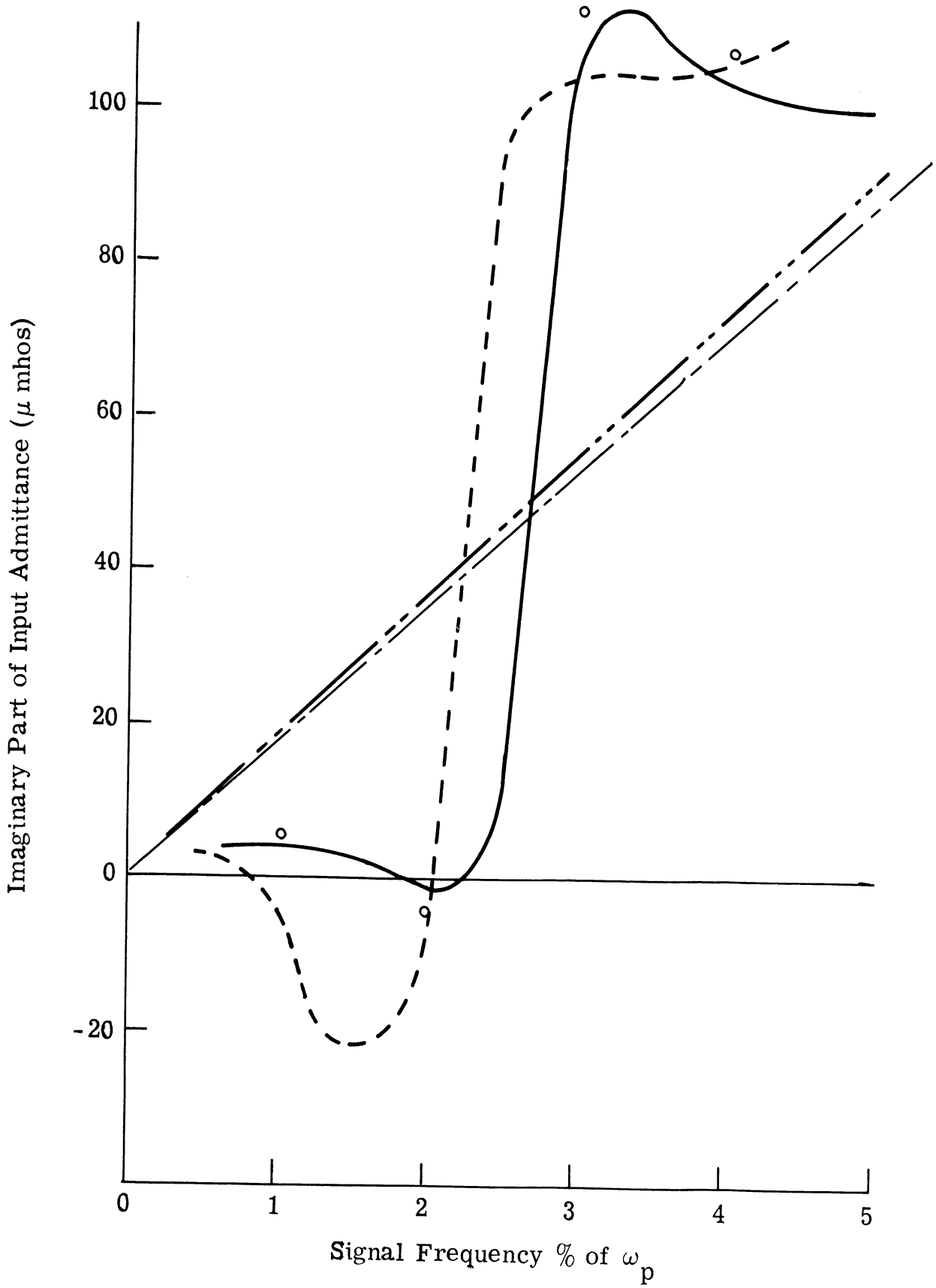

Fig. 7.14b. Comparison of methods for computing the imaginary part of the input admittance of the lumped circuit

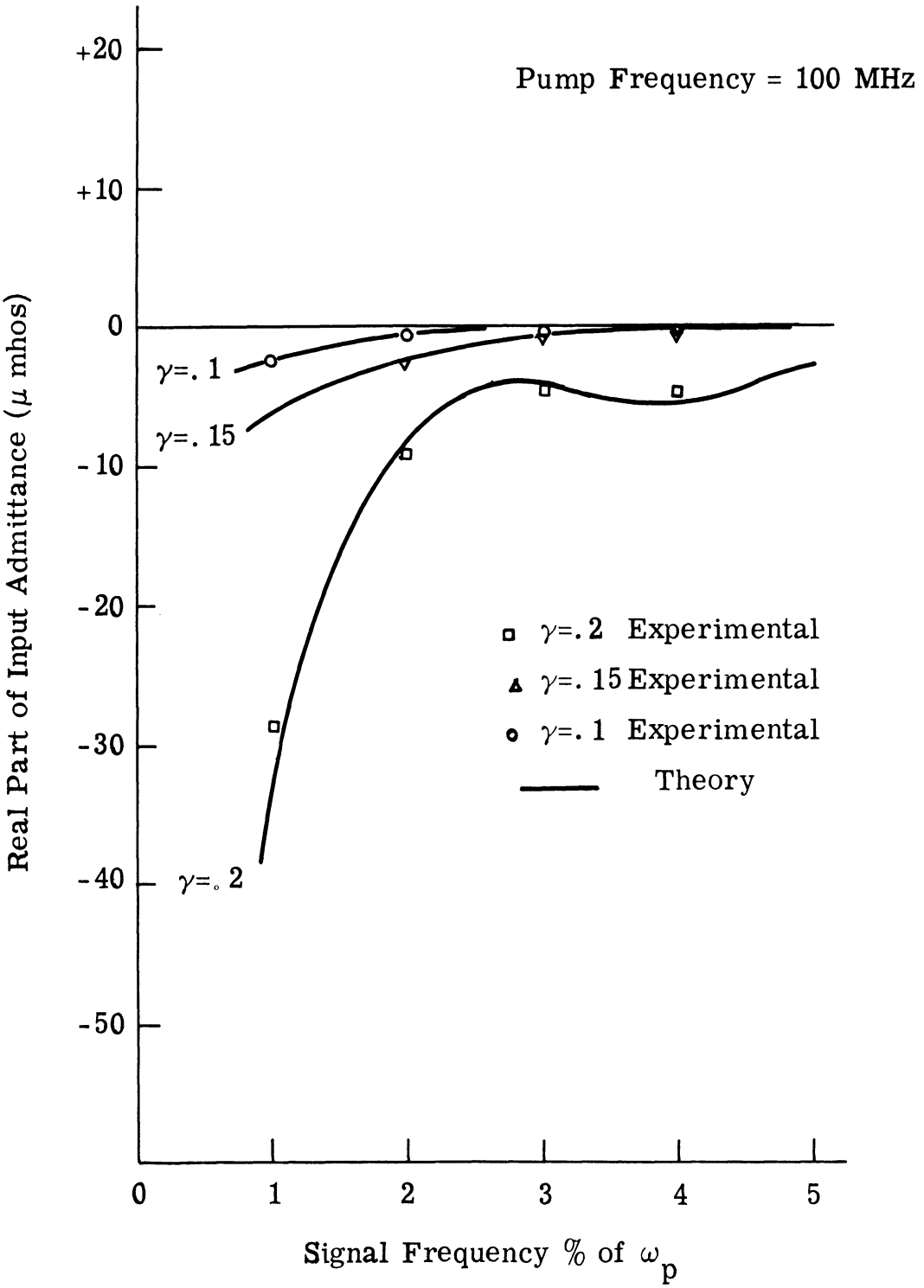

Fig. 7. 15a. Real part of the input admittance of the distributed circuit

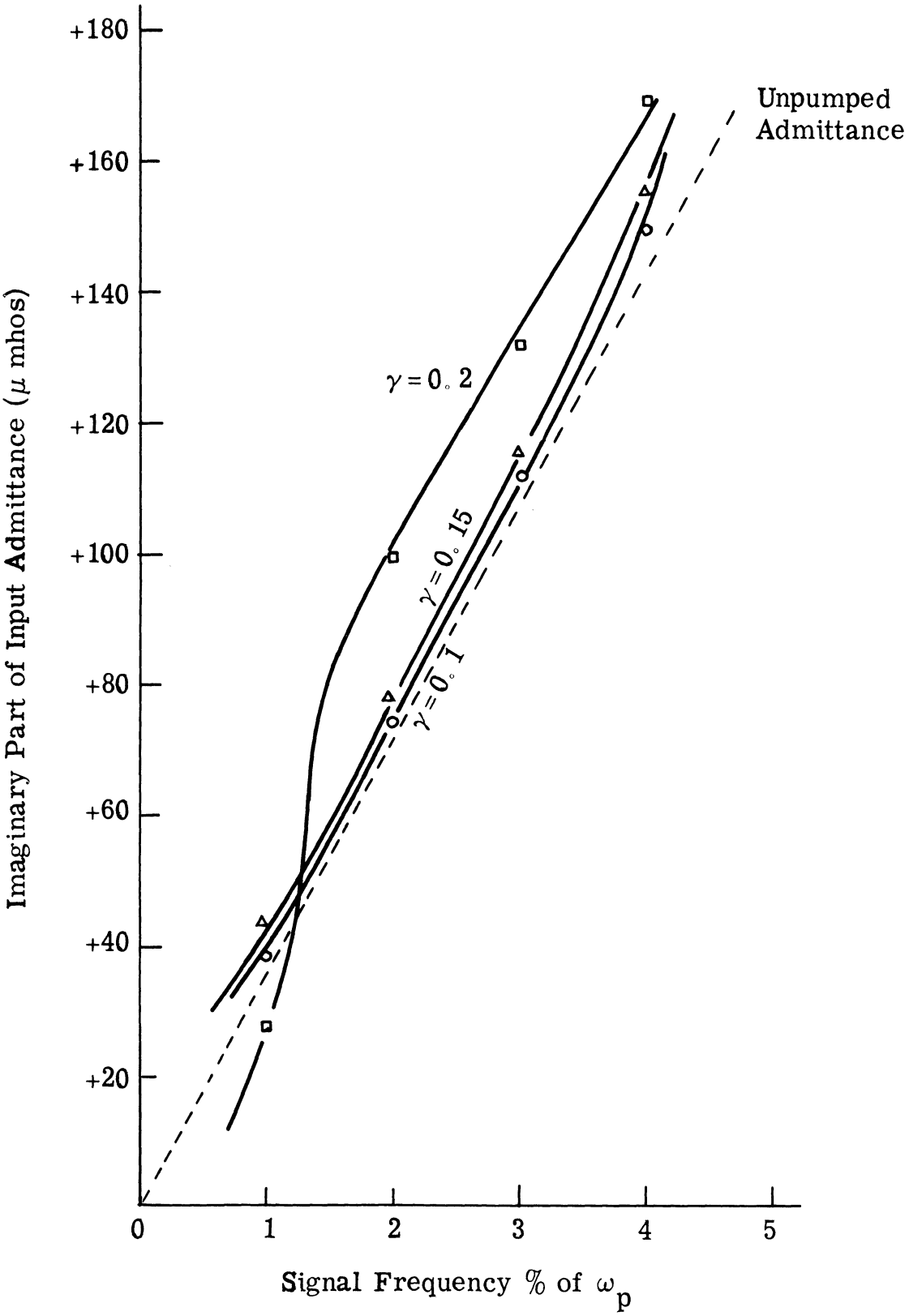

Fig. 7.15b. Imaginary part of the input admittance of the distributed circuit

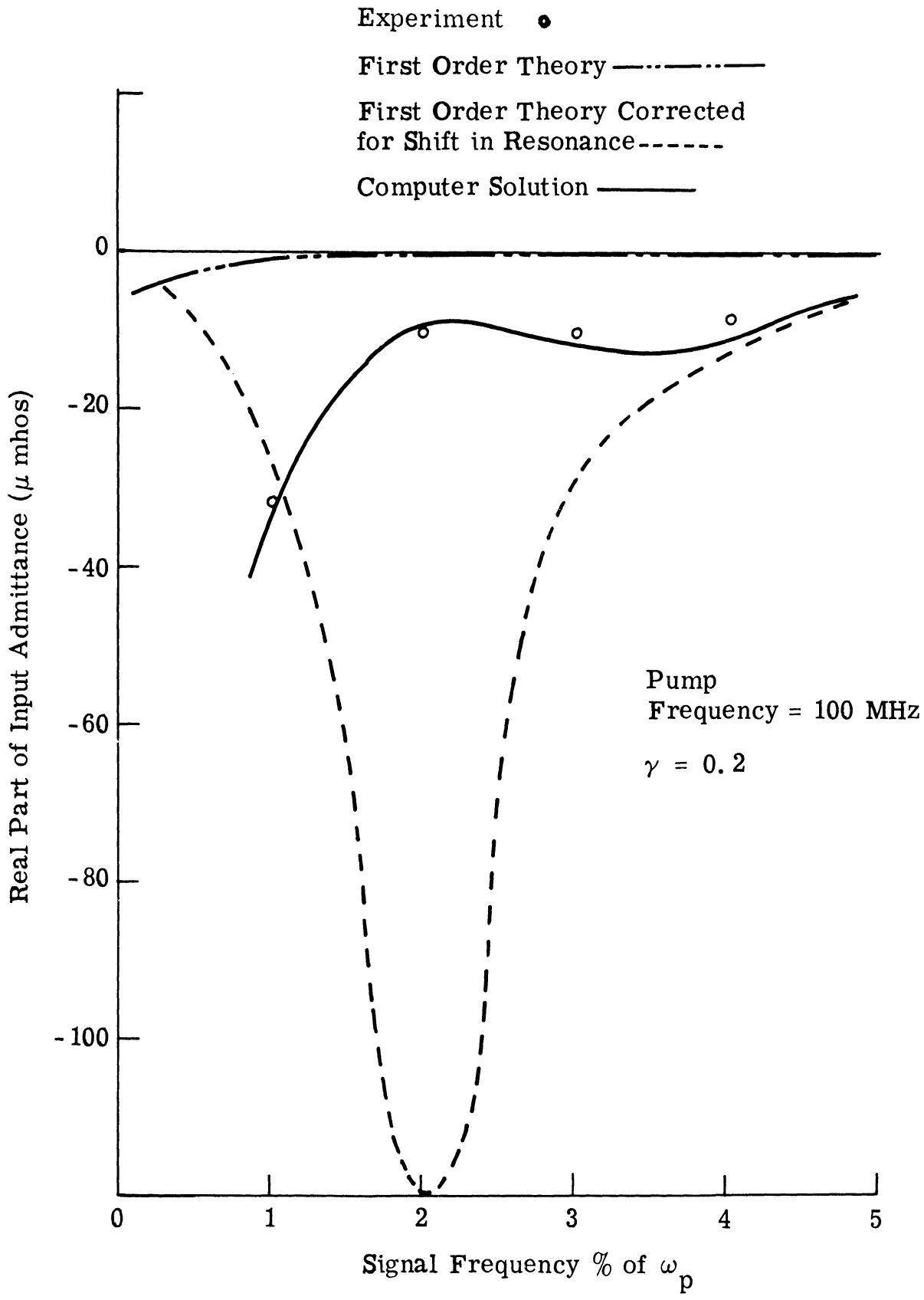

Fig. 7.16a. Comparison of methods for computing the real part of the input admittance of the distributed circuit

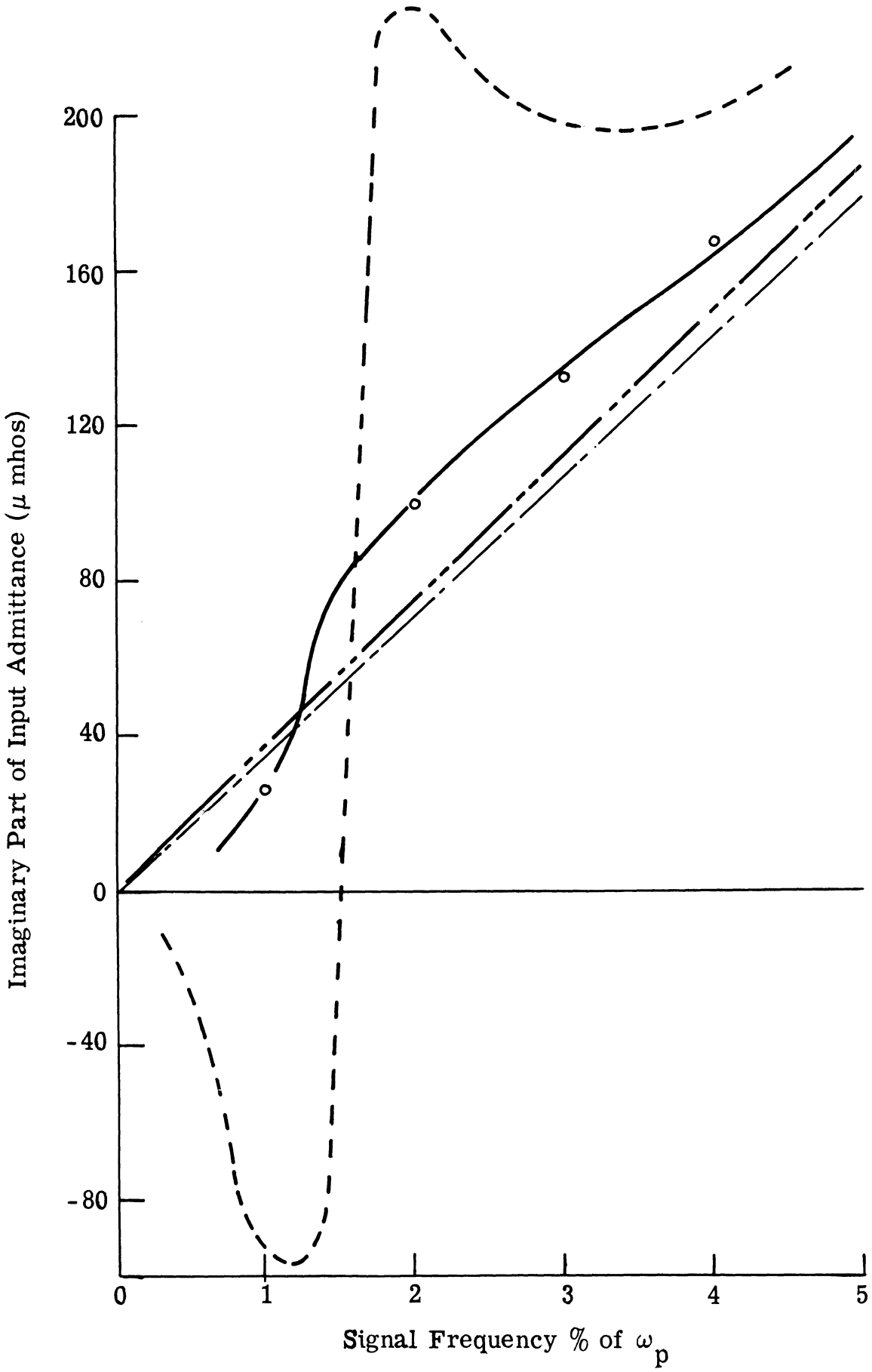

Fig. 7.16b. Comparison of methods for computing the imaginary part of the input admittance of the distributed circuit

only three signal currents (at ω_1, $\omega_p-\omega_1$, and $\omega_p+\omega_1$). The results using this method do not yield accurate results.

The third method is the above first order open circuit theory which assumes a sinusoidal elastance variation, and the existance of only three signal currents, but is modified slightly to account for the variation of the average capacity and the resulting shift in resonant frequency with pump power. This is done by using the first order Eqs. 7.2 and 7.5 to compute the average capacity and the shift in resonant frequency. Except for a small error in the resonant freqeuncy shift, this approximate method can be seen to yield quite accurate results for this circuit.

Figure 7.15 shows the admittance of the "Distributed" circuit (Fig. 7.3, Table 7.2). The unpumped admittance of this circuit is 5.7 pf. Curves are shown for pumping at the small signal resonance (ω_0 = 100 MHz).

In this case, the resonances exhibited by the lumped circuit (Figs. 7.13 and 7.14) are masked by several extraneous effects. First of all, the shift in resonant frequency with pump is not as great for the distributed circuit as for the lumped circuit. This can be seen by comparing Fig. 7.4(a and b). Also, due to the multiple resonances of this structure, sidebands other than ($\omega_p - \omega_1$) and ($\omega_p + \omega_1$) are important. The tuning of these sidebands change with pump in a manner different from the lower sideband, making this case difficult to understand intuitively.

The difficulty in understanding this circuit can be seen

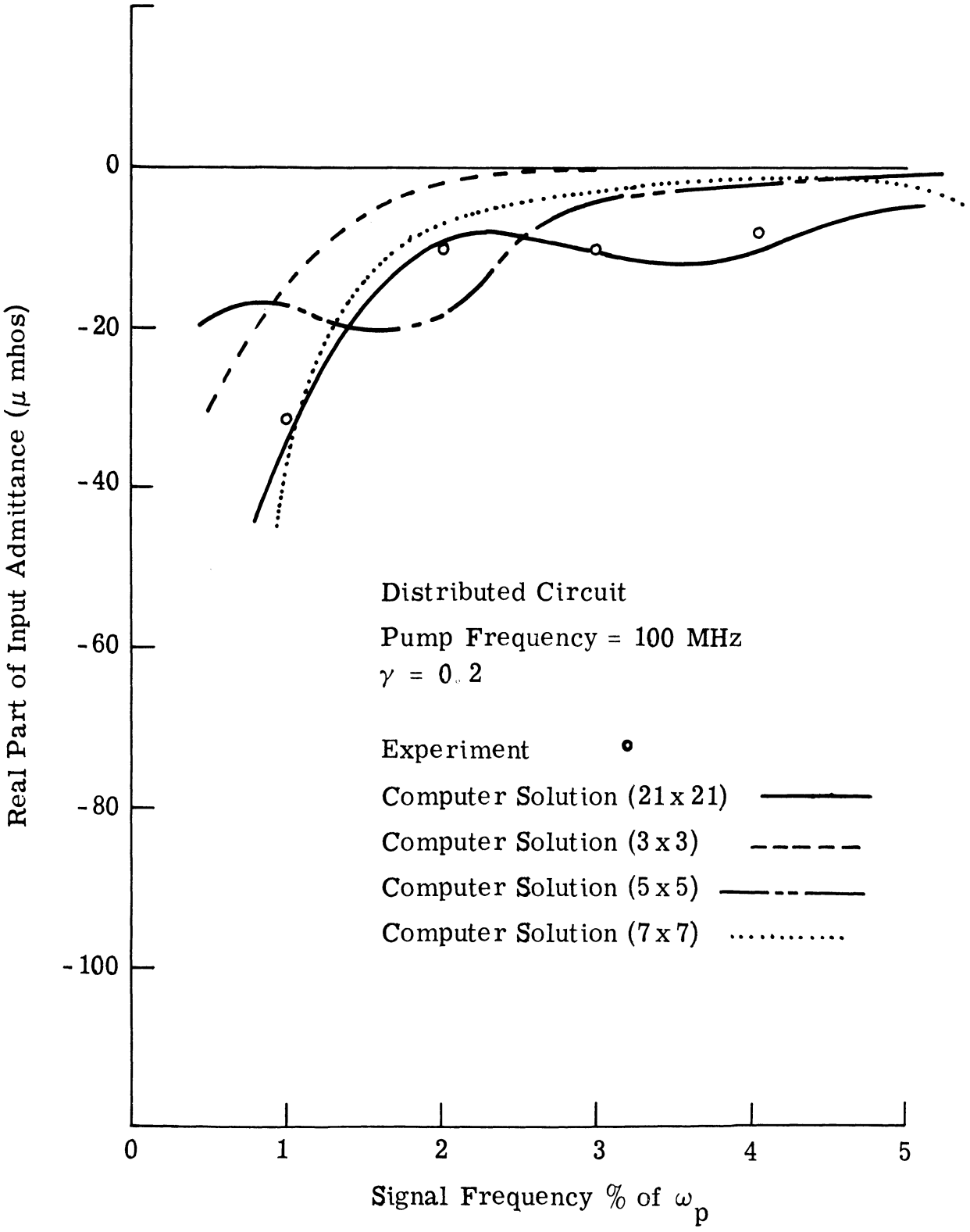

Fig. 7.17a. Effect of harmonics upon the real part of the input admittance

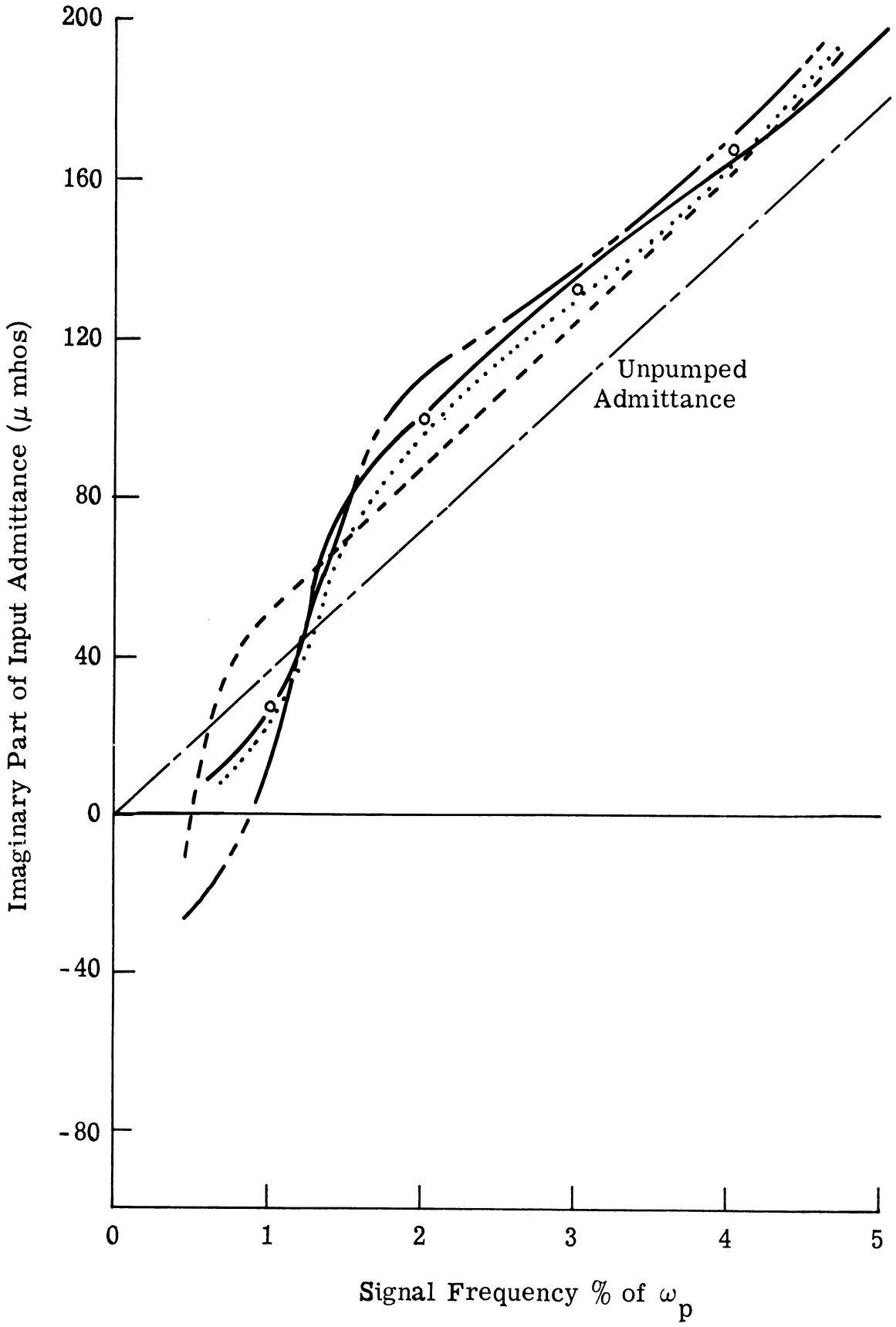

Fig. 7.17b. Effect of harmonics upon the imaginary part of the input admittance

by comparing Fig. 7. 14 with Fig. 7. 16. In Fig. 7. 14 which illustrates the Lumped Circuit, the three current open circuit theory is seen to yield good results when modified by a shift in resonant frequency. However in Fig. 7. 16 in which the distributed circuit is exhibited, this simple modification yield results which are no better than the conventional theory. This can be at least qualitatively explained by referring to Fig. 7. 12 where it is seen that the coefficients of the higher harmonics of elastance are much larger in the Distributed circuit than in the Lumped Circuit. Thus, sidebands around the harmonics of pump have a greater magnitude and therefore play a larger role in the determination of input impedance.

Figure 7. 17 illustrates this concept. The input impedance of the Distributed circuit for $\gamma = 0.2$ was computed using various size impedance matrices of the form (Eq. 5.57) and is plotted here along with the experimental results. The (3 x 3) matrix includes the effects of only ω_1, $(\omega_p - \omega_1)$, and $(\omega_p + \omega_1)$. It differs from the first order short circuit theory only by the inclusion of a shift in average capacity, and the addition of two second harmonic elastance terms.

The (5 x 5) matrix includes, in addition to these effects, signal currents at $(2\omega_p - \omega_1)$ and $(2\omega_p - \omega_1)$, as well as some elastance terms at the third and fourth harmonics. The (7 x 7) matrix includes signal currents at $(3\omega_p - \omega_1)$ and $(3\omega_p + \omega_1)$, and additional higher harmonic elastance terms. It can be seen that even a (7 x 7) matrix differs to some extent from the "correct" solution which in this work is assumed to be obtained from a (21 x 21) matrix. For this circuit,

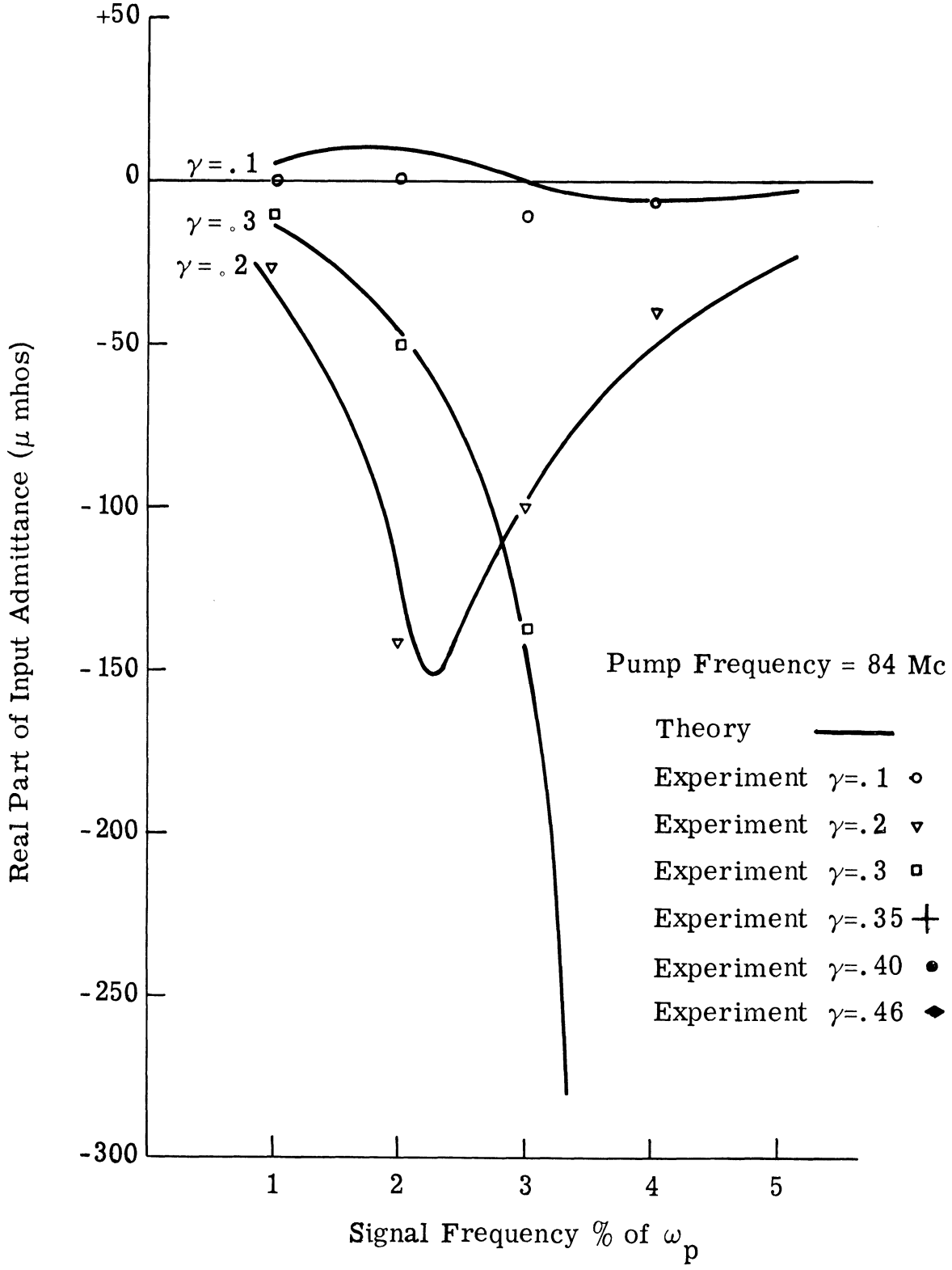

Fig. 7.18a. Real part of the input admittance of the diffusion circuit

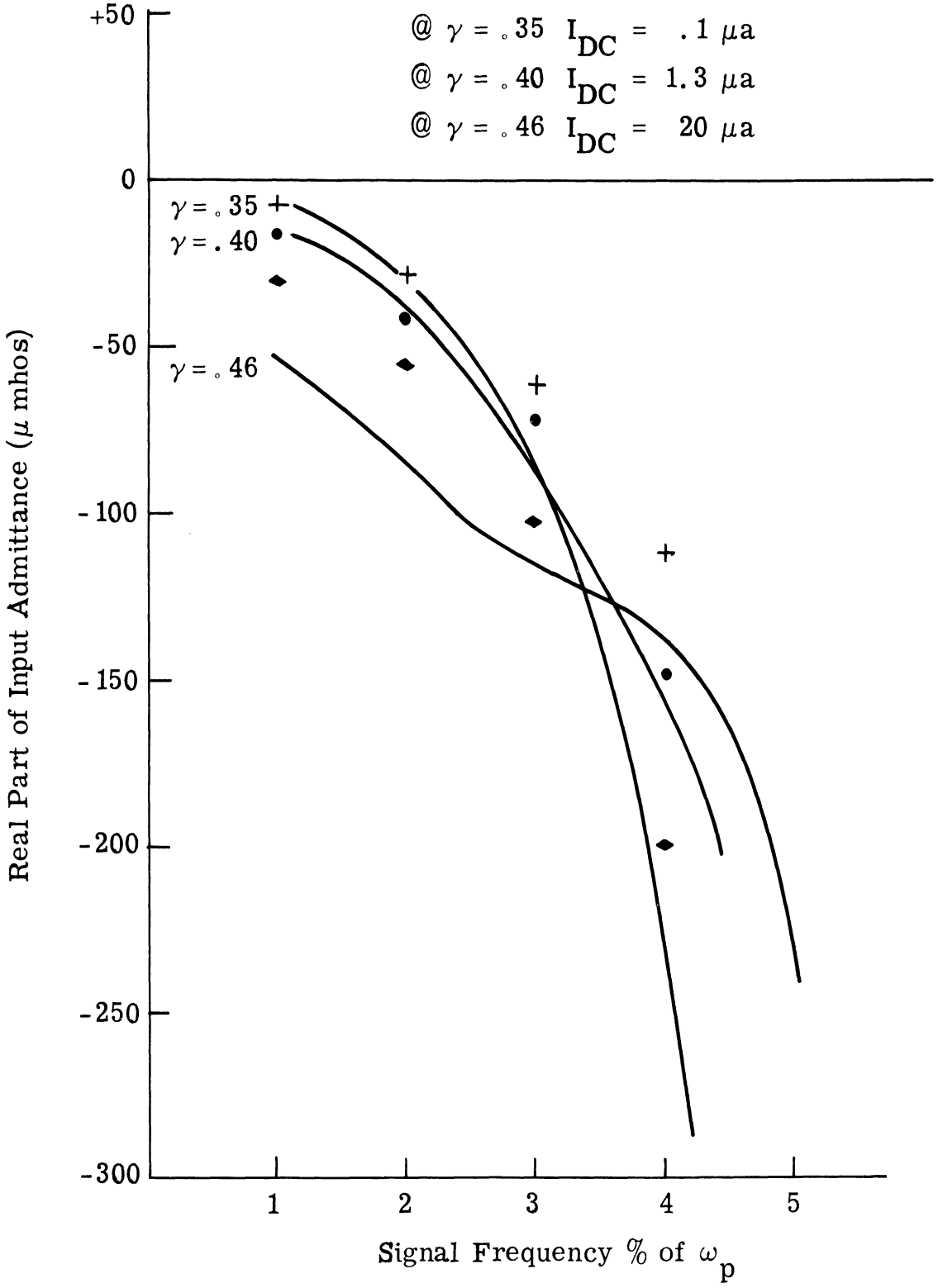

Fig. 7.18b. Real part of the input admittance of the diffusion circuit

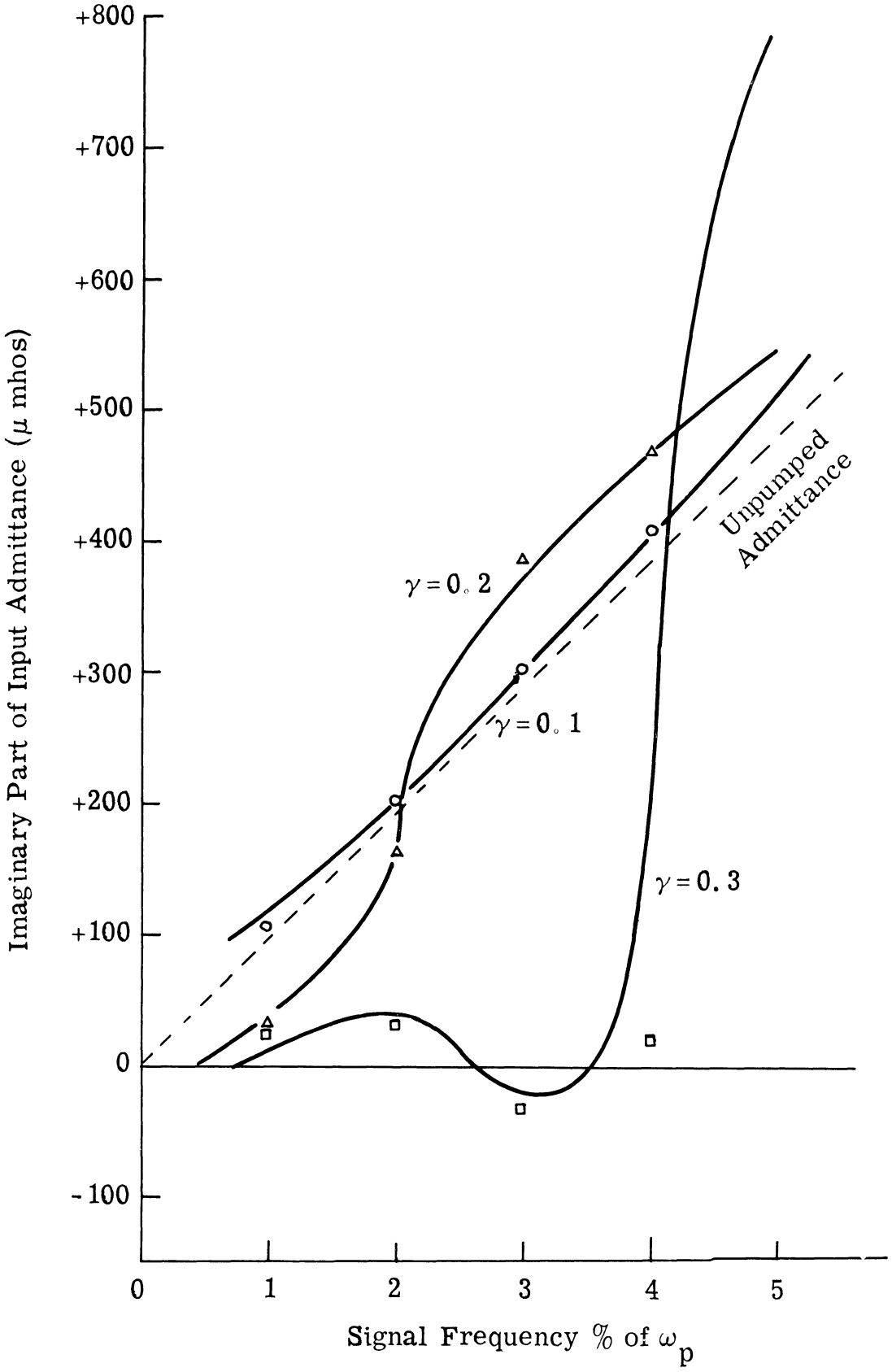

Fig. 7.18c. Imaginary part of the input admittance of the diffusion circuit

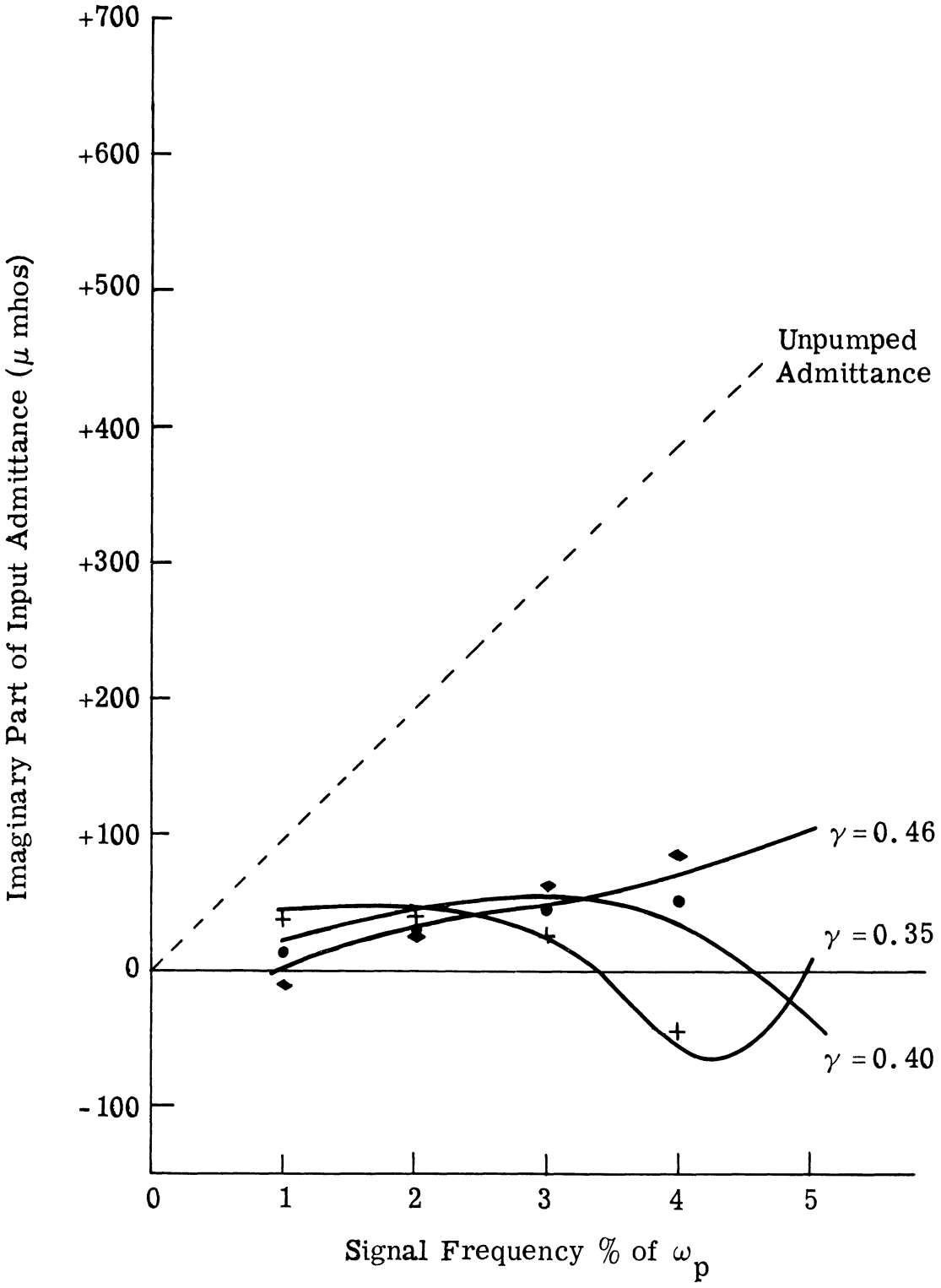

Fig. 7.18d. Imaginary part of the input admittance of the diffusion circuit

the solutions obtained using matrix sizes greater than (13 x 13) are all virtually identical, indicating that signal sidebands around pump harmonics above the 6th are negligible.

The admittance of the "Diffusion" circuit (Fig. 7.2; Table 7.1) is shown in Fig. 7.18, for 6 values of γ. The unpumped admittance of this circuit is 18.4 pf. The curves shown are for pumping at the small signal resonance of the circuit (ω_0 = 84 MHz). For $\gamma < .3$, diffusion capacity is negligible, and as illustrated in Fig. 7.18 (a and c), this circuit exhibits the same sort of resonances as the "Lumped" circuit. However, for $\gamma > .3$, a measurable D.C. current flows through the diode, diffusion and charge storage effects become important, and the results [Fig. 7.18(b and d)] are no longer subject to simple interpretations.

It should be pointed out here that, whenever diffusion effects are important, the concept of γ to denote pumping level must be approached with some care. The parameter γ as ordinarily used and as defined in Eq. 7.1 refers to a time varying, but frequency independent capacitor. This is a valid concept for dealing with depletion layer capacitance. In one sense, diffusion capacity is not really a capacitor at all; it is merely an admittance with a positive imaginary part, onto which we have applied the name capacity. Mathematically, it must be considered as a time varying, frequency dependent admittance, nothing more. The parameter γ as used in Fig. 7.18 refers only to the depletion layer portion of the diode admittance; diffusion

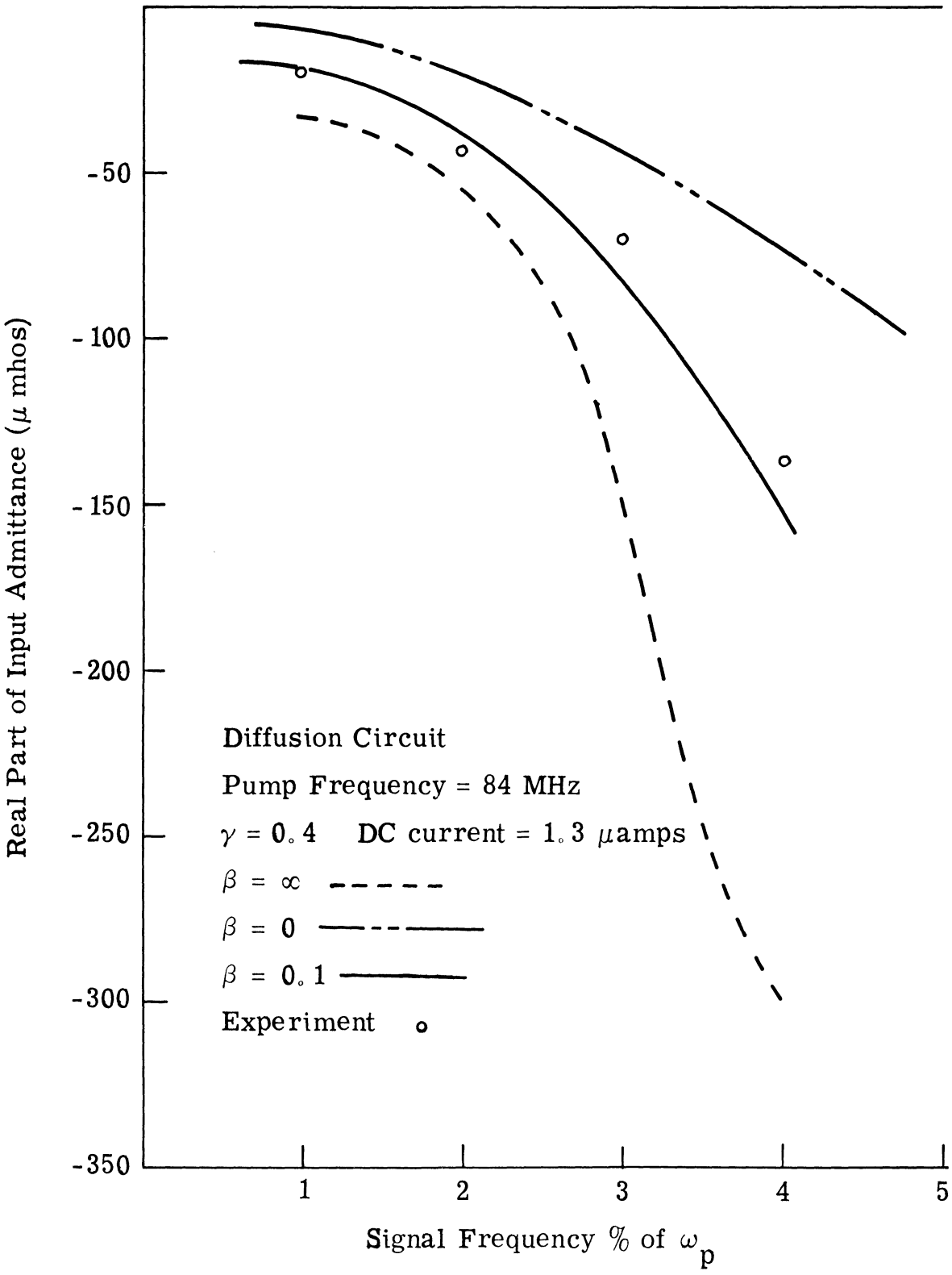

Fig. 7.19a. Effect of the diode model upon the real part of the input admittance

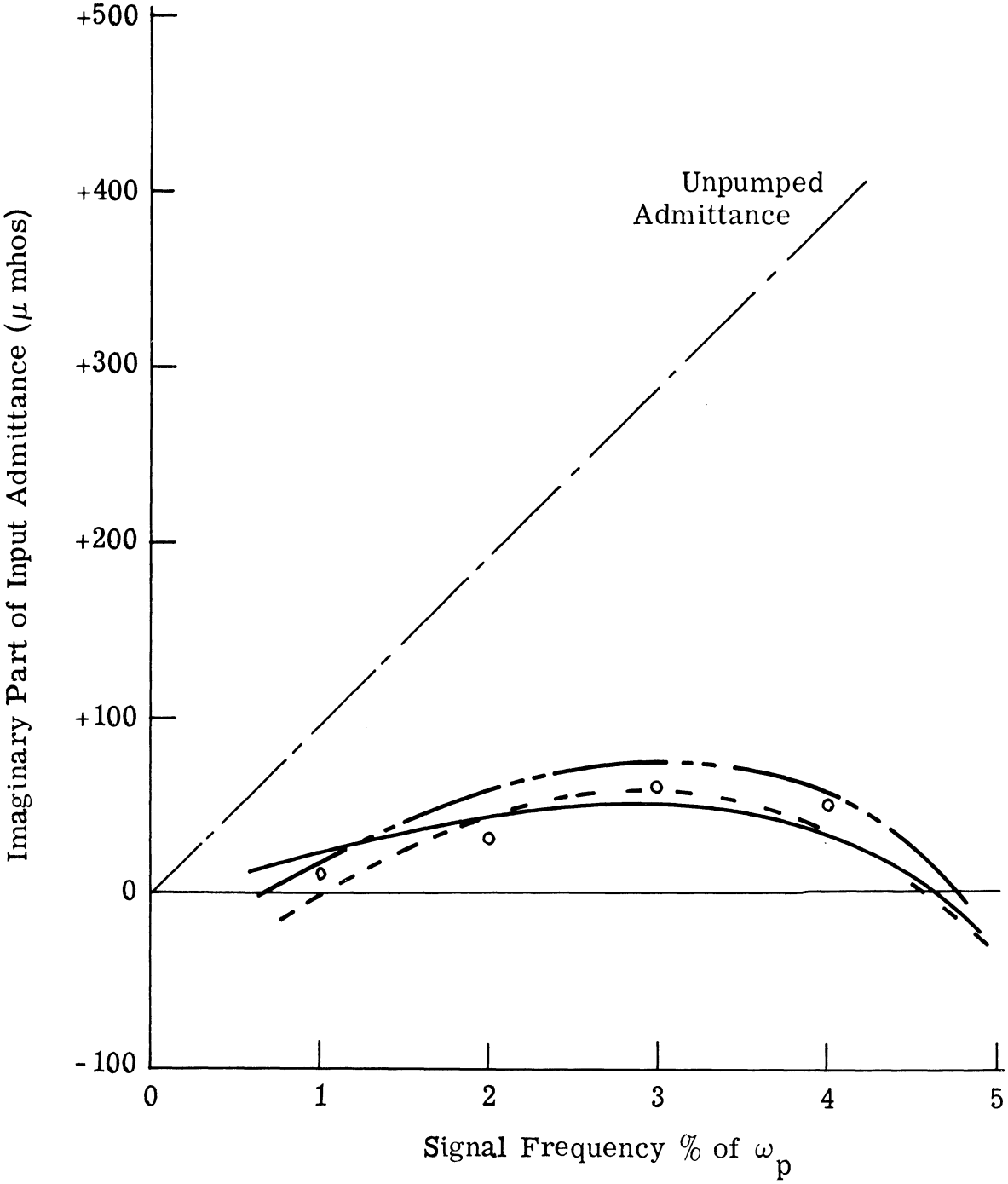

Fig. 7.19b. Effect of the diode model upon the imaginary part of the input admittance

effects were ignored in computing it.

Figure 7. 19 illustrates the effect of the varactor diffusion current model upon the input admittance. The admittance is plotted for three values of junction electric field. This field is seen to have a large effect upon the real part, but little effect upon the real part. Some understanding of this very complex situation may be obtained by recalling that $\beta=0$ corresponds to a retarding electric field with an infinite magnitude. This is the ideal step recovery diode case (Appendix E). The high electric field prevents carriers from diffusing into the n-region; this raises the Q of the diffusion capacity, and results in low losses which are reflected in a small real part of the admittance.

On the other hand, $\beta = \infty$ corresponds to zero electric field in the n-region. This is the situation in an ideal p - n junction diode. The Q of the diffusion capacity is always less than one in this type of diode. The result is higher losses which are reflected in a larger real part of the admittance.

The carrier density and lifetime have similar effects upon the circuit performance.

It is interesting to note that the voltage waveform and the elastance coefficients are affected very little by changes in electric field, carrier density, and carrier lifetime. Changes in these quantities affect the input impedance mainly by altering the terminations of sidebands at harmonics of the pump.

In constructing the set of curves (Figs. 7.13 - 7.19), every effort was made to plot the results using a consistent set of γ's. This, however, proved to be impractical. For example, the maximum value of γ obtainable in the lumped circuit was limited by the onset of diffusion effects. For harder pumping, D.C. current flows and diffusion effects become appreciable.

Also, γ is limited by pump power. The oscillator used as the pump source has a maximum output (into a matched load) of 200 mW. In addition, the circuit tuning changes as the pump power is varied. The maximum value of γ obtainable in the distributed circuit was limited by these effects.

In general, the agreement between the theory and experiment can be seen to be excellent. There are a few minor discrepancies, however, probably caused by some idealizing of the varactor diode model.

7.4 Conclusions

This paper has presented the theoretical development and the experimental results of an investigation into pumped varactor circuits. In view of the evidence presented in the previous section, it may be concluded that the theoretical development given in this work is adequate to analyze a pumped varactor circuit with some accuracy. The quantity of experimental verification is insufficient to be totally conclusive, but enough data was presented to indicate that the analysis

is valid for a wide variety of situations.

The small amplitude pump restrictions of previous analyses have been totally eliminated by using numerical techniques to solve the nonlinear differential equations which describe the behavior of varactor diode circuits which are driven by large amplitude sources. The reactive mixing between the non-sinusoidal pump and the signal was investigated by using a matrix formulation. All significant mixing products were taken into account by using a large matrix. This matrix was then manipulated by using numerical techniques. The only assumptions made were certain general assumptions as to the nature of the diode, and an assumption that the signal amplitude (not the pump amplitude) is small.

The work has been exploratory in nature, and it is difficult to summarize precisely. However, it is possible to make a few generalizations. The most practical of these deal with the character of circuit model and the nature of analysis which should be used when studying pumped varactor circuits. An engineer, who has some computer time at his disposal, can utilize the methods of this paper to analyze practical circuit configurations. He can do this with some confidence, because the theory yields good correlation with experiment, correlation which is better than any previous work.

Specifically, it is possible to make the following practical suggestions on modeling a pumped varactor circuit:

1) The "Uhlir" model, with some modifications, adequately represents the actual diode. Good experimental - theoretical correlation is obtained by using the equivalent circuit of Figs. 2.3 or 2.4, and including in the junction characteristics the effects of diffusion as well as barrier layer capacity. For reverse bias, the use of the barrier layer capacity yields results which can be verified almost exactly with experiment, while for forward voltages, the parallel combination of barrier layer capacity plus diffusion capacity yields results which are almost as good. It is also clear that the variation of series resistance with voltage, which sometimes occurs in high quality varactors, must also be accounted for.

2) Under reverse bias conditions, the details of the capacity-voltage characteristics can be very important. A diode which appears to have only slight deviations from the ideal abrupt junction may actually perform in quite a different fashion when used in a circuit. Likewise, two diodes may have similar characteristics, but very dissimilar performances. The practical implications of this are obvious.

3) Under conditions of forward voltage, the diode junction model consisting of diffusion capacity in parallel with barrier layer capacity appears to give quite adequate results. The diffusion capacity model involves the assumption of a retarding electric field which is uniform with distance. The magnitude of this field may be varied from zero to infinity. Although this is an obvious

oversimplification, this model yields quite accurate results.

4) The concept of treating the linear portion of the network as an equivalent Thevenin or Norton impedance is most useful. This equivalent impedance appears across the terminals of the diode, and terminates the pump harmonics as well as the fundamental and its sidebands. The nature of this impedance, even at the harmonics, has been shown here to influence the circuit behavior significantly. The so-called open circuit and short circuit conditions are the limiting cases of this impedance.

5) The shift in average capacity is very important. For applications where accuracy may not be of the greatest importance, the three frequency open circuit model, modified to account for changes in tuning with pump level, may be good enough. It is also a useful concept in treating the ferro-resonant effect, and is helpful in the intuitive understanding of some experimentally observed phenomenon.

This circuit model is the end product of evolution through a series of models. The first model tried was the first order model which consists of two sidebands and a sinusoidal capacitance (or elastance). In succeeding trials, more exact circuit representations were used, and the discrepancy between theory and experiment narrowed. The present model is not the most accurate model which could be conceived, but it does yield accurate results and is physically meaningful.

In addition to the work on the circuit model, mention should be made of the following original contributions. These results were effected while developing the circuit model, but are not logically placed with the above results.

1) Obtained relationships which clarified the connection between the open circuit and the short circuit equations. These relationships showed that even though sidebands at higher frequencies are terminated in open circuits or short circuits, and therefore carry no power, their presence affects the sidebands which do carry power.

2) Set up and then solved the nonlinear pump circuit differential equation using an accurate circuit model. Computed the reactive mixing between the non-sinusoidal pump and a small sinusoidal signal taking into account all significant components.

3) Devised a practical method for measuring the pumping coefficient, γ. This method is independent of whether the pumping is hard enough to cause DC current to flow. It is fast, reasonably accurate, and requires only two additional pieces of equipment: a signal source, and a detector. Using this method, γ can actually be measured while the circuit is being operated.

4) Obtained good experimental correlation of the analytical portion of the work. The experimental work was carried out using measured values of γ, while the diode parameters used in the analytical work were obtained using simple RF bridge and pulse techniques. The good agreement tends to confirm the accuracy of

the circuit model and the validity of the analytical procedure.

5) Obtained relationships which clarified the ferro-resonant or jump effect. By treating it from an impedance viewpoint, the present treatment avoids many of the complications associated with other interpretations.

This work has presented a procedure for analyzing pumped varactor diode circuits. Using the procedures and models presented here, an engineer can analyze any circuit he chooses to devise. Useful as this may be, the design engineer is still left with a most difficult task. He must still base his design on simplified theory (Ref. 55); and although he can utilize the procedures of this paper to check this design, his method of procedure, should this initial design fail to be satisfactory, is not at all clear. The most profitable extension of this work lies in the development of advanced design tools to make the analysis more useful.

The results of this work can also be used as a basis for the consideration of more practical pumped varactor circuits. The most important of these is the circuit consisting of a diode mounted in a waveguide. Although all the concepts presented in this paper hold true for this circuit, the computation of the impedances at the diode terminals presents some difficulty. In a waveguide designed to propagate the pump fundamental, higher order modes of the pump harmonics will not be cut off. The impedance (both the real and the imaginary parts) must be derived from the solution of field problems

involving the excitation and the propagation of waves in an oversize waveguide.

Work can also be profitably undertaken in the improvement of the diode model. The use of a more accurate diode model, especially in the forward-conduction region, would give even closer correlation between theory and experiment than was obtained here.

APPENDIX A

INVERSION OF MATRICES USED IN CHAPTER III

In Chapter III, the values of $\beta_{11}(n)$, $\beta_{12}(n)$, $\beta_{22}(n)$ were simply quoted. The computation will be carried out in this appendix. $\beta_{11}(n)$, $\beta_{12}(n)$, $\beta_{21}(n)$, $\beta_{22}(n)$ are defined as the upper four elements of the inverse of $\alpha_{22}(n)$.

Where

$$\alpha_{22}(n) = \begin{bmatrix} -j\omega_4 C_0 & 0 & -j\omega_4 C_1 & 0 & 0 & 0 & \cdots \\ 0 & j\omega_5 C_0 & 0 & j\omega_5 C_{-1} & 0 & 0 & \cdots \\ -j\omega_6 C_{-1} & 0 & -j\omega_6 C_0 & 0 & -j\omega_6 C_1 & 0 & \cdots \\ 0 & j\omega_7 C_1 & 0 & j\omega_7 C_0 & 0 & j\omega_7 C_{-1} & \cdots \\ 0 & 0 & -j\omega_8 C_{-1} & 0 & -j\omega_8 C_0 & 0 & \cdots \\ 0 & 0 & 0 & j\omega_9 C_1 & 0 & j\omega_9 C_0 & \cdots \\ \cdot & \cdot & \cdot & \cdot & \cdot & \cdot & \cdot \\ \cdot & \cdot & \cdot & \cdot & \cdot & \cdot & \cdot \\ \cdot & \cdot & \cdot & \cdot & \cdot & \cdot & \cdot \end{bmatrix} \tag{A.1}$$

The symbol n is the order of the original matrix (3.29); $\alpha_{22}(n)$ is of order n-3 (n is greater than 3). The values of the β's can be found by dividing the co-factor corresponding to that β by the determinant of the matrix.

The determinant will be computed first. The computation

can be easily done if the arrangement of zero and non-zero elements are used to advantage. Because there is only one non-zero element below the diagonal in each row (for rows below the second), the matrix can easily be put in upper triangular form. This can be systematized by starting from the top and working down. When this is done, the result is

(See next page)

where

$$\gamma^2 = \frac{C_1 C_{-1}}{C_0^2}$$

The value of the determinate is now just the product of all the diagonal terms.

$$|\alpha_{22}(n)| = F_{(n)}\, C_0^{(n-3)} (1-\gamma^2)^2 \left(1 - \frac{\gamma^2}{1-\gamma^2}\right)^2 \left(1 - \frac{\gamma^2}{1 - \frac{\gamma^2}{1-\gamma^2}}\right)^2 \cdots \tag{A.3}$$

where

$$F_{(n)} = (-j\omega_4)(+j\omega_5) \ldots\ldots [(-1)^{n+1} j\omega_n] \text{ , and}$$

γ^2 appears $\left(\sum_{\ell=6}^{n} \left[\frac{\ell - \frac{7}{2} - (-1)^{\ell} \frac{1}{2}}{2} \right] \right)$ times.

To complete the evaluation of $\beta_{11}(n)$, the co-factor $B_{11}(n)$

$$\alpha_{22}(n) = \begin{vmatrix} -j\omega_4 C_0 & 0 & -j\omega_4 C_1 & 0 & 0 & \cdots \\ 0 & j\omega_5 C_0 & 0 & j\omega_5 C_{-1} & 0 & \cdots \\ 0 & 0 & -j\omega_6 C_0(1-\gamma^2) & 0 & -j\omega_6 C_1 & \cdots \\ 0 & 0 & 0 & j\omega_7 C_0(1-\gamma^2) & 0 & \cdots \\ 0 & 0 & 0 & 0 & -j\omega_8 C_0\left(1 - \frac{\gamma^2}{1-\gamma^2}\right) & \cdots \\ 0 & 0 & 0 & 0 & 0 & j\omega_9 C_0\left(1 - \frac{\gamma^2}{1-\gamma^2}\right) \cdots \\ \vdots & \vdots & \vdots & \vdots & \vdots & \ddots \end{vmatrix}$$

(A. 2)

of the (1, 1) element is also needed. This is a matrix of order n - 4, which has the same form as $|\alpha_{22}(n)|$.

$$B_{11}(n) = \begin{vmatrix} j\omega_5 C_0 & 0 & j\omega_5 C_{-1} & 0 & 0 & \cdots \\ 0 & -j\omega_6 C_0 & 0 & -j\omega_6 C_1 & 0 & \cdots \\ j\omega_7 C_1 & 0 & j\omega_7 C_0 & 0 & j\omega_7 C_{-1} & \cdots \\ 0 & -j\omega_8 C_{-1} & 0 & -j\omega_8 C_0 & 0 & \cdots \\ 0 & 0 & j\omega_9 C_1 & 0 & j\omega_9 C_0 & \cdots \\ \vdots & \vdots & \vdots & \vdots & \vdots & \end{vmatrix} \tag{A. 4}$$

This can be evaluated by the same procedure used to evaluate (A. 1). The result is

$$B_{11}(n) = F'(n)\, C_0^{(n-4)} (1-\gamma^2)^2 \left(1 - \frac{\gamma^2}{1-\gamma^2}\right)^2 \left(1 - \frac{\gamma^2}{1 - \frac{\gamma^2}{1-\gamma^2}}\right)^2 \cdots \tag{A. 5}$$

where

$$F'(n) = (j\omega_5)(-j\omega_6) \cdots [(-1)^{n+1} j\omega_n], \text{ and}$$

γ^2 appears $\left(\sum_{\ell=6}^{n-1} \left[\frac{\ell - \frac{7}{2} - (-1)^{\ell} \frac{1}{2}}{2}\right]\right)$ times.

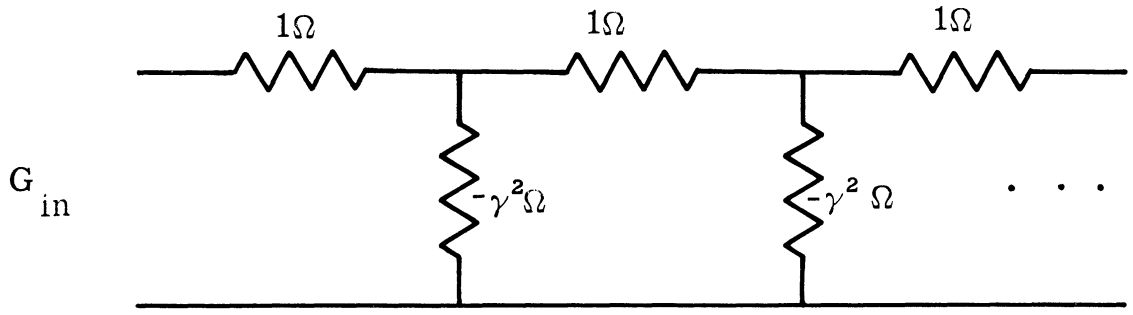

Fig. A. 1. Resistive ladder network

Now that both the co-factor of the (1, 1) element, $B_{11}(n)$ and the determinate of the matrix $|\alpha_{22}(n)|$ are known, the inverse element can be found.

$$\beta_{11}(n) = \frac{B_{11}(n)}{|\alpha_{22}(n)|} = \frac{1}{(-j\omega_4)\, C_0 \left(1 - \frac{\gamma^2}{1 - \frac{\gamma^2}{1 - \gamma^2}}\right)} \quad \text{(A.6)}$$

Only the first and last terms in $|\alpha_{22}(n)|$ are left after the division is carried out. γ^2 appears $(\frac{n}{2} - 2)$ times for n even and $(\frac{n}{2} - \frac{5}{2})$ times for n odd.

In the limit as $n \to \infty$, the expansion of Eq. A.6 can be put in a very simple form. This can be accomplished by giving the expansion a physical interpretation (Ref. 44). Consider the ladder network Fig. A.1 which consists of 1 ohm and $(-\gamma^2)$ ohm resistors. Except for the multiplicative factor $\frac{1}{(-j\omega_4) C_0}$, the input admittance of this network can be put in the same form as Eq. A.6, where the network has $(\frac{n}{2} - 2)$ nodes for n even and $(\frac{n}{2} - \frac{5}{2})$ nodes for n odd.

For $n \to \infty$, the admittance can be put in a very simple form by using standard image parameter theory.

$$G_{in} = \frac{1}{\left(\frac{1}{2} + \sqrt{\frac{1}{4} - \gamma^2}\right)} \quad \text{(A.7)}$$

Then:

$$\beta_{11}(\infty) = \frac{1}{-j\omega_4 C_0 \left(\frac{1}{2} + \sqrt{\frac{1}{4} - \gamma^2}\right)} \tag{A.8}$$

The computation for $\beta_{22}(n)$ is carried out in exactly the same manner.

$$\beta_{22}(n) = \frac{1}{(j\omega_5) C_0 \left(1 - \frac{\gamma^2}{1 - \frac{\gamma^2}{1 - \gamma^2}}\right)} \tag{A.9}$$

The continued fraction expansion is carried out until γ^2 appears $(\frac{n}{2} - 2)$ times for n even and $(\frac{n}{2} - \frac{5}{2})$ times for n odd. In the infinite case

$$\beta_{22}(n) = \frac{1}{(j\omega_5) C_0 \left(\frac{1}{2} + \sqrt{\frac{1}{4} - \gamma^2}\right)} \tag{A.10}$$

To evaluate $\beta_{12}(n)$, the co-factor of the (2, 1) element is needed. This can be shown by induction to equal zero for all n.

$$B_{2,1}(n) = \begin{vmatrix} 0 & -j\omega_4 C_1 & 0 & 0 & 0 & 0 & \cdots \\ 0 & -j\omega_6 C_0 & 0 & -j\omega_6 C_1 & 0 & 0 & \cdots \\ j\omega_7 C_1 & 0 & j\omega_7 C_0 & 0 & j\omega_7 C_{-1} & 0 & \cdots \\ 0 & -j\omega_8 C_{-1} & 0 & -j\omega_8 C_0 & 0 & -j\omega_8 C_1 & \cdots \\ 0 & 0 & j\omega_9 C_1 & 0 & j\omega_9 C_0 & 0 & \cdots \\ \cdot & \cdot & \cdot & \cdot & \cdot & \cdot & \\ \cdot & \cdot & \cdot & \cdot & \cdot & \cdot & \\ \cdot & \cdot & \cdot & \cdot & \cdot & \cdot & \end{vmatrix}$$

(A. 11)

For all n greater than 6, the form of the lower right hand corner is

$$\begin{vmatrix} \cdot & \cdot & \cdot & \cdot & \cdot & \cdot & \cdot & \cdot \\ \cdot & \cdot & \cdot & \cdot & \cdot & \cdot & \cdot & \cdot \\ \cdot & \cdot & \cdot & \cdot & \cdot & \cdot & \cdot & 0 \\ \cdots & X & 0 & X & 0 & X & 0 & 0 \\ \cdots & 0 & X & 0 & X & 0 & X & 0 \\ \cdots & 0 & 0 & X & 0 & X & 0 & j\omega_{n-2} C_1 \\ \cdots & 0 & 0 & 0 & X & 0 & X & 0 \\ \cdots & 0 & 0 & 0 & 0 & j\omega_n C_1 & 0 & j\omega_n C_0 \end{vmatrix} \qquad \text{(A. 12)}$$

the X's simply denote the presence of a non-zero element. Now, the nth row can be multiplied by $\frac{-\omega_{n-2} C_1}{\omega_n C_0}$ and then added to the

(n-2)th row. This operation changes the value of the (n - 2, n - 2) element, and makes the (n - 2, n) element zero. The determinate can be expanded along the nth column, which now has only one element.

$$B_{2,1}(n) = j\omega_n C_0 B'_{2,1}(n-1) \qquad \text{(A. 13)}$$

The (') indicates that the $B_{2,1}(n-1)$ matrix has been changed by the alteration of its (n - 2, n - 2) diagonal term. However, if $B_{2,1}(n-1)$ is equal to zero simply by virtue of the arrangement of zero and non-zero elements, then $B'_{2,1}(n-1)$ must also equal zero, because this arrangement has not been disturbed. By inspection, $B_{2,1}(4) = B_{2,1}(5) = B_{2,1}(6) = 0$, because of their arrangement of zero and non-zero elements. Then $B'_{2,1}(4) = B'_{2,1}(5) = B'_{2,1}(6) = 0$.

Thus, by induction, $B_{2,1}(n)$ equals zero for all n. Now

$$\beta_{1,2}(n) = \frac{B_{2,1}(n)}{|\alpha_{22}(n)|} \qquad \text{(A. 14)}$$

and $|\alpha_{22}(n)|$ has been shown to be non-zero for all n.

Therefore, $\beta_{1,2}(n) = 0$ for all n.

$\beta_{1,2}(n)$ can be shown to equal zero for all n by the same reasoning.

APPENDIX B

VOLTAGE AND CURRENT PUMPING

In Chapter V, an iterative technique is used to compute the elastance of a pumped varactor. This technique is applicable to any circuit containing one varactor (see Fig. 5.1), but it is laborious to execute and the results are in numerical form. In this appendix, two special cases, for which a power series form of solution can be obtained, are presented.

1) The linear network can be approximated by a sinusoidal voltage source with negligible internal impedance. In this case, currents may flow at harmonics of the pump frequency, but the voltage must remain sinusoidal (Ref. 56).

2) The linear network can be approximated by a sinusoidal current source with very high internal impedance. In this case, voltages may exist at harmonics of the pump frequency, but the current is constrained to be sinusoidal.

The depletion layer capacity of a varactor diode is given by (see Section 2.2)

$$\frac{dq_t}{dv_t} = C_M = \frac{C_a}{\left(1 - \frac{v_t}{\phi}\right)^{\frac{1}{M}}} \qquad (2.1)$$

The voltage of a pumped varactor can be written as the sum of a DC bias voltage plus a time varying voltage. That is, let

$$v_t = V_{Bias} + K_1 V_M(t) \tag{B. 1}$$

then

$$C_M = \frac{C_a \phi^{\frac{1}{M}}}{(\phi - V_{Bias})^{\frac{1}{M}}} \cdot \frac{1}{\left(1 - \frac{K_1 V_M(t)}{\phi - V_{Bias}}\right)^{\frac{1}{M}}} \tag{B. 2}$$

Now define C_B as the small signal capacity at the bias point, and normalize the time varying voltage.

$$C_B \triangleq \frac{C_a \phi^{\frac{1}{M}}}{(\phi - V_{Bias})^{\frac{1}{M}}}$$

$$K_1 = -\phi + V_{Bias}$$

Then Eq. B. 2 can be rewritten as

$$\frac{dq_t}{dv_t} \triangleq C_M = C_B(1+V_M)^{-\frac{1}{M}} \tag{B. 3}$$

and

$$S_M = \frac{1}{C_B}(1+V_M)^{\frac{1}{M}} \qquad \text{(B.4)}$$

where

$$V_M > -1$$

In the case of sinusoidal voltage pumping

$$V_M = a \cos t$$

where

$$|a| < 1 .$$

The charge stored in the diode can be found by integrating Eq. B.3.

$$q_t = C_B\left(1 - \frac{1}{M}\right)^{-1}\left[1+V_M\right]^{1-\frac{1}{M}} + Q_c \qquad \text{(B.5)}$$

where Q_c is a constant of integration.

The total charge equals a constant, or bias, charge plus a charge due to the pump.

$$q_t = Q_{Bias} + K_3\, Q_M(t)$$

Q_{Bias} can be chosen such that $Q_M = 0$ when $V_M = 0$, and the time varying charge can be normalized

$$Q_{Bias} = C_B(1 - \frac{1}{M})^{-1} + Q_c$$

$$K_3 = C_B(1 - \frac{1}{M})^{-1}$$

Equation B. 5 can be written in terms of the new charge variables, and solved for V_M

$$V_M = [1 + Q_M]^{\frac{M}{M-1}} - 1 \qquad (B.6)$$

Combine Eqs. B. 3 and B. 6 to obtain an expression for the capacity in terms of the charge.

$$C_M = C_B[1 + Q_M]^{-\frac{1}{M-1}} \qquad (B.7)$$

$$S_M = \frac{1}{C_B}[1 + Q_M]^{\frac{1}{M-1}} \qquad (B.8)$$

where

$$Q_M > -1$$

For the case of sinusoidal current pumping:

$$Q_M = a \cos t$$

where

$$|a| < 1$$

Under sinusoidal pumping conditions, the expressions for the capacity of the voltage pumped diode (B. 3), for the elastance of the voltage pumped diode (B. 4) for the capacity of the current pumped diode (B. 7), and for the elastance of the current pumped diode (B. 8) have the same form:

$$K_N' = (1 + a \cos t)^{-\frac{1}{N}} \qquad \text{(B. 9)}$$

where

$N = M$ for voltage pumped capacitance

$N = -M$ for voltage pumped elastance

$N = M-1$ for current pumped capacitance

$N = -(M-1)$ for current pumped elastance

It is convenient to put this relationship in the form of a Fourier series. To do this, the expression (B.) can first be expanded in a power series.

$$K_N' = \sum_{\ell=0}^{\infty} \frac{(N+1)(2N+1) \ldots ([\ell-1]\,N+1)\, a^{\ell} (\cos t)^{\ell}}{\ell !\, N^{\ell}\, (-1)^{\ell}} \qquad \text{(B. 10)}$$

The terms of the form $(\cos t)^{\ell}$ can be expanded by using trigonometric identities.

$$(\cos t)^{\ell} = \frac{[1 + (-1)^{\ell}]\,(\ell)!}{2^{\ell+1}\,(\frac{\ell}{2})!\,(\frac{\ell}{2})!} + \frac{1}{2^{\ell-1}} \sum_{k=0}^{\left[\frac{\ell-1}{2}\right]} \frac{\ell!\,\cos\,(\ell - 2k)\,t}{(\ell-k)!\,(k)!}$$

Using this identity, the expression for $K_N^{'}$ becomes

$$K_N^{'} = \sum_{\ell=0}^{\infty} \frac{[1 + (-1)^{\ell}]\,(N+1)(2N+1)\,\ldots\,([\ell-1]\,N+1)\,a^{\ell}}{2^{\ell+1}\,(\frac{\ell}{2})!\,(\frac{\ell}{2})!\,N^{\ell}} +$$

$$\sum_{\ell=1}^{\infty} \sum_{k=0}^{\left[\frac{\ell-1}{2}\right]} \frac{(N+1)(2N+1)\,\ldots\,([\ell-1]\,N+1)\,a^{\ell}\,\cos\,(\ell - 2k)\,t}{(-1)^{\ell}\,N^{\ell}\,2^{\ell-1}\,(\ell-k)!\,(k)!}$$

This expansion can be put in the form

$$K_N^{'} = \sum_{\ell=0}^{\infty} \frac{(N+1)(2N+1)\,\ldots\,([2\ell-1]\,N+1)\,a^{2\ell}}{4^{\ell}\,(\ell)!\,(\ell)!\,N^{2\ell}} + \qquad \text{(B. 11)}$$

$$\sum_{\ell=1}^{\infty} \left[\sum_{k=0}^{\infty} \frac{(N+1)(2N+1)\,\ldots\,([\ell+2k-1]N+1)\,a^{\ell+2k}}{2^{\ell+2k-1}\,N^{\ell+2k}\,(-1)^{\ell}\,(\ell+k)!\,(k)!} \right] \cos \ell t$$

Equation B. 11 can easily be put into exponential form

$$K_N^{'} = \sum_{\ell=-\infty}^{+\infty} K_{\ell}\, e^{j\ell t}$$

where the average value is

$$K_0 = \sum_{\ell=0}^{\infty} \frac{(N+1)(2N+1)\,\ldots\,([2\ell-1]\,N+1)\,a^{2\ell}}{4^{\ell}\,(\ell)!\,(\ell)!\,N^{2\ell}} \qquad \text{(B. 12)}$$

and the coefficient of the $\ell^{\underline{th}}$ harmonic is given by

$$K_\ell = \left(-\frac{a}{2}\right)^\ell \sum_{k=0}^{\infty} \frac{(N+1)(2N+1) \ldots ([\ell + 2k - 1]\, N + 1)\, a^{2k}}{2^{2k}\, N^{2k} (\ell + k)!\, (k)!} \qquad \text{(B. 13)}$$

The values of the first 24 of these coefficients have been computed for various values of N. The results are presented in tabular form in Tables B. 1 through B. 8. The values of ℓ are in the left column; the values of a are in the top row.

FOURIER COEFFICIENTS

N = 1.000

ℓ \ a	.1	.2	.3	.4	.5	.6	.7	.8	.9
0	1.005038	1.020621	1.048285	1.091089	1.154700	1.250000	1.400280	1.666666	2.294155
1	-.050378	-.103104	-.160949	-.227724	-.309401	-.416667	-.571829	-.833333	-1.437952
2	.002525	.010416	.024712	.047529	.082904	.138889	.233516	.416667	.901292
3	-.000127	-.001052	-.003794	-.009920	-.022214	-.046296	-.095360	-.208333	-.564920
4	.000006	.000106	.000583	.002070	.005952	.015432	.038942	.104167	.354086
5	-.000000	-.000011	-.000089	-.000432	-.001595	-.005144	-.015903	-.052083	-.221937
6	.000000	.000001	.000014	.000090	.000427	.001715	.006494	.026042	.139103
7	-.000000	-.000000	-.000002	-.000019	-.000115	-.000572	-.002652	-.013021	-.087191
8	.000000	.000000	.000000	.000004	.000031	.000191	.001083	.006510	.054650
9	.000000	-.000000	-.000000	-.000001	-.000008	-.000064	-.000442	-.003255	-.034254
10	.000000	.000000	.000000	.000000	.000002	.000021	.000181	.001628	.021470
11	.000000	.000000	-.000000	-.000000	-.000001	-.000007	-.000074	-.000814	-.013457
12	.000000	.000000	.000000	.000000	.000000	.000002	.000030	.000407	.008435
13	.000000	.000000	.000000	-.000000	-.000000	-.000001	-.000012	-.000203	-.005287
14	.000000	.000000	.000000	.000000	.000000	.000000	.000005	.000102	.003314
15	.000000	.000000	.000000	.000000	-.000000	-.000000	-.000002	-.000051	-.002077
16	.000000	.000000	.000000	.000000	.000000	.000000	.000001	.000025	.001302
17	.000000	.000000	.000000	.000000	-.000000	-.000000	-.000000	-.000013	-.000816
18	.000000	.000000	.000000	.000000	.000000	.000000	.000000	.000006	.000511
19	.000000	.000000	.000000	.000000	.000000	-.000000	-.000000	-.000003	-.000321
20	.000000	.000000	.000000	.000000	.000000	.000000	.000000	.000002	.000201
21	.000000	.000000	.000000	.000000	.000000	.000000	-.000000	-.000001	-.000126
22	.000000	.000000	.000000	.000000	.000000	.000000	.000000	.000000	.000079
23	.000000	.000000	.000000	.000000	.000000	.000000	.000000	-.000000	-.000049
24	.000000	.000000	.000000	.000000	.000000	.000000	.000000	.000000	.000031

Table B. 1 Fourier coefficients for N= 1.0

a	.1	.2	.3	.4	.5	.6	.7	.8	.9
ℓ									
0	1.001885	1.007669	1.017761	1.032954	1.054649	1.085357	1.129987	1.199854	1.331821
1	-.025118	-.050963	-.078364	-.108395	-.142612	-.183556	-.235984	-.310739	-.443336
2	.000944	.003863	.009033	.016999	.028749	.046116	.072832	.117946	.212854
3	-.000039	-.000325	-.001156	-.002959	-.006429	-.012842	-.024881	-.049450	-.112405
4	.000002	.000029	.000155	.000541	.001509	.003751	.008912	.021716	.062066
5	-.000000	-.000003	-.000021	-.000102	-.000364	-.001126	-.003280	-.009797	-.035174
6	.000000	.000000	.000003	.000019	.000089	.000344	.001229	.004499	.020277
7	-.000000	-.000000	-.000000	-.000004	-.000022	-.000107	-.000467	-.002092	-.011832
8	.000000	.000000	.000000	.000001	.000006	.000033	.000179	.000981	.006967
9	.000000	-.000000	-.000000	-.000000	-.000001	-.000011	-.000069	-.000464	-.004131
10	.000000	.000000	.000000	.000000	.000000	.000003	.000027	.000221	.002463
11	.000000	.000000	-.000000	-.000000	-.000000	-.000001	-.000010	-.000105	-.001475
12	.000000	.000000	.000000	.000000	.000000	.000000	.000004	.000050	.000887
13	.000000	.000000	.000000	-.000000	-.000000	-.000000	-.000002	-.000024	-.000535
14	.000000	.000000	.000000	.000000	.000000	.000000	.000001	.000012	.000324
15	.000000	.000000	.000000	.000000	-.000000	-.000000	-.000000	-.000006	-.000196
16	.000000	.000000	.000000	.000000	.000000	.000000	.000000	.000003	.000119
17	.000000	.000000	.000000	.000000	.000000	-.000000	-.000000	-.000001	-.000073
18	.000000	.000000	.000000	.000000	.000000	.000000	.000000	.000001	.000044
19	.000000	.000000	.000000	.000000	.000000	.000000	-.000000	-.000000	-.000027
20	.000000	.000000	.000000	.000000	.000000	.000000	.000000	.000000	.000017
21	.000000	.000000	.000000	.000000	.000000	.000000	.000000	-.000000	-.000010
22	.000000	.000000	.000000	.000000	.000000	.000000	.000000	.000000	.000006
23	.000000	.000000	.000000	.000000	.000000	.000000	.000000	-.000000	-.000004
24	.000000	.000000	.000000	.000000	.000000	.000000	.000000	.000000	.000002

Table B.2 Fourier coefficients for N= 2.0

FOURIER COEFFICIENTS

N = 3.000

ℓ \ a	.1	.2	.3	.4	.5	.6	.7	.8	.9
0	1.001117	1.004533	1.010465	1.019321	1.031818	1.049209	1.073874	1.111075	1.176859
1	-.016732	-.033865	-.051851	-.071266	-.092920	-.118101	-.149130	-.191060	-.259339
2	.000559	.002282	.005312	.009932	.016645	.026360	.040877	.064375	.110414
3	-.000022	-.000179	-.000635	-.001614	-.003474	-.006849	-.013028	-.025173	-.054354
4	.000001	.000015	.000081	.000281	.000776	.001905	.004443	.010524	.028562
5	-.000000	-.000001	-.000011	-.000051	-.000180	-.000551	-.001575	-.004571	-.015579
6	.000000	.000000	.000001	.000009	.000043	.000163	.000572	.002035	.008706
7	-.000000	-.000000	-.000000	-.000002	-.000010	-.000049	-.000212	-.000922	-.004948
8	.000000	.000000	.000000	.000000	.000003	.000015	.000079	.000423	.002848
9	.000000	-.000000	-.000000	-.000000	-.000001	-.000005	-.000030	-.000196	-.001655
10	.000000	.000000	.000000	.000000	.000000	.000001	.000011	.000091	.000969
11	.000000	.000000	-.000000	-.000000	-.000000	-.000000	-.000004	-.000043	-.000571
12	.000000	.000000	.000000	.000000	.000000	.000000	.000002	.000020	.000339
13	.000000	.000000	.000000	-.000000	-.000000	-.000000	-.000001	-.000010	-.000201
14	.000000	.000000	.000000	.000000	.000000	.000000	.000000	.000005	.000120
15	.000000	.000000	.000000	.000000	-.000000	-.000000	-.000000	-.000002	-.000072
16	.000000	.000000	.000000	.000000	.000000	.000000	.000000	.000001	.000043
17	.000000	.000000	.000000	.000000	.000000	-.000000	-.000000	-.000001	-.000026
18	.000000	.000000	.000000	.000000	.000000	.000000	.000000	.000000	.000016
19	.000000	.000000	.000000	.000000	.000000	.000000	-.000000	-.000000	-.000010
20	.000000	.000000	.000000	.000000	.000000	.000000	.000000	.000000	.000006
21	.000000	.000000	.000000	.000000	.000000	.000000	.000000	-.000000	-.000004
22	.000000	.000000	.000000	.000000	.000000	.000000	.000000	.000000	.000002
23	.000000	.000000	.000000	.000000	.000000	.000000	.000000	.000000	-.000001
24	.000000	.000000	.000000	.000000	.000000	.000000	.000000	.000000	.000001

Table B.3 Fourier coefficients for N=3.0

FOURIER COEFFICIENTS

N = 4.000

a / l	.1	.2	.3	.4	.5	.6	.7	.8	.9
0	1.000785	1.003184	1.007338	1.013516	1.022184	1.034150	1.050924	1.075779	1.118372
1	-.012544	-.025360	-.038752	-.053104	-.068950	-.087126	-.109111	-.138051	-.183244
2	.000393	.001602	.003721	.006937	.011574	.018218	.028008	.043533	.072923
3	-.000015	-.000121	-.000429	-.001087	-.002329	-.004563	-.008603	-.016401	-.034563
4	.000001	.000010	.000053	.000184	.000507	.001237	.002860	.006682	.017691
5	-.000000	-.000001	-.000007	-.000033	-.000116	-.000351	-.000994	-.002845	-.009458
6	.000000	.000000	.000001	.000006	.000027	.000102	.000355	.001246	.005200
7	.000000	-.000000	-.000000	-.000001	-.000006	-.000030	-.000130	-.000557	-.002916
8	.000000	.000000	.000000	.000000	.000002	.000009	.000048	.000253	.001659
9	.000000	-.000000	-.000000	-.000000	-.000000	-.000003	-.000018	-.000116	-.000954
10	.000000	.000000	.000000	.000000	.000000	.000001	.000007	.000054	.000554
11	.000000	.000000	.000000	-.000000	-.000000	-.000000	-.000003	-.000025	-.000324
12	.000000	.000000	.000000	.000000	.000000	.000000	.000001	.000012	.000190
13	.000000	.000000	.000000	.000000	-.000000	-.000000	-.000000	-.000006	-.000112
14	.000000	.000000	.000000	.000000	.000000	.000000	.000000	.000003	.000067
15	.000000	.000000	.000000	.000000	.000000	-.000000	-.000000	-.000001	-.000040
16	.000000	.000000	.000000	.000000	.000000	.000000	.000000	.000001	.000024
17	.000000	.000000	.000000	.000000	.000000	.000000	-.000000	-.000000	-.000014
18	.000000	.000000	.000000	.000000	.000000	.000000	.000000	.000000	.000009
19	.000000	.000000	.000000	.000000	.000000	.000000	-.000000	-.000000	-.000005
20	.000000	.000000	.000000	.000000	.000000	.000000	.000000	.000000	.000003
21	.000000	.000000	.000000	.000000	.000000	.000000	.000000	-.000000	-.000002
22	.000000	.000000	.000000	.000000	.000000	.000000	.000000	.000000	.000001
23	.000000	.000000	.000000	.000000	.000000	.000000	.000000	.000000	-.000001
24	.000000	.000000	.000000	.000000	.000000	.000000	.000000	.000000	.000000

Table B. 4 Fourier coefficients for N=4.0

FOURIER COEFFICIENTS

N = -1.000

ℓ \ a	.1	.2	.3	.4	.5	.6	.7	.8	.9
0	1.000000	1.000000	1.000000	1.000000	1.000000	1.000000	1.000000	1.000000	1.000000
1	.050000	.100000	.150000	.200000	.250000	.300000	.350000	.400000	.450000
2	.000000	.000000	.000000	.000000	.000000	.000000	.000000	.000000	.000000
3	.000000	.000000	.000000	.000000	.000000	.000000	.000000	.000000	.000000
4	.000000	.000000	.000000	.000000	.000000	.000000	.000000	.000000	.000000
5	.000000	.000000	.000000	.000000	.000000	.000000	.000000	.000000	.000000
6	.000000	.000000	.000000	.000000	.000000	.000000	.000000	.000000	.000000
7	.000000	.000000	.000000	.000000	.000000	.000000	.000000	.000000	.000000
8	.000000	.000000	.000000	.000000	.000000	.000000	.000000	.000000	.000000
9	.000000	.000000	.000000	.000000	.000000	.000000	.000000	.000000	.000000
10	.000000	.000000	.000000	.000000	.000000	.000000	.000000	.000000	.000000
11	.000000	.000000	.000000	.000000	.000000	.000000	.000000	.000000	.000000
12	.000000	.000000	.000000	.000000	.000000	.000000	.000000	.000000	.000000
13	.000000	.000000	.000000	.000000	.000000	.000000	.000000	.000000	.000000
14	.000000	.000000	.000000	.000000	.000000	.000000	.000000	.000000	.000000
15	.000000	.000000	.000000	.000000	.000000	.000000	.000000	.000000	.000000
16	.000000	.000000	.000000	.000000	.000000	.000000	.000000	.000000	.000000
17	.000000	.000000	.000000	.000000	.000000	.000000	.000000	.000000	.000000
18	.000000	.000000	.000000	.000000	.000000	.000000	.000000	.000000	.000000
19	.000000	.000000	.000000	.000000	.000000	.000000	.000000	.000000	.000000
20	.000000	.000000	.000000	.000000	.000000	.000000	.000000	.000000	.000000
21	.000000	.000000	.000000	.000000	.000000	.000000	.000000	.000000	.000000
22	.000000	.000000	.000000	.000000	.000000	.000000	.000000	.000000	.000000
23	.000000	.000000	.000000	.000000	.000000	.000000	.000000	.000000	.000000
24	.000000	.000000	.000000	.000000	.000000	.000000	.000000	.000000	.000000

Table B. 5 Fourier coefficients for N=-1.0

FOURIER COEFFICIENTS

N = -2.000

l \ a	.1	.2	.3	.4	.5	.6	.7	.8	.9
0	.999374	.997476	.994251	.989596	.983343	.975224	.964798	.951263	.932819
1	.025024	.050190	.075655	.101596	.128237	.155886	.185002	.216381	.251768
2	-.000313	-.001266	-.002895	-.005272	-.008511	-.012804	-.018472	-.026129	-.037230
3	.000008	.000064	.000222	.000549	.001135	.002118	.003729	.006415	.011309
4	-.000000	-.000004	-.000021	-.000071	-.000190	-.000439	-.000945	-.001983	-.004344
5	.000000	.000000	.000002	.000010	.000035	.000102	.000269	.000689	.001881
6	-.000000	-.000000	-.000000	-.000002	-.000007	-.000025	-.000082	-.000257	-.000875
7	.000000	.000000	.000000	.000000	.000001	.000007	.000026	.000100	.000428
8	.000000	-.000000	-.000000	-.000000	-.000000	-.000002	-.000009	-.000041	-.000217
9	.000000	.000000	.000000	.000000	.000000	.000001	.000003	.000017	.000113
10	.000000	.000000	-.000000	-.000000	-.000000	-.000000	-.000001	-.000007	-.000060
11	.000000	.000000	.000000	.000000	.000000	.000000	.000000	.000003	.000032
12	.000000	.000000	.000000	.000000	-.000000	-.000000	-.000000	-.000001	-.000018
13	.000000	.000000	.000000	.000000	.000000	.000000	.000000	.000001	.000010
14	.000000	.000000	.000000	.000000	.000000	-.000000	-.000000	-.000000	-.000005
15	.000000	.000000	.000000	.000000	.000000	.000000	.000000	.000000	.000003
16	.000000	.000000	.000000	.000000	.000000	.000000	-.000000	-.000000	-.000002
17	.000000	.000000	.000000	.000000	.000000	.000000	.000000	.000000	.000001
18	.000000	.000000	.000000	.000000	.000000	.000000	.000000	-.000000	-.000001
19	.000000	.000000	.000000	.000000	.000000	.000000	.000000	.000000	.000000
20	.000000	.000000	.000000	.000000	.000000	.000000	.000000	.000000	-.000000
21	.000000	.000000	.000000	.000000	.000000	.000000	.000000	.000000	.000000
22	.000000	.000000	.000000	.000000	.000000	.000000	.000000	.000000	-.000000
23	.000000	.000000	.000000	.000000	.000000	.000000	.000000	.000000	.000000
24	.000000	.000000	.000000	.000000	.000000	.000000	.000000	.000000	.000000

Table B. 6 Fourier coefficients for N=-2.0

FOURIER COEFFICIENTS

N = -3.000

ℓ \ a	.1	.2	.3	.4	.5	.6	.7	.8	.9
0	.999443	.997753	.994869	.990683	.985012	.977561	.967833	.954883	.936473
1	.016690	.033522	.050649	.068254	.086570	.105924	.126826	.150202	.178213
2	-.000279	-.001128	-.002588	-.004733	-.007690	-.011668	-.017036	-.024519	-.035945
3	.000008	.000063	.000221	.000548	.001142	.002151	.003839	.006738	.012283
4	-.000000	-.000004	-.000023	-.000076	-.000204	-.000477	-.001041	-.002231	-.005073
5	.000000	.000000	.000003	.000012	.000040	.000116	.000311	.000814	.002313
6	-.000000	-.000000	-.000000	-.000002	-.000008	-.000030	-.000099	-.000316	-.001121
7	.000000	.000000	.000000	.000000	.000002	.000008	.000033	.000127	.000566
8	.000000	-.000000	-.000000	-.000000	-.000000	-.000002	-.000011	-.000053	-.000295
9	.000000	.000000	.000000	.000000	.000000	.000001	.000004	.000023	.000157
10	.000000	.000000	-.000000	-.000000	-.000000	-.000000	-.000001	-.000010	-.000085
11	.000000	.000000	.000000	.000000	.000000	.000000	.000000	.000004	.000047
12	.000000	.000000	.000000	.000000	-.000000	-.000000	-.000000	-.000002	-.000026
13	.000000	.000000	.000000	.000000	.000000	.000000	.000000	.000001	.000015
14	.000000	.000000	.000000	.000000	.000000	-.000000	-.000000	-.000000	-.000008
15	.000000	.000000	.000000	.000000	.000000	.000000	.000000	.000000	.000005
16	.000000	.000000	.000000	.000000	.000000	.000000	-.000000	-.000000	-.000003
17	.000000	.000000	.000000	.000000	.000000	.000000	.000000	.000000	.000002
18	.000000	.000000	.000000	.000000	.000000	.000000	.000000	-.000000	-.000001
19	.000000	.000000	.000000	.000000	.000000	.000000	.000000	.000000	.000001
20	.000000	.000000	.000000	.000000	.000000	.000000	.000000	-.000000	-.000000
21	.000000	.000000	.000000	.000000	.000000	.000000	.000000	.000000	.000000
22	.000000	.000000	.000000	.000000	.000000	.000000	.000000	.000000	-.000000
23	.000000	.000000	.000000	.000000	.000000	.000000	.000000	.000000	.000000
24	.000000	.000000	.000000	.000000	.000000	.000000	.000000	.000000	.000000

Table B.7 Fourier coefficients for N=-3.0

FOURIER COEFFICIENTS

N = -4.000

ℓ \ a	.1	.2	.3	.4	.5	.6	.7	.8	.9
0	.999530	.998102	.995662	.992107	.987271	.980878	.972454	.961088	.944555
1	.012521	.025167	.038076	.051412	.065386	.080300	.096634	.115278	.138379
2	-.000235	-.000953	-.002190	-.004015	-.006545	-.009977	-.014660	-.021299	-.031720
3	.000007	.000056	.000196	.000488	.001021	.001934	.003475	.006165	.011445
4	-.000000	-.000004	-.000021	-.000070	-.000188	-.000442	-.000973	-.002109	-.004891
5	.000000	.000000	.000002	.000011	.000038	.000110	.000297	.000789	.002286
6	-.000000	-.000000	-.000000	-.000002	-.000008	-.000029	-.000096	-.000311	-.001130
7	.000000	.000000	.000000	.000000	.000002	.000008	.000032	.000128	.000580
8	.000000	-.000000	-.000000	-.000000	-.000000	-.000002	-.000011	-.000054	-.000306
9	.000000	.000000	.000000	.000000	.000000	.000001	.000004	.000023	.000165
10	.000000	.000000	-.000000	-.000000	-.000000	-.000000	-.000001	-.000010	-.000090
11	.000000	.000000	.000000	.000000	.000000	.000000	.000001	.000004	.000050
12	.000000	.000000	.000000	.000000	-.000000	-.000000	-.000000	-.000002	-.000028
13	.000000	.000000	.000000	.000000	.000000	.000000	.000000	.000001	.000016
14	.000000	.000000	.000000	.000000	.000000	-.000000	-.000000	-.000000	-.000009
15	.000000	.000000	.000000	.000000	.000000	.000000	.000000	.000000	.000005
16	.000000	.000000	.000000	.000000	.000000	.000000	-.000000	-.000000	-.000003
17	.000000	.000000	.000000	.000000	.000000	.000000	.000000	.000000	.000002
18	.000000	.000000	.000000	.000000	.000000	.000000	.000000	-.000000	-.000001
19	.000000	.000000	.000000	.000000	.000000	.000000	.000000	.000000	.000001
20	.000000	.000000	.000000	.000000	.000000	.000000	.000000	-.000000	-.000000
21	.000000	.000000	.000000	.000000	.000000	.000000	.000000	.000000	.000000
22	.000000	.000000	.000000	.000000	.000000	.000000	.000000	.000000	-.000000
23	.000000	.000000	.000000	.000000	.000000	.000000	.000000	.000000	.000000
24	.000000	.000000	.000000	.000000	.000000	.000000	.000000	.000000	.000000

Table B.8 Fourier coefficients for N=-4.0

APPENDIX C

THE COMPUTER FLOW DIAGRAM TO SOLVE THE PUMP CIRCUIT EQUATION FOR SINGLE TUNING

This appendix presents the computer flow block diagram for the solution of Eq. 5.14. This equation describes the behavior of the circuit in the absence of signal, and is valid for an abrupt junction diode, although it can be easily modified for any other type of reversed bias diode.

$$Q_p(t) = L^{-1}\left\{\frac{1}{s\,Z(s)}\left[E_{in}(s) - L\left\{\frac{Q_p^{\,2}(t)}{4} + Q_p(t)\right\}\right]\right\} \qquad (5.14)$$

The method of solution which is diagrammed here implements the iterative procedure described in Section 5.3. It is useful whenever the impedance of the linear portion of the circuit is such that

$$\left| n\omega_p\, Z(n\omega_p) \right| > 2 \qquad (5.32)$$

when $n = 2, 3, \ldots$

The notation used in the block diagram is consistent with that introduced in Chapter V. The computer block diagram is shown in Fig. C.1. It computes both the waveform of the diode charge, $Q_p(t)$, and the Fourier analysis of this waveform. The input data needed includes $Q_A(1)$, L, R_s, G and C_s.

The theoretical results presented in Chapter VII were obtained by an algorithm of this procedure programmed in MAD for an IBM 7090 computer. From four to twelve iterations were necessary to obtain one millivolt accuracy. This number of iterations varied depending upon both the pump level and the accuracy of the initial estimate, $Q_0(t)$. On the average, each iteration took about one second of computer running time.

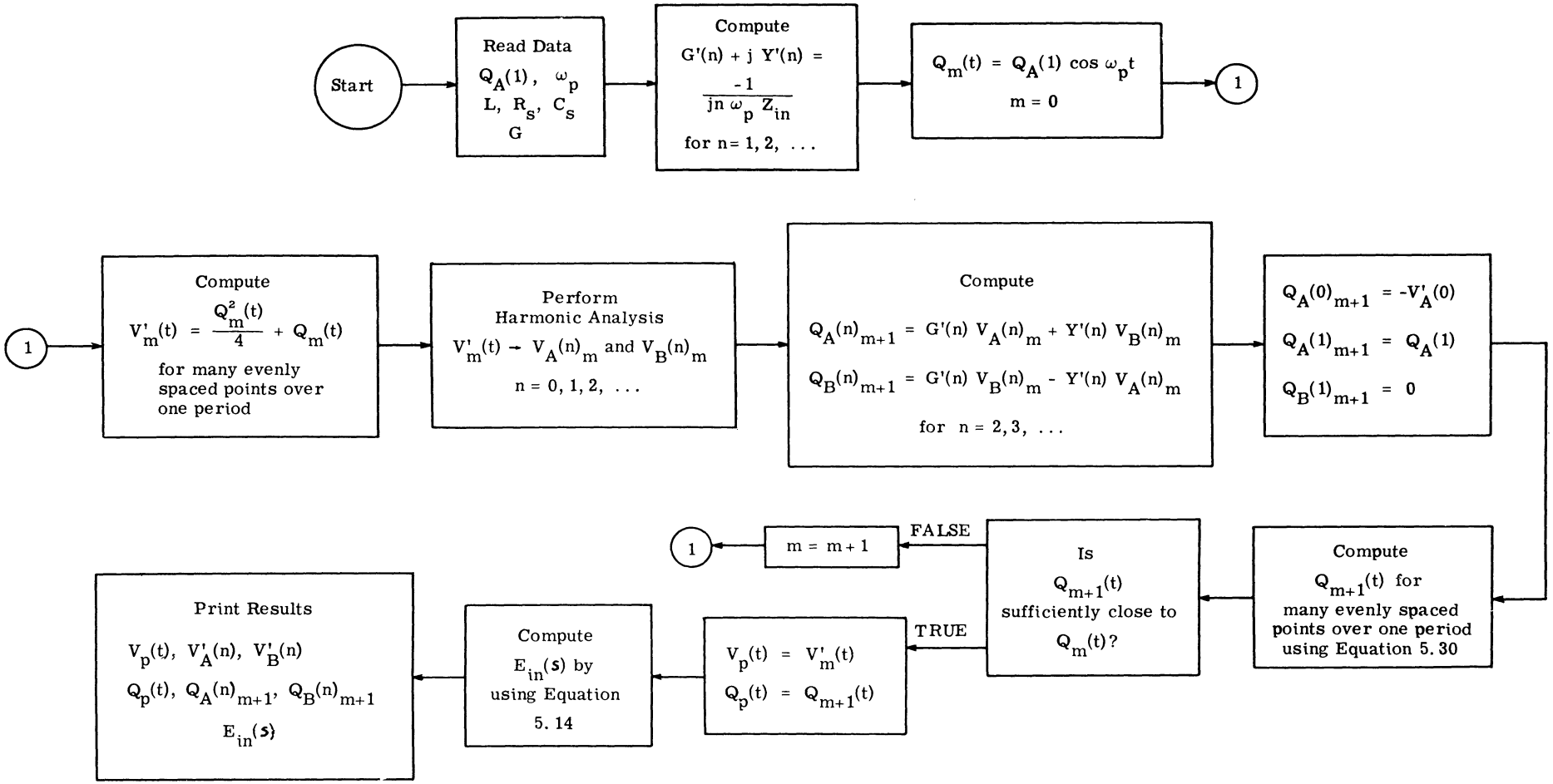

Fig. C.1. The computer flow diagram to solve the pump circuit equation for single tuning.

APPENDIX D

THE COMPUTER FLOW DIAGRAM TO SOLVE THE DISTRIBUTED CIRCUIT EQUATION

This appendix presents the computer flow block diagram for the solution of Eq. 5.13. This equation describes pump circuit behavior in the absence of signal, and is valid for an abrupt junction diode. However, both the equation, and the program may be adapted to fit any type of reversed biased varactor.

$$0 = E_{in}(s) - s\,Z(s)\,Q_p(s) - L\left\{Q_p(t) + \frac{Q_p^{\,2}(t)}{4}\right\} \qquad (5.13)$$

The method of solution diagrammed here implements the iteration procedure of Section 5.4. It is useful for all circuit configurations which contain one varactor. However, it is more complex than the method of Appendix C, and generally, the computer running time is longer. The computer block diagram is shown in Fig. D.1. The notation used is consistent with that introduced in Chapter V. Both the waveform of the diode charge $Q_p(t)$, and the Fourier analysis of this waveform are computed. The input data needed includes $Q_A(1)$, ω_p, and $Z(s)$ [or at least enough data to determine $Z(s)$].

In Step (2) of the m^{th} iteration, it is necessary to set up and solve the following set of equations for $\epsilon'_m(t)$.

$$\delta_m(s) = \epsilon'_m(s)\,[-1 - s\,Z(s)] - L\left\{\frac{Q_m(t)\,\epsilon'_m(t)}{2}\right\} \qquad (D.1)$$

where because only the "steady state" solution is of interest the equation error can be written as

$$\delta_m(t) = \frac{\delta_A(0)_m}{2} + \sum_{n=2}^{\infty}\left[\delta_A(n)_m \cos n\omega_p t + \delta_B(n)_m \sin n\omega_p t\right] \qquad (D.2)$$

and the desired correction term is

$$\epsilon'_m(t) = \frac{\epsilon'_A(0)_m}{2} + \sum_{n=2}^{\infty}\left[\epsilon'_A(n)_m \cos n\omega_p t + \epsilon'_B(n)_m \sin n\omega_p t\right] \qquad (D.3)$$

The left side of Eq. D. 1 can be expressed in the time domain as a Fourier series. In the time domain the first two terms of the right side of the equation can be written as

$$L^{-1}\{\epsilon'_m(s)\,[1 + s\,Z(s)]\} = \sum_{n=2}^{\infty}\left[\epsilon'_{Am}(n)\,R'(n) + \epsilon'_{Bm}(n)\,X'(n)\right]\cos n\omega_p t + \sum_{n=2}^{\infty}\left[\epsilon'_{Bm}(n)\,R'(n) - \epsilon'_{Am}(n)\,X'(n)\right]\sin n\omega_p t \qquad (D.4)$$

where the Thevenin linear impedance at pump harmonic is expressed as

$$Z(n\omega_p) = R(n) + j\,X(n) \qquad (5.12)$$

and

$$(-1 - Z(n\omega)\,p) \triangleq R'(n) + j\,X'(n) \qquad \text{(D. 5)}$$

for $n = 1, 2, 3, \ldots$

In the time domain, the last term on the left side of the equation (Eq. D. 1) can be written as the product of two infinite Fourier series. The result, of course, is a third Fourier series, whose coefficients are combinations of $Q_{Am}(n)$, $Q_{Bm}(n)$, $\epsilon'_{Am}(n)$, and $\epsilon'_{Bm}(n)$. An infinite set of simultaneous linear equations can now be generated by equating coefficients of the $\cos n\omega_p t$ terms and the $\sin n\omega_p t$ terms in Eq. D. 1. The $n = 1$ term can be omitted from this set of equations, because both $\delta_m(t)$ and $\epsilon'_m(t)$ have no components at frequency ω_p.

This infinite set of equations can be reduced to a finite set by truncating each of the series and neglecting all harmonics beyond the ℓth.

The remaining equations can be put into the form of a $(2\ell - 1) \times (2\ell - 1)$ matrix.

$$
\left[\begin{array}{c|ccc|ccc}
\eta_{1,1} & \eta_{1,2} & \cdots & \eta_{1,\ell} & \eta_{1,\ell+1} & \cdots & \eta_{1,2\ell-1} \\
\hline
\eta_{2,1} & \eta_{2,2} & & & \eta_{2,\ell+1} & & \\
 & \cdot & & & \cdot & & \\
 & \cdot & & & \cdot & & \\
 & \cdot & & & \cdot & & \\
\eta_{\ell,1} & & & \eta_{\ell,\ell} & & & \eta_{\ell,2\ell-1} \\
\hline
 & \eta_{\ell+1,2} & & & \eta_{\ell+1,\ell+1} & & \\
 & \cdot & & & \cdot & & \\
 & \cdot & & & \cdot & & \\
 & \cdot & & & \cdot & & \\
\eta_{2\ell-1,1} & & & \eta_{2\ell-1,\ell} & & & \eta_{2\ell-1,2\ell-1}
\end{array}\right]
\times
\left|\begin{array}{c}
\epsilon'_A(0) \\
\hline
\epsilon'_A(2) \\
\epsilon'_A(3) \\
 \\
 \\
 \\
\epsilon'_A(\ell) \\
\hline
\epsilon'_B(2) \\
\epsilon'_B(3) \\
\cdot \\
\cdot \\
\cdot \\
\epsilon'_B(\ell)
\end{array}\right|
=
\left|\begin{array}{c}
\delta_A(0) \\
\hline
\delta_A(2) \\
\delta_A(3) \\
\delta_A(4) \\
\cdot \\
\cdot \\
\cdot \\
\delta_A(\ell) \\
\hline
\delta_B(2) \\
\delta_B(3) \\
\cdot \\
\cdot \\
\cdot \\
\delta_B(\ell)
\end{array}\right|
$$

(D. 6)

Every term in this matrix has the subscript m implied. The ϵ' terms are coefficients of sines and cosines which are multiplied by constants [the R'(n) and X'(n) terms] and by other sine and cosine terms $[Q_m(t)]$.

The resulting terms are, of course, also sine and cosine terms, whose coefficients are the δ's. The individual elements of the η matrix are constants plus the coefficients of products which have one of the forms:

(a) [sin r] x [sin s]

(b) [sin r] x [cos s]

or (c) [cos r] x [cos s] .

Using the formula for products of trigonometric functions and after much labor, the matrix elements can be found to be

r and s are dummy indices $2 \leq r \leq \ell$, $2 \leq s \leq \ell$

$$\eta_{1,1} = \frac{1}{2} Q_A(0) + 1 \qquad \text{(D. 7)}$$

$$\eta_{1,r} = \frac{1}{4} Q_A(r) \qquad \text{(D. 8)}$$

$$\eta_{r,1} = \frac{1}{2} Q_A(r) \qquad \text{(D. 9)}$$

$$\eta_{1,r+\ell-1} = \frac{1}{4} Q_B(r) \qquad \text{(D. 10)}$$

$$\eta_{r+\ell-1,1} = \frac{1}{2} Q_B(r) \qquad \text{(D. 11)}$$

$$\eta_{r,\,r} = \frac{1}{2} Q_A(0) + \frac{1}{4} Q_A(2r) + R'(r) \qquad \text{(D. 12)}$$

$$\eta_{r+\ell-1,\,r+\ell-1} = \frac{1}{2} Q_A(0) - \frac{1}{4} Q_A(2r) + R'(r) \qquad \text{(D. 13)}$$

$$\eta_{r,\,r+\ell-1} = \frac{1}{4} Q_B(2r) + X'(r) \qquad \text{(D. 14)}$$

$$\eta_{r+\ell-1,\,r} = \frac{1}{4} Q_B(2r) - X'(r) \qquad \text{(D. 15)}$$

The following hold only for $s \neq r$

$$\eta_{s,\,r} = \frac{1}{4} Q_A(s+r) + \frac{1}{4} Q_A(|s-r|) \qquad \text{(D. 16)}$$

$$\eta_{s+\ell-1,\,r+\ell-1} = \frac{1}{4} Q_A(|s-r|) - \frac{1}{4} Q_A(s+r) \qquad \text{(D. 17)}$$

$$\eta_{s,\,r+\ell-1} = \frac{1}{4} Q_B(|s-r|) \pm \frac{1}{4} Q_B(s+r) \qquad \text{(D. 18)}$$

$$\eta_{s+\ell-1,\,r} = \frac{1}{4} Q_B(s+r) \pm \frac{1}{4} Q_B(|s-r|) \qquad \text{(D. 19)}$$

In (D. 18) use + when $s > r$, - when $s < r$

In (D. 19) use - when $s > r$, + when $s < r$.

The theoretical results presented in this paper were obtained by an algorithm of this procedure programmed in MAD for an IBM 7090 computer. The number of iterations needed to compute each pump voltage waveform varies depending upon the accuracy of the initial estimate, $Q_0(t)$, and the accuracy desired for the solution.

For the data presented in this paper from three to eleven iterations were necessary to obtain one millivolt accuracy. The computer

running time for each iteration depends upon the size of the η matrix and whether diffusion effects are included in the program. For the distributed network and a matrix large enough to include the first eight harmonics between three and eight iterations are necessary. The running time for each iteration is approximately three seconds.

The running time increases considerably when the matrix size is increased to include the first twenty harmonics, and diffusion effects are included. Under these conditions, the number of iterations averages nine to eleven, and the running time for each iteration is approximately ten seconds.

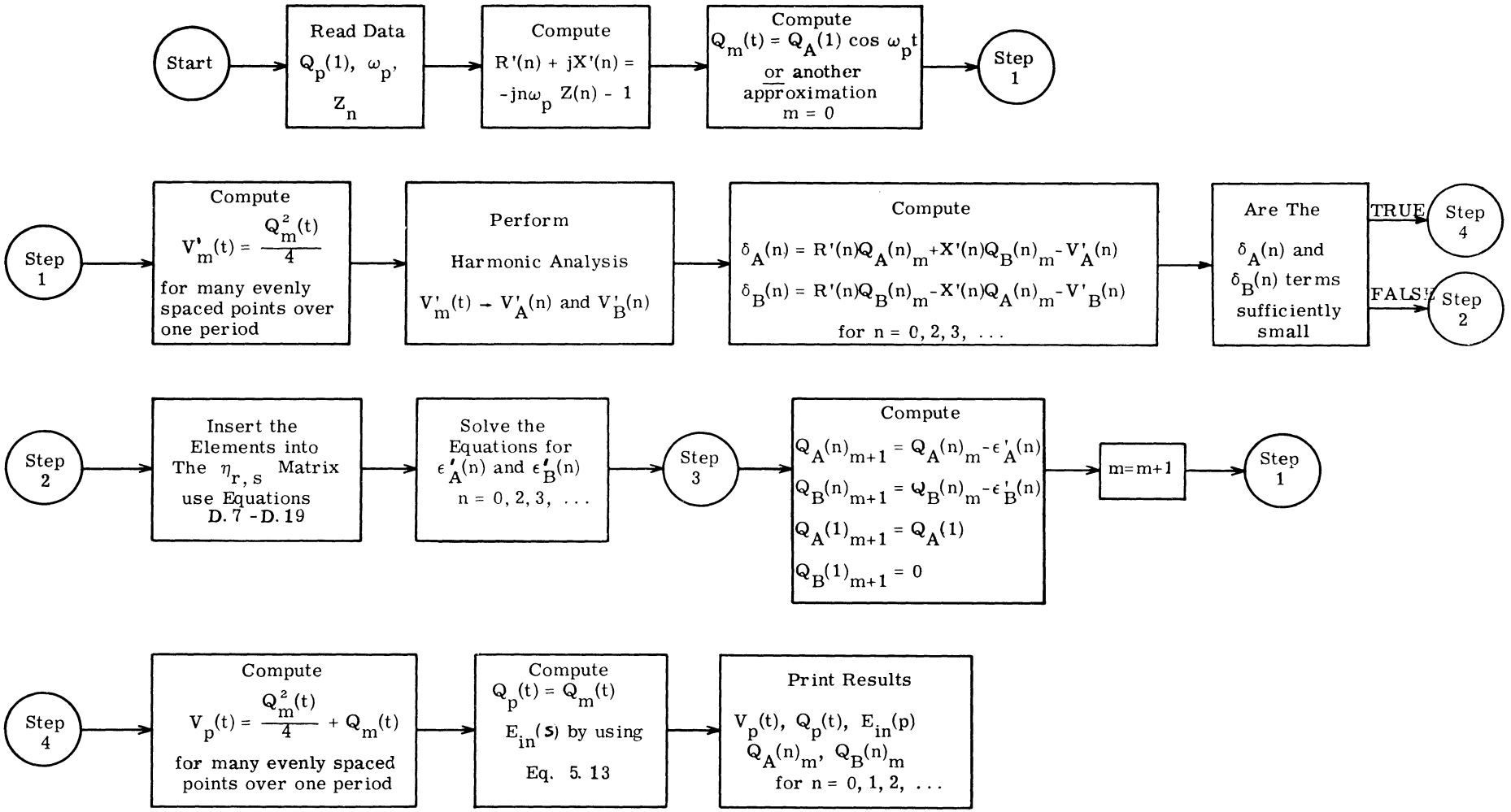

Fig. D.1. The computer flow diagram to solve the distributed circuit equation.

APPENDIX E

MEASUREMENT OF VARACTOR DIODES

This appendix presents the measured characteristics of the diodes used in the experiments. A summary of the measurements which were performed is shown in Table E. 1, the data itself is shown in Fig. E. 2 and Table E. 2. It can be seen from Table E. 1 that a complete set of measurements was not performed on every diode. In every case, however, enough information was obtained to produce a model which represents the diode under circuit conditions. The measurement techniques are briefly described below.

Diode Number	Used In Circuit	Data Presented In:		
		Barrier Layer Capacity	Q-V Relation	Diffusion Capacity P_n, τ, β
PC 1430 D	"Lumped"	Fig. E. 1(a)	Fig. E. 2(a)	
PC 0642 C	"Distributed"	Fig. E. 1(b)	Fig. E. 2(b)	
PC 0622 C	"Diffusion"	Fig. E. 1(c)		Table E. 2
Ideal abrupt junction			Fig. E. 2(c)	

Table E. 1. Varactor Measurements

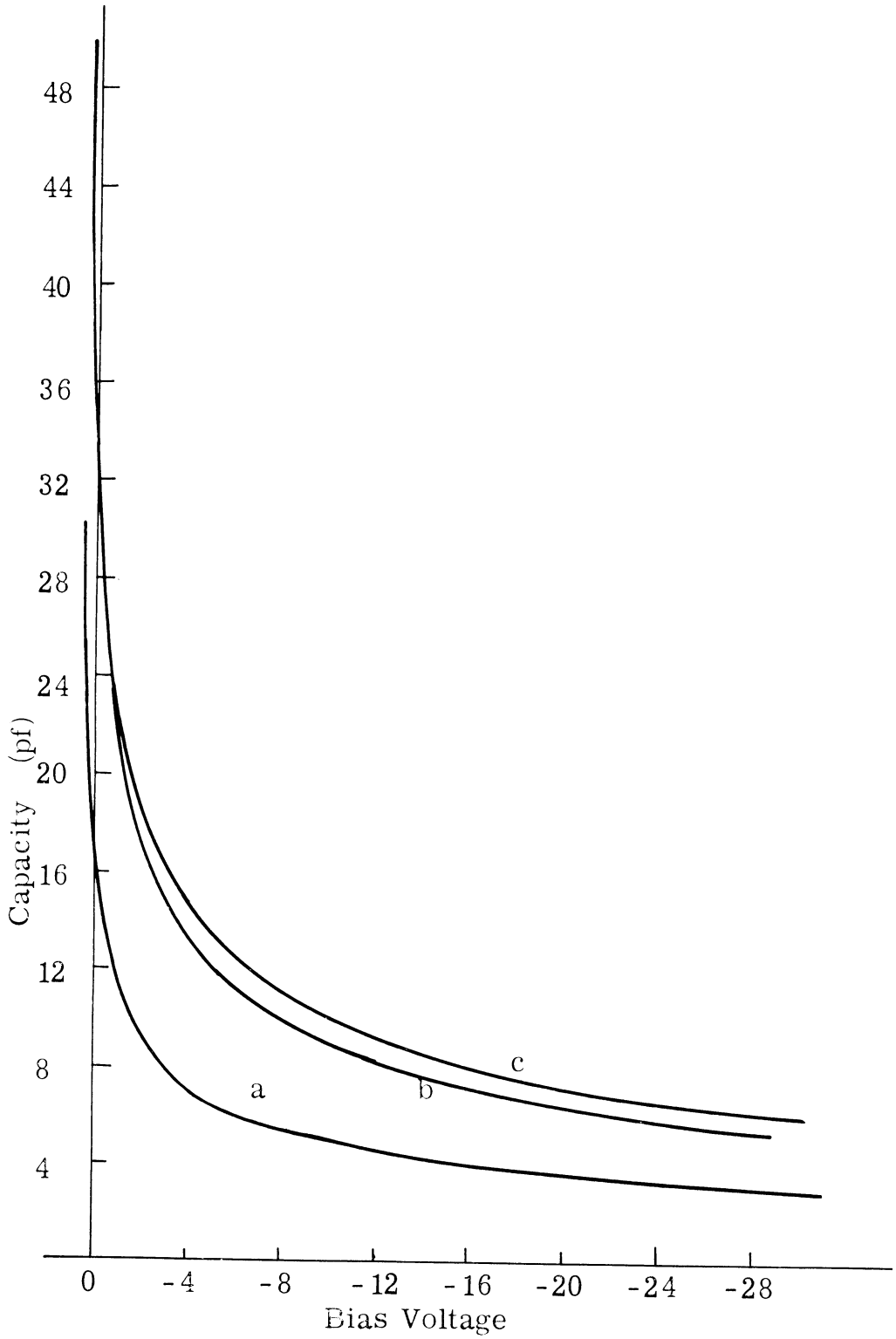

Fig. E. 1. Measured depletion layer capacity

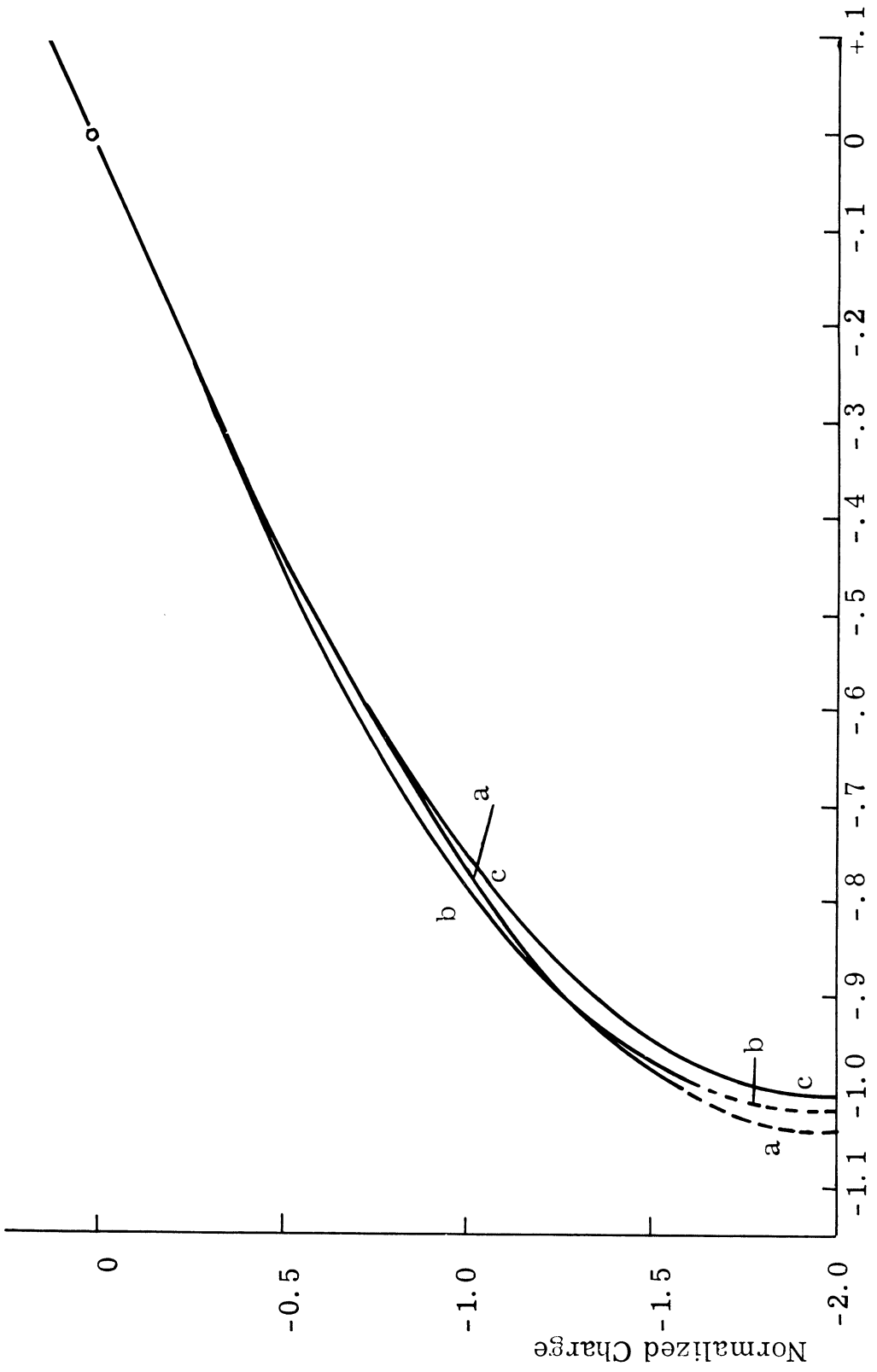

Fig. E. 2. Measured stored charge

Measurements of barrier layer capacity were made on the GR 821-A Parallel-T bridge. All these were taken at 1 MHz, and are ordinary RF bridge measurements, except for two minor points:

a) The circuit was arranged so as to minimize the effect of the DC. bias supply on the HF signal. By supplying the diode bias through the bridge terminals, the entire bias supply circuitry was kept at RF ground.

b) Great care was taken to ensure that the signal across the diode was really "small": that the differential quantity $C \triangleq \frac{dq_t}{dv_t}$ was really the quantity being measured.

The plots of q_t versus v_t were obtained directly from the $\frac{dq_t}{dv_t}$ curves by graphical integration and are normalized according to the procedure in Section 2.2.

The techniques used to measure diffusion capacity were somewhat more novel. Using the diffusion capacity model (and the notation) introduced in Section 2.3, the diode can be completely characterized if the following data is known:

a) P_n the normalized carrier density

b) τ the carrier lifetime

c) β the electric field term

A relation between β and P_n can be obtained from the forward DC current-voltage relation. From evaluation of this data and using Eq. 2.34, it is possible to obtain the value of

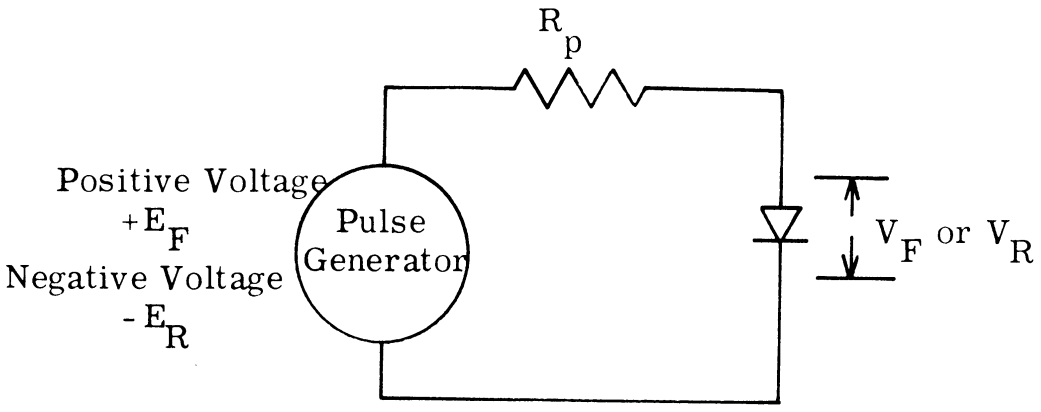

Fig. E.3. Test circuit for pulse measurements

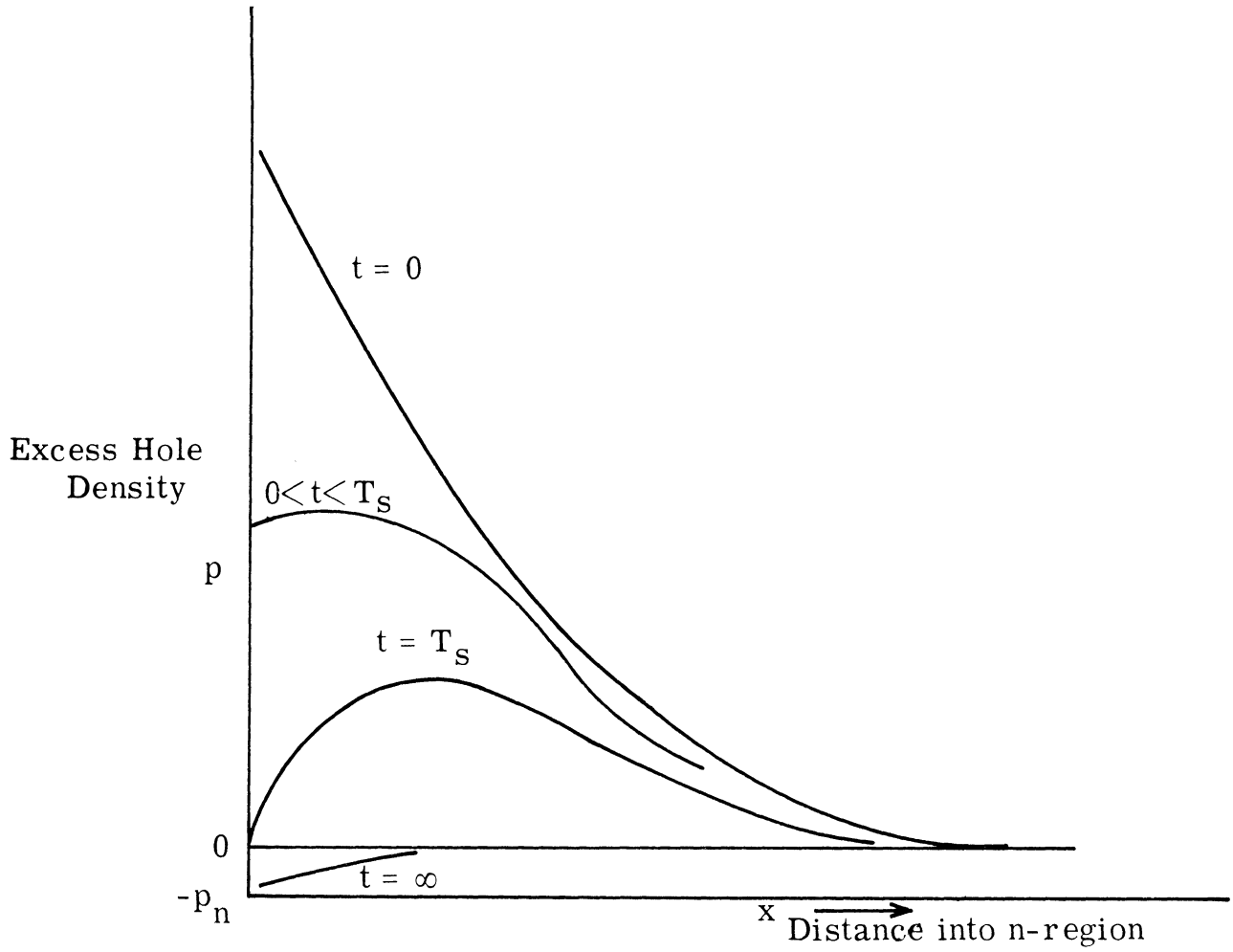

Fig. E. 4. Minority carrier density in base of diode

$$\frac{P_n}{1 + \sqrt{1 + \beta}} \qquad \text{(E. 1)}$$

The quantities τ and β can be obtained from pulse measurements. The carrier lifetime τ, of course, has been measured by several workers. However they have either used the assumption that $\beta = 0$ (Refs. 57, 58) or the assumption that $\beta = \infty$ (Refs. 59, 60, 61).

The method used involves formulating an expression for the reverse current pulse which appears when the diode is switched from forward to reverse bias with a square wave. The circuit is shown in Fig. E.3. The generator voltage, E_F, and the resistor, R_p, can be considered large enough so that during forward conduction, the forward voltage drop, V_F, across the diode may be neglected and

$$I_F = \frac{E_F}{R_p} \qquad \text{(E. 2)}$$

It is further assumed that the duration of forward current is long so that steady state conditions are established. Before switching, the holes set up a distribution in the base as shown in Fig. E.4. When the diode is switched to reverse bias, the n region becomes a source of positive carriers and reverse current flows until these carriers have been removed. By Eq. 2.27 between the time the generator is switched ($t = 0$) and the time when the excess hole concentration at the junction becomes zero ($t = T_s$), the voltage across the diode is small.

$$0 \leq V_R \leq V_F \quad \text{for} \quad 0 \leq t \leq T_s \tag{E.3}$$

Then between $t=0$ and $t=T_s$, the current can be considered to be constant and equal to

$$I_R = \frac{E_R}{R_p} \tag{E.4}$$

After time T_s, however, the voltage magnitude across the junction increases very rapidly as more carriers are removed, and the current magnitude drops rapidly to the normal reverse current value. The result is an almost rectangular pulse, of reverse current.

To determine T_s, consider the behavior of holes in the base region. In the one dimensional situation they are governed by

$$D \frac{\partial^2 P(x,t)}{\partial x^2} = \frac{\partial P(x,t)}{\partial t} + \frac{P(x,t)}{\tau} - \mu E \frac{\partial P(x,t)}{\partial x} \tag{2.24}$$

The current through the diode is given by

$$I(t)_{\text{Total}} = -q\,DA \frac{\partial P(x,t)}{\partial x}\bigg|_{x=0} - q\,A\,E\mu\,P(x,t)\bigg|_{x=0} \tag{2.26}$$

where, as in Section 2.3, the junction is taken to be at the origin of the coordinate system. The base region extends indefinitely in the positive x direction.

$$P(\infty, t) = 0$$

At $t=0$, the current is switched instantaneously from I_F to $-I_R$. A boundary value problem may be set up and then $P(0,t)$ may be solved using conventional Laplace transform methods. The result is found (use Transform No. 42 in Ref. 62) after some labor

$$P(0,t) = \left(\frac{I_F + I_R}{\beta}\right)\left[e^{-\frac{t}{\tau}}\left(1 + \operatorname{erf}\sqrt{\frac{t}{\tau\beta}}\right) - \sqrt{1+\beta}\ \operatorname{erf}\sqrt{\frac{(1+\beta)t}{\tau\beta}} - 1\right] + \frac{I_F}{\beta}\left[1 + \sqrt{1+\beta}\right] \quad \text{(E. 5)}$$

by the definition of T_s, $P(0, T_s) = 0$

and

$$\frac{I_F}{I_F + I_R} = \frac{1 + \sqrt{1+\beta}\ \operatorname{erf}\sqrt{\frac{(1+\beta)\,T_s}{\tau\beta}} - e^{-\frac{T_s}{\tau}}\left(1 + \operatorname{erf}\sqrt{\frac{T_s}{\tau\beta}}\right)}{1 + \sqrt{1+\beta}} \quad \text{(E. 6)}$$

For the case of 0 electric field ($\beta = \infty$), this relation reduces to that of an ideal PN junction.

$$\frac{I_F}{I_F + I_R} = \operatorname{erf}\sqrt{\frac{T_s}{\tau}} \quad \text{(E. 7)}$$

Likewise, for the infinite electric field case ($\beta = 0$) the function reduces to that of the ideal step recovery diode which is

modeled by a parallel RC circuit

$$\frac{I_F}{I_F + I_R} = 1 - e^{\left(\frac{-T_s}{\tau}\right)} \qquad \text{(E.8)}$$

Figure E. 5 shows the function $I_F/(I_F+I_R)$ plotted as a function of T_s/τ for various values of β. Both τ and β can be estimated by using this graph in conjunction with a similar plot of measured values of $I_F/(I_F+I_R)$ versus T_s. The values of τ and β for diode number PC0622C which were measured using this technique are presented in Table E. 2 along with an estimate of P_n. It should be noted that the curves near $\beta = 0$ become very close together and an accurate estimate for β is difficult, and so the very good comparison of values obtained using pulse methods with those values which correlate with measured values of pumped varactor input impedance may be somewhat fortuitous. However, even if the comparison should not be this good, the use of this diode model and this means of measuring the diode constants still apparently have some merits.

Measured Parameters of Diode PC 0622 C		
P_n	τ	β
10^{-12}	0. 5 μsec.	$\approx$ 0. 1

Table E. 2.

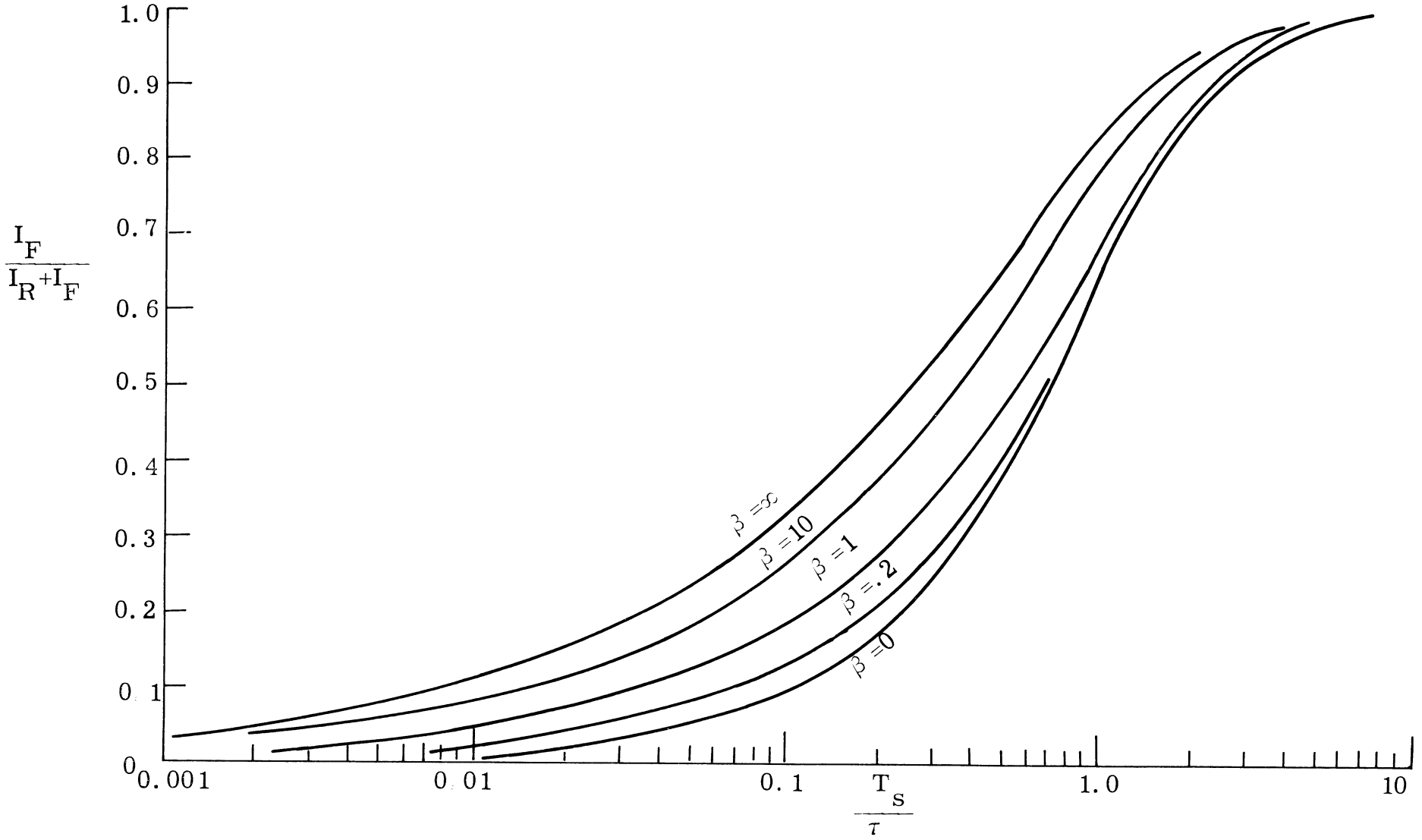

Fig. E. 5. Normalized switching time for diode with charge storage

REFERENCES

1. W. W. Mumford, "Some Notes on the History of Parametric Transducers," Proc. IRE, 1960, 48, No. 5, 848-853.

2. E. F. W. Alexanderson, "A Magnetic Amplifier for Radio Telephony," Proc. IRE, 1916, 4, 101-149.

3. H. C. Torrey & C. A. Whitmer, Crystal Rectifiers (M. I. T. Rad. Lab. Series), New York, McGraw-Hill Book Co., Inc., 1948, Vol. 15.

4. A. van der Ziel, "Noise Figure of Reactance Converters and Parametric Amplifiers," J. of Appl. Phys., 1959, 30, No. 9, 1449.

5. A. Uhlir, Jr., "The Potential of Semiconductor Diodes in High-Frequency Communications," Proc. IRE, 1958, 46, No. 6, 1099, 1115.

6. A. E. Bakanowski, N. G. Cranna, & A. Uhlir, Jr., "Diffused Silicon Nonlinear Capacitors," IRE Trans. on Electron Devices, 1959, ED-6, No. 4, 384-390.

7. B. A. Bryce, Microwave Parametric Amplifiers and Related Parametric Devices--An Annotated Bibliography, Autonetics Technical Report No. EM-6644, 10 May, 1961.

8. J. M. Manley & H. E. Rowe, "Some General Properties of Nonlinear Elements: Part I - General Energy Relations," Proc. IRE, 1956, 44, No. 7, 904-913.

9. J. M. Manley & H. E. Rowe, "General Energy Relations in Nonlinear Reactances," Proc. IRE, 1959, 47, No. 12, 1271.

10. H. Suhl, "Proposal for a Ferromagnetic Amplifier in the Microwave Range," Phys. Rev., 1957, 106, Part 2, 384-385.

11. M. T. Weiss, "Solid-State Microwave Amplifier and Oscillator Using Ferrites," Phys. Rev., 1957, 107, Part 1, 317.

12. S. Bloom & K. K. N. Chang, "Theory of Parametric Amplification Using Nonlinear Reactances," RCA Review, 1957, 18, No. 4, 578-593.

13. H. Heffner & G. Wade, "Gain, Bandwidth, and Noise Characteristics of the Variable-Parameter Amplifier," J. of Appl. Phys., 1958, 29, No. 9, 1321-1331.

REFERENCES (Cont.)

14. H. E. Rowe, "Some General Properties of Nonlinear Elements: Part II - Small Signal Theory," Proc. IRE, 1958, 46, No. 5, 850, 860.

15. D. Leenov, "Gain and Noise Figure of a Variable-Capacitance Up-Converter," Bell System Tech. J., 1958, 37, 989-1008.

16. B. J. Robinson, "Theory of Variable-Capacitance Parametric Amplifiers," Proc. IEE, Monograph No. 480E, 1961, 108C, 198.

17. P. Penfield, Jr. & R. P. Rafuse, Varactor Applications, Cambridge, Massachusetts: The M. I. T. Press, 1962.

18. K. Kurakawa & M. Uenohara, "Minimum Noise Figure of the Variable-Capacitance Amplifier," Bell System Tech. Jour., 1961, XL, No. 3, 695-722.

19. D. K. Adams, A Study of Double-Sideband Reactive Mixers, Cooley Electronics Laboratory Technical Report No. 134, (Prepared for Signal Corps., Department of the Army, Contr. No. DA-36-039 sc-89227). Ann Arbor, Michigan: The University of Michigan, December 1962.

20. A. Korpel & V. Ramaswamy, "Input Conductance of a Four-Frequency Parametric Up-Converter," IEEE Trans. on Micro. Theor. & Tech., 1965, MTT-13, No. 1, 96-106.

21. A. Korpel & V. Ramaswamy, "Ferroresonant Effect Caused by Nonlinear Capacitors," Proc. IEEE, 1964, 52, No. 1, 82.

22. L. A. Blackwell & K. L. Kotzebue, Semiconductor-Diode Parametric Amplifiers, Englewood Cliffs, New Jersey: Prentice-Hall, Inc , 1961.

23. K. K. N. Chang, Parametric and Tunnel Diodes, Englewood Cliffs, New Jersey: Prentice-Hall, Inc., 1964.

24. S. T. Eng, "Characterization of Microwave Variable Capacitance Diodes," IRE Trans., 1961, MTT-9, No. 1, 11, 21.

25. L. S. Lototskii, "Comparison of Static and Dynamic Characteristics of Germanium Diodes under Negative Bias," Radio Engrg. and Elec. Phys., 1961, 6, No. 11, 1717-1721.

26. S. P. Morgan & F. M. Smits, "Potential Distribution and Capacitance of a Graded P-N Junction " Bell System Tech. J., 1960, 39, No. 6, 1573-160

REFERENCES (Cont.)

27. D. B. Leeson, Large-Signal Analysis of Parametric Frequency Multipliers, Stanford Electronics Laboratories Technical Report No. 1710-1. [Prepared under Office of Naval Research Contract Nonr-225(31), AD 287 001.] Stanford, California: Stanford Electronics Laboratories, May 1962.

28. A. van der Ziel, Electronics, Boston: Allyn and Bacon, 1966.

29. Y.-F. Chang, Transient Phenomena in Semiconductor Diodes, Cruft Laboratory Technical Report No. 294. [Prepared for the Office of Naval Research, Contract No. 1866(16) NR-372-012.] Cambridge, Massachusetts: Cruft Laboratory, Harvard University, January 1959.

30. D. Koehler, "A New Charge Control Equivalent Circuit for Diodes and Transistors and Its Relation to Other Large Signal Models," Internat. Solid-State Circuits Conf. Digest of Tech. Papers, 1965, 38-39.

31. D. Koehler, "The Charge-Control Concept in the Form of Equivalent Circuits," Bell System Tech. J., 1967, 46, 523-567.

32. J. L. Moll, Physics of Semiconductors, New York: McGraw-Hill, 1964, pp. 110-140.

33. L. P. Hunter, Handbook of Semiconductor Electronics, New York: McGraw-Hill, 1956, pp. 3-1 to 3-17.

34. R. Fekete, "Varactors in Voltage Tuning Applications," Microwave J., 1964, 7, No. 7, 53-61.

35. D. E. Crook, "A Simplified Technique for Measuring High Quality Varactor Parameters," Solid State Design, 1965, 6, No. 8, 31-33.

36. R. V. Garver & J. A. Rosado, "Microwave Diode Cartridge Impedance," IRE Trans. MTT, 1960, MTT-8, No. 1, 104-107.

37. A. P. Epperly, "Varactor Fabrication for Microwave Applications," Proc. NEC, 1962, 18, 406-413.

38. B. J. Levin, "The Modified Series Model for an Abrupt-Junction Varactor Frequency Doubler," IRE Trans., Microwave Theo. & Tech., 1966, MTT-14, 184-188.

39. S. T. Eng & W. P. Waters, "A Gold Bonded Germanium Diode for Parametric Amplification," Proc NEC, 1959, 15, 83-91.

REFERENCES (Cont.)

40. A. P. Bolie, "Application of Complex Symbolism to Linear Variable Networks," IRE Trans., 1955, CT-2, No. 1, 32-35.

41. H. Heffner, "Capacitance Definitions for Parametric Operation," IRE Trans. MTT, 1961, MTT-9, No. 1, 98-99.

42. G. L. Matthaei, "A Study of the Optimum Design of Wideband Parametric Amplifiers and Up-Converters," IRE Trans. on Micro. Theor. & Tech., 1961, MTT-9, No. 1, 23-38.

43. M. Uenohara, "Noise Consideration of the Variable Capacitance Parametric Amplifier," Proc. IRE, 1960, 48, No. 12, 1973-1987.

44. C. A. Desoer, "Steady State Transmission through a Network Containing a Single Time-Varying Element," IRE Trans. on Circuit Theory, 1959, CT-6, 244-252.

45. A. A. Kharkevich, Nonlinear and Parametric Phenomena in Radio Engineering, New York: John F. Rider, 1962.

46. J. J. Stoker, Nonlinear Vibrations, New York: Interscience, 1950.

47. C. Hayashi, Forced Oscillations in Nonlinear Systems, Osaka, Japan: Nippon Printing and Publishing, 1953.

48. W. Kaplan, Operational Methods for Linear Systems, Reading, Massachusetts: Addison-Wesley, 1966.

49. J. L. Cockrell, The Phase Synchronization of a Parametric Subharmonic Oscillator, Cooley Electronics Laboratory Technical Report No. 178, [Prepared for USAEC, Fort Monmouth, N. J. Contract No. DA 28-043-AMC-01870(E)] Ann Arbor, Michigan, The University of Michigan, April 1967.

50. S. Ramo & J. R. Whinnery, Fields and Waves in Modern Radio, New York: John Wiley and Sons, 1953.

51. V. Volterra, Lecons sur les Equationes Integrales, Paris: Gauthier-Villar 1913.

52. R. E. Scott, Linear Circuits, Reading, Massachusetts: Addison-Wesley, 1966

REFERENCES (Cont.)

53. C. S. Bunus, An Iterative Procedure for the Analysis of Nonlinear Networks, Stanford Electronics Laboratories Technical Report No. 6657-1 [Prepared under Office of Naval Research Contract Nonr-225(83), NR 373 360.] Stanford, California: Stanford Electronics Laboratories, August 1965.

54. K. Siegel, "Anomalous Reverse Current in Varactor Diodes," Proc. IRE, 1960, 48, 1159-1160.

55. B. Albrecht, J. Kliphuis, & D. Heuf, "Universal Performance Curves Speed Parametric Amplifier Design," Microwaves, 1966, 5, No. 7, 20-24.

56. A. L. Helgesson, "Varactor Charge-Voltage Expansions for Large Pumping Conditions," Proc. IRE, 1962, 50, No. 8, 1846-1847.

57. S. Krakaur, J. L. Moll, & R. Shen, "P-N Junction Charge-Storage Diodes," Proc. IRE, 1962, 50, No. 1, 43-53.

58. C. Culwell, E. H. Devletoglou, & L. E. Niemann, Jr., Negative Resistance Study--Phase I., Rome Air Development Center Technical Report RADC-TR-66-231, 1966, June. New York: Griffiss Air Force Base, Rome Air Development Center.

59. J. G. Gardiner & D. P. Howson, "Influence of Minority-Carrier Storage on Performance of Semiconductor-Diode Modulator," Proc. IEE, 1964, 111, 1393-1400.

60. R. H. Kingston, "Switching Time in Junction Diode," Proc. IRE, 1954, 25, 829-834.

61. B. Lax & S. F. Neustadter, "Transient Response of a P-N Junction, J. Appl. Phys., 1954, 25, 1148-1152.

62. R. V. Churchill, Operational Mathematics, New York: McGraw-Hill Book Co., 1958.

DISTRIBUTION LIST

No. of Copies	
10	Defense Documentation Center ATTN: DDC-IRS Cameron Station (Bldg. 5) Alexandria, Virginia 22314
1	Office of Assistant Secretary of Defense (Research Engineering) ATTN: Technical Library, Rm 3E1065 Washington, D. C. 20301
1	Defense Intelligence Agency ATTN: DIARD Washington, D. C. 20301
1	Bureau of Ships Technical Library ATTN: Code 312 Main Navy Building, Room 1528 Washington, D. C. 20325
1	Chief, Bureau of Ships ATTN: Code 454 Department of the Navy Washington, D. C. 20360
2	Director U. S. Naval Research Laboratory ATTN: Code 2027 Washington, D. C. 20390
1	Commanding Officer and Director U. S. Navy Electronics Laboratory ATTN: Library San Diego, California 92101
1	Commander U. S. Naval Ordnance Laboratory ATTN: Technical Library White Oak, Silver Spring, Maryland 20910

DISTRIBUTION LIST (Cont.)

No. of Copies	
1	AFSC STLO (RTSND) Naval Air Development Center Johnsville, Warminster, Pa. 18974
1	Rome Air Development Center (EMTLD) ATTN: Documents Library Griffiss Air Force Base New York 13440
1	Systems Engineering Group (SEPIR) AVWW Wright-Patterson Air Force Base Ohio 45433
2	Electronic Systems Division (ESTI) L. G. Hanscom Field Bedford, Massachusetts 01731
1	Air Proving Ground CTR (PGBPS-12) ATTN: PGAPI Eglin Air Force Base, Florida 32542
1	Air University Library (3T) Maxwell Air Force Base Alabama 36112
2	Chief of Research and Development Department of the Army Washington, D. C. 20315
2	Commanding General U. S. Army Materiel Command ATTN: R & D Directorate Washington, D. C. 20315
1	Commanding General U. S. Army Combat Developments Command ATTN: CDCMR-E Fort Belvoir, Virginia 22060

DISTRIBUTION LIST (Cont.)

No. of Copies	
3	Commanding Officer U. S. Army Combat Developments Command Communications-Electronics Agency Fort Monmouth, New Jersey 07703
1	Commanding Officer U. S. Army Sec Agcy Combat Dev Actv Arlington Hall Station Arlington, Virginia 22212
1	U. S. Army Security Agency ATTN: OACofS, Dev (CDA Arlington Hall Station Arlington, Virginia 22212
1	Harry Diamond Laboratories ATTN: Library Connecticut Avenue and Van Ness Street Washington, D. C. 20438
1	Asst Secretary of the Army (R & D) Department of the Army ATTN: Deputy Asst for Army (R & D) Washington, D. C. 20315
1	Commanding Officer U. S. Army Limited War Laboratory Aberdeen Proving Ground, Md. 2100
2	C. G. U. S. Army Security Agency Arlington Hall Station Arlington, Virginia 22207 ATTN: IALOG and IARD
1	Stanford Electronics Laboratory Stanford University Stanford, California ATTN: Dr. D. G. Grace
1	Chief, Mountain View Office Electronic Warfare Lab., USAECOM P. O. Box 205 Mountain View, California 94042

DISTRIBUTION LIST (Cont.)

No. of Copies	
1	Chief, Intelligence Materiel Dev Office Electronic Warfare Lab., USAECOM Fort Holabird, Maryland 21219
1	Chief Missile Electronic Warfare Tech Area EW Lab, USA Electronics Command White Sands Missile Range, N. M. 88002
1	Chief, Willow Run Office CSTA Lab. USAECOM P. O. Box 618 Ann Arbor, Michigan 48107
1	Headquarters U. S. Army Combat Developments Command ATTN: CDCLN-EL Fort Belvoir, Virginia 22060
1	USAECOM Liaison Officer MIT, Bldg 26, Rm 131 77 Massachusetts Avenue Cambridge, Mass. 02139
1	USAECOM Liaison Officer Aeronautical Systems Division ATTN: ASDL-9 Wright-Patterson AF Base, Ohio 45433
1	USAECOM Liasion Office U. S. Army Electronic Proving Ground Fort Hauchuca, Arizona 85613
1	Dir. National Security Agency Fort George G. Meade Maryland 20755
1	Asst Secretary of the Army (R & D) Department of the Army ATTN: Asst for Research Washington, D. C. 20315

DISTRIBUTION LIST (Cont.)

No. of Copies	
16	Commanding General U.S. Army Electronics Command Fort Monmouth, New Jersey 07703 ATTN: AMSEL-EW AMSEL-PP AMSEL-IO-T AMSEL-RD-MAT AMSEL-RD-MAF (Record Copy) AMSEL-RD-LNA AMSEL-RD-LNR AMSEL-XL-D AMSEL-NL-D AMSEL-VL-D AMSEL-KL-D AMSEL-HL-CT-D AMSEL-BL-D AMSEL-WL 3 copies
1	Dr. T.W. Butler, Director Cooley Electronics Laboratory The University of Michigan Ann Arbor, Michigan 48105
7	Cooley Electronics Laboratory The University of Michigan Ann Arbor, Michigan 48105

Security Classification

DOCUMENT CONTROL DATA - R&D

(Security classification of title, body of abstract and indexing annotation must be entered when the overall report is classified)

1. ORIGINATING ACTIVITY (Corporate author) Cooley Electronics Laboratory The University of Michigan Ann Arbor, Michigan	2a. REPORT SECURITY CLASSIFICATION Unclassified 2b. GROUP

3. REPORT TITLE

Impedance Characteristics of Pumped Varactors

4. DESCRIPTIVE NOTES (Type of report and inclusive dates)

Technical Report No. 7695-189 November 1967

5. AUTHOR(S) (Last name, first name, initial)

Oliver, David E.

6. REPORT DATE	7a. TOTAL NO. OF PAGES	7b. NO. OF REFS
November 1967	278	62

8a. CONTRACT OR GRANT NO. DA 28-043-AMC-01870(E) b. PROJECT NO. 1PO 21101 AO42.01.02 c. d.	9a. ORIGINATOR'S REPORT NUMBER(S) C.E.L. Technical Report No. 7695-189 9b. OTHER REPORT NO(S) (Any other numbers that may be assigned this report) ECOM-01870-189

10. AVAILABILITY/LIMITATION NOTICES

This document is subject to special export controls and each transmittal to foreign governments or foreign nationals may be made only with prior approval of CG, U.S. Army Electronics Command, Fort Monmouth, N.J. Attn: AMSEL-WL-S

11. SUPPLEMENTARY NOTES	12. SPONSORING MILITARY ACTIVITY
	U.S. Army Electronics Command AMSEL-WL-S Fort Monmouth, N. J. 07703

13. ABSTRACT A considerable amount of work has been reported on the analysis of pumped varactor diode circuits. However, all these studies have been limited in generality by two simplifying assumptions: the limitation of the pump voltage to low amplitudes, and the restriction of signal power flow to only a few sidebands. The first of these assumptions excludes the possibility of harmonic generation by the nonlinear diode, while the second presupposes the existence of ideal filters in the linear circuitry. This study is concerned with an analysis of pumped varactor diode circuits without these two restrictions.

The input impedances of several basic pumped varactor diode circuits were analyzed theoretically by determining a suitable model for each circuit and then predicting its impedance characteristics. The results showed good correlation with experimental measurements, indicating the adequacy of the circuit model and the validity of the analysis methods.

It was shown that several circuit parameters significantly affect circuit behavior. A practical technique was developed for experimentally measuring the pump voltage amplitude across the diode junction. The most significant outcome of this study is the development of a circuit model which can accurately characterize a varactor diode circuit.

DD FORM 1 JAN 64 1473

Security Classification

14. KEY WORDS	LINK A		LINK B		LINK C	
	ROLE	WT	ROLE	WT	ROLE	WT
Varactor Diode Impedance characteristics Linear networks Pump circuits						

INSTRUCTIONS

1. ORIGINATING ACTIVITY: Enter the name and address of the contractor, subcontractor, grantee, Department of Defense activity or other organization *(corporate author)* issuing the report.

2*a*. REPORT SECURITY CLASSIFICATION: Enter the overall security classification of the report. Indicate whether "Restricted Data" is included. Marking is to be in accordance with appropriate security regulations.

2*b*. GROUP: Automatic downgrading is specified in DoD Directive 5200.10 and Armed Forces Industrial Manual. Enter the group number. Also, when applicable, show that optional markings have been used for Group 3 and Group 4 as authorized.

3. REPORT TITLE: Enter the complete report title in all capital letters. Titles in all cases should be unclassified. If a meaningful title cannot be selected without classification, show title classification in all capitals in parenthesis immediately following the title.

4. DESCRIPTIVE NOTES: If appropriate, enter the type of report, e.g., interim, progress, summary, annual, or final. Give the inclusive dates when a specific reporting period is covered.

5. AUTHOR(S): Enter the name(s) of author(s) as shown on or in the report. Enter last name, first name, middle initial. If military, show rank and branch of service. The name of the principal author is an absolute minimum requirement.

6. REPORT DATE: Enter the date of the report as day, month, year; or month, year. If more than one date appears on the report, use date of publication.

7*a*. TOTAL NUMBER OF PAGES: The total page count should follow normal pagination procedures, i.e., enter the number of pages containing information.

7*b*. NUMBER OF REFERENCES: Enter the total number of references cited in the report.

8*a*. CONTRACT OR GRANT NUMBER: If appropriate, enter the applicable number of the contract or grant under which the report was written.

8*b*, 8*c*, & 8*d*. PROJECT NUMBER: Enter the appropriate military department identification, such as project number, subproject number, system numbers, task number, etc.

9*a*. ORIGINATOR'S REPORT NUMBER(S): Enter the official report number by which the document will be identified and controlled by the originating activity. This number must be unique to this report.

9*b*. OTHER REPORT NUMBER(S): If the report has been assigned any other report numbers *(either by the originator or by the sponsor)*, also enter this number(s).

10. AVAILABILITY/LIMITATION NOTICES: Enter any limitations on further dissemination of the report, other than those imposed by security classification, using standard statements such as:

(1) "Qualified requesters may obtain copies of this report from DDC."

(2) "Foreign announcement and dissemination of this report by DDC is not authorized."

(3) "U. S. Government agencies may obtain copies of this report directly from DDC. Other qualified DDC users shall request through _____."

(4) "U. S. military agencies may obtain copies of this report directly from DDC. Other qualified users shall request through _____."

(5) "All distribution of this report is controlled. Qualified DDC users shall request through _____."

If the report has been furnished to the Office of Technical Services, Department of Commerce, for sale to the public, indicate this fact and enter the price, if known.

11. SUPPLEMENTARY NOTES: Use for additional explanatory notes.

12. SPONSORING MILITARY ACTIVITY: Enter the name of the departmental project office or laboratory sponsoring *(paying for)* the research and development. Include address.

13. ABSTRACT: Enter an abstract giving a brief and factual summary of the document indicative of the report, even though it may also appear elsewhere in the body of the technical report. If additional space is required, a continuation sheet shall be attached.

It is highly desirable that the abstract of classified reports be unclassified. Each paragraph of the abstract shall end with an indication of the military security classification of the information in the paragraph, represented as *(TS)*, *(S)*, *(C)*, or *(U)*.

There is no limitation on the length of the abstract. However, the suggested length is from 150 to 225 words.

14. KEY WORDS: Key words are technically meaningful terms or short phrases that characterize a report and may be used as index entries for cataloging the report. Key words must be selected so that no security classification is required. Identifiers, such as equipment model designation, trade name, military project code name, geographic location, may be used as key words but will be followed by an indication of technical context. The assignment of links, rules, and weights is optional.